

# Light Front Field Theory Calculation of Deuteron Properties

Jason Randolph Cooke

A dissertation submitted in partial fulfillment  
of the requirements for the degree of

Doctor of Philosophy

University of Washington

2001

Program Authorized to Offer Degree: Physics



University of Washington  
Graduate School

This is to certify that I have examined this copy of a doctoral dissertation by

Jason Randolph Cooke

and have found that it is complete and satisfactory in all respects,  
and that any and all revisions required by the final  
examining committee have been made.

Chair of Supervisory Committee:

---

Gerald A. Miller

Reading Committee:

---

Gerald A. Miller

---

Daniel R. Phillips

---

Stephen R. Sharpe

Date: \_\_\_\_\_



In presenting this dissertation in partial fulfillment of the requirements for the Doctoral degree at the University of Washington, I agree that the Library shall make its copies freely available for inspection. I further agree that extensive copying of this dissertation is allowable only for scholarly purposes, consistent with "fair use" as prescribed in the U.S. Copyright Law. Requests for copying or reproduction of this dissertation may be referred to Bell and Howell Information and Learning, 300 North Zeeb Road, Ann Arbor, MI 48106-1346, to whom the author has granted "the right to reproduce and sell (a) copies of the manuscript in microform and/or (b) printed copies of the manuscript made from microform."

Signature\_\_\_\_\_

Date\_\_\_\_\_



University of Washington

Abstract

## Light Front Field Theory Calculation of Deuteron Properties

by Jason Randolph Cooke

Chair of Supervisory Committee:

Professor Gerald A. Miller  
Department of Physics

Light front dynamics is a promising approach for solving bound state problems in nuclear physics. It is also ideal for calculating the deuteron form factors at high momentum transfers. However, in light-front dynamics rotational invariance is not manifest, which results in a splitting in the binding energies of states with different magnetic quantum numbers and a breaking of the angular condition for the matrix elements of the deuteron current operator. The objective of this work is to investigate the symptoms of broken rotational invariance for deuterons calculated using one-meson-exchange (OME) and two-meson-exchange (TME) potentials for various models.

We first consider the Wick-Cutkosky model. The binding energies of states with different  $m$  values are split when calculated with the OME potential, but this splitting is reduced for all states when the TME potential is included. In addition, we find that appropriate OME+TME potentials give almost identical results to the ladder and crossed ladder Bethe-Salpeter equation.

Next, we derive light-front nucleon-nucleon OME and TME potentials from an effective nuclear Lagrangian. We consider first the potentials generated by the ex-



change of pions only. There is a large splitting in the binding energies between the  $m = 0$  and  $m = 1$  deuteron states when the one-pion-exchange (OPE) potential is used. Including the chiral two-pion-exchange (TPE) potential in the calculation reduces this splitting. We then proceed to use the potentials generated by all the mesons, and find that the deuteron mass splittings are smaller for both the OME and OME+TME potentials than in the pion-only model.

The deuteron wave functions are used to calculate the electromagnetic and axial current matrix elements and form factors. The matrix elements of the electromagnetic current operator have better transformation properties under rotations when we use the OME potential instead of the OME+TME potential to calculate the wave functions. The axial current matrix elements have about the same transformation properties regardless of whether the OME or OME+TME potential is used. Finally, at momentum transfers greater than about  $2 \text{ GeV}^2$ , the breaking of rotational invariance causes less uncertainty in the  $A$  and  $B$  form factors than do the uncertainties in the nucleon form factors.



# TABLE OF CONTENTS

<b>List of Figures</b>	<b>v</b>
<b>List of Tables</b>	<b>x</b>
<b>Glossary</b>	<b>xii</b>
<b>Chapter 1: Introduction</b>	<b>1</b>
1.1 Theoretical Descriptions of the Deuteron . . . . .	1
1.2 Benefits of Light-front Dynamics . . . . .	3
1.3 Breaking of Rotational Invariance . . . . .	4
1.4 Outline . . . . .	5
<b>Chapter 2: Wick-Cutkosky Model</b>	<b>7</b>
2.1 Formalism . . . . .	7
2.1.1 Light-front Hamiltonian . . . . .	8
2.1.2 Hamiltonian Bound-state Equations . . . . .	10
2.1.3 Further Development of the Light-front Schrödinger Equation	15
2.1.4 Bethe-Salpeter Equation . . . . .	19
2.1.5 Comparison Between the Light-front Schrödinger Equation and the Bethe-Salpeter Equation . . . . .	22
2.2 Wick-Cutkosky Perturbative Potentials . . . . .	23
2.2.1 OBE Potential . . . . .	24
2.2.2 TBE Potentials . . . . .	26

2.2.3	TBE:SB Potential: Connection to the Ladder Bethe-Salpeter Equation . . . . .	30
2.3	Wick-Cutkosky Non-perturbative Potentials . . . . .	31
2.3.1	Symmetrized-mass Approximation . . . . .	31
2.3.2	Instantaneous and Retarded Approximations . . . . .	33
2.3.3	Three-dimensional Reduction of the Bethe-Salpeter Equation . . . . .	34
2.3.4	The Modified-Green's-function Approach . . . . .	37
2.4	Results for the Wick-Cutkosky Model . . . . .	42
2.4.1	Ground State Results . . . . .	43
2.4.2	Excited State Results . . . . .	47
2.5	Conclusions . . . . .	59
<b>Chapter 3: Realistic Nuclear Models</b>		<b>61</b>
3.1	Model and Formalism . . . . .	62
3.2	Non-interacting Nucleon-Nucleon Theory . . . . .	63
3.2.1	Free Field Expansions . . . . .	63
3.2.2	Non-interacting Hamiltonians . . . . .	65
3.3	Interacting Nucleon-Nucleon Theory . . . . .	65
3.3.1	Expanding the Pion Interaction . . . . .	66
3.3.2	Elimination of Dependent Fermion Components . . . . .	67
3.3.3	Elimination of Dependent Vector Meson Components . . . . .	69
3.3.4	Interaction Hamiltonians in Momentum Space . . . . .	71
3.4	Feynman Rules for Nucleon-Nucleon Potentials . . . . .	72
3.5	Nucleon-Nucleon Perturbative Potentials . . . . .	74
3.5.1	The Bethe-Salpeter Equation . . . . .	74
3.5.2	OME Potential . . . . .	77
3.5.3	TME Potentials . . . . .	80

3.5.4	Further Development of the Light-front Schrödinger Equation	85
3.6	Results for the Nucleon-Nucleon Potentials . . . . .	86
3.6.1	Pion-only Results . . . . .	87
3.6.2	Light-Front Nucleon-Nucleon Model Results . . . . .	95
<b>Chapter 4:</b>	<b>Form Factors of the Deuteron</b>	<b>104</b>
4.1	Electromagnetic Form Factors . . . . .	104
4.1.1	Covariant Theory . . . . .	105
4.1.2	Light Front Calculation . . . . .	108
4.1.3	Impulse Approximation on the Light Front . . . . .	114
4.1.4	The Nucleon Form Factors . . . . .	117
4.2	Axial Form Factors . . . . .	120
4.3	Results for the Form Factors . . . . .	122
<b>Chapter 5:</b>	<b>Conclusions</b>	<b>136</b>
	<b>Bibliography</b>	<b>139</b>
	<b>Appendix A: Notation, Conventions, and Useful Relations</b>	<b>149</b>
	<b>Appendix B: Conversion to Matrix Form</b>	<b>152</b>
	<b>Appendix C: Azimuthal-angle and Loop Integrals</b>	<b>155</b>
C.1	Azimuthal-angle Integration of the OBE and MGF Potentials . . . . .	155
C.2	Azimuthal-angle and Loop Integration of the TBE Potentials . . . . .	157
	<b>Appendix D: Cosine Integrals</b>	<b>160</b>
	<b>Appendix E: Check of the Uncrossed Approximation</b>	<b>169</b>

<b>Appendix F: Spinors</b>	<b>173</b>
F.1 Definition of the Spinors . . . . .	173
F.2 Two Helicity Spinors in the Center of Momentum Frame . . . . .	178
F.3 Helicity Spinor Summary . . . . .	180
F.4 Breakup of Dirac Spinor Matrix Elements . . . . .	180
F.5 The Gordon Decomposition . . . . .	184
<b>Appendix G: Rotation Matrices</b>	<b>185</b>
G.1 Relations Between Rotation Matrices . . . . .	185
G.2 Jacobi Polynomials . . . . .	189
G.3 Helicity Applied to Potentials with Full Rotational Invariance . . . . .	193
G.4 Helicity Applied to Potentials with Cylindrical Invariance . . . . .	195
G.5 Summary of Transformations . . . . .	196

## LIST OF FIGURES

2.1	The full kernel for the Bethe-Salpeter equation of the Wick-Cutkosky model. . . . .	20
2.2	The ladder (one-boson-exchange) kernel for the Bethe-Salpeter equation. . . . .	20
2.3	The crossed (two-boson-exchange) kernel for the Bethe-Salpeter equation. . . . .	21
2.4	The relation between the Feynman box diagram and non-vanishing light-front time-ordered perturbation theory diagrams. . . . .	24
2.5	The diagrams for the OBE potential. . . . .	25
2.6	The components of the TBE potential, the stretched-box, stretched-crossed, T-crossed, wide-crossed, and Z-crossed diagrams. . . . .	28
2.7	The two-boson crossed and uncrossed Feynman graphs. . . . .	39
2.8	The spectra calculated using the OBE, OBE+TBE:SB and OBE+TBE potentials are displayed in this figure, along with the Bethe-Salpeter spectra for the ladder and ladder plus crossed kernels. . . . .	45
2.9	The spectra of all three of the perturbative light-front potentials (OBE, OBE+TBE:SB, OBE+TBE) and the four non-perturbative light-front potentials (modified-Green's-function, retarded, instantaneous, symmetrized mass) are plotted here along with the spectra for the full solution (FSR). The instantaneous curve lies very close to the symmetrized mass curve, hence the same line style is used for both. . . .	46
2.10	The first three energy bands for the ladder Bethe-Salpeter equation. .	48

2.11	Spectra for the four lowest wave functions of even parity and $m = 0$ (a) for the OBE equation (short-dashed line) and the Bethe-Salpeter equation (solid line), (b) for the OBE+TBE:SB equation (long-dashed line) and the Bethe-Salpeter equation (solid line). . . . .	50
2.12	The fractions of each angular momentum state in several wave functions is plotted as a function of the binding energy $E/M$ . The results for the OBE truncation are shown along with the OBE+TBE:SB truncation. The OBE wave functions, in general, have more support from a larger number of partial waves. . . . .	52
2.13	The spectra for the first $p$ -wave state, the $2p$ state. The Bethe-Salpeter (BS) result is plotted with a solid line, the OBE results with the short- dashed lines, and the OBE+TBE:SB with the long-dashed lines. . .	55
2.14	The spectra for the second $p$ -wave state, the $3p$ state. The Bethe- Salpeter (BS) result is plotted with a solid line, the OBE results with the short-dashed lines, and the OBE+TBE:SB with the long-dashed lines. . . . .	56
2.15	The first $d$ -wave state, the $3d$ state. The Bethe-Salpeter (BS) result is plotted with a solid line, the OBE results with short-dashed lines, and the OBE+TBE:SB results with long-dashed lines. . . . .	58
3.1	The first several terms of the full kernel for the Bethe-Salpeter equation of the nuclear model with chiral symmetry. . . . .	74
3.2	The non-vanishing diagrams for pion-nucleon scattering at threshold: (a) $\mathcal{M}_U$ , (b) $\mathcal{M}_X$ , and (c) $\mathcal{M}_C$ . The mesons here are pions. . . . .	76
3.3	The two diagrams which contribute to the OME potential for each meson. . . . .	77

3.4	The non-contact TME potentials: the Mesa potential, the stretched box potential, the stretched instantaneous potential, and the stretched double instantaneous potential. . . . .	81
3.5	The contact TME potentials: the contact potential, the stretched contact potential, the stretched instantaneous contact potential, and the stretched double contact potential. . . . .	82
3.6	The values of the binding energy for the $m = 0$ and $m = 1$ states for different pion-only light-front potentials. Three different pion-nucleon form factors are used. . . . .	94
3.7	The values of the binding energy for the $m = 0$ and $m = 1$ states for different nucleon-nucleon light-front potentials. The $\sigma$ coupling constant factor is $f_\sigma = 1.22$ . . . . .	101
3.8	The values of the binding energy for the $m = 0$ and $m = 1$ states for different nucleon-nucleon light-front potentials. The $\sigma$ coupling constant factor is $f_\sigma = 1.2815$ . . . . .	103
4.1	The Feynman diagram for one-photon-exchange electron-deuteron scattering. . . . .	105
4.2	The lowest-order graphs which contribute to the deuteron current matrix element. . . . .	109
4.3	The $F_1$ and $-F_2$ isoscalar nucleon form factors for six different models: the dipole model, Hohler, Gari:1985, Gari:1992, Mergell, and Lomon. . . . .	119
4.4	The matrix elements of $I_{(1)m'm}^+$ , the component of the electromagnetic current which multiplies the nucleon $F_1$ form factor, calculated with the wave function from the OME, OME+TME, OME+TPE, and Bonn potentials. . . . .	125

4.5	The matrix elements of $I_{(2)m'm}^+$ , the component of the electromagnetic current which multiplies the nucleon $F_2$ form factor, calculated with the wave function from the OME, OME+TME, OME+TPE, and Bonn potentials. . . . .	126
4.6	The matrix elements of $I_{(5)m'm}^+$ , the deuteron axial current including the nucleon axial form factor, calculated with the wave function from the OME, OME+TME, OME+TPE, and Bonn potentials. . . . .	127
4.7	The matrix elements for $F_1 I_{(1)m'm}^+$ , $F_2 I_{(2)m'm}^+$ , and $I_{m'm}^+$ calculated with the OME wave functions. The Gari:1985 nucleon isoscalar form factors are used for $F_1$ and $F_2$ . . . . .	129
4.8	The form factors $A$ , $B$ , $T_{20}$ , and $F_A$ calculated using the various choices of the “bad” matrix element. The definitions of the “bad” matrix elements are given in Sections 4.1.2 and 4.2. The OME wave function is used, along with the Lomon nucleon form factors for the electromagnetic form factors, and the Liesenfeld nucleon form factor for the axial form factor. . . . .	130
4.9	The form factors $A$ , $B$ , $T_{20}$ , and $F_A$ calculated using the various choices of the “bad” matrix element. The definitions of the “bad” matrix elements are given in Sections 4.1.2 and 4.2. The OME+TME wave function is used, along with the Lomon nucleon form factors for the electromagnetic form factors, and the Liesenfeld nucleon form factor for the axial form factor. . . . .	131

4.10	The electromagnetic form factors $A$ , $B$ , and $T_{20}$ calculated using the various choices of the nucleon isoscalar form factors. The OME wave function is used, along with the FFS choice of the “bad” deuteron current matrix. The axial form factor is not shown since its dependence on different form factors is trivial. . . . .	133
4.11	The $A$ , $B$ , $T_{20}$ , and $F_A$ form factors for the OME and OME+TME potentials, along with data. See the accompanying text for an explanation of the data. . . . .	135
E.1	The spectra for the potential derived from the TBE truncation of the uncrossed approximation, the TBE potential, the ladder plus crossed Bethe-Salpeter equation, and the modified-Green’s-function potential. Except for the MGF spectrum, all the curves lie close to each other.	172

## LIST OF TABLES

3.1	Binding energies for deuterons calculated with several potentials and two different pion-nucleon form factors for the scalar-pion-only model. The $n$ parameter of the form factor is 1, the coupling constant is $\frac{g^2}{4\pi} = 0.424$ , and the pion mass is used as the mass of the exchanged meson.	89
3.2	Binding energies for deuterons calculated with several potentials and two different pion-nucleon form factors for the (pseudoscalar) pion-only model. The $n$ parameter of the form factor is 1, the coupling constant is $\frac{g^2}{4\pi} = 14.6$ , and the pion mass is used as the mass of the exchanged meson. The negative binding energy for the light-front potentials in the first column indicates that the states are not bound. . . . .	90
3.3	The values of the binding energy, percentage of the wave function in the D state, and the percentage of the wave function in the $J = 1$ state for the $m = 0$ and $m = 1$ states for different potentials. The pion-nucleon form factor uses $n = 1$ and $\Lambda = 1.9$ GeV. . . . .	92
3.4	A pion-nucleon form factor with $n = 1$ and $\Lambda = 2.1$ GeV is used to calculate the same quantities as shown in Table 3.3. . . . .	93
3.5	A pion-nucleon form factor with $n = 2$ and $\Lambda = 2.9$ GeV is used to calculate the same quantities as shown in Table 3.3. . . . .	95
3.6	The parameters for the $\pi$ , $\eta$ , $\rho$ , $\omega$ , $\delta$ , and $\sigma$ mesons. The $\sigma$ meson is also known as $f_0(400 - 1200)$ , and the $\delta$ meson is the $a_0(980)$ . . . . .	96

3.7	The values of $f_\sigma$ required to give the physical value of the deuteron mass for a given potential and state with $J_z = m$ . The percent of the wave function in the D-state and in the $J = 1$ state are also shown. .	97
3.8	The values of the binding energy, percentage of the wave function in the D state, and the percentage of the wave function in the $J = 1$ state for the $m = 0$ and $m = 1$ states for different potentials. The $\sigma$ coupling constant factor is $f_\sigma = 1.22$ . . . . .	100
3.9	The $\sigma$ coupling constant factor used here, $f_\sigma = 1.2815$ , distinguishes this table from Table 3.8. . . . .	102

## GLOSSARY

BSE: The Bethe-Salpeter equation.

DEUTERON: The only stable bound state of a proton and a neutron. Also a life giving material (for theses at least).

EQUAL-TIME DYNAMICS: A Hamiltonian theory based on quantization of fields on a hyperplane defined at one instant in time. Such a plane contains all points in space at the same time.

FSR: The Feynman-Schwinger representation of the two-particle Green's function.

LFTOPT: Light-front time-ordered perturbation theory.

LIGHT-FRONT DYNAMICS: A Hamiltonian theory based on quantization of fields on a hyperplane defined at one instant in light-front time. Such a plane is traced out by the front of a plane wave of light.

LIGHT-FRONT TIME: The light-front time  $x^+$  of a space-time location is defined by  $x^+ = x^0 + x^3$ , where  $x^0$  and  $x^3$  are the time and  $z$  direction ordinates of the event.

MGF: Modified Green's Function (potential).

NCTME: Non-chiral two-meson-exchange (potential).

NCTPE: Non-chiral two-pion-exchange (potential).

OBE: One-boson-exchange (potential).

OME: One-meson-exchange (potential).

OPE: One-pion-exchange (potential).

TBE: Two-boson-exchange (potential).

TME: Two-meson-exchange (potential).

TPE: Two-pion-exchange (potential).

## ACKNOWLEDGMENTS

Most of the work described here was done in collaboration with Gerald A. Miller (my advisor) and with Daniel R. Phillips. I want to express my deepest gratitude to Jerry for teaching me about nuclear theory and light-front dynamics, and for guiding me through this work. I am grateful to Daniel for providing useful advice and productive discussions on many occasions.

This work is supported in part by the U.S. Dept. of Energy under Grant No. DE-FG03-97ER4014.

I have also benefited from numerous conversations about our respective research topics with Daniel Arndt, Jiunn-Wei Chen, Patrick Fox, Gautam Rupak, and Brian Tiburzi. I also owe a lot to my friends H. Pieter Mumm and Paul Bedrosian, who “experienced” the first-year with me, and to my undergraduate research advisor and friend, Madappa Prakash.

Most of all, I thank my wife for her patience and love during graduate school, and my son for supporting me by saying “You can do it, Daddy!”

# DEDICATION

For Sam



## Chapter 1

# INTRODUCTION

“If you always do what interests you, at least one person is pleased.”

—*Katharine Hepburn*

Recent experiments at Thomas Jefferson National Accelerator Facility have measured the  $A(Q^2)$  structure function of the deuteron for momentum transfers up to 6  $(\text{GeV}/c)^2$  [1], and measurements for  $B(Q^2)$  are planned. At such large momentum transfers, a relativistic description of the deuteron is required. Even at lower momentum transfers, a relativistic description is important to understand the details of the form factors. In addition, incorporating relativity is important for the deuteron wave function to transform correctly under boosts to large momentum, which is important for calculating form factors.

One approach that gives a relativistic description of the deuteron is light-front dynamics. The subject of this work is to investigate the consequences of combining light front dynamics with various nuclear models to calculate bound state wave functions, and using them to calculate the deuteron form factors.

### ***1.1 Theoretical Descriptions of the Deuteron***

In principle, the two-particle deuteron wave function is obtained by solving the full quantum field theory that describes the interacting nucleons for the lowest energy bound state. In practice, many approximations must be made before even a numeric solution is possible.

There are many approximations that can be used to obtain relativistic two-particle wave functions. One approach is to use the Feynman-Schwinger representation (FSR) of the two-particle Green's function [2], which effectively includes *all* two-particle to two-particle ladder and crossed ladder diagrams. However, it requires a path integral to be done numerically, and intensive computation is required to obtain an accurate answers. While the FSR has been applied to scalar theories, such as the Wick-Cutkosky model, it has not been used with more realistic models of the deuteron involving spin.

Another approach comes from using the Bethe-Salpeter equation (BSE) [3–7]. Solving the BSE is equivalent to solving the FSR with a truncated kernel. This simplification allows the BSE to be solved much more quickly than the FSR, however, the truncation of the BSE kernel causes the BSE results to differ from the FSR results. It is well known that any finite truncation of the kernel yields bound-state wave functions with problems, such as the incorrect one-body limit [8]. In addition, other approximations can be made to the propagators used in the BSE to obtain a quasi-potential equation [8–11] which addresses some of the problems with the BSE.

Constructing potentials from a relativistic Hamiltonian theory provides yet another approach. It can be shown that the potentials derived in this manner are physically equivalent to the Bethe-Salpeter equation. There are several different forms of Hamiltonian dynamics [12], each associated with a hypersurface on which the commutation relations for the fields are defined. Equal-time dynamics is the most commonly known form of Hamiltonian dynamics, but we will consider light-front dynamics in this work, where the orientation of the light-front is fixed.

There is another light-front dynamics approach that is in use, explicitly covariant light-front dynamics [13,14]. In that approach, manifest covariance is kept by using a null-plane whose orientation is variable. Although that approach has some benefits, we are interested in numerical calculations, for which the usual light-front dynamics is best suited.

## 1.2 Benefits of Light-front Dynamics

The utility of the light-front dynamics was first discussed by Dirac [12]. Light-front dynamics makes use of the light-front coordinate system, where a four-vector  $x^\mu$  is expressed as  $x^\mu = (x^+, x^-, x^1, x^2)$ , with  $x^\pm = x^0 \pm x^3$ . This is simply a change of variables, but an especially convenient one. Using this coordinate system and defining the commutation relations at equal light-front time ( $x^+ = t_{\text{LF}}$ ), we obtain a light-front Hamiltonian [15–17]. We use Hamiltonian in the light-front Schrödinger equation to solve for bound states. There are many desirable features of the light-front dynamics and the use of light-front coordinates.

First of all, high-energy experiments are naturally described using light-front coordinates. The wave front of a beam of high-energy particles traveling in the (negative) three-direction is defined by a surface where  $x^+$  is (approximately) constant. Such a beam can probe the wave function of a target described in terms of light-front variables [15, 18]: the Bjorken  $x$  variable used to describe high-energy experiments is simply the ratio of the plus momentum of the struck constituent particle to the total plus momentum ( $p^+$ ) of the bound state.

Secondly, the vacuum for a theory with massive particles can be very simple on the light front. This is because all massive particles and anti-particles have positive plus momentum, and the total plus momentum is a conserved quantity. Thus, the naïve vacuum (with  $p^+ = 0$ ) is empty, and diagrams that couple to this vacuum are zero. This greatly reduces the number of non-trivial light-front time-ordered diagrams.

Thirdly, the generators of boosts in the one, two, and plus directions are kinematic, meaning they are independent of the interaction. Thus, even when the Hamiltonian is truncated, the wave functions will transform correctly under boosts. Thus, light-front dynamics is useful for describing form factors at high momentum transfers.

Finally, it is easy to perform relativistic calculations using light-front dynamics. This is partly due to the simplicity of the vacuum, and partly due the the fact that,

with light-front variables, center-of-momentum variables can be cleanly separated from the relative momentum variables. This allows us to write relativistic equations which have the simple form of a non-relativistic Schrödinger equation.

### 1.3 *Breaking of Rotational Invariance*

One serious drawback of light-front dynamics is that rotational invariance is not manifest in any light-front Hamiltonian<sup>1</sup>. This is a result of selecting a particular direction in space for the orientation of the light-front.

An untruncated light-front Hamiltonian will commute with the total relative angular momentum operator, since the total momentum commutes with the relative momentum. Thus, eigenstates of the full Hamiltonian will also be eigenstates of the angular momentum. However, as mentioned earlier, a Fock-space truncation of the light-front Hamiltonian results in the momentum operator four-vector losing covariance under rotations. Hence  $J^2$  and the truncated Hamiltonian do not commute and this implies that the eigenstates of the truncated Hamiltonian will not be eigenstates of the angular momentum.

How will this violation of rotational invariance affect physical observables? One way to observe this violation is to note that on the light front, rotational invariance about the  $z$ -axis is maintained. This allows us to classify states as eigenstates of  $J_3$  with eigenvalues  $m$ . We compare the energies of states with the same angular momentum quantum number  $j$  but different  $m$  values. If the Hamiltonian were rotationally invariant, the energies should be the same; the breaking of rotational invariance causes the energies to be different [19].

We expect that the higher Fock-space components of the full Hamiltonian will be small if the coupling constant is small enough. Thus, truncation at successively higher orders in the Fock-space expansion should reduce the violation of rotational

---

<sup>1</sup>This problem is not unique to light-front dynamics. In any form of Hamiltonian dynamics, at least three of the Poincaré group generators are dynamic, and thus complicated.

invariance of the truncated Hamiltonian. In particular, by retaining enough terms in the perturbation expansion of the Hamiltonian, the violation of rotational invariance can be reduced to an arbitrarily small amount, provided only that a perturbation expansion is valid. Thus, the only real question is: How many terms are required?

#### **1.4 Outline**

In chapter 2, the massive Wick-Cutkosky model is used to investigate the degree to which rotational invariance is broken for deeply bound states. We use light-front dynamics to obtain one-meson-exchange (OME) and two-meson-exchange (TME) potentials, and then we use those potentials to calculate the bound states. We develop several methods for quantifying the extent to which rotational invariance is broken by the bound states. The binding energies we calculate are compared with those calculated using other methods in the literature, such as the Bethe-Salpeter equation [20,21] and the Feynman-Schwinger representation of the Greens function [2,22].

A brief discussion about the approximation we use for the Wick-Cutkosky potentials is in order. It is well known that the vacuum of the full Wick-Cutkosky model is unstable [23] due to the cubic coupling which provides the interaction. However, when the bound-state calculation is restricted to the two-particle sector, the quenched approximation is used, and the self-energy and vertex-renormalization diagrams are neglected, then the theory has a well defined ground state. In this chapter, we compare the results of our light-front Hamiltonian calculation to the Bethe-Salpeter and Feynman-Schwinger representation calculations, both of which use the same approximations. The use of these simplifying approximations allows us to highlight the differences between the various approaches. The inclusion of the self-energy diagrams and counterterms for the light-front Hamiltonian [24] and for the Feynman-Schwinger representation [25–27] will not be discussed here.

In chapter 3, we introduce a model Lagrangian for nuclear physics which includes

chiral symmetry [18]. The methods introduced in chapter 2 are generalized for use with this nuclear model. The Hamiltonian is derived and used to calculate the OME and TME potentials for a new light-front nucleon-nucleon potential. We also formulate a new light-front pion-only model. The potentials are used to calculate the binding energy of the deuteron. We have some freedom in how to choose the TME potentials, and we consider several different choices.

We are interested mainly in the rotational properties of the potentials and wave functions, not in achieving detailed agreement with experimental data. This is because detailed agreement between calculations in light-front dynamics and experimental data cannot be achieved until the problems of rotational invariance have been addressed. From this standpoint, we may simplify our calculations by omitting effects that are formally rotationally invariant, such as crossed TME potentials, but are required for precise calculations.

The wave functions obtained in chapter 3 are used in chapter 4 to calculate the electromagnetic and axial form factors of the deuteron. Although rotational invariance demands that there be only three independent matrix elements of the deuteron current, the light-front calculation of the deuteron current results in four independent matrix elements. This is a result of the lack of manifest rotational invariance on the light front. There are several prescriptions for choosing which deuteron current matrix element should be eliminated, and in principle this choice will affect the form factors. We attempt to find currents that transform correctly (or well enough) under rotations so that the choice of “bad” component does not matter too much.

## Chapter 2

### WICK-CUTKOSKY MODEL

The Wick-Cutkosky model is an ideal starting point for any investigation of the deuteron. The model, introduced with an analytic solution in 1954 by Wick [28] and Cutkosky [29], is concerned with the interaction of two heavy scalar particles mediated by a massless scalar particle. The model can be extended by allowing the exchange particle to have a mass. The massive Wick-Cutkosky model cannot be solved analytically, but it is amenable to numeric calculations [14, 22, 30–35].

A large amount of the material presented in this chapter is based on previously published work by the author in Refs. [36, 37].

#### 2.1 Formalism

We consider an isospin doublet of two uncharged scalars  $\phi = (\phi_1, \phi_2)$  with mass  $M$  (which we will refer to as *nucleons*), that couple to a third, uncharged scalar  $\chi$  with mass  $\mu$  (which we will refer to as a *meson*) by a  $\phi^2\chi$  interaction. This is denoted as a  $\phi^2\chi$  theory, which is an extension of the Wick-Cutkosky model [28, 29] to include massive mesons. This model has been used on the light front to study scattering states [14] as well as bound states [38]. The Lagrangian is

$$\mathcal{L} = \frac{1}{2} (\partial_\mu \phi \partial^\mu \phi - M^2 \phi^2) + \frac{1}{2} (\partial_\mu \chi \partial^\mu \chi - \mu^2 \chi^2) + g \frac{M}{2} \phi^2 \chi, \quad (2.1)$$

where  $g$  is a dimensionless coupling constant and  $\phi^2 = \phi_1^2 + \phi_2^2$ . This Lagrangian will be used in two formalisms, the Bethe-Salpeter equation and the Hamiltonian approach.

### 2.1.1 Light-front Hamiltonian

To obtain the light-front Hamiltonian from the Lagrangian in Eq. (2.1), we follow the approach of by Miller [18] and many others (see the review in Ref. [15]) to write the light-front Hamiltonian ( $P^-$ ) as the sum of a free, non-interacting part and a term containing the interactions. We use the conventions given in Appendix A. The operators can be expressed in terms of Fock space operators since for this theory in light-front dynamics, the physical vacuum is the Fock space vacuum, and thus the Hilbert space is simply the Fock space. The Hamiltonian is obtained by using the energy-momentum tensor  $T^{\mu\nu}$  in

$$P^\mu = \frac{1}{2} \int dx^- d^2x_\perp T^{+\mu}(x^+ = 0, x^-, \mathbf{x}_\perp). \quad (2.2)$$

The usual relations determine  $T^{+\mu}$ , with

$$T^{\mu\nu} = -g^{\mu\nu} \mathcal{L} + \sum_r \frac{\partial \mathcal{L}}{\partial(\partial_\mu \phi_r)} \partial^\nu \phi_r, \quad (2.3)$$

in which the degrees of freedom (the fields  $\phi$  and  $\chi$ ) are labeled by  $\phi_r$ .

It is worthwhile to consider the limit in which the interactions between the fields are removed. This will allow us to define the free Hamiltonian  $P_0^-$  and to display the necessary commutation relations. The energy-momentum tensor of the non-interacting fields is defined as  $T_0^{\mu\nu}$ . Use of Eq. (2.3) leads to the result

$$T_0^{\mu\nu} = \partial^\mu \phi \partial^\nu \phi - \frac{g^{\mu\nu}}{2} [\partial_\sigma \phi \partial^\sigma \phi - M^2 \phi^2] + \partial^\mu \chi \partial^\nu \chi - \frac{g^{\mu\nu}}{2} [\partial_\sigma \chi \partial^\sigma \chi - \mu^2 \chi^2], \quad (2.4)$$

with

$$T_0^{+-} = \nabla_\perp \phi \cdot \nabla_\perp \phi + M^2 \phi^2 + \nabla_\perp \chi \cdot \nabla_\perp \chi + \mu^2 \chi^2. \quad (2.5)$$

The scalar nucleon fields can be expressed in terms of creation and destruction operators:

$$\phi_i(x) = \int \frac{d^2k_\perp dk^+ \theta(k^+)}{(2\pi)^{3/2} \sqrt{2k^+}} \left[ a_i(\mathbf{k}) e^{-ik \cdot x} + a_i^\dagger(\mathbf{k}) e^{ik \cdot x} \right], \quad (2.6)$$

where  $i = 1, 2$  is a particle index,  $k \cdot x = \frac{1}{2}(k^- x^+ + k^+ x^-) - \mathbf{k}_\perp \cdot \mathbf{x}_\perp$  with  $k^- = \frac{M^2 + \mathbf{k}_\perp^2}{k^+}$ , and  $\mathbf{k} \equiv (k^+, \mathbf{k}_\perp)$ . Note that  $k^-$  is such that the particles are on the mass shell, which is a consequence of using a Hamiltonian theory. The  $\theta$  function restricts  $k^+$  to positive values. Likewise, the scalar meson field is given by

$$\chi(x) = \int \frac{d^2 k_\perp dk^+ \theta(k^+)}{(2\pi)^{3/2} \sqrt{2k^+}} [a_\chi(\mathbf{k}) e^{-ik \cdot x} + a_\chi^\dagger(\mathbf{k}) e^{ik \cdot x}], \quad (2.7)$$

where  $k^- = \frac{\mu^2 + \mathbf{k}_\perp^2}{k^+}$ , so that the mesons are also on the mass shell. The non-vanishing commutation relations are

$$[a_\alpha(\mathbf{k}), a_\alpha^\dagger(\mathbf{k}')] = \delta(\mathbf{k}_\perp - \mathbf{k}'_\perp) \delta(k^+ - k'^+), \quad (2.8)$$

where  $\alpha = 1, 2, \chi$  is a particle index. The commutation relations are defined at equal light-front time,  $x^+ = 0$ . It is useful to define

$$\delta^{(2,+)}(\mathbf{k} - \mathbf{k}') \equiv \delta(\mathbf{k}_\perp - \mathbf{k}'_\perp) \delta(k^+ - k'^+), \quad (2.9)$$

which will be used throughout this work.

We write a ket in the two-distinguishable-particle sector of the Fock space as

$$|k_1, k_2\rangle = a_1^\dagger(k_1) a_2^\dagger(k_2) |0\rangle. \quad (2.10)$$

This implies that the identity operator in this Fock space sector can be written as

$$I_2 = \int d^2 k_{1,\perp} dk_1^+ \int d^2 k_{2,\perp} dk_2^+ |k_1, k_2\rangle \langle k_1, k_2|. \quad (2.11)$$

The derivatives appearing in the quantity  $T_0^{+-}$  are evaluated and then one sets  $x^+$  to 0 to obtain the result

$$P_0^- = \int_k \left[ \frac{M^2 + \mathbf{k}_\perp^2}{k^+} \left( a_1^\dagger(k) a_1(k) + a_2^\dagger(k) a_2(k) \right) + \frac{\mu^2 + \mathbf{k}_\perp^2}{k^+} a_\chi^\dagger(k) a_\chi(k) \right], \quad (2.12)$$

with  $\int_k = \int d^2 k_\perp dk^+ \theta(k^+)$ . Eq. (2.12) has the interpretation of an operator that counts the light-front energy  $k^-$  (which is  $\frac{M^2 + \mathbf{k}_\perp^2}{k^+}$  for the nucleons and  $\frac{\mu^2 + \mathbf{k}_\perp^2}{k^+}$  for the mesons) of all of the particles.

We now consider the interacting part of the Lagrangian,  $\mathcal{L}_I$ . An analysis similar to that for the non-interacting parts yields the interacting part of the light-front Hamiltonian  $P_I^-$ ;

$$\begin{aligned}
P_I^- = \sum_{i=1,2} \frac{M}{2} \int_k \int_{k'} \frac{1}{(2\pi)^{3/2} \sqrt{2k^+ k'^+ (k^+ + k'^+)}} \\
\times \left\{ \left[ 2a_i^\dagger(k+k') a_\chi(k') a_i(k) + a_\chi^\dagger(k+k') a_i(k') a_i(k) \right] \right. \\
\left. + \text{Hermitian conjugate} \right\}. \tag{2.13}
\end{aligned}$$

The interaction Hamiltonian is self-adjoint since the Hilbert space is the Fock space. The total light-front Hamiltonian is given by  $P^- = P_0^- + gP_I^-$ .

### 2.1.2 Hamiltonian Bound-state Equations

We will be studying the bound states of two distinguishable nucleons. The technology of time-ordered (old-fashioned) perturbation theory is used to construct the light-front time-ordered perturbation theory (LFTOPT) for our Hamiltonian. We start with the light-front Schrödinger equation in the full Fock space,

$$(P_0^- + gP_I^-) |\psi_F\rangle = |\psi_F\rangle P^-, \tag{2.14}$$

where  $P_0^- + gP_I^-$  is the Hamiltonian in the full Fock-space basis,  $|\psi_F\rangle$  is the wave function in the full Fock space, and  $P^-$  is the light-front energy of that state. Recall that  $P_0^-$ , the non-interacting part of the Hamiltonian, is diagonal in the momentum basis, while  $P_I^-$ , which contains the interaction, has only off-diagonal elements.

A serious drawback of this equation is that the wave function  $|\psi_F\rangle$  has support from infinitely many sectors of the Fock space, since  $P_I^-$  changes the total number of particles. However, the components of the wave function with many particles will be small compared to the two-particle component if the coupling constant is not too large and the exchange particle  $\chi$  is massive. We will construct the two-particle light-front

Schrödinger equation which the two-particle component of the wave function satisfies. From this construction, we will obtain the rules for the LFTOPT.

We start by introducing the projection operators  $\mathcal{P}$  and  $\mathcal{Q}$ . The operator  $\mathcal{P}$  projects out the sector of Fock space with two distinguishable nucleons and no mesons, while  $\mathcal{Q} = I - \mathcal{P}$  projects out all the other sectors. We define

$$\mathcal{P}|\psi_F\rangle \equiv |\psi\rangle, \quad (2.15)$$

$$\mathcal{Q}|\psi_F\rangle \equiv |\psi_Q\rangle, \quad (2.16)$$

so that  $|\psi_F\rangle = |\psi\rangle + |\psi_Q\rangle$ . Since the free Hamiltonian does not change the number of particles,  $[P, P_0^-] = [\mathcal{Q}, P_0^-] = 0$ . The interaction Hamiltonian changes the particle number, so it cannot connect the two-particle sector to itself, thus  $\mathcal{P}P_I^- \mathcal{P} = 0$ .

Using these projection operators, Eq. (2.14) can be broken up into two parts,

$$P_0^- |\psi\rangle + g\mathcal{P}P_I^- \mathcal{Q}|\psi_Q\rangle = |\psi\rangle P^-, \quad (2.17)$$

$$(P_0^- + g\mathcal{Q}P_I^- \mathcal{Q}) |\psi_Q\rangle + g\mathcal{Q}P_I^- \mathcal{P}|\psi\rangle = |\psi_Q\rangle P^-. \quad (2.18)$$

Eliminating the  $|\psi_Q\rangle$  and using the expression of the identity given in Eq. (2.11) we obtain the two-particle effective light-front Schrödinger equation

$$\begin{aligned} & \int d^2 p_{1,\perp} dp_1^+ \int d^2 p_{2,\perp} dp_2^+ \langle \mathbf{k}_1, \mathbf{k}_2 | [P_0^- + V(g, P^-)] | \mathbf{p}_1, \mathbf{p}_2 \rangle \langle \mathbf{p}_1, \mathbf{p}_2 | \psi \rangle \\ & = \langle \mathbf{k}_1, \mathbf{k}_2 | \psi \rangle P^-, \end{aligned} \quad (2.19)$$

where  $P_0^-$  and the potential  $V$  act in the two-nucleon basis. The two-particle potential is given by

$$V(g, P^-) = g^2 \mathcal{P} P_I^- \frac{\mathcal{Q}}{P^- - P_0^- - g\mathcal{Q}P_I^- \mathcal{Q}} P_I^- \mathcal{P}. \quad (2.20)$$

Note that Eq. (2.19) is similar to Eq. (2.14), except for two main differences. Here we have a two-nucleon wave function, which makes it simpler. However, the potential depends on the light-front energy  $P^-$ , thus making it more complicated.

The denominator in the definition of the potential is non-diagonal in the full Fock space, so the matrix inversion that it represents is highly non-trivial. This problem is avoided by expanding the inversion in powers of the coupling constant  $g$  to get

$$V(g, P^-) = \mathcal{P} P_I^- \left[ \frac{g^2 \mathcal{Q}}{P^- - P_0^-} \sum_{n=0}^{\infty} \left( P_I^- \frac{g \mathcal{Q}}{P^- - P_0^-} \right)^n \right] P_I^- \mathcal{P}. \quad (2.21)$$

This can be simplified further by noting that in the two-nucleon sector of our theory, every meson emitted must be absorbed, so there must be an even number of interactions. Thus, the full potential can be written as the sum of  $n$  meson exchange potentials,

$$V(P^-, g) = \sum_{n=1}^{\infty} g^{2n} V_{(2n)}(P^-), \quad (2.22)$$

where  $V_{(2n)}$  is the potential due to the exchange of  $n$  mesons, given by

$$V_{(2n)}(P^-) = \mathcal{P} \left( P_I^- \frac{\mathcal{Q}}{P^- - P_0^-} \right)^{2n-1} P_I^- \mathcal{P}. \quad (2.23)$$

To see how to write a sum of diagrams for the potential, we express what what Eq. (2.23) represents in words. We start off with two particles, then the interaction occurs. There are two possibilities of what can happen; nucleon 1 or 2 can emit a meson. Each possibility has a separate diagram. After the interaction, there is propagation with the light-front Green's function,

$$G_{\text{LF}}(P^-) = \frac{1}{P^- - P_0^-}, \quad (2.24)$$

until another interaction occurs, and so on. We simply sum up all of the possible orderings of the interaction to get the full potential. The  $n^{\text{th}}$  order potential is simply the sum of all possible diagrams with  $n$ -meson exchanges.

Each intermediate state in Eq. (2.23) has more than two particles, so the diagrams are two-particle irreducible with respect to the two-particle Green's function  $G_{2\text{LF}} = \mathcal{P} G_{\text{LF}} \mathcal{P}$ . We can represent  $G_{2\text{LF}}$  by its diagonal matrix elements,

$$G_{2\text{LF}}(\mathbf{k}_1, \mathbf{k}_2; P^-) = \frac{1}{P^- - k_1^- - k_2^-}. \quad (2.25)$$

In the diagrams we draw, the nucleons will be represented by solid lines and the mesons by dashed lines. Although the states we will be considering consist of two distinguishable nucleons, we will not label the nucleon lines. Energy denominator terms are represented by vertical, thin, dotted lines. We will be using the quenched approximation (so there are no nucleon loops) and neglect the mass and vertex renormalization diagrams (so the physical masses and coupling constant are used, and each meson emitted from one nucleon must be absorbed by the other nucleon). It is not expected that these restrictions will lead to qualitatively different results than the true full solution when the states are not too deeply bound. The quenched approximation is reasonable when the masses of the nucleon fields are large compared to the binding energy. Use of the physical masses and coupling constant are reasonable as well when the momenta are not too large.

A truncation must be made for the potential in Eq. (2.22), since in a Hamiltonian theory the infinite sum of graphs cannot be calculated. However, all the graphs are required to obtain manifest Lorentz invariance. We stress again that we will compare various truncations of the light-front Hamiltonian to other calculations which do not include renormalization diagrams. This is because we want to determine the effect of truncation on the light-front Hamiltonian. The differences between our calculation and those which include the self-energy graphs [24,32], which may be large for deeply-bound states, are not considered here.

The rules for drawing the  $n$ -meson-exchange graphs that correspond to this approximation are:

1. Draw all topologically distinct time-ordered diagrams with  $n$  mesons. Use solid lines for the nucleons and dashed lines for the mesons.
2. Delete all graphs which couple particles to the vacuum. In the massive theory we consider here, these diagrams always vanish since the vacuum has zero plus momentum and massive particles always have positive plus momentum.

3. Our quenched approximation and use of the physical masses and coupling constant requires us to delete all graphs that have nucleon loops or have mesons that are emitted and absorbed from the same nucleon.

Once the diagrams are drawn, we use the following rules to convert the sum of diagrams into the potential  $\langle \mathbf{k}_{1f}, \mathbf{k}_{2f} | V_{(2n)}(P^-) | \mathbf{k}_{1i}, \mathbf{k}_{2i} \rangle$ :

1. Overall factor of  $\frac{\delta^{(2,+)}(\mathbf{k}_{1f} + \mathbf{k}_{2f} - \mathbf{k}_{1i} - \mathbf{k}_{2i})}{2(2\pi)^3 \sqrt{k_{1f}^+ k_{2f}^+ k_{1i}^+ k_{2i}^+}}$ . This delta function says that the total light-front three-momentum is conserved. We define the light-front three-momentum  $\mathbf{P} \equiv \mathbf{k}_{1f} + \mathbf{k}_{2f}$ .
2. To each internal line, assign a light-front three-momentum  $\mathbf{q}_i$  where  $1 \leq i \leq N$  and  $N$  is the number of internal lines. The light-front energy for particle  $i$  with mass  $m_i$  is  $q_i = \frac{m_i^2 + q_{i,\perp}^2}{q_i^+}$ . It is useful to define  $z_i = q_i^+ / P^+$ .
3. A factor of  $\frac{\theta(z_i^+)}{z_i^+}$  for each internal line.
4. An extra factor of  $\frac{M^2}{P^+ P^-}$  for each internal meson line.
5. A factor of  $\frac{P^-}{(P^- - \sum_i q_i^-)}$  between consecutive vertices, where the sum is over only the particles that exist in the intermediate time between those vertices.
6. Use light-front three-momentum conservation to eliminate all the independent momenta.
7. Integrate with  $\int \frac{d^2 q_{i,\perp} dz_i}{2P^+ P^- (2\pi)^3}$  over all remaining free internal momenta.
8. Symmetry factor of  $\frac{1}{2}$  when two nucleons are created or destroyed at the same time.

With these rules, one can calculate the effective potential for any order.

### 2.1.3 Further Development of the Light-front Schrödinger Equation

Once the potential is calculated, we can plug it into Eq. (2.19), which we write as

$$\begin{aligned} & \int d^2k_{1i,\perp} dk_{1i}^+ \int d^2k_{2i,\perp} dk_{2i}^+ \langle \mathbf{k}_{1f}, \mathbf{k}_{2f} | [P_0^- + V(g(P^-), P^-)] | \mathbf{k}_{1i}, \mathbf{k}_{2i} \rangle \langle \mathbf{k}_{1i}, \mathbf{k}_{2i} | \psi \rangle \\ & = \langle \mathbf{k}_{1f}, \mathbf{k}_{2f} | \psi \rangle P^-, \end{aligned} \quad (2.26)$$

where  $P^-$  is an arbitrary light-front energy and  $g(P^-)$  is the coupling constant which yields the bound-state wave function with  $P^-$  as the bound-state energy. We call this  $g(P^-)$  the spectrum of the light-front Schrödinger equation for the corresponding wave function.

The total momentum  $\mathbf{P} = \mathbf{k}_{1f} + \mathbf{k}_{2f}$  is conserved by the potential given in Eq. (2.22), so the wave function in Eq. (2.26) can be parameterized by the total momentum. To make the calculations easier later, we choose to be in the center-of-momentum frame, where the components of the total momentum can be written as  $\mathbf{P}_\perp = 0$  and  $P^+ = P^- = E$ . The energy,  $E$ , is the same as the mass of the bound state. In terms of the binding energy  $B$ ,  $E = 2M - B$ . In the center-of-momentum frame, the wave function is parameterized by  $E$ , so we can define

$$\langle \mathbf{k}_{1f}, \mathbf{k}_{2f} | \psi_M \rangle = \delta^{(2,+)}(\mathbf{k}_{1f} + \mathbf{k}_{2f} - \mathbf{P}) \psi(\mathbf{k}_{1f}), \quad (2.27)$$

$$\langle \mathbf{k}_{1f}, \mathbf{k}_{2f} | V_{(2n)}(P^-) | \mathbf{k}_{1i}, \mathbf{k}_{2i} \rangle = \delta^{(2,+)}(\mathbf{k}_{1f} + \mathbf{k}_{2f} - \mathbf{k}_{1i} - \mathbf{k}_{2i}) V_{(2n)}(E; \mathbf{k}_{1f}; \mathbf{k}_{1i}). \quad (2.28)$$

With these, Eq. (2.26) effectively becomes a one-particle equation, where particle 2's momentum is determined by  $\mathbf{k}_{2f} = \mathbf{P} - \mathbf{k}_{1f}$ . The minus component (the light-front energy) of particle 2 is defined by the requirement that the particle 2 is on mass shell, so  $k_{2f}^- = (M^2 + \mathbf{k}_{2f,\perp}^2)/k_{2f}^+$ . We also define

$$x \equiv k_{1f}^+/P^+ = x_{Bj}, \quad (2.29)$$

where  $x_{Bj}$  is the Bjorken  $x$  variable, so that  $k_{2f}^+/P^+ = 1 - x$ . Likewise, we write the Bjorken variables that correspond to the momenta  $\mathbf{k}_{1i}$  and  $\mathbf{q}_1$  as  $y \equiv k_{1i}^+/P^+$  and  $z \equiv q_1^+/P^+$ .

Using Eqs. (2.27), (2.28), and the fact that the plus momentum of both nucleons is positive, we can write the light-front Schrödinger equation Eq. (2.26) as

$$\int d^2 k_{1i,\perp} \int_0^E dk_{1i}^+ V(g(E), E; \mathbf{k}_{1f}; \mathbf{k}_{1i}) \psi(\mathbf{k}_{1i}) = \psi(\mathbf{k}_{1f}) (E - k_{1f}^- - k_{2f}^-). \quad (2.30)$$

It is useful to convert from light-front coordinates  $\mathbf{k}_1 = (k_1^+, \mathbf{k}_\perp)$  to “equal-time” coordinates  $\mathbf{k}_{\text{ET}} = (\mathbf{k}_\perp, k^3)$ , using an implicit definition of  $k^3$  [39]

$$k_1^+ = \frac{E}{2k^0(\mathbf{k}_{\text{ET}})} [k^0(\mathbf{k}_{\text{ET}}) + k^3], \quad (2.31)$$

$$k^0(\mathbf{k}_{\text{ET}}) = \sqrt{M^2 + \mathbf{k}_{\text{ET}}^2}, \quad (2.32)$$

or an explicit transformation [40]

$$k^0(k_1^+, \mathbf{k}_\perp) = \frac{E}{2} \sqrt{\frac{M^2 + \mathbf{k}_\perp^2}{k_1^+ k_2^+}} = \sqrt{\frac{M^2 + \mathbf{k}_\perp^2}{4x(1-x)}}, \quad (2.33)$$

$$k^3 = (k_1^+ - k_2^+) \frac{k^0}{E} = (2x - 1)k^0. \quad (2.34)$$

Often the explicit dependence of  $k^0$  on  $\mathbf{k}_{\text{ET}}$  will not be shown. It is worth emphasizing that this is just a convenient change of variables;  $\psi(\mathbf{k}_{\text{ET}})$  is not the usual equal-time wave function. With this transformation, we can express  $k_1^-$  and  $k_2^-$  as

$$k_1^- = \left(1 - \frac{k^3}{k^0}\right) \frac{2(k^0)^2}{E}, \quad (2.35)$$

$$k_2^- = \left(1 + \frac{k^3}{k^0}\right) \frac{2(k^0)^2}{E}. \quad (2.36)$$

We may also write

$$k_1^+ = \left(1 + \frac{k^3}{k^0}\right) \frac{E}{2}, \quad (2.37)$$

$$k_2^+ = \left(1 - \frac{k^3}{k^0}\right) \frac{E}{2}. \quad (2.38)$$

Using Eqs. (2.35-2.38), we can rewrite Eq. (2.30) as

$$\int d^3 k_{i,\text{ET}} \frac{2k_{1i}^+ k_{2i}^+}{k_i^0} V(g(E), E, \mathbf{k}_{f,\text{ET}}; \mathbf{k}_{i,\text{ET}}) \psi(\mathbf{k}_{i,\text{ET}}) = \psi(\mathbf{k}_{f,\text{ET}}) [E^2 - (2k_f^0)^2]. \quad (2.39)$$

Now consider the exchange of the particle labels 1 and 2. This causes

$$\mathbf{k}_{1,\perp} \rightarrow \mathbf{k}_{2,\perp} = -\mathbf{k}_{1,\perp}, \quad (2.40)$$

$$k_1^+ \rightarrow k_2^+ = E - k_1^+, \quad (2.41)$$

which means that  $k^3$  as defined in Eq. (2.31) transforms as  $k^3 \rightarrow -k^3$ , so  $\mathbf{k}_{\text{ET}} \rightarrow -\mathbf{k}_{\text{ET}}$ . Consequently, exchange of particle labels 1 and 2 is the same as parity for  $\mathbf{k}_{\text{ET}}$ .

For scattering states, the OBE potential computed for on-shell nucleons and used in the Weinberg integral equation [41] (which is essentially the scattering analogue of Eq. (2.26)) leads to manifestly rotationally invariant results when written in terms of the relative momenta [18]. The similarity between that rotationally invariant result and the usual equal-time result implies that this equal-time momentum  $\mathbf{k}$  can be interpreted as the relative momentum of the two particles. For bound states, this exact simplification does not occur, since for bound states the potential is, of necessity, evaluated off the energy shell (but on the mass shell). However, we expect that the OBE potential, written in terms of the relative momentum, is *approximately* spherically symmetric for lightly-bound states. Thus, the wave functions are approximate eigenfunctions of the “relative angular momentum”, which we define by the operator  $\mathbf{L} = \mathbf{x} \times \mathbf{k}$ . Our “relative angular momentum operator” is not the same as the true orbital angular momentum operator which is obtained from the Lagrangian via the energy-momentum tensor in a way similar to the Hamiltonian.

Since the two nucleons are identical except for the particle label, the effective potential commutes with parity to all orders in  $g^2$ . Furthermore, the light-front Hamiltonian is explicitly invariant under rotations about the three-axis. These considerations allow us to classify the wave functions as having eigenvalues  $p$  of parity ( $\mathcal{P}$ ) and  $m$  of the three-component of the angular momentum operator ( $J_3$ ). We label

the wave function as  $\langle k_1 | \psi_{m,p} \rangle$ , where

$$\langle k_1 | J_3 | \psi_{m,p}^n \rangle = \langle k_1 | \psi_{m,p}^n \rangle m, \quad (2.42)$$

$$\langle k_1 | \mathcal{P} | \psi_{m,p}^n \rangle = \langle k_2 | \psi_{m,p}^n \rangle, \quad (2.43)$$

$$= \langle k_1 | \psi_{m,p}^n \rangle p. \quad (2.44)$$

With this, we may write the OBE truncation of full uncrossed Hamiltonian as

$$P_{\text{OBE}}^-(g, E) = P_0^- + g^2 V_{\text{OBE}}(E), \quad (2.45)$$

which gives OBE light-front Schrödinger equation

$$P_{\text{OBE}}^- \left( g_{\text{OBE}}^{n,m,p}(E), E \right) | \psi_{m,p}^{n,\text{OBE}} \rangle = | \psi_{m,p}^{n,\text{OBE}} \rangle E, \quad (2.46)$$

where  $E$  is an arbitrary energy,  $| \psi_{m,p}^{n,\text{OBE}} \rangle$  is the  $n^{\text{th}}$  wave function with parity  $p$  and  $J_3$  quantum number  $m$ , and  $g_{\text{OBE}}^{n,m,p}(E)$  is the coupling constant which yields that bound-state wave function with  $E$  as the bound-state energy.

For the OBE+TBE truncation, we have

$$P_{\text{TBE}}^-(g, E) = P_0^- + g^2 V_{\text{OBE}}(E) + g^4 V_{\text{TBE}}(E), \quad (2.47)$$

which gives TBE light-front Schrödinger equation

$$P_{\text{TBE}}^- \left( g_{\text{TBE}}^{n,m,p}(E), E \right) | \psi_{m,p}^{n,\text{TBE}} \rangle = | \psi_{m,p}^{n,\text{TBE}} \rangle E, \quad (2.48)$$

where the quantities here are defined in an analogous way to Eq. (2.46). By comparing the spectra  $g_{\text{OBE}}^{n,m,p}(E)$  and  $g_{\text{TBE}}^{n,m,p}(E)$ , we can see what effect adding the TBE potential to the OBE potential has on the coupling constant for a given bound-state energy.

The quantum numbers  $m$  and  $p$  of the wave function can be used to rewrite Eq. (2.39) as

$$\begin{aligned} & \int_0^\infty dk_{i,\text{ET}} \int_0^{\pi/2} d\theta_i \frac{2k_{1i}^+ k_{2i}^+ k_{i,\text{ET}}^2 \sin \theta_i}{k_i^0} V_{p,m}(k_{f,\text{ET}}, \theta_f; k_{i,\text{ET}}, \theta_f) \psi_{p,m}(k_{i,\text{ET}}, \theta_i) \\ & = \psi_{p,m}(k_{f,\text{ET}}, \theta_f) [E^2 - 4(k_f^0)^2], \end{aligned} \quad (2.49)$$

where

$$\begin{aligned} V_{p,m}(k_{f,\text{ET}}, \theta_f; k_{i,\text{ET}}, \theta_i) \\ = \frac{1}{2} \left[ V_m(k_{f,\text{ET}}, \theta_f; k_{i,\text{ET}}, \theta_i) + pV_m(k_{f,\text{ET}}, \theta_f; k_{i,\text{ET}}, \pi - \theta_i) \right] \end{aligned} \quad (2.50)$$

$$\begin{aligned} V_m(k_{f,\text{ET}}, \theta_f; k_{i,\text{ET}}, \theta_i) \\ = \iint_0^{2\pi} \frac{d\phi_f d\phi_i}{2\pi} e^{im(\phi_f - \phi_i)} V(\mathbf{k}_{f,\text{ET}}; \mathbf{k}_{i,\text{ET}}). \end{aligned} \quad (2.51)$$

We call  $V(k_{f,\text{ET}}, \theta_f; k_{i,\text{ET}}, \theta_i)$  the azimuthal-angle-integrated potential. The light-front vectors can also be expressed in terms of the azimuthal angle  $\phi$ , the angle between  $\mathbf{k}_\perp$  and the  $x$ -axis. This allows the azimuthal-angle-integrated potential to be written in light-front coordinates

$$V_m(k_{1f}^+, k_{1f,\perp}; k_{1i}^+, k_{1i,\perp}) = \iint_0^{2\pi} \frac{d\phi_f d\phi_i}{2\pi} e^{im(\phi_f - \phi_i)} V(\mathbf{k}_{1f}; \mathbf{k}_{1i}). \quad (2.52)$$

All of the simplifications of Eq. (2.49) based on physical considerations have been addressed. However, further rearrangements need to be done before Eq. (2.49) is fit to be solved on the computer. Since these involve only numerical techniques, they are relegated to Appendix B.

#### 2.1.4 Bethe-Salpeter Equation

The Bethe-Salpeter equation [3–7] provides a way of describing bound states based on Feynman propagators and kernels constructed from covariant quantum field theory, and thus is manifestly covariant. The equation for the bound state of nucleons 1 and 2 can be written as

$$GK\psi = \psi, \quad (2.53)$$

$G$  is the free two-particle propagator, which is the product of two one-particle propagators,  $G = S_1 S_2$ ,  $\psi$  is the four-dimensional Bethe-Salpeter amplitude, and  $K$  is the sum of all two-particle irreducible two-to-two Feynman graphs, shown in Fig. 2.1.

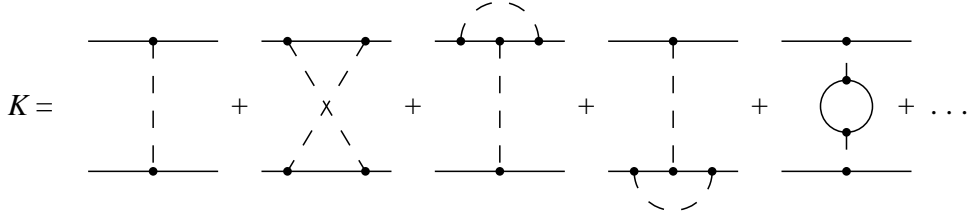


Figure 2.1: The full kernel for the Bethe-Salpeter equation of the Wick-Cutkosky model.

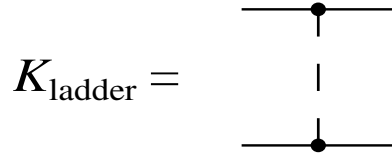


Figure 2.2: The ladder (one-boson-exchange) kernel for the Bethe-Salpeter equation.

There are no nucleon exchange graphs since we treat only the case where the two nucleons are distinguishable.

We consider the ladder approximation to the Bethe-Salpeter equation,

$$g^2 G \tilde{K}_{\text{ladder}} \psi = \psi, \quad (2.54)$$

which is obtained by replacing  $K$  in Eq. (2.53) with  $g^2 \tilde{K}_{\text{ladder}}$ . We define  $\tilde{K}_{\text{ladder}} = \frac{1}{g^2} K_{\text{ladder}}$ , where  $K_{\text{ladder}}$  is the graph due to one-boson-exchange, shown in Fig 2.2. This definition of  $\tilde{K}_{\text{ladder}}$  makes it independent of the coupling constant. Making this approximation leaves the Bethe-Salpeter equation covariant. This implies that the Bethe-Salpeter amplitudes  $\psi$  have definite angular momentum  $l$ , and hence the energies of the states are degenerate for different  $m$  projections of the same angular momentum.

This equation can be simplified in the center-of-momentum frame. In that frame, once the total energy is defined as  $P^0$ , the four-momentum of the second particle is

$$K_{\text{crossed}} = \begin{array}{c} \text{---} \bullet \text{---} \bullet \text{---} \\ \diagdown \quad \diagup \\ \vee \\ \diagup \quad \diagdown \\ \text{---} \bullet \text{---} \bullet \text{---} \end{array}$$

Figure 2.3: The crossed (two-boson-exchange) kernel for the Bethe-Salpeter equation.

given by  $k_2^\mu = P^\mu - k_1^\mu$ , and thus the Bethe-Salpeter equation is effectively a one-particle equation. The remainder of the discussion in this section will be done using the center-of-momentum frame. We then can rewrite Eq. (2.54), taking into account the explicit symmetries of the equation, as

$$\left[ g_{\text{LBSE}}^{n,l,m}(E) \right]^2 G(E) \tilde{K}_{\text{ladder}}(E) \psi_{n,l,m} = \psi_{n,l,m}, \quad (2.55)$$

where  $E$  is an arbitrary energy,  $\psi_{n,l,m}$  is the  $n^{\text{th}}$  Bethe-Salpeter amplitude with angular momentum  $l$  and three-projection  $m$ , and  $g_{\text{LBSE}}^{n,l,m}(E)$  is the coupling constant which yields that bound-state Bethe-Salpeter amplitude with  $E$  as the bound-state energy. We call this  $g(E)$  the spectrum of the ladder Bethe-Salpeter equation for the corresponding Bethe-Salpeter amplitude. The Greens function  $G(E)$  and the ladder kernel  $\tilde{K}_{\text{ladder}}(E)$  are functions of the energy in the c.m. frame and are implicitly effective one-particle operators.

We may also take the kernel to be  $\tilde{K} = \tilde{K}_{\text{ladder}} + \tilde{K}_{\text{crossed}}$ , where  $\tilde{K}_{\text{crossed}} = \frac{1}{g^2} K_{\text{crossed}}$ , and  $K_{\text{crossed}}$  is the crossed diagram is shown in Fig. 2.3. Since this kernel is also covariant, the discussion given above for the ladder kernel also applies for the ladder plus crossed kernel. In particular, the bound states calculated by using kernel with the Bethe-Salpeter equation will be angular momentum eigenstates.

The comparison we draw is only between the ladder (or ladder plus crossed) Bethe-Salpeter equation and the light-front Hamiltonian that corresponds to that approximation. The exact nature of the correspondence is discussed in section 2.1.2. Since

we are not looking at the solutions to the full theory, for our purposes it does not matter that there are sizeable differences between the solutions to the full Bethe-Salpeter equation and the ladder approximation when the coupling constant is large [22,33–35].

### 2.1.5 Comparison Between the Light-front Schrödinger Equation and the Bethe-Salpeter Equation

The solution to the untruncated light-front Schrödinger equation in the uncrossed approximation is equivalent to the solution of the ladder Bethe-Salpeter equation. When the full uncrossed Hamiltonian is truncated, differences will be introduced. Thus, here we think of the ladder Bethe-Salpeter equation as the exact theory which the truncated light-front Schrödinger equations approximate. As more graphs are included in the truncated light-front Hamiltonian potential, the agreement with the Bethe-Salpeter equation will obviously be better. The question we wish to answer is how well the spectra  $g(E)$  for the two different truncations [Eqs. (2.46) and (2.48)] approximate the spectra for the “exact” theory, the BSE results.

The lack of manifest rotational invariance of the truncated Hamiltonian theory causes a breaking of the degeneracy of the spectra of the truncated light-front Schrödinger equations for different  $m$  states — unlike the case for the Bethe-Salpeter equation. The wave functions from the Hamiltonian approach are classified by their dominant angular momentum contribution  $l$ , so that we can compare the spectra for different  $m$  projections of the same total angular momentum  $l$ . By doing this, we can compare how the degeneracy of the spectra is broken for the OBE and the OBE+TBE truncations, and also compare to the spectra obtained from the ladder Bethe-Salpeter equation.

We want to approximate our potential  $V$  so that Eq. (2.26) is physically equivalent to the ladder Bethe-Salpeter equation. This approximation of  $V$  will be called the *uncrossed approximation*. By physically equivalent, we mean that the spectra of the potential  $V$  should reproduce the spectrum for the states of the Bethe-Salpeter equation,

excluding the so-called “abnormal” states [28,29]. It is well known how to reduce the Bethe-Salpeter equation to a physically equivalent Hamiltonian (Schrödinger-type) equation. For an extensive discussion of this issue of defining the potential equivalent to a sum of Feynman graphs in the equal-time case see, for instance, Klein [42], Phillips and Wallace [43], Lahiff and Afnan [44], and, for examples on the light front, Ligterink and Bakker [45] and Schoonderwoerd and Bakker [46]. The general procedure to get the effective potential due to  $n$  boson exchange takes two steps. First, write the sum of all Feynman graphs obtained from iteration of the Bethe-Salpeter kernel with  $n$  boson exchanges. Then, write that sum in terms of LFTOPT graphs, and discard all graphs which are not two-particle-irreducible with respect to the light-front two-body propagator,

$$G_{\text{LF}}(P^-) = \frac{1}{P^- - P_0^-}. \quad (2.56)$$

The graphs which remain after this procedure constitute the  $V_{\text{nBE}}$ .

As an example, we construct the TBE potential. When the ladder Bethe-Salpeter equation is used, only one Feynman graph contributes, the box diagram arising from the iteration of the Feynman OBE kernel. This gives six non-vanishing LFTOPT diagrams. (The other diagrams vanish because the vacuum is simple on the light front.)

The first four diagrams are iterations of the OBE potential and are reducible with respect to  $G_{\text{LF}}$ . The last two are two-particle-irreducible and thus constitute the TBE potential,  $V_{\text{TBE}}$ .

## 2.2 Wick-Cutkosky Perturbative Potentials

A truncation must be made of the expansion of the potential given in Eq. (2.22), since it is not feasible to calculate the infinite sum of graphs for the potential in this Hamiltonian theory. For this investigation we consider three truncations of the potential derived from the field theory. First, the OBE potential and the TBE potentials are

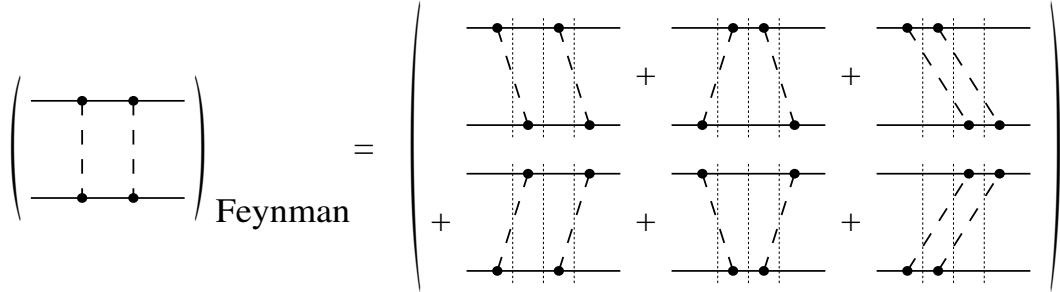


Figure 2.4: The relation between the Feynman box diagram and non-vanishing light-front time-ordered perturbation theory diagrams.

calculated. Then, we note that a subset of the TBE diagrams, the stretched-box diagrams, correspond to the truncated potential derived from the ladder Bethe-Salpeter equation. Thus, three truncated potentials are obtained that have a physical interpretation.

The matrix elements of these potentials are written in the two-particle momentum basis, denoting the momentum of the incoming particles by  $\mathbf{k}_{1i}$  and  $\mathbf{k}_{2i}$ , and the outgoing particles  $\mathbf{k}_{1f}$  and  $\mathbf{k}_{2f}$ . For simplicity, we choose to work in the center-of-momentum frame. By inspecting the rules for converting a light-front time-ordered diagram into a potential given in section 2.1.2, and looking at Eq. (2.28), we find that each piece of the effective-one-particle potential  $V(E; \mathbf{k}_{1f}, \mathbf{k}_{1i})$  is proportional to

$$\frac{E}{2(2\pi)^3 \sqrt{k_{1f}^+ k_{2f}^+ k_{1i}^+ k_{2i}^+}}. \quad (2.57)$$

(The factor of  $E$  in the numerator is included to simplify later equations.) This term will be suppressed in all of the potentials written in this chapter.

### 2.2.1 OBE Potential

We start by drawing all the allowed and non-vanishing time-ordered diagrams with one meson exchange. These diagrams are shown in Fig. 2.5. The light-front time-



written in terms of the equal-time coordinates. A reorganization of Eq. (2.58) yields

$$\begin{aligned}
V_{\text{OBE}}(E; \mathbf{k}_{f,\text{ET}}; \mathbf{k}_{i,\text{ET}}) &= \left(\frac{M}{E}\right)^2 E \left[ \frac{\theta(x-y)}{(k_{1f}^+ - k_{1i}^+)(E - k_{1i}^- - k_{2f}^-) - \mu^2 - (\mathbf{k}_{i\perp} - \mathbf{k}_{f\perp})^2} \right. \\
&\quad \left. + \frac{\theta(y-x)}{(k_{1i}^+ - k_{1f}^+)(E - k_{1f}^- - k_{2i}^-) - \mu^2 - (\mathbf{k}_{i\perp} - \mathbf{k}_{f\perp})^2} \right]. \quad (2.61)
\end{aligned}$$

Using the relations in Eqs. (2.35-2.38), we find

$$\begin{aligned}
(k_{1f}^+ - k_{1i}^+)(E - k_{1i}^- - k_{2f}^-) &= \left(\frac{k_f^3}{k_f^0} - \frac{k_i^3}{k_i^0}\right) \left(\frac{E^2 - 4M^2}{2} - k_{i,\text{ET}}^2 - k_{f,\text{ET}}^2\right) \\
&\quad + \frac{k_f^3 k_i^3}{k_f^0 k_i^0} (k_f^0 - k_i^0)^2 - (k_f^3 - k_i^3)^2. \quad (2.62)
\end{aligned}$$

Under the exchange  $k_f \leftrightarrow k_i$ , the only thing that changes in Eq. (2.62) is that the first term picks up a minus sign. This observation allows Eq. (2.61) to be rewritten as

$$V_{\text{OBE}}(E; \mathbf{k}_{f,\text{ET}}; \mathbf{k}_{i,\text{ET}}) = \left(\frac{M}{E}\right)^2 \frac{E}{\left|\frac{k_f^3}{k_f^0} - \frac{k_i^3}{k_i^0}\right| \Delta + \frac{k_f^3 k_i^3}{k_f^0 k_i^0} (q_{\text{ET}}^0)^2 - \mathbf{q}_{\text{ET}}^2 - \mu^2}, \quad (2.63)$$

where

$$\Delta = \frac{E^2 - 4M^2}{2} - k_{i,\text{ET}}^2 - k_{f,\text{ET}}^2, \quad (2.64)$$

$$q_{\text{ET}}^\mu = k_{f,\text{ET}}^\mu - k_{i,\text{ET}}^\mu. \quad (2.65)$$

Note that  $q_{\text{ET}}^-$  is not the light-front energy of the meson, since in a Hamiltonian theory only the light-front three-momenta are conserved; the four-momenta are not conserved. Equation (2.63) will be useful in the context of approximations based on the physical arguments that we will discuss in section 2.3.

### 2.2.2 TBE Potentials

As in the previous section, we start by drawing all the allowed, non-vanishing time-ordered diagrams with two meson exchanges shown in Fig. 2.6. The diagrams are

classified according to the behavior of the intermediate particles. The total TBE potential is given by the sum of all the diagrams, so

$$V_{\text{TBE}} = V_{\text{TBE:SB}} + V_{\text{TBE:SX}} + V_{\text{TBE:TX}} + V_{\text{TBE:WX}} + V_{\text{TBE:ZX}}. \quad (2.66)$$

In the diagrams for the TBE potential in Fig. 2.6, the intermediate loop momenta can be parameterized by  $\mathbf{k}_{1m}$  or  $\mathbf{k}_{2m}$ . The dependent variable is defined by the relation  $\mathbf{P} = \mathbf{k}_{1i} + \mathbf{k}_{2i}$ . The Bjorken  $x$  variable that corresponds to  $\mathbf{k}_{1m}$  ( $\mathbf{k}_{2m}$ ) is labeled with  $z$  ( $1 - z$ ). We use the Feynman rules to calculate all of these potentials, starting with

$$\begin{aligned} & V_{\text{TBE:SB}}(E; \mathbf{k}_{1f}; \mathbf{k}_{1i}) \\ &= \left(\frac{M}{E}\right)^4 \int \frac{d^2 k_{m\perp}}{2(2\pi)^3} \left[ \int_0^1 dz \frac{\theta(z-y)\theta(x-z)}{z(1-z)(z-y)(x-z)} \right. \\ & \quad \times \frac{1}{E - k_{1m}^- - k_{2f}^- - \omega^-(\mathbf{k}_{1f} - \mathbf{k}_{1m})} \\ & \quad \times \frac{1}{E - k_{1i}^- - k_{2f}^- - \omega^-(\mathbf{k}_{1f} - \mathbf{k}_{1m}) - \omega^-(\mathbf{k}_{1m} - \mathbf{k}_{1i})} \\ & \quad \left. \times \frac{1}{E - k_{1i}^- - k_{2m}^- - \omega^-(\mathbf{k}_{1m} - \mathbf{k}_{1i})} \right] \\ & + \{1 \leftrightarrow 2\}. \end{aligned} \quad (2.67)$$

The symbol  $\{1 \leftrightarrow 2\}$  means that all labels 1 are replaced with 2 and vice versa, as well as replacing the Bjorken variables  $x$ ,  $y$ , and  $z$  with  $1 - x$ ,  $1 - y$ , and  $1 - z$ . This is a way of explicitly stating the symmetry of the potential under exchange of particles 1 and 2. A detailed discussion of the evaluation of the loop integral in Eq. (2.67) is given in Appendix C.2.

$$\begin{aligned}
(a) \quad V_{\text{TBE:SB}} &= \left( \begin{array}{c} \text{Diagram 1} \\ \text{Diagram 2} \end{array} \right) + \left( \begin{array}{c} \text{Diagram 3} \\ \text{Diagram 4} \end{array} \right) \\
(b) \quad V_{\text{TBE:SX}} &= \left( \begin{array}{c} \text{Diagram 5} \\ \text{Diagram 6} \end{array} \right) + \left( \begin{array}{c} \text{Diagram 7} \\ \text{Diagram 8} \end{array} \right) \\
(c) \quad V_{\text{TBE:TX}} &= \left( \begin{array}{c} \text{Diagram 9} \\ \text{Diagram 10} \end{array} \right) + \left( \begin{array}{c} \text{Diagram 11} \\ \text{Diagram 12} \end{array} \right) \\
(d) \quad V_{\text{TBE:WX}} &= \left( \begin{array}{c} \text{Diagram 13} \\ \text{Diagram 14} \end{array} \right) + \left( \begin{array}{c} \text{Diagram 15} \\ \text{Diagram 16} \end{array} \right) \\
(e) \quad V_{\text{TBE:ZX}} &= \left( \begin{array}{c} \text{Diagram 17} \\ \text{Diagram 18} \end{array} \right) + \left( \begin{array}{c} \text{Diagram 19} \\ \text{Diagram 20} \end{array} \right)
\end{aligned}$$

Figure 2.6: The components of the TBE potential, (a) the stretched-box, (b) stretched-crossed, (c) T-crossed, (d) wide-crossed, and (e) Z-crossed diagrams. Here,  $\hat{k}_{1m} = k_{1f} + k_{1i} - k_{1m}$  and  $\hat{k}_{2m} = k_{2f} + k_{2i} - k_{2m}$ .

It is straightforward to calculate the other parts of the TBE potential,

$$\begin{aligned}
& V_{\text{TBE: SX}}(E; \mathbf{k}_{1f}; \mathbf{k}_{1i}) \\
&= \left(\frac{M}{E}\right)^4 \int \frac{d^2 k_{m\perp}}{2(2\pi)^3} \left[ \int_0^1 dz \frac{\theta(x-z)\theta(z-y)}{z(x-z)(1+z-x-y)(z-y)} \right. \\
&\quad \times \frac{1}{E - k_{1m}^- - k_{2f}^- - \omega^-(\mathbf{k}_{1f} - \mathbf{k}_{1m})} \\
&\quad \times \frac{1}{E - k_{1i}^- - k_{2f}^- - \omega^-(\mathbf{k}_{1f} - \mathbf{k}_{1m}) - \omega^-(\mathbf{k}_{1m} - \mathbf{k}_{1i})} \\
&\quad \left. \times \frac{1}{E - k_{1i}^- - \widehat{k}_{2m}^- - \omega^-(\mathbf{k}_{1f} - \mathbf{k}_{1m})} \right] \\
&\quad + \{1 \leftrightarrow 2\}, \tag{2.68}
\end{aligned}$$

where we have denoted the light-front energy of particle 2 by  $\widehat{k}_{2m}^-$ , given by

$$\widehat{k}_{2m}^- = \epsilon^-(\mathbf{P} + \mathbf{k}_{1m} - \mathbf{k}_{1i} - \mathbf{k}_{1f}), \tag{2.69}$$

$$\epsilon^-(\mathbf{k}) = \frac{M^2 + \mathbf{k}_\perp^2}{k^+}. \tag{2.70}$$

The rest of the TBE potential is given by

$$\begin{aligned}
& V_{\text{TBE: TX}}(E; \mathbf{k}_{1f}; \mathbf{k}_{1i}) \\
&= \left(\frac{M}{E}\right)^4 \int \frac{d^2 k_{m\perp}}{2(2\pi)^3} \left[ \int_0^1 dz \frac{\theta(x-z)\theta(1+z-x-y)\theta(y-z)}{z(x-z)(1+z-x-y)(y-z)} \right. \\
&\quad \times \frac{1}{E - k_{1m}^- - k_{2f}^- - \omega^-(\mathbf{k}_{1f} - \mathbf{k}_{1m})} \\
&\quad \times \frac{1}{E - k_{1m}^- - \widehat{k}_{2m}^- - \omega^-(\mathbf{k}_{1f} - \mathbf{k}_{1m}) - \omega^-(\mathbf{k}_{1i} - \mathbf{k}_{1m})} \\
&\quad \left. \times \frac{1}{E - k_{1i}^- - \widehat{k}_{2m}^- - \omega^-(\mathbf{k}_{1f} - \mathbf{k}_{1m})} \right] \\
&\quad + \{1 \leftrightarrow 2\}, \tag{2.71}
\end{aligned}$$

$$\begin{aligned}
& V_{\text{TBE:WX}}(E; \mathbf{k}_{1f}; \mathbf{k}_{1i}) \\
&= \left(\frac{M}{E}\right)^4 \int \frac{d^2 k_{m\perp}}{2(2\pi)^3} \left[ \int_0^1 dz \frac{\theta(x-z)\theta(1+z-x-y)\theta(y-z)}{z(x-z)(1+z-x-y)(y-z)} \right. \\
&\quad \times \frac{1}{E - k_{1m}^- - k_{2f}^- - \omega^-(\mathbf{k}_{1f} - \mathbf{k}_{1m})} \\
&\quad \times \frac{1}{E - k_{1m}^- - \widehat{k}_{2m}^- - \omega^-(\mathbf{k}_{1f} - \mathbf{k}_{1m}) - \omega^-(\mathbf{k}_{1i} - \mathbf{k}_{1m})} \\
&\quad \left. \times \frac{1}{E - k_{1m}^- - k_{2i}^- - \omega^-(\mathbf{k}_{1i} - \mathbf{k}_{1m})} \right] \\
&\quad + \{1 \leftrightarrow 2\}, \tag{2.72}
\end{aligned}$$

$$\begin{aligned}
& V_{\text{TBE:ZX}}(E; \mathbf{k}_{1f}; \mathbf{k}_{1i}) \\
&= \left(\frac{M}{E}\right)^4 \int \frac{d^2 k_{m\perp}}{2(2\pi)^3} \left[ \int_0^1 dz \frac{\theta(x+y-1-z)}{z(x-z)(x+y-1-z)(y-z)} \right. \\
&\quad \times \frac{1}{E - k_{1m}^- - k_{2f}^- - \omega^-(\mathbf{k}_{1f} - \mathbf{k}_{1m})} \\
&\quad \times \frac{1}{E - k_{1m}^- - k_{2f}^- - k_{2i}^- - \epsilon^-(\mathbf{k}_{1i} + \mathbf{k}_{1i} - \mathbf{P} - \mathbf{k}_{1m})} \\
&\quad \left. \times \frac{1}{E - k_{1m}^- - k_{2i}^- - \omega^-(\mathbf{k}_{1i} - \mathbf{k}_{1m})} \right] \\
&\quad + \{1 \leftrightarrow 2\}. \tag{2.73}
\end{aligned}$$

The loop integrals in the expressions for the TBE potentials and the azimuthal-angle integrations are discussed in Appendix C.2.

### 2.2.3 TBE:SB Potential: Connection to the Ladder Bethe-Salpeter Equation

As discussed in Section 2.1.5, a truncated kernel of the Bethe-Salpeter equation is physically equivalent to a Hamiltonian potential which does not include all the graphs that the full theory allows. In particular, consider the Bethe-Salpeter equation when the ladder kernel is used. The physically equivalent light-front potential will not include any graphs where the meson lines cross, so to order  $g^4$ , the potential is given

by  $g^2V_{\text{OBE}} + g^4V_{\text{TBE:SB}}$ . Therefore, by considering the TBE:SB truncation, we can test how well the light-front Hamiltonian approach approximates the full ladder Bethe-Salpeter equation. This concept is discussed more thoroughly in Refs. [36, 38, 45].

### 2.3 Wick-Cutkosky Non-perturbative Potentials

The potentials discussed in this section are derived from the OBE field theory potential, but additional approximations are made to simplify the expressions.

#### 2.3.1 Symmetrized-mass Approximation

Krautgärtner, Pauli and Wölz [47], and Trittmann and Pauli [19] studied positronium with a large coupling constant in light-front dynamics. The one-photon-exchange potential they obtain has a colinear singularity due to the sum of the instantaneous photon exchange graph and a gauge-dependent factor from the spin sum. They argue that the singularity is not physical, and therefore must be canceled by higher-order terms in the potential. The effect of those terms can be simulated by choosing the bound-state energy so that the coefficient of the singular term vanishes. They find that this condition is met when the light-front energy  $P^-$  in the one-photon-exchange potential is replaced with the operator  $\omega$ , expressed here in the two-particle basis,

$$P^- \Rightarrow \omega(\mathbf{k}_{1f}, \mathbf{k}_{2f}; \mathbf{k}_{1i}, \mathbf{k}_{2i}) \equiv \frac{1}{2} (k_{1i}^- + k_{2i}^- + k_{1f}^- + k_{2f}^-). \quad (2.74)$$

This approximation is called the *symmetrized mass* [47], the average of the total  $P^-$  in the initial and final states. It is important to note that this approximation affects not only the singular term, but also the energy denominator in the rest of the OBE potential. The modified denominators simulate the effects of the non-perturbative higher-order terms that are not included explicitly in the OBE potential. Potentials obtained with this approximation are similar to those given by the unitary transformation method [48, 49], where the potentials depend explicitly on the initial- and final-state energies.

In our model, there are no singularities associated with the OBE graphs because we deal only with scalar fields. However, we may use their approximation to obtain a new light-front OBE potential that should incorporate some non-perturbative effects. Recalling that the only place where  $P^-$  occurred in Eq. (2.58) was in the denominator, the  $E$  in the denominator of the OBE potential is replaced with  $\omega$  to get

$$V_\omega(\mathbf{k}_{1f}; \mathbf{k}_{1i}) = \left(\frac{M}{E}\right)^2 \left[ \frac{\theta(x-y)/|x-y|}{\frac{1}{2}(-k_{1i}^- + k_{2i}^- + k_{1f}^- - k_{2f}^-) - \omega^-(\mathbf{k}_{1f} - \mathbf{k}_{1i})} + \frac{\theta(y-x)/|y-x|}{\frac{1}{2}(+k_{1i}^- - k_{2i}^- - k_{1f}^- + k_{2f}^-) - \omega^-(\mathbf{k}_{1i} - \mathbf{k}_{1f})} \right] \quad (2.75)$$

$$= \left(\frac{M}{E}\right)^2 \frac{E}{\frac{1}{2}(k_{1f}^+ - k_{1i}^+) (-k_{1i}^- + k_{2i}^- + k_{1f}^- - k_{2f}^-) - \mu^2 - (\mathbf{k}_{f\perp} - \mathbf{k}_{i\perp})^2}. \quad (2.76)$$

Writing the light-front variables in the denominator in terms of the equal-time variables, as prescribed in Eqs. (2.35-2.38), we find

$$\frac{1}{2}(k_{1f}^+ - k_{1i}^+) (-k_{1i}^- + k_{2i}^- + k_{1f}^- - k_{2f}^-) = -(k_f^3 - k_i^3)^2 + \frac{k_f^3 k_i^3}{k_f^0 k_i^0} (k_f^0 - k_i^0)^2. \quad (2.77)$$

Thus, Eq. (2.76) can be rewritten as

$$V_\omega(\mathbf{k}_{f,\text{ET}}; \mathbf{k}_{i,\text{ET}}) = \left(\frac{M}{E}\right)^2 \frac{E}{\frac{k_f^3 k_i^3}{k_f^0 k_i^0} (k_f^0 - k_i^0)^2 - (\mathbf{k}_{f,\text{ET}} - \mathbf{k}_{i,\text{ET}})^2 - \mu^2}. \quad (2.78)$$

This result can also be obtained more directly by considering the first term in Eq. (2.62). Recall that the  $E^2$  that appears in the denominator is written as  $P^+P^-$  in an arbitrary frame, so in the symmetrized-mass approximation, the  $E^2$  term is replaced with  $E\omega$ . This causes the  $\Delta$  term in the denominator of Eq. (2.63) to vanish, so that the equation reduces to Eq. (2.78). Also, note that by writing this new potential, we attempt to incorporate physics from higher-order graphs than just the OBE graphs.

The singularity structure of the symmetrized-mass potential is easily analyzed. When scattering states are used, in the center-of-momentum frame the total energy

of the state is  $E = 2k_f^0 = 2k_i^0$ , so the relations in Eqs. (2.35-2.38) become

$$k_1^\pm = k^0 \pm k^3, \quad (2.79)$$

$$k_2^\pm = k^0 \mp k^3. \quad (2.80)$$

Using these relations, the symmetrized mass is  $\omega = E$ . Thus, for scattering states, this potential is same as the OBE scattering potential and the singularity structure is the same.

### 2.3.2 Instantaneous and Retarded Approximations

For our bound states,  $k_{\text{ET}}^2 \ll M^2$ , so that the  $\frac{k_f^3 k_i^3}{k_f^0 k_i^0} (k_f^0 - k_i^0)^2$  will be much smaller than the other terms in the denominator of Eq. (2.78). Therefore, we may approximate the symmetrized-mass potential  $V_\omega$  by the instantaneous potential,

$$V_{\text{Inst}}(\mathbf{k}_{f,\text{ET}}; \mathbf{k}_{i,\text{ET}}) = \left(\frac{M}{E}\right)^2 \frac{-E}{(\mathbf{k}_{f,\text{ET}} - \mathbf{k}_{i,\text{ET}})^2 + \mu^2}. \quad (2.81)$$

Alternatively, we may also argue that since the energy difference term is small, we can also approximate  $V_\omega$  by the retarded potential,

$$V_{\text{Ret}}(\mathbf{k}_{f,\text{ET}}; \mathbf{k}_{i,\text{ET}}) = \left(\frac{M}{E}\right)^2 \frac{E}{(k_f^0 - k_i^0)^2 - (\mathbf{k}_{f,\text{ET}} - \mathbf{k}_{i,\text{ET}})^2 - \mu^2} \quad (2.82)$$

$$= \left(\frac{M}{E}\right)^2 \frac{E}{(k_{f,\text{ET}} - k_{i,\text{ET}})^2 - \mu^2}, \quad (2.83)$$

where  $k_{f,\text{ET}}$  and  $k_{i,\text{ET}}$  represent four-vectors, defined by the equal-time three-vectors and the condition that  $k_{f,\text{ET}}^2 = k_{i,\text{ET}}^2 = M^2$ . These potentials resemble the three-dimensional Blankenbecler-Sugar [10] or Gross [11] quasi-potentials.

Both of these approximations are reasonable if the energy difference between the initial and final states is small, which is valid for lightly-bound states. The instantaneous potential is a better approximation of the symmetrized-mass potential, since, if we expand the symmetrized-mass potential to second-order in perturbation theory about  $k_f^0 = k_i^0$ , we get  $V_\omega = V_{\text{Inst}}$ . Also, note that these potentials are explicitly

rotationally invariant in terms of our equal-time parameterization, which provides significant computational advantages.

### 2.3.3 Three-dimensional Reduction of the Bethe-Salpeter Equation

We now consider a non-perturbative approximation used by Wallace and Mandelzweig [50,51]. The basic idea is to first make an approximation of the Bethe-Salpeter equation, then reduce that modified Bethe-Salpeter equation to the physically equivalent Hamiltonian equation. This approach was used by Phillips and Wallace [43] for the model we use, however, they obtained an equal-time Hamiltonian, while we seek a light-front Hamiltonian. Before we do this, we first review the basic mechanics of the three-dimensional reduction, as presented in Sales *et al.* [38] and specialized to our particular case. We postpone the discussion of the approximation until section 2.3.4.

The Bethe-Salpeter equation can be written in matrix form as  $\Gamma = KG_0\Gamma$ , or explicitly in function form in the momentum basis as

$$\Gamma(k_{1f}; P) = \int \frac{d^4 k_{1i}}{(2\pi)^4} K(k_{1f}, k_{1i}; P) G_0(k_{1i}; P) \Gamma(k_{1i}; P). \quad (2.84)$$

Here,  $\Gamma$  is the four-dimensional vertex function,  $K$  is the four-dimensional kernel, and  $G_0$  is the two-particle four-dimensional Green's function. The momenta are  $P$ , the total four-momentum, and  $k_1$ , the four-momentum of particle 1. Particle 2's momentum is implicitly  $P - k_1$ . The four-dimensional Green's function is given by

$$G_0(k_1; P) = id(k_1)d(P - k_1), \quad (2.85)$$

where  $d$  is the one-particle Green's function. On the light front,  $d$  can be written as

$$d(p) = \left( \frac{1}{p^+} \right) \frac{1}{p^- - \text{Sign}(p^+) \epsilon^-(\mathbf{p})}, \quad (2.86)$$

where the light-front energy  $\epsilon^-$  is given by

$$\epsilon^-(\mathbf{p}) = \frac{M^2 + \mathbf{p}_\perp^2}{|p^+|} - i\eta. \quad (2.87)$$

The real part of  $\epsilon^-$  is a positive definite quantity, and  $\eta$  is positive infinitesimal.

The Bethe-Salpeter equation can be rewritten [52] as

$$\Gamma = W\widehat{G}_0\Gamma, \quad (2.88)$$

where  $\widehat{G}_0$  is an auxiliary Green's function, and  $W$  is defined by

$$W = K + K(G_0 - \widehat{G}_0)W. \quad (2.89)$$

The advantage of this rearrangement is that we are free to choose the form of the auxiliary Green's function,  $\widehat{G}_0$ . The choice of  $\widehat{G}_0$  advocated in Ref. [38] is

$$\widehat{G}_0(k_{1f}, k_{1i}; P) = G_0(k_{1f}; P) \frac{\delta^{(2,+)}(\mathbf{k}_{1f} - \mathbf{k}_{1i})}{g_0(\mathbf{k}_{1f}; P)} G_0(k_{1i}; P), \quad (2.90)$$

where

$$g_0(\mathbf{k}_1, P) = \int \frac{dk_1^-}{2(2\pi)} G_0(k_1; P). \quad (2.91)$$

There is an extra factor of 2 in the denominator of Eq. (2.91) when compared to the equal-time formalism. This is due to the Jacobian of the light-front coordinates.

Using the definition of  $\widehat{G}_0$  given in Eq. (2.90), we can integrate the modified Bethe-Salpeter equation, in Eq. (2.88), over the light-front energy to get

$$\gamma(\mathbf{k}_{1f}; P) = \int \frac{d^2k_{1i,\perp} dk_{1i}^+}{(2\pi)^3} w(\mathbf{k}_{1f}, \mathbf{k}_{1i}; P) g_0(\mathbf{k}_{1i}; P) \gamma(\mathbf{k}_{1i}; P), \quad (2.92)$$

where

$$w(\mathbf{k}_{1f}, \mathbf{k}_{1i}; P) \equiv \frac{1}{g_0(\mathbf{k}_{1f}; P)} \langle G_0 W G_0 \rangle(\mathbf{k}_{1f}, \mathbf{k}_{1i}; P) \frac{1}{g_0(\mathbf{k}_{1i}; P)}, \quad (2.93)$$

$$\gamma(\mathbf{k}_1; P) \equiv \frac{1}{g_0(\mathbf{k}_1; P)} \int \frac{dk_1^-}{2(2\pi)} G_0(k_1; P) \Gamma(k_1; P). \quad (2.94)$$

The functional  $\langle f \rangle$  is defined by its action on an arbitrary function  $f(k_{1f}, k_{1i})$ , where  $k_{1f}$  and  $k_{1i}$  are four-vectors, as

$$\langle f \rangle(\mathbf{k}_{1f}, \mathbf{k}_{1i}) = \int \frac{dk_{1f}^-}{2(2\pi)} \frac{dk_{1i}^-}{2(2\pi)} f(k_{1f}, k_{1i}). \quad (2.95)$$

We proceed by calculating the specific form of  $g_0$ ,

$$g_0(\mathbf{k}_1; P) = \frac{\theta(k_1^+)\theta(k_2^+)}{2k_1^+k_2^+} \frac{1}{P^- - k_1^- - k_2^-}, \quad (2.96)$$

where  $k_i^- = \epsilon^-(\mathbf{k}_i)$ . As  $g_0$  is a three-dimensional quantity, it is clear that  $k_i^-$  is not the independent minus component of a momentum four-vector. With this expression for  $g_0$ , we can specialize Eq. (2.92) to the center-of-momentum frame and obtain

$$\begin{aligned} & (E - k_{1f}^- - k_{2f}^-) \psi(\mathbf{k}_{1f}; E) \\ &= \int d^2k_{1i,\perp} \int_0^E dk_{1i}^+ \frac{w(\mathbf{k}_{1f}, \mathbf{k}_{1i}; E)}{2(2\pi)^3 \sqrt{k_{1f}^+ k_{2f}^+ k_{1i}^+ k_{2i}^+}} \psi(\mathbf{k}_{1i}; E), \end{aligned} \quad (2.97)$$

where

$$\psi(\mathbf{k}_1; E) = \frac{g_0(\mathbf{k}_1; E)}{\sqrt{k_1^+ k_2^+}} \gamma(\mathbf{k}_1; E). \quad (2.98)$$

By comparing this equation to Eq. (2.30), we find that the full light-front two-nucleon effective potential that corresponds to the kernel  $K$ , after suppressing the coefficient given in Eq. (2.57), is

$$V(\mathbf{k}_{1f}, \mathbf{k}_{1f}; E) = \frac{1}{E} w(\mathbf{k}_{1f}, \mathbf{k}_{1f}; E). \quad (2.99)$$

Thus, we can calculate light-front potentials directly from the Bethe-Salpeter equation using this method.

The potential  $V$  can be expanded in powers of the coupling constant, as done in LFTOPT. We find that when the auxiliary Green's function given in Eq. (2.90) and the OBE kernel are used, the lowest order parts of the potential (as calculated in Ref. [38]) are the same as our OBE and TBE:SB potentials. Thus, we conclude that this method produces the physically equivalent Hamiltonian theory to the Bethe-Salpeter equation being used. We will use this in the next section to derive a Hamiltonian potential for a situation where LFTOPT cannot be applied.

### 2.3.4 The Modified-Green's-function Approach

Now that the technology for the three-dimensional reduction has been reviewed, we derive an approximate kernel for the Bethe-Salpeter equation. We will follow the approach of Phillips and Wallace [43] and works cited therein. The idea is to start with the Bethe-Salpeter equation where the kernel is truncated to only include ladder (one-boson-exchange, see Fig. 2.2) and crossed (two-boson-exchange, see Fig. 2.3) parts,

$$\Gamma = (K_{\text{ladder}} + K_{\text{cross}})G_0\Gamma. \quad (2.100)$$

An uncrossed approximation is used where the crossed part of the kernel is approximated by  $K_{\text{cross}} \approx K_{\text{ladder}}G_C K_{\text{ladder}}$ . Our job is to find a valid modified Green's function,  $G_C$ . Using this uncrossed approximation,

$$\Gamma \approx (K_{\text{ladder}} + K_{\text{ladder}}G_C K_{\text{ladder}})G_0\Gamma. \quad (2.101)$$

One can attempt to rewrite Eq. (2.100) as an equation linear in  $K_{\text{ladder}}$ , to obtain the modified-Green's-function Bethe-Salpeter equation,

$$\Gamma_{\text{MGF}} = K_{\text{ladder}}(G_0 + G_C)\Gamma_{\text{MGF}}. \quad (2.102)$$

By iterating this integral equation for  $\Gamma_C$ , we obtain

$$\Gamma_{\text{MGF}} = \left[ K_{\text{ladder}} + \sum_{n=1}^{\infty} K_{\text{ladder}} (G_C K_{\text{ladder}})^n \right] G_0 \Gamma_{\text{MGF}}. \quad (2.103)$$

The part of Eq. (2.102) that plays the role of the kernel includes the uncrossed approximation of the original kernel  $K_{\text{ladder}} + K_{\text{ladder}}G_C K_{\text{ladder}}$  as well as many more terms. We note that the higher-order terms approximate some of the higher-order terms that should be included in the full kernel, such as three-boson-exchange diagrams where several meson lines cross. However, this approach undercounts the higher-order terms which it approximates, and also leaves out some terms completely. Therefore, this

new Bethe-Salpeter equation will give results that are closer to the full solution than Eq. (2.100), but will not give the exact solution. The articles by Wallace and Mandelzweig [50, 51] demonstrate that this approach, by effectively summing an infinite set of interactions, gives the correct one-body limit, which is something that the usual Bethe-Salpeter equation with a truncated kernel cannot do.

The modified Bethe-Salpeter equation in Eq. (2.102) is reduced to a Hamiltonian equation via the technique discussed in the previous section. The equal-time Hamiltonian has been derived by Phillips and Wallace [43]. They found that this modified-Green's-function approach gave a spectra that lies closer to the full ground-state spectra than the other approximations they considered. We will use the light-front reduction to obtain the light-front potential for the Hamiltonian equation physically equivalent to Eq. (2.102).

To clearly see what role  $G_C$  plays, we compare the crossed and uncrossed Feynman graphs in Fig. 2.7. Using the Feynman rules,

$$K_{\text{crossed}} \propto \int \frac{d^4 k_{1m}}{(2\pi)^4} \frac{1}{(k_{1f} - k_{1m})^2 - \mu^2} d(k_{1m}) d(\widehat{k}_{2m}) \frac{1}{(k_{1i} - k_{1m})^2 - \mu^2}, \quad (2.104)$$

$$K_{\text{uncrossed}} \propto \int \frac{d^4 k_{1m}}{(2\pi)^4} \frac{1}{(k_{1f} - k_{1m})^2 - \mu^2} d(k_{1m}) d(k_{2m}) \frac{1}{(k_{1i} - k_{1m})^2 - \mu^2}, \quad (2.105)$$

where  $d$  is the one-particle propagator given in Eq. (2.86), and  $\widehat{k}_{2m} = -k_{2m} + k_{2i} + k_{2f}$ . The only difference between these two graphs is that the crossed one has  $d(\widehat{k}_{2m})$  while the uncrossed one has  $d(k_{2m})$ .

We want an approximate one-particle Green's function  $d_C$  that only depends on  $q_1$  and  $P$ , so that

$$d_C(k_1; P) \approx d(\widehat{k}_2). \quad (2.106)$$

Substitution of  $d_C(k_1; P)$  for  $d(\widehat{k}_2)$  in the crossed graph causes the graph to become uncrossed. The penalty for this simplification is that a modified Green's function propagates in the intermediate state, namely  $id(k_1)d_C(k_1; P)$ . It is important that

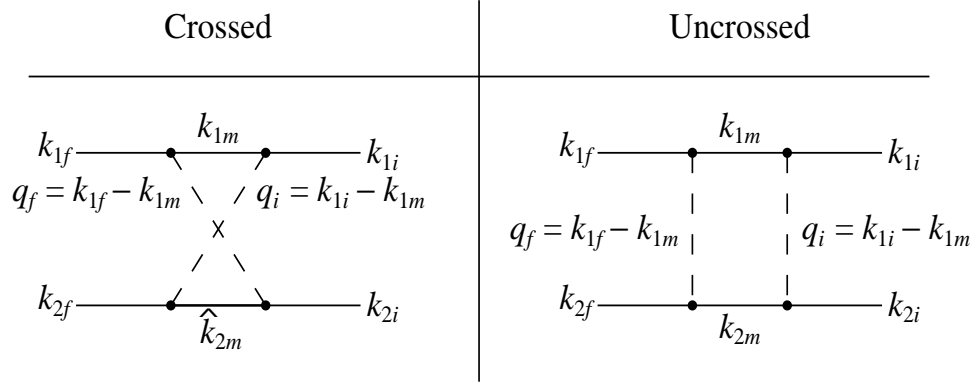


Figure 2.7: The two-boson crossed and uncrossed Feynman graphs. Here,  $\hat{k}_{2m} = -k_{2m} + k_{2i} + k_{2f}$ .

this approximation be invariant under relabeling particle labels, so we explicitly symmetrize by defining

$$G_C = \frac{i}{2} [d(k_1)d_C(k_1; P) + d(k_2)d_C(k_2; P)]. \quad (2.107)$$

How should we approximate  $d_C$ ? Since we are interested in obtaining a bound state, a low-energy approximation is chosen. Specializing to the center-of-momentum frame in this limit, the external momenta are half the total momentum, so  $k_{2i} = k_{2f} = P/2$  and  $\hat{k}_{2m} = P - k_{2m} = k_{1m}$ . This approximation is similar to the one used by Phillips and Wallace. Thus, we define  $d_C(k_1; P) \equiv d(k_1)$  so

$$G_C(k_1; P) = G_1(k_1; P) + G_2(k_1; P), \quad (2.108)$$

where we define  $G_1$  and  $G_2$  by

$$G_1(k_1; P) = \frac{i}{2} d(k_1)^2, \quad (2.109)$$

$$G_2(k_1; P) = \frac{i}{2} d(P - k_1)^2. \quad (2.110)$$

This approximation for  $G_C$  is valid for this model for the energy range we study, as discussed in Appendix E.

We can write the modified-Green's-function Bethe-Salpeter equation as

$$\Gamma_{\text{MGF}} = K_{\text{ladder}} \tilde{G}_0 \Gamma_{\text{MGF}}, \quad (2.111)$$

where

$$\tilde{G}_0 = G_0 + G_1 + G_2. \quad (2.112)$$

This is used as the starting point of three-dimensional reduction discussed in Section 2.3.3, where  $\tilde{G}_0$  is considered as the Green's function. Before doing the reduction, note that the two poles of  $G_1$  and  $G_2$  lie in the same half plane for each function, so

$$\tilde{g}_0(\mathbf{k}_1, P) \equiv \int \frac{dk_1^-}{2(2\pi)} \tilde{G}_0(k_1, ; P) \quad (2.113)$$

$$= g_0(\mathbf{k}_1, P). \quad (2.114)$$

Proceeding with the three-dimensional reduction of Eq. (2.111) in the center-of-momentum frame, we obtain

$$\begin{aligned} & (E - k_{1f}^- - k_{2f}^-) \tilde{\psi}(\mathbf{k}_{1f}; E) \\ &= \int d^2 k_{1i, \perp} \int_0^E dk_{1i}^+ \frac{\tilde{w}(\mathbf{k}_{1f}, \mathbf{k}_{1i}; E)}{2(2\pi)^3 \sqrt{k_{1f}^+ k_{2f}^+ k_{1i}^+ k_{2i}^+}} \tilde{\psi}(\mathbf{k}_{1i}; E), \end{aligned} \quad (2.115)$$

where

$$\tilde{w}(\mathbf{k}_{1f}, \mathbf{k}_{1i}; P) = \frac{1}{g_0(\mathbf{k}_{1f}; P)} \langle \tilde{G}_0 \tilde{W} \tilde{G}_0 \rangle(\mathbf{k}_{1f}, \mathbf{k}_{1i}; P) \frac{1}{g_0(\mathbf{k}_{1i}; P)}, \quad (2.116)$$

$$\tilde{\psi}(\mathbf{k}_1; E) = \frac{1}{\sqrt{k_1^+ k_2^+}} \int \frac{dk_1^-}{2(2\pi)} \tilde{G}_0(k_1; P) \Gamma_{\text{MGF}}(k_1; P), \quad (2.117)$$

and the modified kernel  $\tilde{W}$  is given by

$$\tilde{W} = K_{\text{ladder}} + K_{\text{ladder}} \left[ \tilde{G}_0 - \hat{\tilde{G}}_0 \right] \tilde{W}, \quad (2.118)$$

$$\hat{\tilde{G}}_0(k_{1f}, k_{1i}; P) = \tilde{G}_0(k_{1f}; P) \frac{\delta^{(2,+)}(\mathbf{k}_{1f} - \mathbf{k}_{1i})}{g_0(\mathbf{k}_{1f}; P)} \tilde{G}_0(k_{1i}; P). \quad (2.119)$$

It is a feature of the light front that  $\tilde{g}_0 = g_0$ , so that the uncrossed approximation only affects the potential, and Eq. (2.115) has the same form as Eq. (2.92). In the

equal-time calculation [43]  $\tilde{g}_0 \neq g_0$ , so the approximation changes both the Green's function as well as the potential.

We now expand  $\tilde{W}$  in powers of the coupling constant, and keep only the lowest order term,  $K_{\text{ladder}}$ . According to Eq. (2.99), the light-front potential that corresponds to this truncation of the kernel is the modified-Green's-function (MGF) potential  $V_{\text{MGF}}$ ,

$$V_{\text{MGF}}(\mathbf{k}_{1f}, \mathbf{k}_{1i}; P) = \frac{1}{E} \frac{1}{g_0(\mathbf{k}_{1f}; P)} \langle \tilde{G}_0 K_{\text{ladder}} \tilde{G}_0 \rangle(\mathbf{k}_{1f}, \mathbf{k}_{1i}; P) \frac{1}{g_0(\mathbf{k}_{1i}; P)}. \quad (2.120)$$

The one-boson-exchange kernel  $K_{\text{ladder}}$  is given by the Feynman diagram, so

$$\begin{aligned} K_{\text{ladder}}(k_{1f}, k_{1i}; P) &= \frac{(iM)^2}{(k_{1f} - k_{1i})^2 - \mu^2 + i\eta} \\ &= \left( \frac{1}{k_{1f}^+ - k_{1i}^+} \right) \frac{M^2}{(k_{1f}^- - k_{1i}^-) - \text{Sign}(k_{1f}^+ - k_{1i}^+) \omega^-(\mathbf{k}_{1f} - \mathbf{p}_{1i})}, \end{aligned} \quad (2.121)$$

where the light-front energy of the meson is given by

$$\omega^-(\mathbf{q}) = \frac{\mu^2 - \mathbf{q}_\perp^2}{|q^+|} - i\eta. \quad (2.122)$$

By examining the locations of all the poles in the  $k^-$  integrals for  $V_{\text{MGF}}$ , we find the integrals are non-vanishing only when both  $x$  and  $y$  are between 0 and 1. The sign functions in the denominator of  $K_{\text{ladder}}$  naturally divide  $V_{\text{MGF}}$  into two parts, one for  $x < y$  and the other for  $x > y$ . The integrals in  $V_{\text{MGF}}$  are straightforward, but quite lengthy and tedious. Therefore, we show only the final answer,

$$\begin{aligned} V_{\text{MGF}}(\mathbf{k}_{1f}, \mathbf{k}_{1i}; P) &= \left( \frac{M}{E} \right)^2 \left[ \frac{\theta(x-y)}{|x-y|} \left( \frac{1}{D_1} + \frac{N_{i,21} + N_{f,12}}{2D_1^2} + \frac{N_{i,21}N_{f,12}}{2D_1^3} \right) \right. \\ &\quad \left. + \frac{\theta(y-x)}{|y-x|} \left( \frac{1}{D_2} + \frac{N_{f,21} + N_{i,12}}{2D_2^2} + \frac{N_{i,12}N_{f,21}}{2D_2^3} \right) \right], \end{aligned} \quad (2.123)$$

where

$$N_{f,12} = \frac{k_{1f}^+}{k_{2f}^+} (E - k_{1f}^- - k_{2f}^-), \quad (2.124)$$

$$N_{f,21} = \frac{k_{2f}^+}{k_{1f}^+} (E - k_{1f}^- - k_{2f}^-), \quad (2.125)$$

$$D_1 = E - k_{1i}^- - k_{2f}^- - \omega^-(\mathbf{k}_{1f} - \mathbf{k}_{2i}), \quad (2.126)$$

$$D_2 = E - k_{1f}^- - k_{2i}^- - \omega^-(\mathbf{k}_{1i} - \mathbf{k}_{2f}). \quad (2.127)$$

The expressions for  $N_{i,12}$  and  $N_{i,21}$  are obtained by replacing  $f$  with  $i$  in  $N_{f,12}$  and  $N_{f,21}$ .

What is the physical interpretation of this modified-Green's-function potential? The first term multiplying each  $\theta$  function gives the OBE potential we derived before from the perturbation theory. There the  $D$  in the denominators corresponds to one meson exchange. The second and third terms multiplying the  $\theta$  functions, with  $D^2$  and  $D^3$  in the denominators appear to be effective two- and three-meson-exchange terms. Since time-ordered perturbation theory does not apply to the modified Bethe-Salpeter equation that we use, the exact nature of these terms is not easy to understand. However, it is clear that these terms increase the strength of the potential, and should mimic the higher-order diagrams that are not being included explicitly.

The only dependence on the direction of the perpendicular components of  $k_f$  and  $k_i$  comes from the  $D$ 's. This allows the azimuthal-angle integration of  $V_{\text{MGF}}$  to be done easily, as shown in Appendix C.1.

## 2.4 Results for the Wick-Cutkosky Model

For our numerical work, we pick the meson mass to be 0.15 times that of the nucleon, so  $\mu = 0.15M$ . This is chosen so that our ground state can be considered a toy model of deuterium, and also to facilitate comparison with the results of Nieuwenhuis and Tjon [22], Phillips and Afnan [20], and Schoonderwoerd, Bakker, and Karmanov [14].

Nieuwenhuis and Tjon used the Feynman-Schwinger representation (FSR) of the two-particle Green's function [2] in the quenched approximation without the mass and vertex renormalization terms [22]. Their result is to be considered the full solution that the Bethe-Salpeter and Hamiltonian equations approximate. For the Bethe-Salpeter equation, computation of the bound-state energies for models similar to ours have been done for the ladder [53] and ladder plus crossed [35] kernels over 30 years ago. More recent results are found in Refs. [20,54], where the solutions are compared to those given by the FSR approach.

#### 2.4.1 *Ground State Results*

We want to examine the ground state energies obtained for each of the light-front potentials derived in this chapter, and see how they compare the energies calculated in other approaches. Our main interest is in finding out how well the light-front potentials approximate the Bethe-Salpeter results, and also in how well both the perturbative and non-perturbative potential agree with the Feynman-Schwinger representation approach.

Consider first how the light-front Hamiltonian approach fits in with the other approaches. As discussed in section 2.2.3, different light-front potentials can be derived from Bethe-Salpeter equations with different kernels. We have mentioned that the OBE+TBE:SB potential should approximate the ladder Bethe-Salpeter equation, and similarly the OBE+TBE potential should approximate the Bethe-Salpeter equation when the ladder plus crossed kernel is used. The best that these truncated Hamiltonians can do is approximate their respective Bethe-Salpeter equations.

With this in mind, we evaluate the coupling constant versus bound-state energy curves (which we will call the spectrum) for the Hamiltonian equation with the OBE potential, the OBE+TBE:SB potential, and the OBE+TBE potential. For the range of values we use here, we find numerical errors in the value of  $g^2$  are less than 2%. Our results (without error bars) are plotted along with the results obtained with

the ladder BSE [20], and ladder plus crossed BSE [21] in Fig. 2.8. We note that the OBE+TBE:SB potential agrees well with the ladder BSE, and the OBE+TBE potential agrees with the ladder plus crossed BSE. This is the best that a Hamiltonian can do, so this result is interpreted as evidence that, in general, the higher-order diagrams are very small for the ground state on the light front.

If all one wanted was a way to approximate the spectra for Bethe-Salpeter equations with different kernels, one could just use the truncated potentials that the LFTOPT provide. However, the true goal is to approximate the spectra for the full ground state, which in this model is given by the FSR approach [22]. We expect that the non-perturbative potentials should give a better approximation of the full solution than the perturbative potentials, since the non-perturbative potentials attempt to incorporate physics from higher-order diagrams, although this is not immediately clear by looking at the forms of the potentials used. We plot the results for all of the light-front potentials described in this chapter, the three truncated potentials (OBE, OBE+TBE:SB, and OBE+TBE) and the four non-perturbative potentials (symmetrized mass, retarded, instantaneous, and modified Green's function) along with the results for the full theory in Fig. 2.9. For deeply-bound states, there is considerable disagreement between the perturbative results and the full results, while the non-perturbative results are in better agreement, with the modified-Green's-function (MGF) potential achieving the closest agreement. For lightly-bound states, the results for all of the potentials appear converge to each other, close to the full result.

For the modified-Green's-function potential, only the first term of the expansion in  $g^2$  was kept. In principle, higher-order terms could be calculated. However, since there was fairly good agreement between the OBE potential and the ladder Bethe-Salpeter equation, it is expected that the MGF potential will give results that are close to the ladder Bethe-Salpeter equation using the modified-Green's-function.

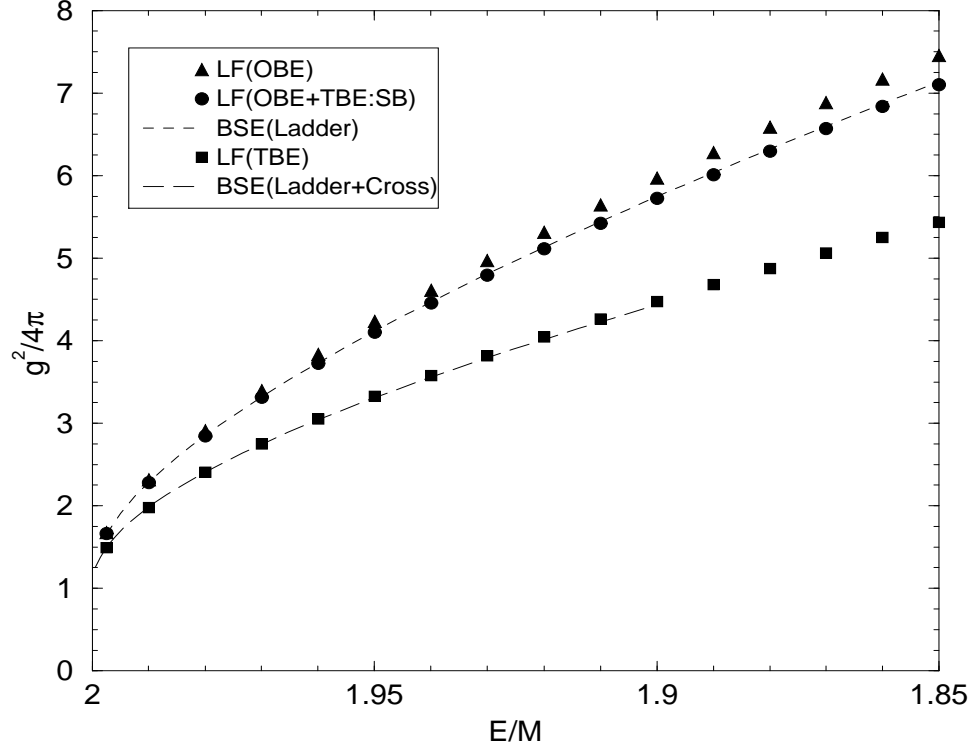


Figure 2.8: The spectra calculated using the OBE, OBE+TBE:SB, and OBE+TBE potentials are displayed in this figure, along with the spectra for the Bethe-Salpeter equation for the ladder and ladder plus crossed kernels. The curves for the ladder (ladder plus crossed) Bethe-Salpeter equation and the light-front OBE+TBE:SB (OBE+TBE) potentials are very close to each other, almost indistinguishable in this figure.  $E$  is the energy of the ground state of two nucleons, and  $M$  is the mass of the nucleons. The meson mass is  $\mu = 0.15M$ . The binding energy  $B$  is related to the bound state energy via  $E = 2M - B$ .

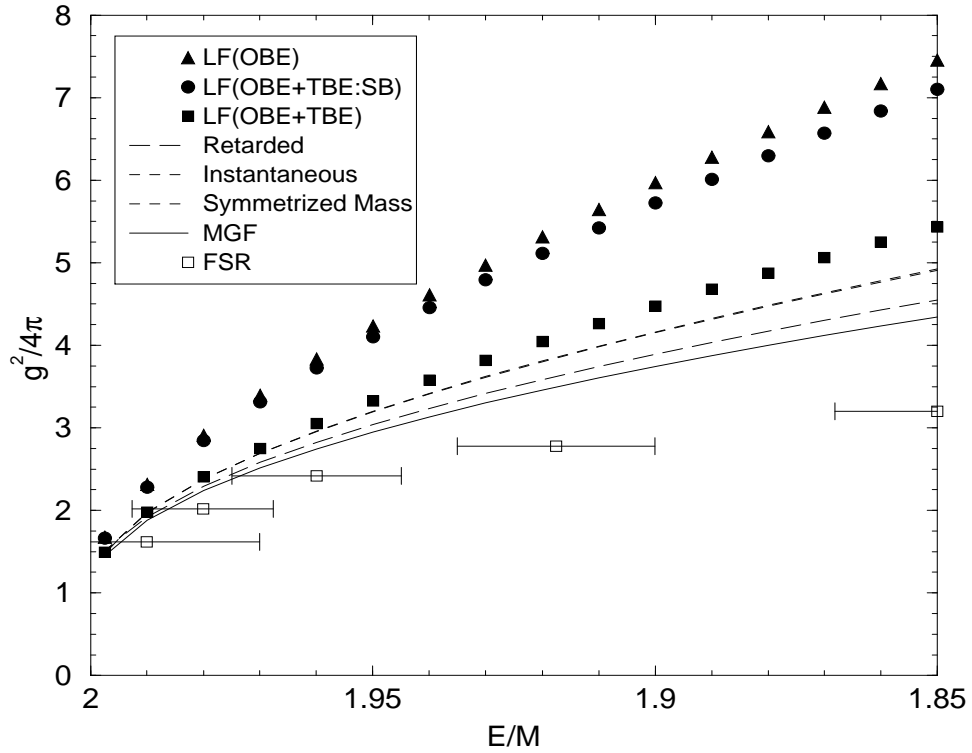


Figure 2.9: The spectra for the seven light-front potentials (OBE, OBE+TBE:SB, OBE+TBE, retarded, instantaneous, symmetrized mass, modified-Green's-function) are plotted here along with the spectra for the full solution (FSR). The instantaneous curve lies very close to the symmetrized mass curve, hence the same line style is used for both.

### 2.4.2 Excited State Results

Now, we are ready to address the problem of rotational invariance of the light-front potentials, and see how the bound states are affected by the breaking of rotational invariance. We expect a splitting of the bound-state energies for different  $m$  states, and we also expect that the states will not be pure angular momentum states. In order to examine these effects, we must have excited states, preferably those with non-zero angular momentum.

Furthermore, since the results of the previous section show that the ground-state energies calculated with the OBE+TBE potentials are in excellent agreement with the Bethe-Salpeter results, we expect that the excited states calculated with the light-front potentials will at least be similar to the Bethe-Salpeter results. This would mean that the excited states should *almost* be angular momentum eigenstates and could be classified easily.

First, we consider the solution for the excited states of the Bethe-Salpeter equation. The technology for doing these bound-state Bethe-Salpeter equation calculations was developed over 30 years ago [33, 34]. Since the eigenstates of the ladder Bethe-Salpeter equation are also eigenstates of the total angular momentum, there is exact degeneracy in the energies of the different  $m$  states for the same angular momentum. For the range of parameters used in this study, we find that the numerical errors in  $g^2$  are less than 0.5%. The numerical errors are largest for the most deeply-bound states ( $E \approx 1.85M$ ) with the largest coupling constants ( $g^2/4\pi \approx 50$ ).

The solutions to the ladder Bethe-Salpeter equation form bands where excited states with different orbital angular momentum are approximately degenerate with each other, as shown in Fig. 2.10. This approximate degeneracy is due to the fact that when  $\mu \rightarrow 0$ , this model can be shown to have the same degeneracies as the non-relativistic hydrogen atom [28, 29]. Thus, in that limit, all states with the same principal quantum number have the same energy. When  $\mu \neq 0$ , that degeneracy is

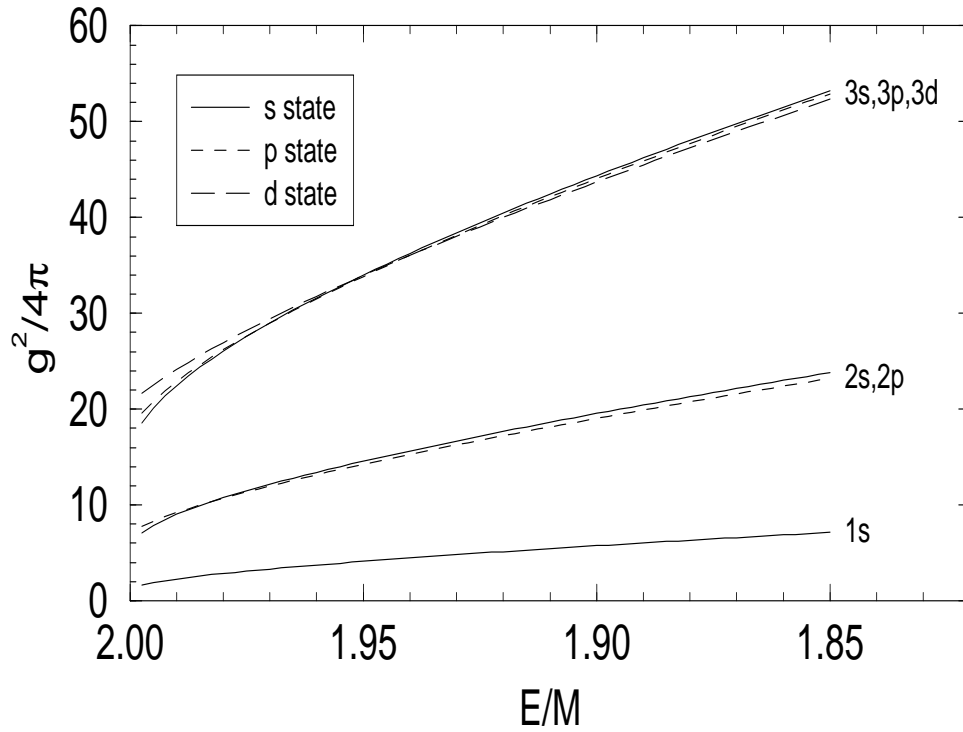


Figure 2.10: The first three energy bands for the ladder Bethe-Salpeter equation.  $E$  is the energy of the bound state of two nucleons, and  $M$  is the mass of each of the two nucleons. The mass of the meson is  $\mu = 0.15M$ .

broken, but only slightly, as we can see from Fig. 2.10. Because of this, we will label our states using atomic spectroscopy notation.

Next, we consider the two light-front Schrödinger equations given by Eqs. (2.46) and (2.48). These equations are solved numerically (for each parity and several  $m$  values) for the spectrum  $g(E)$  for a range of bound-state energies  $E$ . The symmetries of the light-front Hamiltonian allow us to classify the states according to  $m$  and the action under parity, so as an example, we calculate the spectra with even parity and  $m = 0$ . For the range of values we use, we find the numerical errors in  $g^2$  are less than 2%. The errors are largest for the most deeply bound states with the largest coupling constants, as was the case for the Bethe-Salpeter equation.

We plot both the OBE spectra [in Fig. 2.11(a)] and the OBE+TBE:SB spectra [in Fig. 2.11(b)] along with the Bethe-Salpeter spectra for the even parity and  $m = 0$  states. Based on the energies, we see that the  $n = 1$  state is expected to be the  $1s$  state, the  $n = 2$  state the  $2s$  state, and the  $n = 3$  and  $n = 4$  states the  $3s$  or  $3d$  states respectively. We see approximate agreement between both of the truncated Hamiltonian results and the Bethe-Salpeter results for lightly-bound systems (where  $E \approx 2M$ ).

Our states are not manifest eigenstates of total angular momentum  $J^2$ . However, if our approximation of the Hamiltonian potential was good enough, we would be able to identify the  $n = 3$  and  $n = 4$  states of the light-front Hamiltonian calculation with  $3s$  and  $3d$  states of the Bethe-Salpeter equation unambiguously. This would determine the angular momentum of the light-front Schrödinger equation wave functions. From Fig. 2.11, we see both that the addition of the TBE:SB potential brings the  $n = 3$  and  $n = 4$  states closer to the Bethe-Salpeter results, and that in the lightly-bound region the  $n = 3$  and  $n = 4$  states can be identified as  $3s$  and  $3d$  states. For more deeply-bound states, this identification cannot be made.

An alternative approach to assigning angular momenta labels would be to perform a partial-wave decomposition of the wave functions in the real angular momentum ba-

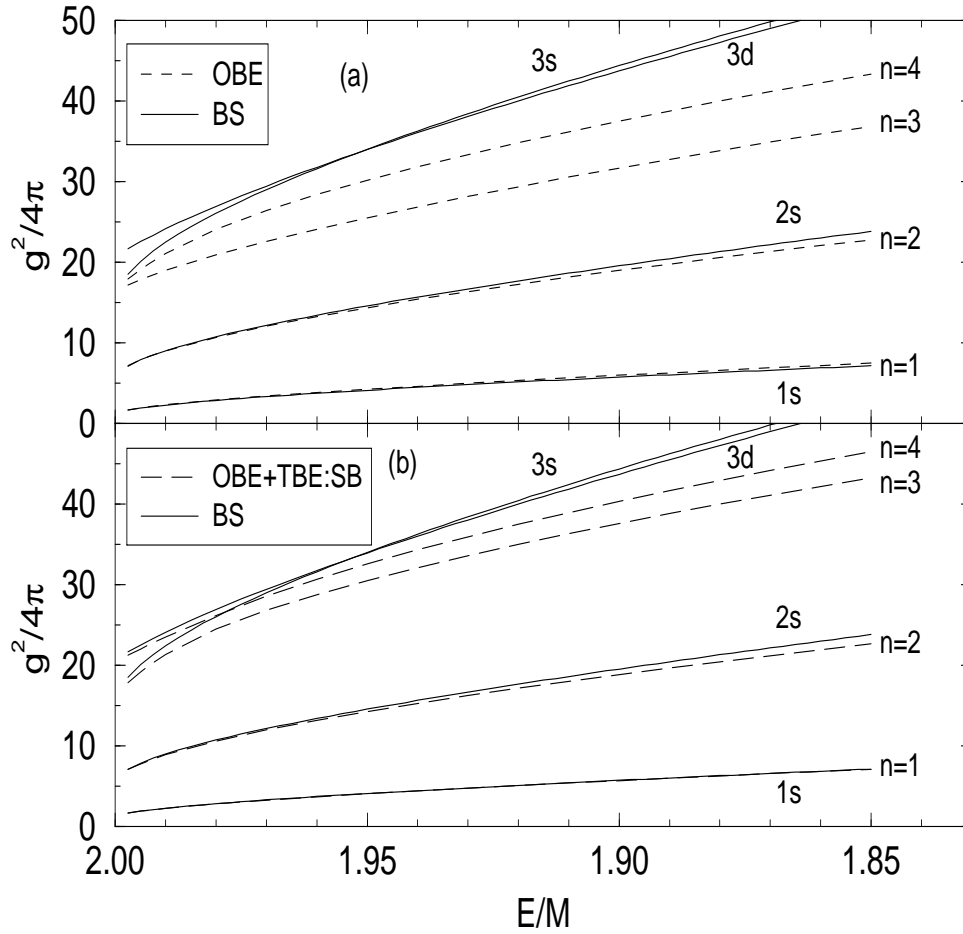


Figure 2.11: Spectra for the four lowest wave functions of even parity and  $m = 0$  (a) for the OBE equation (short-dashed line) and the Bethe-Salpeter equation (solid line), (b) for the OBE+TBE:SB equation (long-dashed line) and the Bethe-Salpeter equation (solid line). The curves are labeled by  $n$ , which indicates that the curve belongs to the  $n^{\text{th}}$  eigenvector. The curve for the  $1s$  state for the Bethe-Salpeter equation and the curve for the first OBE+TBE:SB wave function are very close together, but distinct.

sis. The wave functions could then be labeled by the angular momentum component which is dominant. In light-front dynamics, this is difficult to do since the perpendicular components of the real angular momentum operator ( $J_x$  and  $J_y$ ) are dynamical, which makes the angular momentum operator as complicated as the Hamiltonian. We are encouraged to look for an alternative operator which is easier to use, yet approximates the behavior of the real angular momentum. We shall use the “relative angular momentum”, defined by  $\mathbf{L} = \mathbf{x} \times \mathbf{k}$ , where the vectors are equal-time three-vectors. The relative momentum  $\mathbf{k}$  is defined by Eq. (2.31) and  $\mathbf{x}$  is canonically conjugate to  $\mathbf{k}$ . The “relative angular momentum”  $\mathbf{L}$  is used to help analyze our solutions, and is not the same as the real angular momentum that can be derived from the Lagrangian using the energy-momentum tensor. However, we will see that the “relative angular momentum” gives results that are expected from the real angular momentum, so our use of the “relative angular momentum” in place of the real one appears to be justified.

A partial-wave decomposition is performed on the wave functions (represented in the relative momentum basis) to obtain the radial wave functions  $R_{l,m}$  for all “relative angular momentum” states  $Y_{l,m}$ . Since the potential is not manifestly rotationally invariant when written in terms of the relative momentum, our wave functions will have support from many different partial waves. Not all partial waves are allowed; only those partial-wave states with the same  $J_3$  and parity quantum numbers as the wave function give non-vanishing radial wave functions. We have

$$\langle \mathbf{k} | \psi_{m,p}^n \rangle = \sum_{l=m}^{\infty} Y_l^m(\theta, \phi) R_{l,m}^{n,p}(k). \quad (2.128)$$

We define the fraction of the wave function with “relative angular momentum”  $l$  as

$$f_l^n = \int_0^{\infty} dk k^2 |R_{l,m}^{n,p}(k)|^2. \quad (2.129)$$

The fractions  $f_l^n$  are a measure of the amount of “relative angular momentum” state  $l$  in the  $n^{\text{th}}$  eigenfunction.

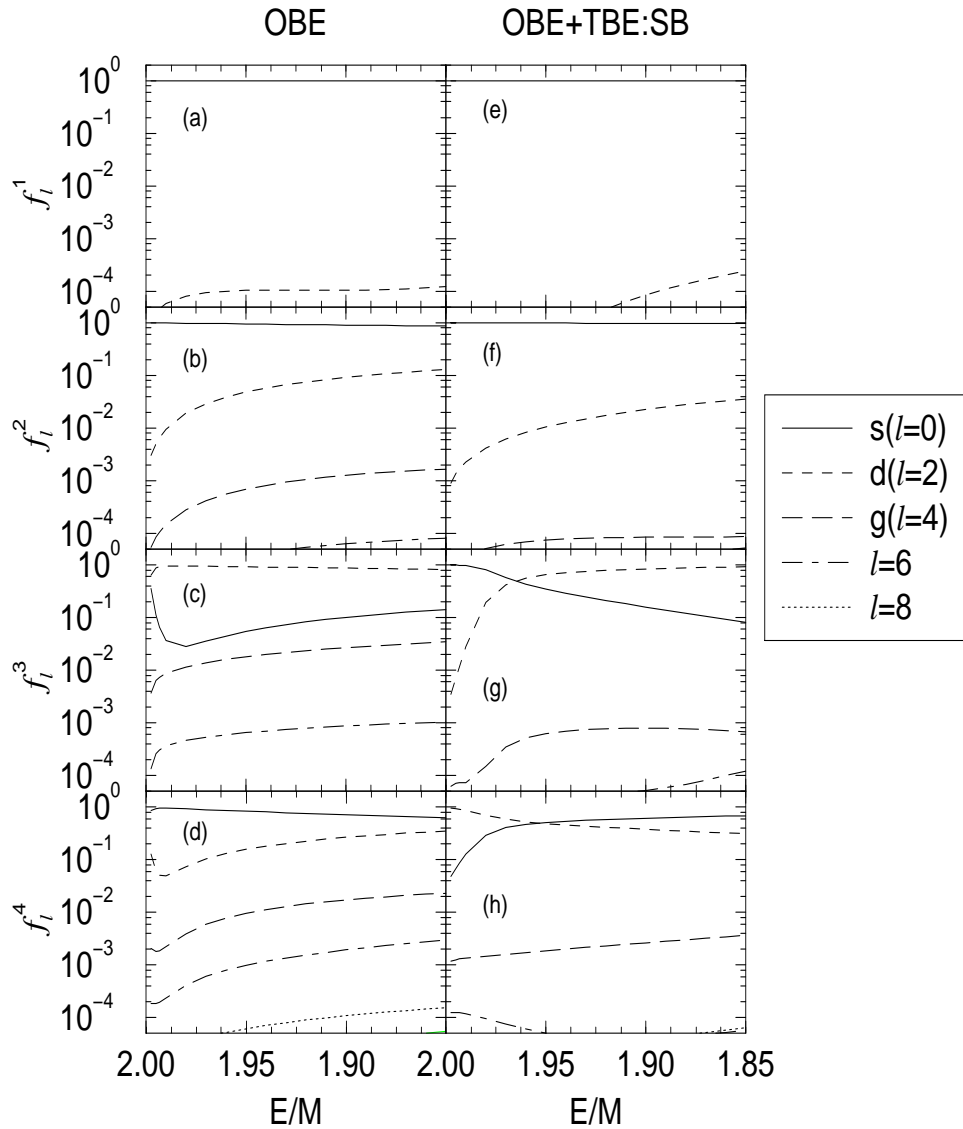


Figure 2.12: The fractions of each angular momentum state in several wave functions is plotted as a function of the binding energy  $E/M$ . The wave functions chosen are the four lowest coupling constant wave functions with  $m = 0$  and even parity. The results for the OBE truncation are shown on the left, (a-d), and the OBE+TBE:SB truncation are shown on the right, (e-h). Note that the OBE wave functions, in general, have more support from a larger number of partial waves.

To illustrate these “relative angular momentum” fractions, we perform this analysis on the four lowest coupling constant wave functions with even parity and  $m = 0$  for both the OBE and OBE+TBE:SB truncations, the same as in Fig. 2.11. We show  $f_l^n$  as a function of  $E$  in Fig. 2.12. (The plots for the  $m = \pm 1, \pm 2$  states show similar behavior, with different  $l$  values.) Note that more higher “relative angular momentum” states contribute for deeper bound states. This is the same behavior that would be expected if the real angular momentum was used to perform the partial wave decomposition. Recall that the real angular momentum will commute with the full potential if no truncation is made. However, the potentials we use are truncated, and neglecting the higher-order terms breaks the rotational invariance of the potential. Also, both the binding and the importance of the higher-order diagrams increase with the coupling constant. Thus, both truncations we consider will break rotational invariance more when the states are more deeply bound. In the absence of having the real angular momentum fractions, we will use the “relative angular momentum” fractions.

Examination of the  $f_l^n$  curves in Fig. 2.12 shows us that, as postulated earlier, the  $n = 1$  and  $n = 2$  states shown in Figs. 2.12(a,e) and 2.12(b,f) are predominately  $s$ -wave states, which we label the  $1s$  and  $2s$  states respectively. For the OBE truncation, the  $n = 3$  state shown in Fig. 2.12(c) is predominately  $d$ -wave (labeled the  $3d$  state) and the  $n = 4$  state shown in Fig. 2.12(d) is predominately  $s$ -wave (labeled the  $3s$  state), with little mixing between the two states. For the OBE+TBE:SB truncation, the  $n = 3$  and  $n = 4$  states are mixtures of both the  $3s$  and  $3d$  states, as seen in Figs. 2.12(g,h). In fact, we see a level crossing between the  $n = 3, 4$  states in that the  $n = 3$  state is predominantly  $3d$  for lightly-bound systems, but as the binding increases, the  $n = 3$  state becomes predominantly  $3s$ . Again, this type of mixing would also be found if the real angular momentum was used.

If this  $3s$ - $3d$  mixing is ignored, then Fig. 2.12 shows clearly that when the TBE:SB is included the amount of “relative angular momentum” states mixed in actually

*decreases* as compared to the OBE results. This implies that the wave functions of the OBE+TBE:SB equation are better “relative angular momentum” states than the wave functions of the OBE equation. Thus the TBE:SB potential restores some rotational invariance to the OBE calculation.

We attempt to classify the wave functions as states with definite angular momentum. If a wave function has the most support from the “relative angular momentum” state  $l$ , we classify that state as having angular momentum  $l$ . This procedure designates the first two wave functions for both the OBE and the OBE+TBE:SB cases as  $s$ -wave states, which is clearly the right thing to do. For the third and fourth wave functions of the OBE+TBE:SB equation, there are points where the fraction of the  $s$ -wave state equals the fraction of the  $d$ -wave state. Here it no longer clear that such a state should be assigned a definite “relative angular momentum” value; we do so regardless and analyze the consequences later.

We now examine the breaking of rotational invariance of the two truncations based on the comparison of states with different  $m$  projections of the same angular momentum. Since the  $s$ -wave state has only  $m = 0$ , there is nothing to analyse in that case. Further discussion of the ground-state  $s$ -wave appears in Ref. [37]. In Figs. 2.13, 2.14, and 2.15, we plot the Bethe-Salpeter bound-state spectra along with the spectra for the states constructed with the OBE and the OBE+TBE:SB potentials. The different  $m$  states for the Bethe-Salpeter equation are exactly degenerate as a result of the rotational invariance of the equation. The curves from the Hamiltonian theory do not exhibit the exact degeneracy in  $m$ ; the degeneracy is broken whether the OBE or OBE+TBE:SB potentials are used. However, we see that the degeneracy is partially restored when the TBE:SB potential is included, in that for a given binding energy the spread of the coupling constants is always smaller.

In Figs. 2.13 and 2.14, we plot the spectra for the  $2p$  and  $3p$  states, respectively. In both figures, we see that the  $m = 0$  and  $m = \pm 1$  curves move closer together after addition of the TBE:SB potential. However, the average of the two curves for each case

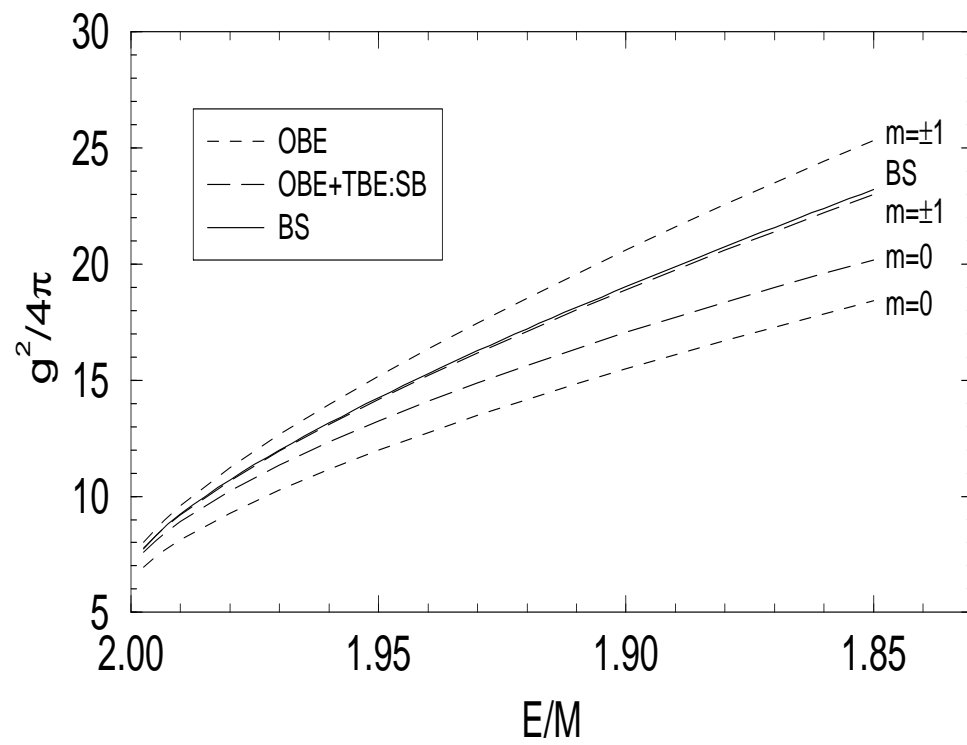


Figure 2.13: The spectra for the first  $p$ -wave state, the  $2p$  state. The Bethe-Salpeter (BS) result is plotted with a solid line, the OBE results with the short-dashed lines, and the OBE+TBE:SB with the long-dashed lines.

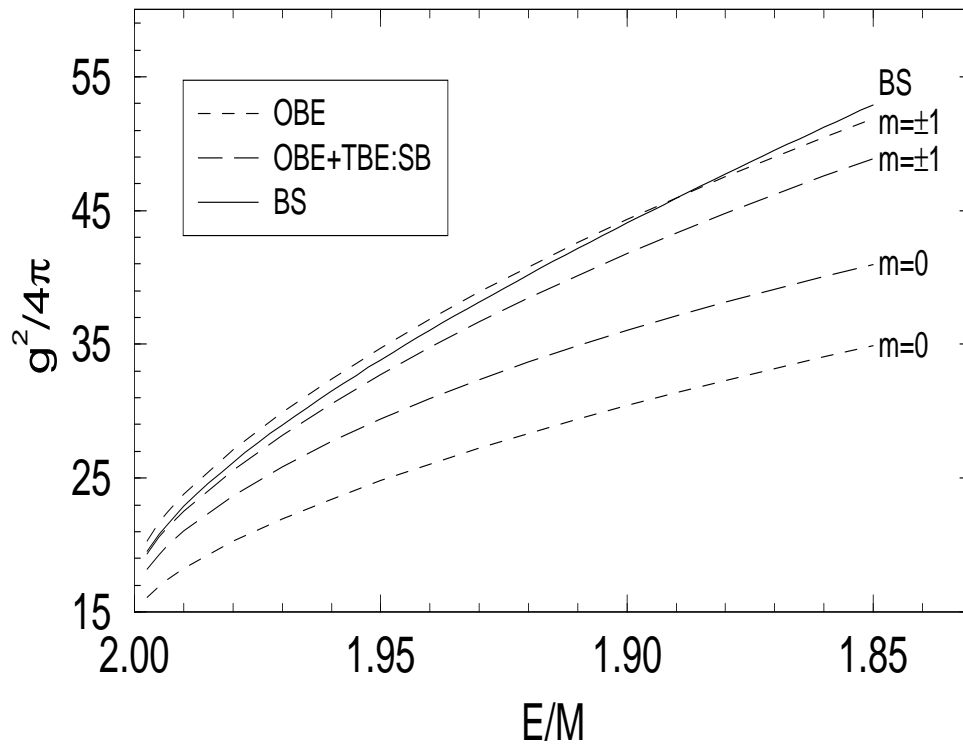


Figure 2.14: The spectra for the second  $p$ -wave state, the  $3p$  state. The Bethe-Salpeter (BS) result is plotted with a solid line, the OBE results with the short-dashed lines, and the OBE+TBE:SB with the long-dashed lines.

does not move much. In fact, for the  $3p$  state in Fig. 2.14, the  $m = \pm 1$  curve moves farther away from the ladder Bethe-Salpeter curve after addition of the TBE:SB. We also note that in Fig. 2.14 the spread of the spectra is larger than in Fig. 2.13 for both the OBE and the OBE+TBE:SB light-front Schrödinger equations. We attribute this to the neglect of the higher-order graphs. Since the states with different  $m$  values would be degenerate if all the higher-order graphs were included, not including them causes a breaking of the degeneracy. Because the coupling constant is larger for the  $3p$  states than for the  $2p$  states with the same binding energy, the omission of the higher-order graphs causes a larger breaking of the degeneracy for the  $3p$  states.

We also consider the first  $d$ -wave states. We see in Fig. 2.15 that, as in Figs. 2.13 and 2.14, the states with different  $m$  values move together after addition of TBE:SB. The effect of the level crossing of the  $3s$  and  $3d$  states shown in Figs. 2.12(g) and 2.12(h) is seen here in that there are two disjoint curves for  $m = 0$ . When the level crossing occurs, at  $E/M \approx 1.96$ , the wave function which originally was the  $3s$  state becomes the  $3d$  state and vice versa.

There are some problems that this level crossing causes. In the intermediate region where the  $3s$  and  $3d$  states are about equally mixed, it is probably not physically sensible to call the state a  $3s$  or  $3d$  state. However, plotting the curves gives us an indication of what the wave functions are doing, and for this case we see that the  $m = 0$  curve is always bounded by the  $m = \pm 1$  and  $m = \pm 2$  curves. A more restrictive classification scheme would leave a gap (in  $E/M$ ) between the two  $m = 0$  curves and it would not be so clear that the bounding of the  $m = 0$  curve which we observe here occurs.

Finally, we note that the spread of the curves in the  $3d$  case is approximately the same as the spread in the  $3p$  case for each truncation. This tells us that the higher-order graphs have the same qualitative effect in both states.

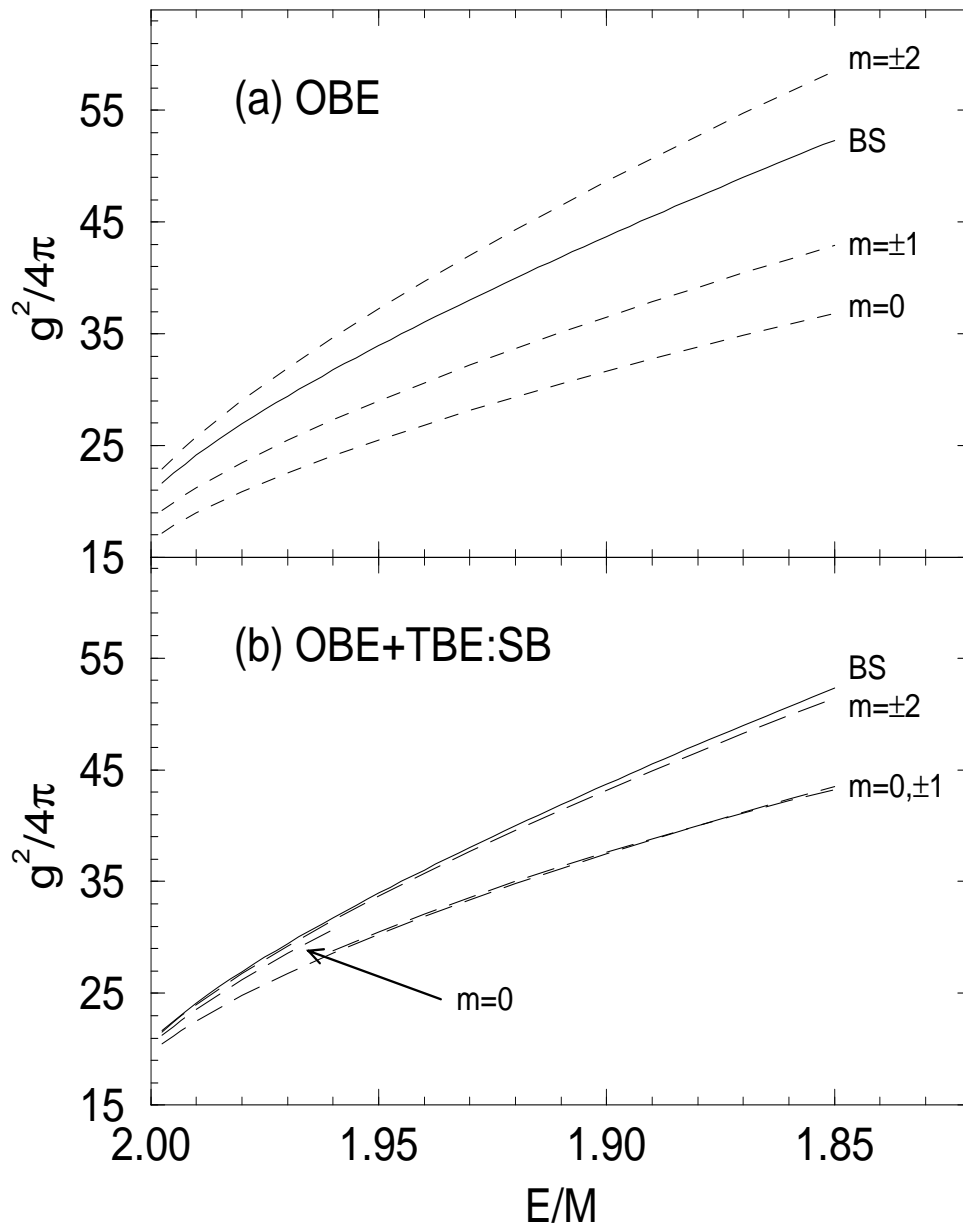


Figure 2.15: The first  $d$ -wave state, the  $3d$  state. The Bethe-Salpeter (BS) result is plotted with a solid line. In (a) the OBE results are the short-dashed lines, and in (b) the OBE+TBE:SB results are the long-dashed lines. Note that there are two separate  $m = 0$  curves when the OBE+TBE:SB are used, one extending a quarter of the way over, and the other hiding under the  $m = \pm 1$  curve with the OBE+TBE:SB.

## 2.5 Conclusions

We have examined several aspects of bound states in a massive Wick-Cutkosky model using several light-front potentials. First, we used three different truncations of the effective potential derived from the perturbative field theory and four approximations that attempt to incorporate non-perturbative physics. For each of these potentials, we calculate the coupling constant that gives the ground-state for a given bound-state energy (the spectrum), and compare to the spectra from different approaches found in the literature. We find fairly good agreement between all the methods for lightly-bound systems.

For the full range of binding energies studied, the results for calculations including one- and two-boson-exchange potentials agree with the Bethe-Salpeter equation using the physically equivalent truncation of the kernel within the numerical errors. (This is a consequence of examining the ground state. For the excited states more higher-order light-front time-ordered graphs are required to get the same level of agreement [36].) The agreement for the case with the stretched box diagrams (OBE+TBE:SB) has been shown previously by Sales *et al.* [38]; the result with the crossed-box contribution (OBE+TBE) is new. This excellent agreement with the Bethe-Salpeter results has an undesirable consequence: The BSE results are known to be a poor approximation of the full solution for deeply bound systems, so the truncated Hamiltonian approach cannot provide a good approximation to the full solution in that regime.

The non-perturbative potentials based on physical considerations give a better approximation of the full solution than the potentials obtained from LFTOPT. For all binding energies, the modified-Green's-function potential achieves the closest agreement with the full solution of all the potentials considered here. However, there is still considerable disagreement between approximate potentials and the full result for deeply bound states. We interpret this as an indication that the approximations, while incorporating some non-perturbative physics, do not go far enough. In the

weakly-bound regime, which is of relevance for deuteron calculations, the spectra for all of the potentials are close together, indicating that light-front dynamics provides a good description of lightly-bound systems.

After examining the ground state thoroughly, we considered the low-lying excited states of the Wick-Cutkosky model. We considered two truncations of the light-front Hamiltonian, the OBE and OBE+TBE:SB truncations. Using these truncations, a “relative angular momentum” operator was used to study the partial-wave decompositions of the bound-state wave functions. We found that the “relative angular momentum” operator acting on those states yield behavior similar to that expected from the real angular momentum. This result encourages the use of this operator to classify the states according to their angular momentum values  $l$ , and to study the degeneracy of the spectra for states with the same  $l$  value but with different projections  $m$ . We found less breaking of the degeneracy when the OBE+TBE:SB potential was used than when the OBE potential was used. Both of these findings indicate that the OBE+TBE:SB truncation of the Hamiltonian breaks rotational invariance less than the OBE truncation alone.

However, there is still some discrepancy between our truncated Hamiltonian spectra and the ladder Bethe-Salpeter spectra. In general, our OBE+TBE:SB results for the  $p$ - and  $d$ -wave states show deeper binding than the Bethe-Salpeter results. Not surprisingly, this disagreement is largest for the most deeply bound-states where the coupling is largest. This difference would be removed if all the higher-order pieces of the potential were included. These higher-order pieces are also needed for the full restoration of rotational invariance.

## Chapter 3

### REALISTIC NUCLEAR MODELS

In this chapter, we start with an effective nuclear Lagrangian [18, 55] for nucleons and six mesons which incorporates a chiral symmetry. We derive the light-front Hamiltonian from the Lagrangian and address some of the difficulties encountered. Then the Hamiltonian is used to construct the Feynman rules for nucleon-nucleon potentials. The issues of the breaking of rotational invariance and chiral symmetry by certain subsets of the potentials are considered and addressed. We use the Feynman rules and the symmetry considerations to construct new one-meson-exchange (OME) and two-meson-exchange (TME) light-front nucleon-nucleon (LFNN) potentials.

The potentials are used in numeric calculations for two families of nuclear models. For our first set of calculations, we assume that the pion is the only meson that interacts with the nucleons, giving us a special case of the full nuclear model. This pion-only model is inspired by the non-relativistic one-pion-exchange model used by Friar, Gibson, and Payne [56]. We generalize their model to form the basis of our pion-only light-front model, which includes relativity automatically.

Our second set of calculations uses the full model with all six mesons ( $\pi$ ,  $\sigma$ ,  $\rho$ ,  $\omega$ ,  $\eta$ , and  $\delta$ ) for the interaction. This model is an extension of the light-front model used by Miller and Machleidt [55]. A new feature of this model is that light-front energy dependent denominators are used in the potentials; the denominators used in Ref. [55] are energy independent.

### 3.1 Model and Formalism

Our starting point is a nuclear Lagrangian [18] which incorporates a non-linear chiral model for the pions. The Lagrangian is based on the linear representations of chiral symmetry used by Gursev [57]. It is invariant (in the limit where  $m_\pi \rightarrow 0$ ) under chiral transformations.

The model prescribes the use of nucleons  $\psi'$  (or  $\psi$ , the free nucleon field, as discussed in Section 3.3.2) and six mesons: the  $\pi$ ,  $\delta$  (also known as the  $a_0(980)$ ),  $\sigma$  (also known as the  $f_0(400 - 1200)$ ),  $\eta$ ,  $\rho$ , and  $\omega$  mesons. The coupling of each meson to the nucleon is governed by the combination of the meson's spin and isospin. The  $\pi$  and  $\eta$  are pseudoscalars, the  $\rho$  and  $\omega$  are vectors, and the  $\delta$  and  $\sigma$  are scalars. Under isospin transformations, the  $\pi$ ,  $\rho$ , and  $\delta$  are isovector particles while the  $\eta$ ,  $\omega$ , and  $\sigma$  are isoscalar particles.

The use of scalar mesons is meant as a simple representation of part of the two-pion-exchange potential which causes much of the medium range attraction between nucleons [58,59]. It can also be interpreted as the effect of fundamental scalar mesons [60–62].

The Lagrangian  $\mathcal{L}$  is based on the one used in Refs. [18,55,63]. It is given by

$$\begin{aligned} \mathcal{L} = & -\frac{1}{4}\boldsymbol{\rho}^{\mu\nu} \cdot \boldsymbol{\rho}_{\mu\nu} + \frac{m_\rho^2}{2}\boldsymbol{\rho}^\mu \cdot \boldsymbol{\rho}_\mu - \frac{1}{4}\omega^{\mu\nu}\omega_{\mu\nu} + \frac{m_\omega^2}{2}\omega^\mu\omega_\mu \\ & + \frac{1}{4}f^2\text{Tr}(\partial_\mu U \partial^\mu U^\dagger) + \frac{1}{4}m_\pi^2 f^2 \text{Tr}(U + U^\dagger - 2) \\ & + \frac{1}{2}(\partial_\mu\sigma\partial^\mu\sigma - m_\sigma^2\sigma^2) + \frac{1}{2}(\partial_\mu\boldsymbol{\delta} \cdot \partial^\mu\boldsymbol{\delta} - m_\delta^2\boldsymbol{\delta}^2) + \frac{1}{2}(\partial_\mu\eta\partial^\mu\eta - m_\eta^2\eta^2) \\ & + \bar{\psi}' \left[ \gamma^\mu(i\partial_\mu - g_\rho\boldsymbol{\rho}_\mu \cdot \boldsymbol{\tau} - g_\omega\omega_\mu) - U(M + g_\sigma\sigma + g_\delta\boldsymbol{\delta} \cdot \boldsymbol{\tau} + ig_\eta\gamma_5\eta) \right] \psi', \end{aligned} \quad (3.1)$$

where the bare masses of the nucleon and the mesons are given by  $M$  and  $m_\alpha$  where  $\alpha = \pi, \eta, \sigma, \delta, \rho, \omega$ . We have defined  $V^{\mu\nu} \equiv \partial^\mu V^\nu - \partial^\nu V^\mu$  for  $V = \rho, \omega$ . The unitary matrix  $U$  can be chosen to have one of the three forms  $U_i$ :

$$U_1 \equiv e^{i\gamma_5\boldsymbol{\tau} \cdot \boldsymbol{\pi}/f}, \quad U_2 \equiv \frac{1 + i\gamma_5\boldsymbol{\tau} \cdot \boldsymbol{\pi}/2f}{1 - i\gamma_5\boldsymbol{\tau} \cdot \boldsymbol{\pi}/2f}, \quad U_3 \equiv \sqrt{1 - \pi^2/f^2} + i\gamma_5\boldsymbol{\tau} \cdot \boldsymbol{\pi}/f, \quad (3.2)$$

which correspond to different definitions of the fields. Note that each of these definitions can be expanded to give

$$U = 1 + i\gamma_5 \frac{\boldsymbol{\tau} \cdot \boldsymbol{\pi}}{f} - \frac{\pi^2}{2f^2} + \mathcal{O}\left(\frac{\pi^3}{f^3}\right). \quad (3.3)$$

In this work, we consider at most two meson exchange potentials, so we consider  $U$  to be defined by Eq. (3.3).

In the limit where  $m_\pi \rightarrow 0$ , this Lagrangian, is invariant under the chiral transformation

$$\psi' \rightarrow e^{i\gamma_5 \boldsymbol{\tau} \cdot \mathbf{a}} \psi', \quad U \rightarrow e^{-i\gamma_5 \boldsymbol{\tau} \cdot \mathbf{a}} U e^{-i\gamma_5 \boldsymbol{\tau} \cdot \mathbf{a}}. \quad (3.4)$$

In this model the other mesons are not affected by the transformation because they are not chiral partners of the pion. This is in contrast to the Lagrangian given in Refs. [18,63], where the mass and scalar interaction terms for the nucleon were written as  $MU + g_s\phi$  instead of  $U(M + g_s\phi)$ .

### 3.2 Non-interacting Nucleon-Nucleon Theory

The light-front Hamiltonian is derived from this Lagrangian using the same approach used in section 2.1, the approach used by Miller [18] and others [64–67]. The basic idea is to write the light-front Hamiltonian ( $P^-$ ) as the sum of a free, non-interacting part and a term containing the interactions. We consider the free part first.

#### 3.2.1 Free Field Expansions

The solutions for the free fields are similar to those obtained by using equal-time dynamics. In fact, the solutions are formally related by a change of variable, and so the most obvious difference between the two is due to the Jacobian. The field equations have the general form (when Lorentz, spinor, and isospin indices are suppressed) of

$$\alpha(x) = \int \frac{d^2k_\perp dk^+ \theta(k^+)}{(2\pi)^{3/2} \sqrt{2k^+}} [a_\alpha(\mathbf{k}) e^{-ik^\mu x_\mu} + a_\alpha^\dagger(\mathbf{k}) e^{+ik^\mu x_\mu}], \quad (3.5)$$

where  $\alpha = \pi, \eta, \sigma, \delta, \rho, \omega, \psi$ . Note that in the exponentials,

$$k^\mu x_\mu = \frac{1}{2} (k^+ x^- + k^- x^+) - \mathbf{k}_\perp \cdot \mathbf{x}_\perp. \quad (3.6)$$

In particular, the solutions for all the mesons and the nucleon field are

$$\boldsymbol{\pi}(x) = \int \frac{d^2 k_\perp dk^+ \theta(k^+)}{(2\pi)^{3/2} \sqrt{2k^+}} [\mathbf{a}_\pi(\mathbf{k}) e^{-ik^\mu x_\mu} + \mathbf{a}_\pi^\dagger(\mathbf{k}) e^{+ik^\mu x_\mu}], \quad (3.7)$$

$$\eta(x) = \int \frac{d^2 k_\perp dk^+ \theta(k^+)}{(2\pi)^{3/2} \sqrt{2k^+}} [a_\eta(\mathbf{k}) e^{-ik^\mu x_\mu} + a_\eta^\dagger(\mathbf{k}) e^{+ik^\mu x_\mu}], \quad (3.8)$$

$$\boldsymbol{\delta}(x) = \int \frac{d^2 k_\perp dk^+ \theta(k^+)}{(2\pi)^{3/2} \sqrt{2k^+}} [\mathbf{a}_\delta(\mathbf{k}) e^{-ik^\mu x_\mu} + \mathbf{a}_\delta^\dagger(\mathbf{k}) e^{+ik^\mu x_\mu}], \quad (3.9)$$

$$\sigma(x) = \int \frac{d^2 k_\perp dk^+ \theta(k^+)}{(2\pi)^{3/2} \sqrt{2k^+}} [a_\sigma(\mathbf{k}) e^{-ik^\mu x_\mu} + a_\sigma^\dagger(\mathbf{k}) e^{+ik^\mu x_\mu}], \quad (3.10)$$

$$\boldsymbol{\rho}^\mu(x) = \int \frac{d^2 k_\perp dk^+ \theta(k^+)}{(2\pi)^{3/2} \sqrt{2k^+}} \sum_{s=1,3} \epsilon^\mu(\mathbf{k}, s) [\mathbf{a}_\rho(\mathbf{k}, s) e^{-ik^\mu x_\mu} + \mathbf{a}_\rho^\dagger(\mathbf{k}, s) e^{+ik^\mu x_\mu}], \quad (3.11)$$

$$\omega^\mu(x) = \int \frac{d^2 k_\perp dk^+ \theta(k^+)}{(2\pi)^{3/2} \sqrt{2k^+}} \sum_{s=1,3} \epsilon^\mu(\mathbf{k}, s) [a_\omega(\mathbf{k}, s) e^{-ik^\mu x_\mu} + a_\omega^\dagger(\mathbf{k}, s) e^{+ik^\mu x_\mu}], \quad (3.12)$$

$$\begin{aligned} \psi(x) = \sqrt{2M} \int \frac{d^2 k_\perp dk^+ \theta(k^+)}{(2\pi)^{3/2} \sqrt{2k^+}} \\ \times \sum_{\lambda=+,-} \sum_{t_3=+,-} [u(\mathbf{k}, \lambda) b(\mathbf{k}) e^{-ik^\mu x_\mu} + v(\mathbf{k}, \lambda) d^\dagger(\mathbf{k}) e^{+ik^\mu x_\mu}] \chi_{t_3}. \end{aligned} \quad (3.13)$$

The polarization vectors are the usual ones. The most general of the commutation relations is

$$[a_{\alpha,i}(\mathbf{k}, s), a_{\beta,j}^\dagger(\mathbf{k}', s')] = \delta_{\alpha,\beta} \delta_{i,j} \delta_{s,s'} \delta^{(2,+)}(\mathbf{k} - \mathbf{k}'), \quad (3.14)$$

where  $\alpha, i,$  and  $s$  denote the meson type, isospin, and spin, and  $\delta^{(2,+)}$  is defined by Eq. (2.9). The anti-commutation relations are

$$\{b(\mathbf{k}, \lambda), b^\dagger(\mathbf{k}', \lambda')\} = \{d(\mathbf{k}, \lambda), d^\dagger(\mathbf{k}', \lambda')\} = \delta_{\lambda,\lambda'} \delta^{(2,+)}(\mathbf{k} - \mathbf{k}'). \quad (3.15)$$

All other (anti-)commutation relations vanish. The spinors are normalized so that  $\bar{u}(\mathbf{p}, \lambda') u(\mathbf{p}, \lambda) = \delta_{\lambda\lambda'}$ . For more information on the definition of the spinors, see Appendix F.

### 3.2.2 Non-interacting Hamiltonians

The general form of the non-interacting Hamiltonian for each meson is

$$P_0^-(\alpha) = \int d^2k_\perp dk^+ \theta(k^+) a_\alpha^\dagger(\mathbf{k}) a_\alpha(\mathbf{k}) \frac{k_\perp^2 + m_\alpha^2}{k^+}. \quad (3.16)$$

For the vector mesons ( $\rho$  and  $\omega$ ), there is an implicit sum over the meson spins. Explicitly, this means that for vector mesons  $a_V^\dagger(\mathbf{k}) a_V(\mathbf{k}) \rightarrow \sum_{s=1,3} a_V^\dagger(\mathbf{k}, s) a_V(\mathbf{k}, s)$ . Likewise, the sum over the isospin of the isovector mesons ( $\pi$ ,  $\delta$ , and  $\rho$ ) is implicit. The sum over isospin can be made explicit by writing  $a_I^\dagger(\mathbf{k}) a_I(\mathbf{k}) \rightarrow \sum_{i=1,3} a_{I,i}^\dagger(\mathbf{k}) a_{I,i}(\mathbf{k})$ . The non-interacting Hamiltonian for the nucleons has a similar form as well,

$$P_0^-(\psi) = \int d^2k_\perp dk^+ \theta(k^+) \left[ \sum_{\lambda=+,-} b^\dagger(\mathbf{k}, \lambda) b(\mathbf{k}, \lambda) + d^\dagger(\mathbf{k}, \lambda) d(\mathbf{k}, \lambda) \right] \frac{k_\perp^2 + M^2}{k^+}. \quad (3.17)$$

These equations are what one expects, since a free particle with momenta  $k_\perp$  and  $k^+$  has light-front energy  $k^- = \frac{k_\perp^2 + m^2}{k^+}$ .

### 3.3 Interacting Nucleon-Nucleon Theory

The interaction Hamiltonians are derived from the Lagrangian in Eq. (3.1) using the techniques presented in chapter 2. However, there are some additional complications due to the structure of the interactions.

One complication is that the chiral coupling of the pion field to the nucleons through the  $U$  matrix generates vertices with any number of pions. This is addressed simply by expanding the  $U$  matrix in powers of  $\frac{1}{f}$ , and considering the interaction Hamiltonians order by order.

Another complication is due to the fact that both the vector mesons and the fermions have components which depend on other components of the field [18, 68–71]. Vector meson fields have four components, but only three degrees of freedom. Likewise, fermion fields have four spinor components, but only two degrees of freedom. When the dependent components are expressed explicitly in terms of the independent

components, we obtain new (effective) interaction Hamiltonians for instantaneous vector mesons and fermions. A complete derivation is given by Miller in Ref. [18], we illustrate only the main points of the derivation here.

### 3.3.1 Expanding the Pion Interaction

We start by Taylor-expanding  $U$  in powers of  $\frac{1}{f}$ , after which the derivation of the one-meson-interaction Hamiltonian  $P_{I,1}^-$  is straightforward. (The prime indicates that it is in terms of  $\psi'$ , not  $\psi$ . We derive the expressions for  $P_{I,1}^-$  in the section 3.3.2.) The result is

$$P_{I,1}^- = \int d^2x_{\perp} dx^- \bar{\psi}'(x) \left[ g_{\rho} \gamma^{\mu} \rho_{\mu,i}(x) \tau_i + g_{\omega} \gamma^{\mu} \omega_{\mu}(x) + g_{\delta} \delta_i(x) \tau_i + g_{\sigma} \sigma(x) + g_{\pi} (i\gamma_5) \tau_i \pi_i(x) + g_{\chi} (i\gamma_5) \chi(x) \right] \psi'(x). \quad (3.18)$$

We have defined a dimensionless coupling constant  $g_{\pi} \equiv \frac{M}{f}$ . To save space and to generalize, we define

$$\Gamma_{\alpha} = \begin{cases} i\gamma^5 & \text{if } \alpha \text{ is a pseudoscalar meson } (\pi, \eta) \\ 1 & \text{if } \alpha \text{ is a scalar meson } (\delta, \sigma) \\ \gamma^{\mu} & \text{if } \alpha \text{ is a vector meson } (\rho, \omega) \end{cases} \quad (3.19)$$

$$T_{\alpha} = \begin{cases} \tau_i & \text{if } \alpha \text{ is an isovector meson } (\pi, \delta, \rho) \\ 1 & \text{if } \alpha \text{ is an isoscalar meson } (\eta, \sigma, \omega) \end{cases} \quad (3.20)$$

and denote the meson fields by  $\Phi_{\alpha}$ . This allows us to write

$$P_{I,1}^- = \sum_{\alpha=\pi,\eta,\sigma,\delta,\rho,\omega} \int d^2x_{\perp} dx^- \bar{\psi}'(x) g_{\alpha} \Gamma_{\alpha} T_{\alpha} \Phi_{\alpha}(x) \psi'(x), \quad (3.21)$$

where the appropriate sums over the meson indices are implicit.

The next step is to derive the two-meson-interaction Hamiltonian which arises

from chiral symmetry,  $P'_{I,2c}$ :

$$P'_{I,2c} = \int d^2x_{\perp} dx^{-} \bar{\psi}'(x) \left[ -\frac{g_{\pi}^2}{2M} \tau_i \tau_j \pi_i(x) \pi_j(x) + \frac{g_{\pi} g_{\phi}}{M} (i\gamma^5) \tau_i \pi_i(x) \phi(x) - \frac{g_{\pi} g_{\chi}}{M} \tau_i \pi_i(x) \chi(x) \right] \psi'(x) \quad (3.22)$$

$$= \sum_{\alpha=\pi,\eta,\sigma,\delta} \frac{g_{\pi} g_{\alpha}}{M} s_{\alpha} \int d^2x_{\perp} dx^{-} \bar{\psi}'(x) [\Gamma_{\pi} T_{\pi} \Phi_{\pi}(x)] [\Gamma_{\alpha} T_{\alpha} \Phi_{\alpha}(x)] \psi'(x), \quad (3.23)$$

where  $s_{\alpha}$  is a symmetry factor, equal to  $\frac{1}{2}$  when  $\alpha = \pi$ , and 1 otherwise. When the contact interaction is used to calculate diagrams, an additional factor is picked up for the  $\pi\pi$  contact term (due to indistinguishability) which cancels the symmetry factor  $s_{\pi}$ . Note that this contact interaction involves only scalar and pseudoscalar mesons.

### 3.3.2 Elimination of Dependent Fermion Components

“It does not do to leave a dragon out of your calculations, if you live near him.”

—*J.R.R. Tolkien*

We are now ready to express the dependent components of  $\psi'$  in terms of the independent components, and address the problem of instantaneous nucleons. The generation of instantaneous interactions is a general feature of theories with interacting fermions in light-front dynamics. This allows us to use a simplified model to demonstrate how these instantaneous nucleons arise. In particular, we want to postpone the discussion of the complication introduced by the vector mesons until the next section. To this end, we choose to remove all mesons except the  $\sigma$  from the Lagrangian given in Eq. (3.1). (The  $\sigma$  is chosen since it has the simplest coupling to the nucleon.) The equation of motion for the nucleons is then

$$i\cancel{D}\psi' = (M + g_{\sigma}\sigma)\psi'. \quad (3.24)$$

Applying the projection operators  $\Lambda_{\pm} = \frac{1}{2}\gamma^0\gamma^{\pm}$  (defined in Appendix A) to Eq. (3.24) splits it into two equations,

$$i\partial^- \psi'_+ = [\boldsymbol{\alpha}_{\perp} \cdot \mathbf{p}_{\perp} + \beta(M + g_{\sigma}\sigma)]\psi'_-, \quad (3.25)$$

$$i\partial^+ \psi'_- = [\boldsymbol{\alpha}_{\perp} \cdot \mathbf{p}_{\perp} + \beta(M + g_{\sigma}\sigma)]\psi'_+, \quad (3.26)$$

where  $\psi'_{\pm} = \Lambda_{\pm}\psi'$ . This split is useful because in Eq. (3.24), all four components of the nucleon field are interrelated, while in Eqs. (3.25) and (3.26), the two components of  $\psi'_+$  are related to the two components of  $\psi'_-$ , and vice versa.

First, notice that Eq. (3.25) involves  $\partial^-$ , a dynamic operator in light-front dynamics. Dynamic operators should be avoided since they involve the interaction, and are therefore complicated. We use Eq. (3.25) to avoid that complication and relate the components of  $\psi$ . Secondly, to keep the relation as simple as possible, we do not attempt to invert the spinor matrix on the right side of Eq. (3.25). Requiring that the equation for the dependent components be both a kinematic equation and simple equation forces us to choose  $\psi'_+$  as the independent components. The dependent components,  $\psi'_-$ , are defined by

$$\psi'_- = \frac{1}{p^+} [\boldsymbol{\alpha}_{\perp} \cdot \mathbf{p}_{\perp} + \beta(M + g_{\sigma}\sigma)]\psi'_+. \quad (3.27)$$

Notice that the dependent components consist of a non-interacting part and an interacting part. We separate these parts by defining  $\psi$  (without a prime) to be the free nucleon field, and  $\xi$  to be the part of  $\psi'$  that is due to interactions. So

$$\psi' = \psi + \xi, \quad (3.28)$$

where

$$\xi = \xi_- = \frac{1}{p^+}\beta(g_{\sigma}\sigma)\psi_+ = \frac{\gamma^+}{2p^+}(g_{\sigma}\sigma)\psi_+. \quad (3.29)$$

This allows us to write

$$\psi' = \psi + \frac{\gamma^+}{2p^+}(g_{\sigma}\sigma)\psi_+ \quad (3.30)$$

$$= \psi + \frac{\gamma^+}{2p^+}(g_{\sigma}\sigma)\psi' \quad (3.31)$$

The last equation follows is obtained from noting that  $(\gamma^+)^2 = 0$ , which implies that  $\gamma^+\psi' = \gamma^+\psi_+$ .

Plugging Eq. (3.31) into Eq. (3.18) and removing all mesons except the  $\sigma$  meson, we obtain

$$P'_{I,1}^- = P_{I,1}^- + P_{I,2}^-, \quad (3.32)$$

$$P_{I,1}^- = \int d^2x_\perp dx^- \bar{\psi}(x) g_\sigma \sigma(x) \psi(x), \quad (3.33)$$

$$P_{I,2}^- = \int d^2x_\perp dx^- \bar{\psi}(x) \left[ g_\sigma \sigma(x) \frac{\gamma^+}{2p^+} g_\sigma \sigma(x) \right] \psi(x). \quad (3.34)$$

We interpret the  $\frac{\gamma^+}{2p^+}$  factor as a type of nucleon propagator that joins any two meson interactions (although having two of these propagators adjacent to each other causes the interaction to vanish since  $(\gamma^+)^2 = 0$ ). Because this propagator does not allow for an energy denominator (as it is already between two potentials),  $\frac{\gamma^+}{2p^+}$  is called an *instantaneous* propagator.

Thus, when constructing the diagrams for the light-front potentials, we must also include instantaneous propagators for the nucleons in addition to the usual propagators. (This is one of the dragons mentioned earlier.)

### 3.3.3 Elimination of Dependent Vector Meson Components

Like the nucleons, the vector mesons have a dependent component that contains interactions and must be eliminated. This process is complicated somewhat by the fact that the dependent nucleon components must be eliminated at the same time. The salient points of the combined elimination of the dependent nucleon and vector meson components are discussed in detail by Miller [18].

The result is that the vector meson field must be redefined and an instantaneous vector meson propagator is generated in addition to an instantaneous nucleon propagator. However, when the nucleon-nucleon potential is calculated, the redefinition of the vector meson field exactly cancels the contribution of the instantaneous vector

meson. The result is that the potentials can formally be calculated using the original vector meson field.

In this work, we use that result to simplify our derivations of nucleon-nucleon potentials by formally using the naïve form of the vector meson field. Thus, we find an interaction Hamiltonian similar to the one shown in Eq. (3.34),

$$P'_{I,1}{}^- = P_{I,1}^- + P_{I,2}^-, \quad (3.35)$$

$$P_{I,1}^- = \sum_{\alpha=\pi,\eta,\sigma,\delta,\rho,\omega} \int d^2x_\perp dx^- \bar{\psi}(x) g_\alpha \Gamma_\alpha T_\alpha \Phi_\alpha(x) \psi(x), \quad (3.36)$$

$$P_{I,2}^- = \sum_{\alpha_1,\alpha_2=\pi,\eta,\sigma,\delta,\rho,\omega} \int d^2x_\perp dx^- \bar{\psi}(x) [g_{\alpha_1} \Gamma_{\alpha_1} T_{\alpha_1} \Phi_{\alpha_1}(x)] \frac{\gamma^+}{2p^+} [g_{\alpha_2} \Gamma_{\alpha_2} T_{\alpha_2} \Phi_{\alpha_2}(x)] \psi(x). \quad (3.37)$$

We may continue to interpret  $\frac{\gamma^+}{2p^+}$  as an instantaneous nucleon propagator, since in the derivation in Ref. [18] it is clear that the potential vanishes when there are two adjacent instantaneous propagators. In Refs. [18,55], sign of the coupling of the vector mesons in the equations equivalent to Eq. (3.37) has the wrong sign; the coupling of the mesons in Eq. (3.37) must be the same as in Eq. (3.36).

Also note that in principle the same prescription has to be applied to the contact interaction, although to the order of two mesons, this simply has the effect of removing the primes. We find that

$$P_{I,2c}^- = \sum_{\alpha=\pi,\eta,\sigma,\delta} \frac{s_\alpha}{M} \int d^2x_\perp dx^- \bar{\psi}(x) [g_\pi \Gamma_\pi T_\pi \Phi_\pi(x)] [g_\alpha \Gamma_\alpha T_\alpha \Phi_\alpha(x)] \psi(x). \quad (3.38)$$

Note that  $P_{I,2c}^-$  and  $P_{I,2}^-$  have forms that are very similar. In fact, we can obtain  $P_{I,2c}^-$  from  $P_{I,2}^-$  by making the following changes:

1. Replace  $\frac{\gamma^+}{2p^+}$  with  $\frac{s_\alpha}{M}$ .
2. Replace  $\alpha_1$  with  $\pi$ .
3. Restrict the sum on  $\alpha_2$  to  $\pi, \eta, \sigma, \delta$ .

### 3.3.4 Interaction Hamiltonians in Momentum Space

We look at the matrix element of the interaction Hamiltonians between initial and final states given by  $|k_i, \lambda_i, \tau_i\rangle = b^\dagger(k_i, \lambda_i)\chi_{\tau_i}|0\rangle$  and  $\langle k_f, \lambda_f, \tau_f| = \langle 0|b(k_f, \lambda_f)\chi_{\tau_f}^\dagger$  where both the bra and the ket have units of  $[M^{-3/2}]$ . We find that

$$P_{I,1}^-(f, i) = \sum_{\alpha=\pi,\eta,\sigma,\delta,\rho,\omega} \frac{g_\alpha 2M}{2(2\pi)^3 \sqrt{k_f^+ k_i^+}} \int \frac{d^2 q_\perp dq^+ \theta(q^+)}{\sqrt{2(2\pi)^3} \sqrt{q^+}} \bar{u}(\mathbf{k}_f, \lambda_f) \Gamma_\alpha u(\mathbf{k}_i, \lambda_i) \chi_{\tau_f}^\dagger T_\alpha \chi_{\tau_i} \int d^2 x_\perp dx^- e^{+ik_f^\mu x_\mu} e^{-ik_i^\mu x_\mu} [a_\alpha(\mathbf{q}) e^{-iq^\mu x_\mu} + a_\alpha^\dagger(\mathbf{q}) e^{+iq^\mu x_\mu}] F_\alpha(\mathbf{q}), \quad (3.39)$$

where  $\mathbf{q} = (q^+, \mathbf{q}_\perp)$  and there are implicit  $\theta$ -functions on  $q^+$  for each particle to ensure that the light-front energy is positive. These are occasionally suppressed to simplify the equations. We include a meson-nucleon form factor  $F_\alpha$  to phenomenologically account for the fact that the mesons and nucleons are composite objects.

Now, we evaluate  $P^-$  at  $x^+ = 0$  and use

$$\int d^2 x_\perp dx^- e^{i(k_f - k_i - q)^\mu x_\mu} = 2(2\pi)^3 \delta^{(2,+)}(k_f - k_i - q), \quad (3.40)$$

to write

$$P_{I,1}^-(f, i) = \sum_{\alpha=\pi,\eta,\sigma,\delta,\rho,\omega} g_\alpha 2M \frac{\bar{u}(\mathbf{k}_f, \lambda_f) \Gamma_\alpha u(\mathbf{k}_i, \lambda_i)}{\sqrt{2(2\pi)^3} \sqrt{k_f^+ k_i^+ q^+}} \chi_{\tau_f}^\dagger T_\alpha \chi_{\tau_i} [a_\alpha(\mathbf{q}) \theta(k_f^+ - k_i^+) + a_\alpha^\dagger(\mathbf{q}) \theta(-(k_f^+ - k_i^+))] F_\alpha(\mathbf{q}). \quad (3.41)$$

We define  $\mathbf{q} \equiv \text{sign}(k_f^+ - k_i^+) (\mathbf{k}_f - \mathbf{k}_i)$ , which ensures that the  $q^+$  of the meson is positive.

Next we consider the two-meson interactions. First take the interaction with the

instantaneous propagator given by Eq. (3.37). Plugging in the field definitions gives

$$\begin{aligned}
P_{I,2}^-(f, i) &= \sum_{\alpha_1, \alpha_2 = \pi, \eta, \sigma, \delta, \rho, \omega} \frac{g_{\alpha_1} g_{\alpha_2} 2M}{2(2\pi)^3 \sqrt{k_f^+ k_i^+}} \int \frac{d^2 q_{1\perp} dq_1^+ \theta(q_1^+)}{(2\pi)^{3/2} \sqrt{2q_1^+}} \int \frac{d^2 q_{2\perp} dq_2^+ \theta(q_2^+)}{(2\pi)^{3/2} \sqrt{2q_2^+}} \\
&\quad \frac{\theta(k_m^+)}{2k_m^+} \bar{u}(\mathbf{k}_f, \lambda_f) \Gamma_{\alpha_2} \gamma^+ \Gamma_{\alpha_1} u(\mathbf{k}_i, \lambda_i) \chi_{\tau_f}^\dagger T_{\alpha_2} T_{\alpha_1} \chi_{\tau_i} \\
&\quad \int d^2 x_\perp dx^- e^{+ik_f^\mu x_\mu} e^{-ik_i^\mu x_\mu} \left[ a_{\alpha_2}(\mathbf{q}_2) e^{-iq_2^\mu x_\mu} + a_{\alpha_2}^\dagger(\mathbf{q}_2) e^{+iq_2^\mu x_\mu} \right] F_{\alpha_2}(\mathbf{q}_2) \\
&\quad \left[ a_{\alpha_1}(\mathbf{q}_1) e^{-iq_1^\mu x_\mu} + a_{\alpha_1}^\dagger(\mathbf{q}_1) e^{+iq_1^\mu x_\mu} \right] F_{\alpha_1}(\mathbf{q}_1) \tag{3.42}
\end{aligned}$$

$$\begin{aligned}
&= \sum_{\alpha_1, \alpha_2 = \pi, \eta, \sigma, \delta, \rho, \omega} g_{\alpha_1} g_{\alpha_2} 2M \frac{\bar{u}(\mathbf{k}_f, \lambda_f) \Gamma_{\alpha_2} \gamma^+ \Gamma_{\alpha_1} u(\mathbf{k}_i, \lambda_i)}{2(2\pi)^3 \sqrt{k_f^+ k_i^+}} \\
&\quad \left[ \chi_{\tau_f}^\dagger T_{\alpha_2} T_{\alpha_1} \chi_{\tau_i} \right] \int \frac{d^2 k_{m\perp} dk_m^+ \theta(k_m^+)}{2k_m^+ \sqrt{q_1^+ q_2^+}} \\
&\quad \left[ a_{\alpha_2}(k_f - k_m) \theta(k_f^+ - k_m^+) + a_{\alpha_2}^\dagger(k_m - k_f) \theta(k_m^+ - k_f^+) \right] F_{\alpha_2}(\mathbf{q}_2) \\
&\quad \left[ a_{\alpha_1}(k_m - k_i) \theta(k_m^+ - k_i^+) + a_{\alpha_1}^\dagger(k_i - k_m) \theta(k_i^+ - k_m^+) \right] F_{\alpha_1}(\mathbf{q}_1) \tag{3.43}
\end{aligned}$$

Note that the momenta  $q_1$  and  $q_2$  are implicitly functions of the momenta  $k_f$ ,  $k_m$ , and  $k_i$ .

We could also write out the contact interaction given by Eq. (3.38) in momentum space, but it is related to Eq. (3.43) by replacing  $\frac{\theta(p^+) \gamma^+}{2p^+}$  with  $\frac{s_\alpha}{M}$  and restricting the allowed values of the  $\alpha$ 's.

### 3.4 Feynman Rules for Nucleon-Nucleon Potentials

Now that we have the one-meson- and two-meson-exchange expressed in momentum space, we are now ready to write out the Feynman rules for diagrams in our model. For simplicity, the only diagrams considered are those where a meson emitted by one nucleon is absorbed by the other nucleon. Since we are only interested in the two-nucleon to two-nucleon potentials, we follow the same approach as outlined in section 2.1.2 to derive the rules. We denote a ‘‘normal’’ nucleon propagator by a solid line with an arrow, an instantaneous nucleon propagator by a solid line with a stroke

across it, mesons of all type by a dashed line, and energy denominator terms by a vertical, light, dotted line.

1. Overall factor of  $\frac{4M^2\delta^{\perp,+}(P_f-P_i)}{2(2\pi)^3\sqrt{k_{1f}^+k_{2f}^+k_{1i}^+k_{2i}^+}}$ .
2. Usual light-front rules for  $p_\perp$  and  $p^+$  momentum conservation.
3. Factor of  $\frac{\theta(q_i)}{q_i}$  for each internal line, including any instantaneous nucleon lines.
4. A factor of  $\frac{1}{P^--\sum_i q_i^-}$  for each energy denominator.
5. Each meson connects the two nucleons, and each end of the meson line has a factor of  $g_\alpha\Gamma_\alpha T_\alpha F_\alpha(q)$ . The indices of the isospin factors on each end of the meson are contracted together. The Lorentz indices of the gamma matrices are contracted with  $-g^{\mu\nu}$  for the vector mesons.
6. For each contact vertex, multiply by a factor of  $\frac{1}{M}$ . If the vertex is a  $\pi - \pi$  vertex, symmetrize the  $T_\pi T_\pi = \tau_i\tau_j$  by replacing it with  $\delta_{i,j}$ .
7. Factor of  $\frac{k^+M}{2M} = \sum_\lambda u(k, \lambda)\bar{u}(k, \lambda)$  for each propagating nucleon and  $\frac{\gamma^+}{2}$  for an instantaneous nucleon.
8. Integrate with  $4M^2 \int \frac{d^2k_\perp dk^+}{2(2\pi)^3}$  over any internal momentum loops.
9. Put the spinor factors for nucleon 1 and 2 between  $\bar{u}u$ 's and the isospin factors between the initial and final state isospin.

From this list, it is useful to summarize what needs to be done to convert a graph with an instantaneous nucleon to one with a contact interaction:

1. Replace  $\frac{\theta(k^+)\gamma^+}{k^+}$  with  $\frac{1}{M}$ .
2. If both mesons are pions, replace  $T_i T_j$  with  $\delta_{i,j}$ .

These rules make it easy to write down what various potentials are.

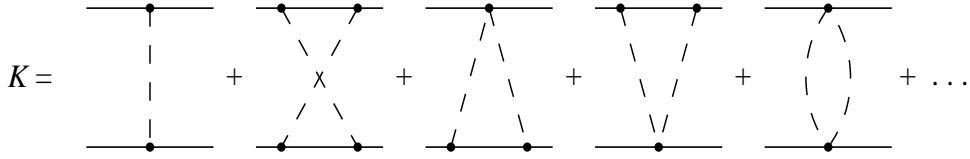


Figure 3.1: The first several terms of the full kernel for the Bethe-Salpeter equation of the nuclear model with chiral symmetry.

### 3.5 Nucleon-Nucleon Perturbative Potentials

The meson exchange potentials have the same basic form as in Section 2.1.2, however we must include the contact interaction and instantaneous nucleon propagators for the nuclear model used here. First, we discuss how to include the contact diagrams from the standpoint of the Bethe-Salpeter equation to maintain chiral symmetry, then we begin to calculate the light-front potentials.

#### 3.5.1 The Bethe-Salpeter Equation

The kernel of the Bethe-Salpeter equation [3–7] for this nuclear model is richer than the one presented in section 2.1.4 for the Wick-Cutkosky model. This is due mainly to the presence of the contact interactions which are generated by the chirally invariant coupling of the pion to the nucleon. Several of the lowest-order pieces of the full kernel  $K$  are shown in Fig. 3.1. (Note that for Feynman diagrams, it is useful to combine the “normal” nucleon propagator with the instantaneous nucleon propagator [72–74], and denote the combination with a solid line.)

As discussed in section 2.1.4, each of these Feynman diagrams is covariant. This means that we may choose any of the diagrams from  $K$  to construct a new kernel  $K'$ , and the infinite series of potential diagrams physically equivalent (Sec. 2.1.5) to  $K'$  will also be covariant.

In practice, this means that when deciding which two-meson-exchange potentials

to include for calculating the deuteron wave function, we may neglect the crossed diagrams. Although including only the box and contact two-meson-exchange diagrams may affect the exact binding energy calculated, we should find a partial restoration of rotational invariance. We reiterate that the focus of this work is on understanding the effects of the breaking of rotational invariance and how to restore it; our goal is not precise agreement with experimental results.

### *Chiral Symmetry*

We also want to keep the potentials chirally symmetric as well. Whereas Lorentz symmetry is maintained by using a kernel with any Feynman diagrams (with potentially arbitrary coefficients), chiral symmetry relates the strength of the  $\pi\pi$  contact interaction to the strength of the pion-nucleon coupling.

Chiral symmetry tells us that for pion-nucleon scattering at threshold, the time-ordered graphs approximately cancel [18]. Furthermore, upon closer examination, we find that all the light-front time-ordered graphs for the scattering amplitude vanish except for the two graphs with instantaneous nucleons and the contact graph. These graphs are shown in Fig. 3.2. Using the Feynman rules, and denoting the nucleon momentum by  $k$  and the pion momentum by  $q$ , we find that

$$\mathcal{M}_U = C \frac{\tau_i \tau_j}{2(k^+ + q^+)} u(k') \gamma^+ u(k), \quad (3.44)$$

$$\mathcal{M}_X = C \frac{\tau_j \tau_i}{2(k^+ - q^+)} u(k') \gamma^+ u(k), \quad (3.45)$$

$$\mathcal{M}_C = C \frac{-\delta_{ij}}{M} u(k') u(k), \quad (3.46)$$

where the factors common to all amplitudes are denoted by  $C$ .

For threshold scattering, we take  $k = k' = M$  and  $q = q' = m_\pi$ . In that limit, we

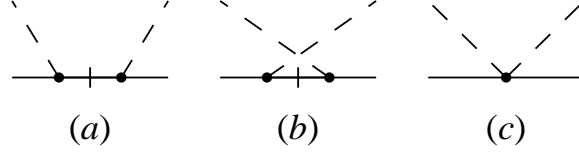


Figure 3.2: The non-vanishing diagrams for pion-nucleon scattering at threshold: (a)  $\mathcal{M}_U$ , (b)  $\mathcal{M}_X$ , and (c)  $\mathcal{M}_C$ . The mesons here are pions.

find

$$\mathcal{M}_U = C' \frac{\delta_{i,j} + i\epsilon_{i,j,k}\tau_k}{2(M + m_\pi)}, \quad (3.47)$$

$$\mathcal{M}_X = C' \frac{\delta_{i,j} - i\epsilon_{i,j,k}\tau_k}{2(M - m_\pi)}, \quad (3.48)$$

$$\mathcal{M}_C = C' \frac{-\delta_{i,j}}{M}, \quad (3.49)$$

where  $C' = C\bar{u}(k')u(k)$ . In the limit that  $m_\pi \rightarrow 0$ , the sum of these three terms vanishes. The term in these equations proportional to  $\tau_k$  is the famous Weinberg-Tomazowa term [75, 76].

The fact that the amplitudes cancel only when the contact interaction is included demonstrates that chiral symmetry can have a significant effect on calculations. In terms of two-pion-exchange potentials, this result means that the contact potentials cancel strongly with both the iterated box potentials and the crossed potentials. This serves to reduce the strength of the total two-pion-exchange potential, which should lead to more stable results.

However, since we do not use the crossed graphs for the nucleon-nucleon potential, we must come up with a prescription which divides the contact interactions into two parts which cancel the box and crossed diagrams separately. We do this by formally defining two new contact interactions, so that

$$\mathcal{M}_{C_U} \equiv \frac{M}{2(M + m_\pi)} \mathcal{M}_C, \quad (3.50)$$

$$\mathcal{M}_{C_X} \equiv \mathcal{M}_C - \mathcal{M}_{C_U}. \quad (3.51)$$

$$V_{\text{OME}} = \left( \begin{array}{c} k_{1f} \leftarrow \bullet \leftarrow k_{1i} \\ q = k_{1f} - k_{1i} \\ k_{2f} \leftarrow \bullet \leftarrow k_{2i} \end{array} \right) + \left( \begin{array}{c} k_{1f} \leftarrow \bullet \leftarrow k_{1i} \\ q = k_{1i} - k_{1f} \\ k_{2f} \leftarrow \bullet \leftarrow k_{2i} \end{array} \right)$$

Figure 3.3: The two diagrams which contribute to the OME potential for each meson.

With these definitions, we find that at threshold and in the chiral limit,

$$\mathcal{M}_U + \mathcal{M}_{C_U} = 0, \quad (3.52)$$

$$\mathcal{M}_X + \mathcal{M}_{C_X} = 0. \quad (3.53)$$

This indicates that we can incorporate approximate chiral symmetry without including crossed graphs simply by weighting each graph with a contact interaction by a factor of  $\frac{M}{2(M+m_\pi)}$ .

### 3.5.2 OME Potential

The one meson exchange (OME) potential connects an initial state with two nucleons to a final state with two nucleons, has one meson in the intermediate state, and has the meson emitted and absorbed by different nucleons. With these restrictions, along with the fact that in light-front dynamics the interaction does not allow for particles to be created from the vacuum, we find that there each meson has only two diagrams for the OME potential. These diagrams are shown in Fig. 3.3.

Note that chiral symmetry does not impose restrictions when considering the OME potential alone. It does affect the TME potentials considered, as discussed in the following section.

The Feynman rules derived in the previous section are used to derive the potential for these diagrams. We factor out an overall factor of  $\frac{4M^2\delta(k_{1f}+k_{2f}-k_{1i}-k_{2i})}{2\sqrt{k_{1f}^+k_{1i}^+k_{2f}^+k_{2i}^+}}$  that is

common to all the two-nucleon potentials and suppress it from now on. Then we get

$$V_{\text{OME},\alpha} = \frac{g_\alpha^2 \mathbf{T}_{\alpha,1} \cdot \mathbf{T}_{\alpha,2}}{(2\pi)^3} \bar{u}(\mathbf{k}_{1f}, \lambda_{1f}) \Gamma_\alpha u(\mathbf{k}_{1i}, \lambda_{1i}) \bar{u}(\mathbf{k}_{2f}, \lambda_{2f}) \Gamma_\alpha u(\mathbf{k}_{2i}, \lambda_{2i}) F_\alpha^2(\mathbf{q})$$

$$\left[ \frac{\theta(k_{1f}^+ - k_{1i}^+)}{(k_{1f}^+ - k_{1i}^+)(P^- - k_{1i}^- - k_{2f}^-) - m_\alpha^2 - (k_{1i,\perp} - k_{1f,\perp})^2} + \frac{\theta(k_{1i}^+ - k_{1f}^+)}{(k_{1i}^+ - k_{1f}^+)(P^- - k_{1f}^- - k_{2i}^-) - m_\alpha^2 - (k_{1i,\perp} - k_{1f,\perp})^2} \right]. \quad (3.54)$$

To simplify the potential, we define

$$a \equiv [\theta(k_{1f}^+ - k_{1i}^+) \times (k_{1f}^+ - k_{1i}^+)(P^- - k_{1i}^- - k_{2f}^-) + \theta(k_{1i}^+ - k_{1f}^+) \times (k_{1i}^+ - k_{1f}^+)(P^- - k_{1f}^- - k_{2i}^-)] - k_{i,\perp}^2 - k_{f,\perp}^2, \quad (3.55)$$

$$b \equiv 2k_{i,\perp} k_{f,\perp}, \quad (3.56)$$

so

$$V_{\text{OME},\alpha} = \frac{g_\alpha^2 \mathbf{T}_{\alpha,1} \cdot \mathbf{T}_{\alpha,2}}{(2\pi)^3} F_\alpha(\mathbf{q})^2 \frac{\bar{u}(\mathbf{k}_{1f}, \lambda_{1f}) \Gamma_\alpha u(\mathbf{k}_{1i}, \lambda_{1i}) \bar{u}(\mathbf{k}_{2f}, \lambda_{2f}) \Gamma_\alpha u(\mathbf{k}_{2i}, \lambda_{2i})}{[a - m_\alpha^2 + b \cos(\phi_f - \phi_i)]}. \quad (3.57)$$

Now we consider the precise form to use for the meson-nucleon form factor. We assume that it has a  $n$ -pole form [58], so that the denominator of the meson-nucleon form factor has the same form as the denominator of the potential in the scattering regime. In particular,  $\Lambda_\alpha$  playing the role of  $m_\alpha$  for the form factor. For simplicity, we choose that the denominator of the form factor has the same form of the denominator of the potential. Thus,

$$F_\alpha(\mathbf{q}) = \left( \frac{\Lambda_\alpha^2 - m_\alpha^2}{a - \Lambda_\alpha^2 + b \cos(\phi_f - \phi_i)} \right)^{n_\alpha}. \quad (3.58)$$

Inserting the explicit expression of for the meson-nucleon form factor into the potential results in

$$V_{\text{OME},\alpha} = \frac{g_\alpha^2 \mathbf{T}_{\alpha,1} \cdot \mathbf{T}_{\alpha,2}}{(2\pi)^3} (\Lambda_\alpha^2 - m_\alpha^2)^{2n_\alpha} \frac{\bar{u}(\mathbf{k}_{1f}, \lambda_{1f}) \Gamma_\alpha u(\mathbf{k}_{1i}, \lambda_{1i}) \bar{u}(\mathbf{k}_{2f}, \lambda_{2f}) \Gamma_\alpha u(\mathbf{k}_{2i}, \lambda_{2i})}{[a - m_\alpha^2 + b \cos(\phi_f - \phi_i)] [a - \Lambda_\alpha^2 + b \cos(\phi_f - \phi_i)]^{2n_\alpha}}. \quad (3.59)$$

Now, since the light-front potentials have exact rotational invariance about the  $z$ -axis, they conserve the  $J_z$  quantum number  $m$ . Thus, these potentials connect only states with the same value of  $m$ . This means that, in general, light-front potentials may be written as

$$V(\phi_f, \phi_i) = \sum_{m=-\infty}^{\infty} e^{im(\phi_i - \phi_f)} V^m, \quad (3.60)$$

where  $V^m$  is the potential in the magnetic quantum number basis. This relation can be inverted to obtain  $V^m$  in terms of  $V(\phi_f, \phi_i)$ ,

$$V_{\text{OME},\alpha}^m = \frac{g_\pi^2 \mathbf{T}_{\alpha,1} \cdot \mathbf{T}_{\alpha,2}}{(2\pi)^3} (\Lambda_\alpha^2 - m_\alpha^2)^{2n_\alpha} \int \frac{d\phi_f}{2\pi} e^{im\phi_f} \frac{[\bar{u}(\mathbf{k}_{1f}, \lambda_{1f}) \Gamma_\alpha u(\mathbf{k}_{1i}, \lambda_{1i}) \bar{u}(\mathbf{k}_{2f}, \lambda_{2f}) \Gamma_\alpha u(\mathbf{k}_{2i}, \lambda_{2i})]_{\phi_i=0}}{[a - m_\alpha^2 + b \cos(\phi_f)] [a - \Lambda_\alpha^2 + b \cos(\phi_f)]^{2n_\alpha}}. \quad (3.61)$$

To perform the integration, we need an expression for  $\phi_f$  dependence the  $\bar{u}u$  matrix elements. These are calculated in Appendix F. Summarizing, we can write

$$\bar{u}(\mathbf{k}_{1f}, \lambda_{1f}) \Gamma_\alpha u(\mathbf{k}_{1i}, \lambda_{1i}) \bar{u}(\mathbf{k}_{2f}, \lambda_{2f}) \Gamma_\alpha u(\mathbf{k}_{2i}, \lambda_{2i}) = \sum_j C_j(\Gamma_\alpha, \Gamma_\alpha) e^{ij\phi_f}, \quad (3.62)$$

where the  $C$  depends implicitly on all the variables on the left-hand side except  $\phi_f$  and  $\phi_i$ .

Thus,

$$V_{\text{OME},\alpha}^m = g_\alpha^2 (\mathbf{T}_{\alpha,1} \cdot \mathbf{T}_{\alpha,2}) \frac{(\Lambda_\alpha^2 - m_\alpha^2)^{2n_\alpha}}{(2\pi)^3} \sum_j C_j(\Gamma_\alpha, \Gamma_\alpha) \int \frac{d\phi_f}{2\pi} \frac{e^{i(m+j)\phi_f}}{[a - m_\alpha^2 + b \cos(\phi_f)] [a - \Lambda_\alpha^2 + b \cos(\phi_f)]^{2n_\alpha}}. \quad (3.63)$$

The cosine integral is denoted by  $I$ , and is calculated in Appendix D. Substituting  $I$  for the integral, we obtain

$$V_{\text{OME},\alpha}^m = g_\alpha^2 (\mathbf{T}_{\alpha,1} \cdot \mathbf{T}_{\alpha,2}) \frac{(\Lambda_\alpha^2 - m_\alpha^2)^{2n_\alpha}}{(2\pi)^3} \sum_j C_j(\Gamma_\alpha, \Gamma_\alpha) I(m+j, a - m_\alpha^2, 1, a - \Lambda_\alpha^2, 2n_\alpha, b). \quad (3.64)$$

All of the terms in Eq. (3.64) are known, and the potential can now be calculated numerically.

### 3.5.3 TME Potentials

The two-meson-exchange (TME) potentials consider here are the box diagrams (see Fig. 3.4) and the contact diagrams (see Fig. 3.5). We do not consider the crossed diagrams because they are not needed to restore rotational invariance, as shown in Section 3.5.1. We derive a few TME potentials to illustrate the general form that they take.

#### Stretched Box Potential

We use the Feynman rules to write the stretched-box potential shown in Fig. 3.4(b),

$$\begin{aligned}
V_{\text{TME:SB}}^{\alpha_f, \alpha_i} &= \frac{g_{\alpha_f}^2 g_{\alpha_i}^2 4M^2 [\mathbf{T}_{\alpha_f,1} \cdot \mathbf{T}_{\alpha_f,2}] [\mathbf{T}_{\alpha_i,1} \cdot \mathbf{T}_{\alpha_i,2}]}{(2\pi)^3} \int \frac{d^2 k_{2m\perp} dk_{2m}^+}{2(2\pi)^3 k_{1m}^+ k_{2m}^+} \\
& {}_{1f} \langle \left( \Gamma_{\alpha_f} \frac{k_{1m} + M}{2M} \Gamma_{\alpha_i} \right) \rangle_{1m} \times {}_{2f} \langle \left( \Gamma_{\alpha_f} \frac{k_{2m} + M}{2M} \Gamma_{\alpha_i} \right) \rangle_{2m} \\
& \theta(k_{1m}^+) \theta(k_{2m}^+) \theta(k_{2i}^+ - k_{2m}^+) \theta(k_{2m}^+ - k_{2f}^+) \\
& \frac{F_{\alpha_f}(\mathbf{q}_f)^2}{(k_{2m}^+ - k_{2f}^+) (P^- - k_{1m}^- - k_{2f}^-) - m_{\alpha_f}^2 - (\mathbf{k}_{1f\perp} - \mathbf{k}_{1m\perp})^2} \\
& \frac{1}{P^- - k_{1i}^- - k_{2f}^- - q_f^- - q_i^-} \\
& \frac{F_{\alpha_i}(\mathbf{q}_i)^2}{(k_{2i}^+ - k_{2m}^+) (P^- - k_{1i}^- - k_{2m}^-) - m_{\alpha_i}^2 - (\mathbf{k}_{1m\perp} - \mathbf{k}_{1i\perp})^2} \\
& + \{1 \leftrightarrow 2\}. \tag{3.65}
\end{aligned}$$

To compress notation, we defined  ${}_{1f} \langle \equiv \bar{u}(\mathbf{k}_{1f}, \lambda_{1f}) \rangle$ ,  $\rangle_{1i} \equiv u(\mathbf{k}_{1i}, \lambda_{1i})$ , and so on. The symbol  $\{1 \leftrightarrow 2\}$  means that all labels 1 are replaced with 2 and vice versa. This is a way of explicitly stating the potential is invariant under exchange of nucleons 1 and 2.

We also used the following relation to simplify Eq. (3.65):

$$\begin{aligned}
& \sum_{\tau_{2m}} \chi_{\tau_{2f}}^\dagger T_{\alpha_f, j} \chi_{\tau_{2m}} \chi_{\tau_{2m}}^\dagger T_{\alpha_i, i} \chi_{\tau_{2i}} \chi_{\tau_{1f}}^\dagger T_{\alpha_f, j} \chi_{\tau_{1m}} \chi_{\tau_{1m}}^\dagger T_{\alpha_i, i} \chi_{\tau_{1i}} \\
& = \langle \tau_f | [\mathbf{T}_{\alpha_f,1} \cdot \mathbf{T}_{\alpha_f,2}] [\mathbf{T}_{\alpha_i,1} \cdot \mathbf{T}_{\alpha_i,2}] | \tau_i \rangle \\
& = [\mathbf{T}_{\alpha_f,1} \cdot \mathbf{T}_{\alpha_f,2}] [\mathbf{T}_{\alpha_i,1} \cdot \mathbf{T}_{\alpha_i,2}]. \tag{3.66}
\end{aligned}$$



$$\begin{aligned}
(a) \quad V_{\text{TME:C}} &= \left( \begin{array}{c} \begin{array}{c} k_{1f} \leftarrow \text{---} \text{---} \text{---} \leftarrow k_{1i} \\ q_f = k_{2f} - k_{2m} / \quad \backslash \quad q_i = k_{2i} - k_{2m} \\ \text{---} \text{---} \text{---} \leftarrow k_{2i} \\ k_{2f} \leftarrow \text{---} \text{---} \text{---} \leftarrow k_{2i} \\ k_{2m} \end{array} & + & \begin{array}{c} k_{1f} \leftarrow \text{---} \text{---} \text{---} \leftarrow k_{1i} \\ q_f = k_{1i} - k_{1m} / \quad \backslash \quad q_i = k_{1i} - k_{1m} \\ \text{---} \text{---} \text{---} \leftarrow k_{2i} \\ k_{2f} \leftarrow \text{---} \text{---} \text{---} \leftarrow k_{2i} \\ k_{1m} \end{array} \end{array} \right) \\
(b) \quad V_{\text{TME:SBC}} &= \left( \begin{array}{c} \begin{array}{c} k_{1f} \leftarrow \text{---} \text{---} \text{---} \leftarrow k_{1i} \\ q_f = k_{2m} - k_{2f} / \quad \backslash \quad q_i = k_{2i} - k_{2m} \\ \text{---} \text{---} \text{---} \leftarrow k_{2i} \\ k_{2f} \leftarrow \text{---} \text{---} \text{---} \leftarrow k_{2i} \\ k_{2m} \end{array} & + & \begin{array}{c} k_{1f} \leftarrow \text{---} \text{---} \text{---} \leftarrow k_{1i} \\ q_f = k_{1m} - k_{1f} / \quad \backslash \quad q_i = k_{1i} - k_{1m} \\ \text{---} \text{---} \text{---} \leftarrow k_{2i} \\ k_{2f} \leftarrow \text{---} \text{---} \text{---} \leftarrow k_{2i} \\ k_{1m} \end{array} \\ + & \left( \begin{array}{c} \begin{array}{c} k_{1f} \leftarrow \text{---} \text{---} \text{---} \leftarrow k_{1i} \\ q_f = k_{1f} - k_{1m} / \quad \backslash \quad q_i = k_{1m} - k_{1i} \\ \text{---} \text{---} \text{---} \leftarrow k_{2i} \\ k_{2f} \leftarrow \text{---} \text{---} \text{---} \leftarrow k_{2i} \\ k_{1m} \end{array} & + & \begin{array}{c} k_{1f} \leftarrow \text{---} \text{---} \text{---} \leftarrow k_{1i} \\ q_f = k_{2f} - k_{2m} / \quad \backslash \quad q_i = k_{2m} - k_{2i} \\ \text{---} \text{---} \text{---} \leftarrow k_{2i} \\ k_{2f} \leftarrow \text{---} \text{---} \text{---} \leftarrow k_{2i} \\ k_{2m} \end{array} \end{array} \right) \\
(c) \quad V_{\text{TME:SBIC}} &= \left( \begin{array}{c} \begin{array}{c} k_{1f} \leftarrow \text{---} \text{---} \text{---} \leftarrow k_{1i} \\ q_f = k_{1f} - k_{1m} / \quad \backslash \quad q_i = k_{1m} - k_{1i} \\ \text{---} \text{---} \text{---} \leftarrow k_{2i} \\ k_{2f} \leftarrow \text{---} \text{---} \text{---} \leftarrow k_{2i} \\ k_{1m} \end{array} & + & \begin{array}{c} k_{1f} \leftarrow \text{---} \text{---} \text{---} \leftarrow k_{1i} \\ q_f = k_{2f} - k_{2m} / \quad \backslash \quad q_i = k_{2m} - k_{2i} \\ \text{---} \text{---} \text{---} \leftarrow k_{2i} \\ k_{2f} \leftarrow \text{---} \text{---} \text{---} \leftarrow k_{2i} \\ k_{2m} \end{array} \\ + & \left( \begin{array}{c} \begin{array}{c} k_{1f} \leftarrow \text{---} \text{---} \text{---} \leftarrow k_{1i} \\ q_f = k_{2m} - k_{2f} / \quad \backslash \quad q_i = k_{2i} - k_{2m} \\ \text{---} \text{---} \text{---} \leftarrow k_{2i} \\ k_{2f} \leftarrow \text{---} \text{---} \text{---} \leftarrow k_{2i} \\ k_{2m} \end{array} & + & \begin{array}{c} k_{1f} \leftarrow \text{---} \text{---} \text{---} \leftarrow k_{1i} \\ q_f = k_{1m} - k_{1f} / \quad \backslash \quad q_i = k_{1i} - k_{1m} \\ \text{---} \text{---} \text{---} \leftarrow k_{2i} \\ k_{2f} \leftarrow \text{---} \text{---} \text{---} \leftarrow k_{2i} \\ k_{1m} \end{array} \end{array} \right) \\
(d) \quad V_{\text{TME:SBCC}} &= \left( \begin{array}{c} \begin{array}{c} k_{1f} \leftarrow \text{---} \text{---} \text{---} \leftarrow k_{1i} \\ q_f / \quad \backslash \quad q_i \\ \text{---} \text{---} \text{---} \leftarrow k_{2i} \\ k_{2f} \leftarrow \text{---} \text{---} \text{---} \leftarrow k_{2i} \end{array} & + & \begin{array}{c} k_{1f} \leftarrow \text{---} \text{---} \text{---} \leftarrow k_{1i} \\ q_f / \quad \backslash \quad q_i \\ \text{---} \text{---} \text{---} \leftarrow k_{2i} \\ k_{2f} \leftarrow \text{---} \text{---} \text{---} \leftarrow k_{2i} \end{array} \end{array} \right)
\end{aligned}$$

Figure 3.5: The TME potentials that include the contact interaction for (a)  $V_{\text{TME:C}}$  (the contact potential), (b)  $V_{\text{TME:SBC}}$  (the stretched contact potential), (c)  $V_{\text{TME:SBIC}}$  (the stretched instantaneous contact potential), and (d)  $V_{\text{TME:SBCC}}$  (the stretched double contact potential). Note that the graphs on the right side are obtained from the graphs on the left side by relabeling  $1 \leftrightarrow 2$ .

### Mesa Potential

We consider the Mesa potential next,  $V_{\text{TME:M}}$ , shown in Fig. 3.4(a). This is one of the potentials which is due to the instantaneous nucleon, a feature not found in the Wick-Cutkosky model. Using the Feynman rules results in

$$\begin{aligned}
V_{\text{TME:M}}^{\alpha_f, \alpha_i} &= \frac{g_{\alpha_f}^2 g_{\alpha_i}^2 4M^2 [\mathbf{T}_{\alpha_f,1} \cdot \mathbf{T}_{\alpha_f,2}] [\mathbf{T}_{\alpha_i,1} \cdot \mathbf{T}_{\alpha_i,2}]}{(2\pi)^3} \int \frac{d^2 k_{2m\perp} dk_{2m}^+}{2(2\pi)^3 k_{1m}^+ k_{2m}^+} \\
& {}_{1f} \langle \left( \Gamma_{\alpha_f} \frac{\gamma^+}{2} \Gamma_{\alpha_i} \right) \rangle_{1m} \times {}_{2f} \langle \left( \Gamma_{\alpha_f} \frac{k_{2m}^+ + M}{2M} \Gamma_{\alpha_i} \right) \rangle_{2m} \\
& \theta(k_{1m}^+) \theta(k_{2m}^+) \theta(k_{2i}^+ - k_{2m}^+) \theta(k_{2m}^+ - k_{2f}^+) \\
& \frac{F_{\alpha_f}(\mathbf{q}_f)^2}{(k_{2f}^+ - k_{2m}^+) (P^- - k_{1f}^- - k_{2m}^-) - m_{\alpha_f}^2 - (\mathbf{k}_{1f\perp} - \mathbf{k}_{1m\perp})^2} \frac{1}{2M} \\
& \frac{F_{\alpha_i}(\mathbf{q}_i)^2}{(k_{2i}^+ - k_{2m}^+) (P^- - k_{1i}^- - k_{2m}^-) - m_{\alpha_i}^2 - (\mathbf{k}_{1m\perp} - \mathbf{k}_{1i\perp})^2} \\
& + \{1 \leftrightarrow 2\}.
\end{aligned} \tag{3.67}$$

### Contact Potential

The last potential which we calculate explicitly is the contact potential  $V_{\text{TME:C}}$ , shown in Fig. 3.5(a). The rules relate this potential to  $V_{\text{TME:M}}$  in a simple fashion. If both the initial and final mesons are not pions, then the potential is

$$\begin{aligned}
V_{\text{TME:C}}^{\alpha_f, \alpha_i} &= \frac{g_{\alpha_f}^2 g_{\alpha_i}^2 4M^2 [\mathbf{T}_{\alpha_f,1} \cdot \mathbf{T}_{\alpha_f,2}] [\mathbf{T}_{\alpha_i,1} \cdot \mathbf{T}_{\alpha_i,2}]}{(2\pi)^3} \int \frac{d^2 k_{2m\perp} dk_{2m}^+}{2(2\pi)^3 k_{2m}^+ M} \\
& {}_{1f} \langle \left( \Gamma_{\alpha_f} \frac{1}{2} \Gamma_{\alpha_i} \right) \rangle_{1m} \times {}_{2f} \langle \left( \Gamma_{\alpha_f} \frac{k_{2m}^+ + M}{2M} \Gamma_{\alpha_i} \right) \rangle_{2m} \\
& \theta(k_{2m}^+) \theta(k_{2i}^+ - k_{2m}^+) \theta(k_{2m}^+ - k_{2f}^+) \\
& \frac{F_{\alpha_f}(\mathbf{q}_f)^2}{(k_{2f}^+ - k_{2m}^+) (P^- - k_{1f}^- - k_{2m}^-) - m_{\alpha_f}^2 - (\mathbf{k}_{1f\perp} - \mathbf{k}_{1m\perp})^2} \frac{1}{2M} \\
& \frac{F_{\alpha_i}(\mathbf{q}_i)^2}{(k_{2i}^+ - k_{2m}^+) (P^- - k_{1i}^- - k_{2m}^-) - m_{\alpha_i}^2 - (\mathbf{k}_{1m\perp} - \mathbf{k}_{1i\perp})^2} \\
& + \{1 \leftrightarrow 2\}.
\end{aligned} \tag{3.68}$$

To get the contact potential for the pions, the following change has to be made:

$$[\mathbf{T}_{\alpha_f,1} \cdot \mathbf{T}_{\alpha_f,2}] [\mathbf{T}_{\alpha_i,1} \cdot \mathbf{T}_{\alpha_i,2}] \rightarrow \tau_2^2 = 3. \tag{3.69}$$

This is due the additional symmetry that the two pion vertex has.

Before this potential is used in calculations, it must be multiplied by a factor of  $\frac{M}{2(M+m\pi)}$  (as discussed in Section 3.5.1) if the crossed diagrams are not included.

### *Common Features and Simplification*

Each potential in Figs. 3.4 and 3.5 can be written schematically in the following, general form:

$$\begin{aligned}
V_{\text{TME}} = & \frac{g^4 4M^2 T^4 (\Lambda^2 - m^2)^{4n_\alpha}}{(2\pi)^3} \int \frac{d^2 k_{2m\perp} dk_{2m}^+}{2(2\pi)^3} f(k_{1m}^+, k_{2m}^+, q_f^+, q_i^+) \\
& {}_{1f}\langle (\Gamma_{\alpha_f} \mathcal{M}_1 \Gamma_{\alpha_i}) \rangle_{1m} \times {}_{2f}\langle (\Gamma_{\alpha_f} \mathcal{M}_2 \Gamma_{\alpha_i}) \rangle_{2m} \\
& \left[ a_f - m_{\alpha_f}^2 + b_f \cos(\phi_f - \phi_m) \right]^{-n_f} \left[ a_f - \Lambda_{\alpha_f}^2 + b_f \cos(\phi_f - \phi_m) \right]^{-2n_{\alpha_f}} \\
& \left[ a_m + b_{mf} \cos(\phi_f - \phi_m) + b_{mi} \cos(\phi_m - \phi_i) \right]^{-n_m} \\
& \left[ a_i - m_{\alpha_i}^2 + b_i \cos(\phi_m - \phi_i) \right]^{-n_i} \left[ a_i - \Lambda_{\alpha_i}^2 + b_i \cos(\phi_m - \phi_i) \right]^{-2n_{\alpha_i}}, \quad (3.70)
\end{aligned}$$

where the expression for  $F_\alpha$  in Eq. (3.58) was used.

The TME potentials, like the OME potential, have exact rotational invariance about the  $z$ -axis, and thus conserve  $m$ . We project the potential onto states of definite  $m$  by setting  $\phi_i$  to zero and integrating the potential with  $\int d\phi_f e^{im\phi_f} / 2\pi$ .

Now we have to obtain the  $\bar{u}u$  matrix elements explicitly to perform the azimuthal integrations. Appendix F shows that we can write

$$\begin{aligned}
& \left[ {}_{1f}\langle (\Gamma_{\alpha_f} \mathcal{M}_1 \Gamma_{\alpha_i}) \rangle_{1m} \times {}_{2f}\langle (\Gamma_{\alpha_f} \mathcal{M}_2 \Gamma_{\alpha_i}) \rangle_{2m} \right]_{\phi_i=0} \\
& = \sum_{j,k} C_{j,k}(\Gamma_{\alpha_f}, \mathcal{M}_1, \Gamma_{\alpha_i}; \Gamma_{\alpha_f}, \mathcal{M}_2, \Gamma_{\alpha_i}) e^{ij(\phi_f - \phi_m)} e^{ik\phi_m}. \quad (3.71)
\end{aligned}$$

Note that the  $C$  is implicitly a function of the momentum and helicity of the initial and final states, but is independent of the azimuthal angles  $\phi_f$  and  $\phi_i$ .

Then, after a change of variables,  $\phi_m \rightarrow \phi'_i$ ,  $\phi_f - \phi_m \rightarrow \phi'_f$ , and  $\phi_f \rightarrow \phi'_f + \phi'_i$ , the

potential can be written as

$$\begin{aligned}
V_{\text{TME}} = & \frac{g^4 4M^2 T^4 (\Lambda^2 - m^2)^{4n_\alpha}}{(2\pi)^3} \sum_{j,k} \int \frac{dk_{2m\perp} k_{2m\perp} dk_{2m}^+}{2(2\pi)^2} f(k_{1m}^+, k_{2m}^+, q_f^+, q_i^+) \\
& C_{j,k}(\Gamma_{\alpha_f}, \mathcal{M}_1, \Gamma_{\alpha_i}; \Gamma_{\alpha_f}, \mathcal{M}_2, \Gamma_{\alpha_i}) \\
& \int_0^{2\pi} \frac{d\phi'_f}{2\pi} \int_0^{2\pi} \frac{d\phi'_i}{2\pi} e^{i(m+j)\phi'_f} e^{i(m+k)\phi'_i} \\
& \left[ a_f - m_{\alpha_f}^2 + b_f \cos \phi'_f \right]^{-n_f} \left[ a_f - \Lambda_{\alpha_f}^2 + b_f \cos \phi'_f \right]^{-2n_{\alpha_f}} \\
& \left[ a_m + b_{mf} \cos \phi'_f + b_{mi} \cos \phi'_i \right]^{-n_m} \\
& \left[ a_i - m_{\alpha_i}^2 + b_i \cos \phi'_i \right]^{-n_i} \left[ a_i - \Lambda_{\alpha_i}^2 + b_i \cos \phi'_i \right]^{-2n_{\alpha_i}}. \tag{3.72}
\end{aligned}$$

The azimuthal-angle integrals taken together are denoted as  $I$ , and the method for calculating the  $\phi'_m$  and  $\phi'_f$  integrals is discussed in Appendix D. Summarizing, we can write

$$\begin{aligned}
V_{\text{TME}} = & \frac{g^4 4M^2 T^4 (\Lambda^2 - m^2)^{4n_\alpha}}{(2\pi)^3} \sum_{j,k} \int \frac{dk_{2m\perp} k_{2m\perp} dk_{2m}^+}{2(2\pi)^2} f(k_{1m}^+, k_{2m}^+, q_f^+, q_i^+) \\
& C_{j,k}(\Gamma_{\alpha_f}, \mathcal{M}_1, \Gamma_{\alpha_i}; \Gamma_{\alpha_f}, \mathcal{M}_2, \Gamma_{\alpha_i}) \\
& I(a_f - m_{\alpha_f}^2, a_f - \Lambda_{\alpha_f}^2, b_f, n_f, 2n_{\alpha_f}, m + j; \\
& \quad a_m, b_{mf}, b_{mi}, n_m; \\
& \quad a_i - m_{\alpha_i}^2, a_i - \Lambda_{\alpha_i}^2, b_i, n_i, 2n_{\alpha_i}, m + k). \tag{3.73}
\end{aligned}$$

This potential is evaluated using the numerical integration techniques discussed in Appendix C.

### 3.5.4 Further Development of the Light-front Schrödinger Equation

The potentials derived here possess a high degree of symmetry. To solve the light-front Schrödinger equation efficiently, these symmetries should be explicitly exploited, as was done in section 2.1.3. In addition to the invariance of the potentials under parity, there are additional symmetries due to the conservation of nucleon helicity and invariance under time reversal [58].

We follow Machleidt's approach for taking advantage of the symmetry of rotationally invariant potentials with helicity [59]. However, since the light-front potentials derived here do not have full rotational invariance, Machleidt's approach must be modified. The symmetry properties of helicity matrix elements are rederived in Appendix G without assuming full rotational invariance of the potentials. These results allow a modified version of Machleidt's approach to be combined with the exploitation of parity (using the transformation from light-front coordinates to equal-time coordinates) discussed in section 2.1.3. In particular, the potentials are initially calculated in the  $|p_{\text{ET}}, \theta, M, \lambda_1, \lambda_2\rangle$  basis, although the relations in Appendix G.5 are used to transform to the  $|p_{\text{ET}}, J, M, L, S\rangle$  basis, which is useful to solve for the wave functions. Note that the potentials connect states with different  $J$  values in general. Once the symmetries have been explicitly expressed, we can discretize the Schrödinger equation as done in Appendix B.

Note that we apply the transformations to the potential in order to simplify the calculation of the wave functions. Once the wave functions are obtained, we may apply the inverse of the transformations to the wave functions to express them in the helicity basis ( $|\mathbf{p}_\perp, p^+, \lambda_1, \lambda_2\rangle$ ) or, by using Eq. (G.111), the Bjorken and Drell spin basis ( $|\mathbf{p}_\perp, p^+, m_1, m_2\rangle$ ).

### **3.6 Results for the Nucleon-Nucleon Potentials**

The next step towards numerically calculating the bound states for these potentials is to choose the parameters (meson masses, coupling constants, etc.) for the potentials. We consider two models: a pion-only model and a light-front nucleon-nucleon model which incorporates all six mesons used in the Refs. [18, 55].

### 3.6.1 Pion-only Results

As a starting point, we look for inspiration from the non-relativistic one-pion-exchange (OPE) model used by Friar, Gibson, and Payne (FGP) [56]. They use the conventional OPE potential along with a  $n$ -pole pion-nucleon form factor to regulate the high-momentum (short-range) part of the potential. By tuning the form factor parameters to reproduce the physical binding energy of the deuteron, they find that the other the deuteron observables are also reproduced fairly accurately. This leads to the conclusion that this OPE potential model is a good starting point for investigating the deuteron observables.

The basic parameters of the FGP model are the mass of the nucleon ( $M = 938.958$  MeV), the mass of the pion ( $m_\pi = 138.03$  MeV), and the pion decay constant ( $f_0^2 = 0.079$ ), which corresponds to a coupling constant of  $\frac{g_\pi^2}{4\pi} = \frac{4M^2 f_0^2}{m_\pi^2} = 14.6228$  in our formalism. The family of  $n$ -pole pion-nucleon form factors they consider have the form

$$F(q) = \left( \frac{\Lambda^2 - m_\pi^2}{\Lambda^2 + \mathbf{q}^2} \right)^n. \quad (3.74)$$

The parameter  $\Lambda$  is fit to reproduce the deuteron binding energy for a given value of  $n$ .

We can obtain the FGP model from our light-front nucleon-nucleon potential by considering only pion exchanges and performing a non-relativistic reduction. To understand our results, it is important to first consider how well the light-front potential and wave functions approximate the non-relativistic potential and wave functions.

It is useful to start by reviewing some of the properties of the deuteron. First, the deuteron is very lightly bound. Second, although a majority of the deuteron wave function resides in the non-relativistic regime, it has a high-momentum tail that falls off rather slowly [58]. Recalling our experience with the Wick-Cutkosky model, where we found that mass splitting between states with different  $m$  values is small for lightly bound states, it may appear plausible that masses of the  $m = 0$  and  $m = 1$  states of

the deuteron should be approximately the same when calculated with the light-front OPE potential. However, the high-momentum tail of the deuteron enhances the effects of the potential's relativistic components. Since the breaking of rotational invariance is a relativistic effect, as shown in Eq. (2.63), this implies that mass splitting may be large for the deuteron calculated with the light-front potential.

To clearly understand how a large mass splitting might arise in the light-front pion-only model, we take a step back and consider a scalar version of the pion-only model, in which we assume that the pion has a scalar coupling to the nucleon. This allows for a more direct comparison with the Wick-Cutkosky model, since the main difference between the scalar-pion-only potential and the Wick-Cutkosky potential is the pion-nucleon form factor. Since the denominator of the pion-nucleon form factor has the same form as the denominator of the potential, the form factors do not significantly change the rotational properties of the scalar-pion-only potential. Another difference is that factors of  $\bar{u}u$  appear in the numerator of the scalar-pion-only potential, but the effect of these terms is small.

In Table 3.1, we show the binding energies for deuterons calculated with the scalar-pion-only model. Two pion-nucleon form factors are considered, the first one has  $\Lambda = 1.0$  GeV, for which the coupling constant was fit to give the correct binding energy for the non-relativistic potential, and the second form factor uses  $\Lambda = 1.915$  GeV, which was fit to give the correct binding energy for the light-front potential. Those form factors are used to calculate the binding energies for the non-relativistic and light-front potentials, as well as the instantaneous and retarded potentials, which are relativistic and defined by analogy with Eqs. (2.81) and (2.83). We find that the binding energies for all of the potentials have the same order of magnitude, and that the light-front potentials have consistently lower binding energies, which confirms the behavior observed in Fig. 2.9. In addition, the binding energies of the  $m = 0$  and  $m = 1$  light-front potentials are essentially degenerate for both form factors.

Now we ready to consider the (pseudoscalar) pion-only model. The only differ-

Table 3.1: Binding energies for deuterons calculated with several potentials and two different pion-nucleon form factors for the scalar-pion-only model. The  $n$  parameter of the form factor is 1, the coupling constant is  $\frac{g^2}{4\pi} = 0.424$ , and the pion mass is used as the mass of the exchanged meson.

Potential	$\Lambda = 1.0$ GeV	$\Lambda = 1.915$ GeV
Non-relativistic	2.2236 MeV	4.2539 MeV
Instantaneous	2.1581 MeV	4.0862 MeV
Retarded	2.3111 MeV	4.5224 MeV
Light-front, $m = 0$	1.2027 MeV	2.2296 MeV
Light-front, $m = 1$	1.2027 MeV	2.2294 MeV

ence between this potential and the scalar-pion-only potential is that the numerator contains factors of  $\bar{u}i\gamma^5u$  instead of  $\bar{u}u$ . Although this is formally a small change, it has a large effect on the binding energies. The pseudoscalar coupling generates a tensor force, which is more sensitive to the relativistic components of the wave function than the scalar force. In general, this means that the differences in binding energies obtained with different potentials, such as those shown in Table 3.1, will be larger for the pion-only potential.

In Table 3.2, we show the binding energies for deuterons calculated with the pion-only model. Two pion-nucleon form factors are considered, the first one has  $\Lambda = 1.01$  GeV, which was fit for the non-relativistic pion-only model [56], and the second form factor uses  $\Lambda = 1.9$  GeV, which was fit to give the most reasonable binding energy for the light-front potentials. We find that the binding energies vary greatly depending on which potential is used. In fact, the light-front potentials do not bind the deuteron with the first form factor, and with the second form factor, the mass splitting between the  $m = 0$  and  $m = 1$  states is very large. These facts

Table 3.2: Binding energies for deuterons calculated with several potentials and two different pion-nucleon form factors for the (pseudoscalar) pion-only model. The  $n$  parameter of the form factor is 1, the coupling constant is  $\frac{g^2}{4\pi} = 14.6$ , and the pion mass is used as the mass of the exchanged meson. The negative binding energy for the light-front potentials in the first column indicates that the states are not bound.

Potential	$\Lambda = 1.01$ GeV	$\Lambda = 1.9$ GeV
Non-relativistic	2.2244 MeV	227.019 MeV
Instantaneous	0.0146 MeV	28.192 MeV
Retarded	1.3590 MeV	130.472 MeV
Light-front, $m = 0$	-0.0269 MeV	0.788 MeV
Light-front, $m = 1$	-0.0246 MeV	8.856 MeV

indicate that the deuteron wave functions are very sensitive to subtle changes in the relativistic structure of the pion-only potentials.

Now that we understand that relativistic effects are important for the OPE potential, we can start to analyze the TPE potential. We reiterate here that the main objective of this work is to investigate this breaking of rotational invariance and how it is restored. Obtaining results which are in agreement with experimental data is of lesser importance; we must have states that transform correctly under rotations before we can address the experimental data. Naïvely, one might think that we can choose any set of two-pion-exchange graphs which is a truncation of a rotationally-invariant infinite series of graphs. In particular, one might think that using the box graphs shown in Fig. 3.4 (the two-pion-exchange graphs without the graphs mandated by chiral symmetry, denoted as the non-chiral-two-pion-exchange (ncTPE) potential) would be adequate for our analysis of rotational invariance.

Another choice of a set of two-pion-exchange graphs is sum of the box graphs

shown in Fig. 3.4 and the contact graphs shown in Fig. 3.5. To incorporate chiral symmetry as accurately as possible without including the crossed two-pion-exchange potentials, we weight the contact vertex with a factor of  $\frac{M}{2(M+m_\pi)}$ , as explained in Section 3.5.1. Note that in the sum, which we call the two-pion-exchange (TPE) potential, chiral symmetry provides a cancelation between the box diagrams and the contact diagrams. This indicates that the results obtained with the TPE potential will be more stable than those obtained with the ncTPE potential.

To check this stability and the restoration of rotational invariance of the pion-only model, we calculate the energy of the deuteron using the OPE, OPE+TPE, and OPE+ncTPE potentials. We verify that the results are independent of the choice of the pion-nucleon form factor by considering three different choices for the form factor.

For the first form factor, we choose  $n = 1$  and find that  $\Lambda = 1.9$  GeV gives a reasonable range of binding energies. We use the form factor to calculate the lowest energy bound state with arbitrary total angular momentum. In addition, we take the  $J = 1$  component of the potential and use it to perform the same calculation. We expect to obtain similar results since the deuteron is a spin one object.

The results for the first pion-nucleon form factor are shown in Table 3.3. Note that the results do not depend much on whether a restriction to spin one is applied. This shows that even though the eigenstates of the light-front Hamiltonian are not in principle eigenstates of the angular momentum, numerically they are *almost* angular momentum eigenstates. However, this does not mean that rotational invariance is unbroken. Rotations relate the different  $m$  states, and from the mass splittings, we see that the states do not transform correctly.

Table 3.3 also shows that both the mass splitting and the difference in the percentage of the D-state wave function decrease when TME diagrams are included. In addition, the wave functions are almost completely in the  $J = 1$  state. As for the D-state probability, we first note that it increases with the binding energy. It is consistent (given the range of values it and the binding energy take) with the value of

Table 3.3: The values of the binding energy, percentage of the wave function in the D state, and the percentage of the wave function in the  $J = 1$  state for the  $m = 0$  and  $m = 1$  states for different potentials. The values obtained for the full potential (which connects states of arbitrary total angular momentum) are shown along with the values obtained for potentials restricted to the  $J = 1$  sector which are shown in parentheses. The pion-nucleon form factor uses  $n = 1$  and  $\Lambda = 1.9$  GeV.

Potential	Binding Energy (MeV)			D state (%)		$J = 1$ (%)	
	m=0	m=1	Diff	m=0	m=1	m=0	m=1
OPE	-0.7884 (-0.7129)	-8.8561 (-7.6970)	8.0677 (6.9841)	4.09 (3.97)	12.27 (11.99)	99.99 (100)	99.78 (100)
OPE +TPE	-0.6845 (-0.5886)	-2.5606 (-2.0644)	1.8761 (1.4758)	3.98 (3.79)	8.08 (7.61)	99.98 (100)	99.88 (100)
OPE +ncTPE	0.0107 (0.0140)	0.0087 (0.0155)	0.0020 (-0.0015)	0.15 (0.11)	0.66 (0.58)	100.00 (100)	100.00 (100)

6% reported in Ref. [56] for the FGP model.

Another thing to note in Table 3.3 are the effects of using the ncTPE potential is used. As mentioned earlier, this potential is greater in magnitude than the TPE potential and should have a larger effect on the binding energy. In fact, the effect is so large that it serves to unbind the deuteron. (Strictly speaking, this indicates only that the binding energy is very small or zero; the error in the binding energy calculation increases as the binding energy approaches zero.) Because the ncTPE potential has such a large effect by itself, it is impossible to determine what effect it has on the rotational properties of the state. Only the TPE potential can be used to analyze the restoration of the state's rotational invariance.

To make sure that the results found are independent of the pion-nucleon form

Table 3.4: A pion-nucleon form factor with  $n = 1$  and  $\Lambda = 2.1$  GeV is used to calculate the same quantities as shown in Table 3.3.

Potential	Binding Energy (MeV)			D state (%)		$J = 1$ (%)	
	m=0	m=1	Diff	m=0	m=1	m=0	m=1
OPE	-1.7357 (-1.6103)	-14.9116 (-13.2111)	13.1759 (11.6008)	5.60 (5.49)	14.30 (14.14)	99.98 (100)	99.71 (100)
OPE +TPE	-1.6296 (-1.4551)	-4.5609 (-3.8203)	2.9313 (2.3652)	5.62 (5.43)	9.89 (9.53)	99.96 (100)	99.85 (100)
OPE +ncTPE	-0.0219 (-0.0045)	-0.0180 (0.0056)	-0.0039 (-0.0101)	0.69 (0.38)	1.33 (0.86)	99.99 (100)	99.99 (100)

factor, we performed the same calculation with  $n = 1$  and  $\Lambda = 2.1$  GeV (shown in Table 3.4) and with  $n = 2$  and  $\Lambda = 2.9$  GeV (shown in Table 3.5). The results in these two tables are qualitatively the same as the results in Table 3.3, which demonstrates that these results are robust.

The deuteron masses for the different  $m$  states, as shown in Tables 3.3, 3.4, and 3.5, are shown in Fig. 3.6 as a function of which potential was used for the calculation. It is easy to see that the relatively large mass splitting obtained with the OPE potential is significantly reduced by including the TPE potential. The apparent further reduction of the splitting by neglecting the chiral part of the TPE potential (leaving the ncTPE potential) is an artifact of the deuteron becoming unbound. Since the unbound states form a continuum, the lowest energy unbound states will always be essentially degenerate, regardless of how badly rotational invariance is broken.

## Pion-Only Model Mass Splittings

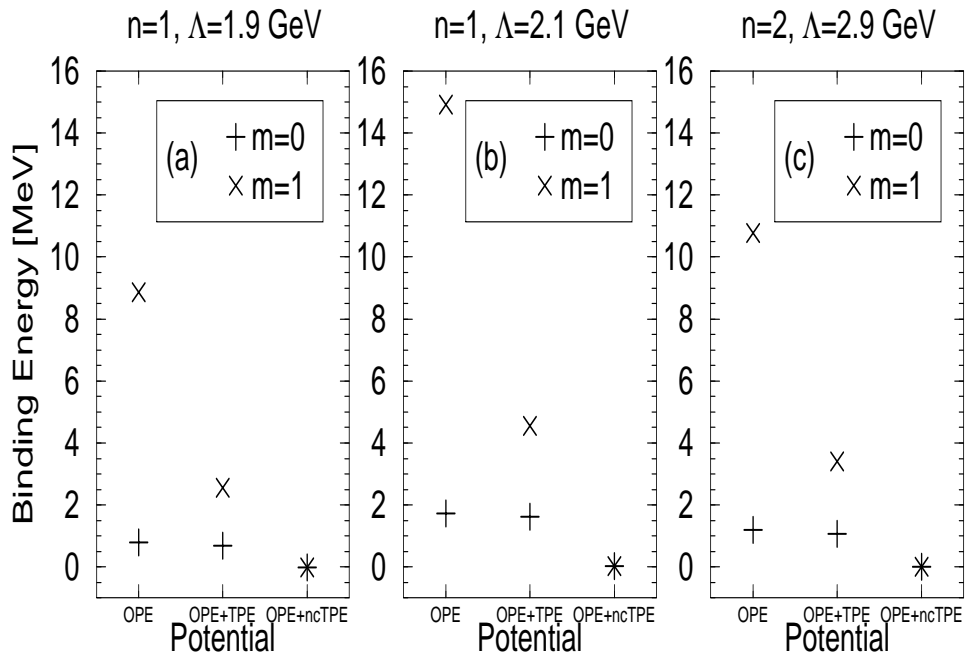


Figure 3.6: The values of the binding energy for the  $m = 0$  and  $m = 1$  states for different pion-only light-front potentials. Three different pion-nucleon form factors are used: (a)  $n = 1$  and  $\Lambda = 1.9$  GeV, (b)  $n = 1$  and  $\Lambda = 2.1$  GeV, and (c)  $n = 2$  and  $\Lambda = 2.9$  GeV.

Table 3.5: A pion-nucleon form factor with  $n = 2$  and  $\Lambda = 2.9$  GeV is used to calculate the same quantities as shown in Table 3.3.

Potential	Binding Energy (MeV)			D state (%)		$J = 1$ (%)	
	m=0	m=1	Diff	m=0	m=1	m=0	m=1
OPE	-1.2060 (-1.1068)	-10.7746 (-9.4180)	9.5686 (8.3112)	4.86 (4.74)	13.06 (12.82)	99.98 (100)	99.75 (100)
OPE +TPE	-1.0781 (-0.9494)	-3.3983 (-2.7863)	2.3202 (1.8369)	4.78 (4.59)	8.95 (8.52)	99.97 (100)	99.87 (100)
OPE +ncTPE	-0.0002 (0.0069)	-0.0028 (0.0106)	0.0026 (-0.0037)	0.30 (0.20)	0.90 (0.68)	100.00 (100)	99.99 (100)

### 3.6.2 Light-Front Nucleon-Nucleon Model Results

Having addressed the simple pion-only model in the previous section, we are now ready to consider the full nuclear model where the nucleon-nucleon interaction is mediated by all the six mesons shown in Table 3.6. For numerical work, use the parameters for the light-front nucleon-nucleon (LFNN) potential from the work of Miller and Machleidt [55]. Those parameters were fit for a potential that used a retarded propagator for the energy in the potentials. Since the potentials used in this paper have energy dependent denominators, the parameters must be modified somewhat. We choose to vary the coupling constant for the  $\sigma$  meson. The parameters are given in table 3.6.

As with all the other deuteron models presented in this paper, the light-front one-meson-exchange (OME) potential breaks rotational invariance and causes a mass splitting of the deuteron states with different magnetic quantum numbers. We expect that the splitting will be removed somewhat by including higher order potentials.

The first step is to determine which two-meson-exchange potentials to use. One

Table 3.6: The parameters for the  $\pi$ ,  $\eta$ ,  $\rho$ ,  $\omega$ ,  $\delta$ , and  $\sigma$  mesons from Ref. [55]. For the meson type, “iv” and “is” stand for isovector and isoscalar, while “ps”, “v”, and “s” stand for pseudoscalar, vector, and scalar. The  $\sigma$  meson is also known as  $f_0(400 - 1200)$ , and the  $\delta$  meson is the  $a_0(980)$ .

Meson	type	mass [MeV]	$\Lambda$ [GeV]	$n$	$\frac{g^2}{4\pi}$	$\frac{f}{g}$
$\pi$	iv,ps	138.04	1.2	1	14.0	
$\eta$	is,ps	547.5	1.5	1	3.0	
$\rho$	iv,v	769.	1.85	2	0.9	6.1
$\omega$	is,v	782.	1.85	2	24.5	0.0
$\delta$	iv,s	983.	2.0	1	2.0723	
$\sigma$	is,s	550.	2.0	1	$f_\sigma \times 8.9602$	

choice is to use only the two-pion-exchange potentials, TPE and ncTPE, as defined in the previous section. However, we expect to get better results using the two-meson-exchange diagrams generated by all the available mesons, including the contact diagrams for the pions, which we denote as the two-meson-exchange (TME) potential. In addition, we can also investigate the effect of leaving out the contact potentials for the pions, resulting in the non-chiral two-meson-exchange (ncTME) potential.

We do not include diagrams with a contact interaction between the nucleon, a pion, and another meson. This is because, as mentioned in section 3.5.1, the infinite series of the box diagrams is rotationally invariant and the contact diagrams are not needed to achieve rotational invariance. Furthermore, they are not required to control the convergence of the series, since there is no strong cancellation between the contact diagram and the instantaneous diagrams.

The first step in analyzing the bound states is to determine what range of  $f_\sigma$  gives reasonable results. We iteratively solve for the binding energy of the deuteron,

Table 3.7: The values of  $f_\sigma$  required to give the physical value of the deuteron mass for a given potential and state with  $J_z = m$ . The percent of the wave function in the D-state and in the  $J = 1$  state are also shown.

Potential	$f_\sigma$			% D state		% $J = 1$	
	m=0	m=1	Diff	m=0	m=1	m=0	m=1
OME	1.2407	1.2125	0.0282	2.87	3.55	99.99	99.97
OME +TPE	1.2829	1.2819	0.0010	2.96	3.23	99.99	99.97
OME +TME	1.2968	1.3079	-0.0111	2.95	3.28	99.99	99.96
OME +ncTPE	1.3064	1.3121	-0.0057	2.99	3.16	99.98	99.97
OME +ncTME	1.3198	1.3397	-0.0199	2.98	3.21	99.98	99.96

varying  $f_\sigma$  until the binding energy matches the physical value of the binding energy, for each of the potentials. The results are shown in Table 3.7. We find that a value of  $f_\sigma$  in the range 1.2 to 1.3 will give reasonable results for the binding energy. Note that D-state probability (about 3%) is lower in this model than for the energy-independent light-front used in Ref. [55], where a value of 4.5% is found. This is expected since the  $f_\sigma$  is greater than 1 in this model, meaning that the scalar interaction is strengthened relative to the tensor interaction, leading to a decrease in amount of the D-state present.

We choose two values of  $f_\sigma$ , one from the low end of the range (1.22) and one from the high end (1.2815) for our investigations. Using two values helps ensure that our results are robust.

First, we examine the bound states for  $f_\sigma = 1.22$ . The results for several different choices of the TME potentials are shown in Table 3.8 and the binding energies are plotted in Fig. 3.7. In addition to the two-meson-exchange potentials mentioned above, we also consider the  $\pi$ - $\sigma$  plus  $\pi$ - $\omega$  Mesa potential. The reason for considering this potential is that Carbonell, Desplanques, Karmanov, and Mathiot [13] have shown that it helps restore rotational invariance of the deuteron.

In particular, they have used manifestly covariant light-front dynamics to analyze the deuteron. They start with a deuteron wave function calculated in equal-time dynamics, then use a light-front one-pion-exchange potential (expanded to lowest order in powers of  $\frac{1}{M}$ ) to calculate the perturbative corrections to the wave function. They find that the resulting wave function has an unphysical dependence on the orientation of the light-front plane, which would manifest itself as a breaking of rotational invariance in our formalism. They also use the  $\pi$ - $\sigma$  and  $\pi$ - $\omega$  Mesa potentials (expanded to lowest order in powers of  $\frac{1}{M}$ ) to calculate the correction to the wave function. When the wave function corrections are combined, they find that the directional dependence of the longest-range part of the deuteron wave function cancels exactly.

This implies that for our model, using the  $\pi$ - $\sigma$  plus  $\pi$ - $\omega$  Mesa potential (which we denote by  $\pi$ -( $\sigma$ - $\omega$ )) should partially restore the rotational invariance of the deuteron, assuming that the breaking of rotational invariance is due primarily to the one-pion-exchange potential. Note that since we solve for the deuteron wave function self-consistently and to all orders for our potentials, we do not expect to find exactly the same result as Ref. [13].

The first thing to notice about the data in Table 3.8 is that the results are essentially the same regardless of if arbitrary angular momentum or is used or if the potential is restricted to the  $J = 1$  sector. This was also seen in the previous section for the pion-only model. It means that the wave functions are numerically approximate to angular momentum eigenstates.

Next we notice the splittings between masses and D state percentages for the

$m = 0$  and  $m = 1$  states. The dependence on  $m$  implies that the states do not transform correctly under rotations. All of the two-meson-exchange potentials used reduce the splittings by similar amounts, by about 60% for the binding energy and by about 70% for the percent D state. Note also that the mass splittings for the pion-only model were much larger.

Examining the effects of the individual two-meson-exchange potentials, we see that  $\pi$ -( $\sigma$ - $\omega$ ) potential does reduce the mass splitting, but it does not fully remove it. This is expected since the OME potential includes more than just the pion potential, and the potential is relativistic.

Next, we compare the ncTME and ncTPE potentials to the TME and TPE potentials. The non-chiral potentials reduce the binding energy more than the chiral potentials, as we expected from our experience from the pion-only model. However, unlike for the pion-only model, we find that the chiral and non-chiral potential have fairly similar effects.

Finally, notice that the mass splitting for the TPE potential is much smaller than for the other two-meson-exchange potentials. By itself, this does not imply that the rotational properties of the deuteron calculated with that potential are significantly better than those from other two-meson-exchange potentials. The individual potentials that make up the TME potential are fairly large in magnitude, but vary in sign. This means that using any subset of those potentials may result in either a larger or smaller mass splitting. In this case, it is smaller. To investigate this further, we examine the currents for the TME and TPE deuteron wave function in Chapter 4.

To verify that our results are independent of the value of  $f_\sigma$ , we recalculate the deuteron properties for each of the potentials with  $f_\sigma = 1.2815$ . The results are summarized in Table 3.9, and the binding energies are shown in Fig. 3.8. The change in  $f_\sigma$  increases the binding of the states, but the rest of the results are qualitatively the same.

Table 3.8: The values of the binding energy, percentage of the wave function in the D state, and the percentage of the wave function in the  $J = 1$  state for the  $m = 0$  and  $m = 1$  states for different potentials. The values obtained for the full potential (which connects states of arbitrary total angular momentum) are shown along with the values obtained for potentials restricted to the  $J = 1$  sector which are shown in parentheses. The  $\sigma$  coupling constant factor is  $f_\sigma = 1.22$ .

Potential	Binding Energy (MeV)			D state (%)		$J = 1$ (%)	
	m=0	m=1	Diff	m=0	m=1	m=0	m=1
OME only	-1.7653 (-1.7141)	-2.4200 (-2.2655)	0.6547 (0.5514)	2.73 (2.72)	3.61 (3.54)	99.99 (100)	99.96 (100)
OME + $\pi$ -( $\sigma$ - $\omega$ ) Mesa	-1.9236 (-1.8625)	-1.7021 (-1.5340)	-0.2215 (-0.3285)	2.80 (2.78)	3.38 (3.25)	99.99 (100)	99.96 (100)
OME +ncTME	-0.4948 (-0.4611)	-0.2646 (-0.2034)	-0.2302 (-0.2577)	1.97 (1.93)	1.76 (1.59)	99.99 (100)	99.98 (100)
OME +ncTPE	-0.6620 (-0.6232)	-0.4825 (-0.4132)	-0.1795 (-0.2100)	2.16 (2.13)	2.09 (1.99)	99.99 (100)	99.98 (100)
OME +TME	-0.7861 (-0.7460)	-0.6060 (-0.5191)	-0.1801 (-0.2269)	2.25 (2.22)	2.31 (2.19)	99.99 (100)	99.97 (100)
OME +TPE	-0.9981 (-0.9531)	-0.9155 (-0.8253)	-0.0826 (-0.1278)	2.42 (2.39)	2.57 (2.48)	99.99 (100)	99.98 (100)

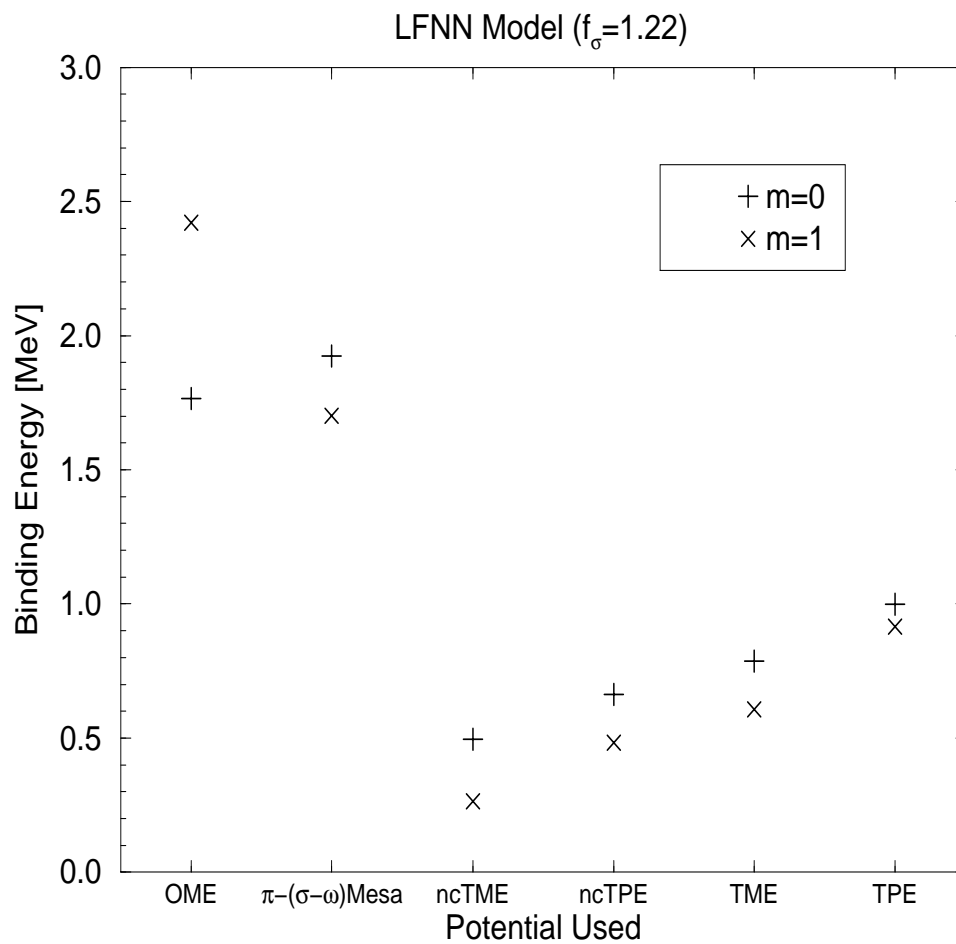


Figure 3.7: The values of the binding energy for the  $m = 0$  and  $m = 1$  states for different nucleon-nucleon light-front potentials. The  $\sigma$  coupling constant factor is  $f_\sigma = 1.22$ .

Table 3.9: The  $\sigma$  coupling constant factor used here,  $f_\sigma = 1.2815$ , distinguishes this table from Table 3.8.

Potential	Binding Energy (MeV)			D state (%)		$J = 1$ (%)	
	m=0	m=1	Diff	m=0	m=1	m=0	m=1
OME only	-3.3500 (-3.2818)	-4.4546 (-4.2622)	1.1046 (0.9804)	3.09 (3.06)	3.97 (3.92)	99.99 (100)	99.96 (100)
OME + $\pi$ -( $\sigma$ - $\omega$ ) Mesa	-3.6331 (-3.5520)	-3.2408 (-3.0194)	-0.3923 (-0.5326)	3.10 (3.10)	3.85 (3.77)	99.99 (100)	99.95 (100)
OME +ncTME	-1.3766 (-1.3230)	-0.9901 (-0.8807)	-0.3865 (-0.4423)	2.67 (2.65)	2.64 (2.54)	99.99 (100)	99.97 (100)
OME +ncTPE	-1.6532 (-1.5939)	-1.4693 (-1.3578)	-0.1839 (-0.2361)	2.81 (2.79)	2.88 (2.81)	99.99 (100)	99.97 (100)
OME +TME	-1.8617 (-1.8021)	-1.6032 (-1.4696)	-0.2585 (-0.3325)	2.85 (2.83)	3.05 (2.97)	99.99 (100)	99.96 (100)
OME +TPE	-2.1915 (-2.1267)	-2.2137 (-2.0831)	0.0222 (-0.0436)	2.95 (2.94)	3.23 (3.17)	99.99 (100)	99.97 (100)

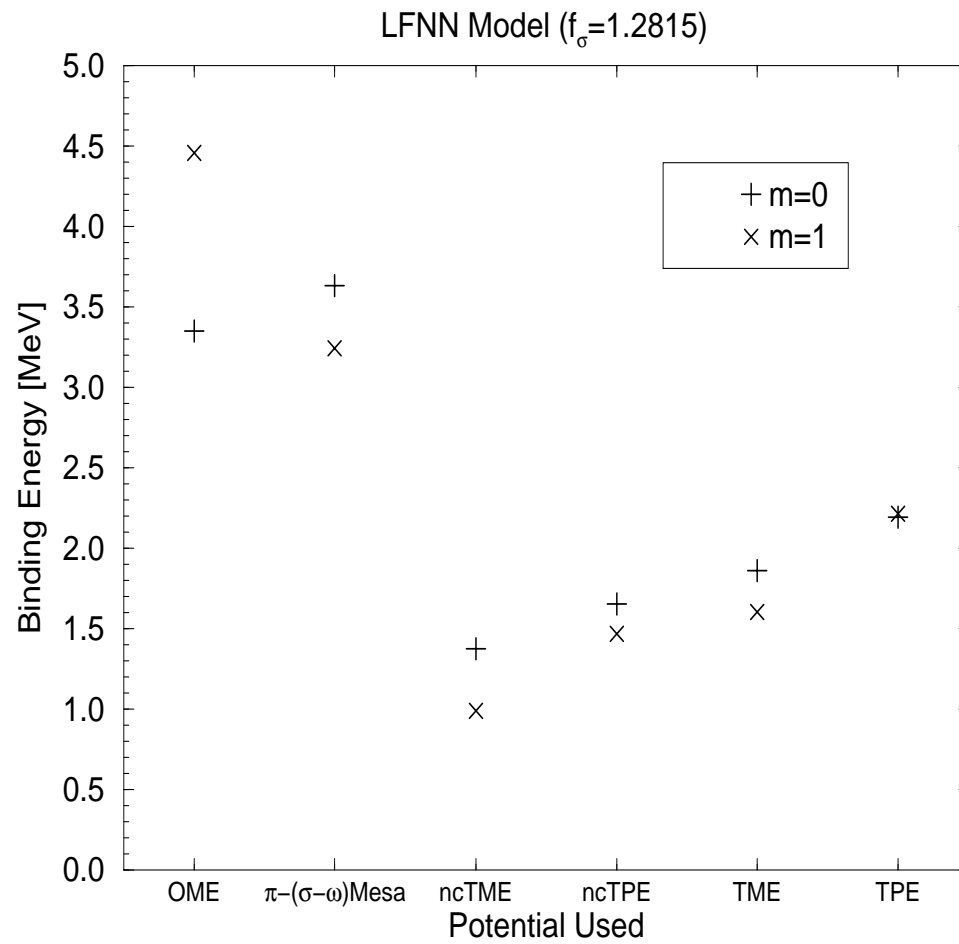


Figure 3.8: The values of the binding energy for the  $m = 0$  and  $m = 1$  states for different nucleon-nucleon light-front potentials. The  $\sigma$  coupling constant factor is  $f_\sigma = 1.2815$ .

## Chapter 4

**FORM FACTORS OF THE DEUTERON**

“It is theory that decides what can be observed.”

—*Albert Einstein*

In Chapter 3, we considered several different truncations of the light-front nucleon-nucleon (LFNN) potential and used them to solve for the deuteron wave function. In this chapter, we use those wave functions to solve for the deuteron current, which is used to calculate the deuteron electromagnetic and axial form factors. We can analyze the rotational properties of the deuteron current like we did for the wave function.

In this chapter, we first outline the covariant theory of the electromagnetic form factors for spin-1 objects, like the deuteron. Then we recall the features of light-front calculations (including the breaking of rotational invariance) of the form factors. After that, we review the covariant and light-front tools for calculating axial form factors. The formalism is then applied to calculate the electromagnetic and axial currents and form factors for the light-front deuteron wave functions.

One notable feature of this calculation is that it is done entirely with light-front dynamics. The covariant Lagrangian generates light-front potentials, which generate light-front wave functions, which are used in a light-front calculation of the deuteron current and form factors. This is different from other approaches which use deuteron wave functions calculated from equal-time dynamics, then transformed to the light front [77–84].

**4.1 Electromagnetic Form Factors**

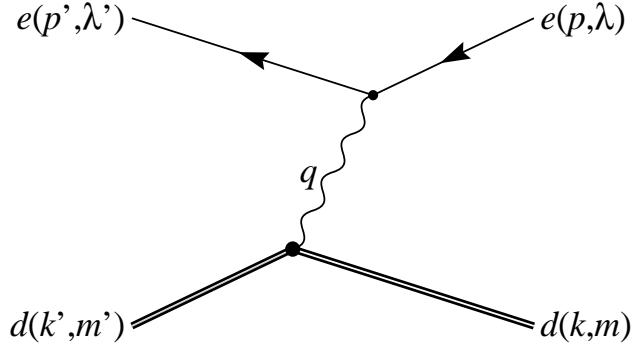


Figure 4.1: The Feynman diagram for one-photon-exchange electron-deuteron scattering.

#### 4.1.1 Covariant Theory

In the one-photon-exchange approximation, shown in Fig. 4.1, the amplitude of the scattering process  $ed \rightarrow ed$  is just the contraction of the electron and deuteron currents, multiplied by the photon propagator,

$$\langle p', \lambda' | j_\mu^e | p, \lambda \rangle \frac{1}{q^2} \langle k', m' | J_d^\mu | k, m \rangle, \quad (4.1)$$

where

$$\langle p', \lambda' | j_\mu^e | p, \lambda \rangle = e \bar{u}(\mathbf{p}', \lambda') \gamma_\mu u(\mathbf{p}, \lambda). \quad (4.2)$$

From Lorentz covariance, current conservation, parity invariance, and time reversal invariance [85–89], we infer that the deuteron form factor can be written as

$$\langle k', m' | J_d^\mu | k, m \rangle = -\frac{e}{2M_d} (e^*)^\rho(\mathbf{k}', m') J_{\rho\sigma}^\mu e^\sigma(\mathbf{k}, m), \quad (4.3)$$

where the spin-1 polarization vectors satisfy

$$e_\mu^*(\mathbf{k}, m) e^\mu(\mathbf{k}, m') = -\delta_{m, m'}, \quad (4.4)$$

$$\sum_m e_\mu^*(\mathbf{k}, m) e_\nu(\mathbf{k}, m) = -g_{\mu\nu} + \frac{k_\mu k_\nu}{M_d^2}, \quad (4.5)$$

$$k_\mu e^\mu(\mathbf{k}, m) = 0, \quad (4.6)$$

and the operator  $J_{\rho\sigma}^\mu$  is given by

$$J_{\rho\sigma}^\mu = (k'_\mu + k_\mu) \left[ g_{\rho\sigma} F_1(q^2) - \frac{q_\rho q_\sigma}{2M_d^2} F_2(q^2) \right] - I_{\rho\sigma}^{\mu\nu} q_\nu G_1(q^2), \quad (4.7)$$

where  $I_{\rho\sigma}^{\mu\nu} = g_\rho^\mu g_\sigma^\nu - g_\rho^\nu g_\sigma^\mu$  is the generator of infinitesimal Lorentz transformations,  $q = k' - k$ , and  $F_1$ ,  $F_2$ , and  $G_1$  are functions of  $q^2$ , the invariant mass of the photon. Some conventions [79, 80] denote  $G_1$  as  $-F_3$ .

The  $F_1$ ,  $F_2$ , and  $G_1$  form factors are related to the deuteron charge, magnetic, and quadrapole form factors, denoted by  $F_C$ ,  $F_M$ , and  $F_Q$  respectively, by [85, 87, 90]

$$F_C = F_1 + \frac{2}{3}\eta [F_1 + (1 + \eta)F_2 - G_1], \quad (4.8)$$

$$F_M = G_1, \quad (4.9)$$

$$F_Q = F_1 + (1 + \eta)F_2 - G_1, \quad (4.10)$$

where

$$\eta = \frac{-q^2}{4M_d^2}. \quad (4.11)$$

Note that since both the initial and final electron and deuteron are on-shell,  $-q^2 > 0$ . We define  $Q^2 = -q^2$ .

At zero-momentum transfer, the deuteron charge, magnetic, and quadrapole form factors are simply

$$F_C(0) = 1, \quad (4.12)$$

$$F_M(0) = \frac{M_d}{m_p} \mu_d = 1.71293, \quad (4.13)$$

$$F_Q(0) = M_d^2 Q_d = 25.8525, \quad (4.14)$$

where  $m_p$  is the mass of the proton,  $\mu_d$  is the magnetic moment of the deuteron (in nuclear magnetons  $\mu_N = \frac{e}{2m_p}$ ), and  $Q_d$  is the electric quadrapole moment of the deuteron (in units of the deuteron mass, although typically it is measured in  $e \cdot \text{barns}$ ). The numerical values of the form factors are determined by using experimentally measured values [88, 91, 92].

Another set of form factors are  $G_0$ ,  $G_1$ , and  $G_2$ , commonly used in light-front dynamics [79,80,83]. They are simply related to the charge, magnetic, and quadrapole form factors,

$$G_0 = F_C, \quad (4.15)$$

$$G_1 = -F_M, \quad (4.16)$$

$$G_2 = \frac{\sqrt{8}}{3}\eta F_Q. \quad (4.17)$$

The electron-deuteron cross-section is measured to determine the deuteron form factors for large momentum transfers. The unpolarized cross-section has the form [88,93]

$$\frac{d\sigma}{d\Omega_e} = \frac{\sigma_{\text{Mott}}}{1 + \frac{2E_e}{M_d} \sin^2 \frac{\theta_e}{2}} \left( A(Q^2) + B(Q^2) \tan^2 \left( \frac{\theta_e}{2} \right) \right), \quad (4.18)$$

where

$$\sigma_{\text{Mott}} = \left( \frac{\alpha \cos \frac{\theta_e}{2}}{2E_e \sin^2 \frac{\theta_e}{2}} \right)^2, \quad (4.19)$$

and  $E_e$  is the electron beam energy,  $\theta_e$  is the angle by which the electron scatters, and  $\alpha$  is the fine-structure constant. The structure functions  $A$  and  $B$  can be expressed in terms of the charge, magnetic, and quadrapole form factors,

$$A = F_c^2 + \frac{8}{9}\eta^2 F_Q^2 + \frac{2}{3}\eta F_M^2, \quad (4.20)$$

$$B = \frac{4}{3}\eta(1 + \eta)F_M^2. \quad (4.21)$$

The three form factors  $F_1$ ,  $F_2$ , and  $G_1$  cannot be determined uniquely from the unpolarized scattering data since that measurement of provides only two structure functions. More information is needed, which can be obtained from experiments where the polarization of the electron and/or deuteron is measured [88,89]. The most commonly measured quantity is the tensor polarization observable,  $T_{20}$ ,

$$T_{20} = - \frac{\frac{8}{3}\eta F_C F_Q + \frac{8}{9}\eta^2 F_Q^2 + \frac{1}{3}\eta F_M^2 (1 + 2(1 + \eta) \tan^2 \frac{\theta_e}{2})}{\sqrt{2} (A + B \tan^2 \frac{\theta_e}{2})}. \quad (4.22)$$

Note that  $T_{20}$  depends on the angle  $\theta_e$ . For ease of comparison, data for  $T_{20}$  is usually presented for  $\theta_e = 70^\circ$ . Alternatively, one can eliminate the angular dependence by defining  $\tilde{T}_{20}$ , which is  $T_{20}$  with  $F_M$  set equal to zero,

$$\tilde{T}_{20} = -\frac{\frac{8}{3}\eta F_C F_Q + \frac{8}{9}\eta^2 F_Q^2}{\sqrt{2}(F_C^2 + \frac{8}{9}\eta^2 F_Q^2)}. \quad (4.23)$$

The extraction of the structure functions from the data is difficult. In practice, each cross-section measurement is performed at a different momentum transfer and angle, making it impossible to exactly disambiguate, for example,  $A$  and  $B$ . One needs to interpolate between values of  $B$  to calculate values for  $A$ , and vice versa. The Jefferson Lab  $t_{20}$  Collaboration used a self-consistent method for obtaining the structure functions from the scattering data [94]. They consider a variety of theoretical models for the deuteron form factors, then fit the parameters of the models to the measured cross-sections. After each model is fit, it is used as the interpolation function to disentangle the structure functions. This two-step process helps minimize model-dependent effects in the values of  $A$  and  $B$ .

#### 4.1.2 Light Front Calculation

Light-front dynamics is particularly well suited to calculating form factors. One reason is that the generators of boosts in the one, two, and plus directions are kinematic, so that wave functions calculated with a truncated potential transform correctly under boosts. This feature is especially important for form factors at high momentum transfer since the wave functions must undergo a large boost.

Another, more subtle, reason for using the light front is that many of the graphs which contribute to the current vanish identically. For example, the three lowest-order graphs for the current are shown in Fig. 4.2. The double line denotes the deuteron, and the vertex of the deuteron lines and the nucleon lines represents the deuteron wave function. The graph labeled (a) does not vanish and is calculated in section 4.1.3.

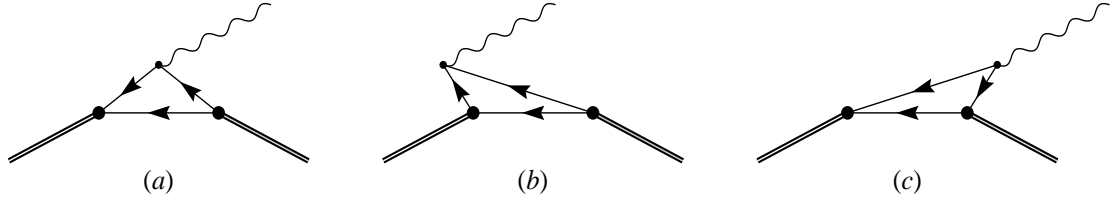


Figure 4.2: The lowest-order graphs which contribute to the deuteron current matrix element.

Fig. 4.2(b) vanishes in light-front dynamics. To see why, we first note three facts: the plus component of each particle in light-front dynamics is non-negative (for massive particles it must be positive), the plus component of the momentum is conserved, and the plus momentum of the vacuum is zero. Combining these facts, we find that any vertex which has particles on one side and vacuum on the other must vanish. In other words, the vacuum is trivially empty, and no graphs couple to it.

For Fig. 4.2(c), the coupling of the photon to the nucleon goes like  $\bar{u}_{\text{LF}}\gamma^\mu v_{\text{LF}}$ , where the light-front spinors are defined in Appendix F. For  $\mu = +$ , this matrix element is suppressed maximally, and thus  $J^+$  is the “good” component of the current [80,82,95]. We calculate only  $J^+$ , since it is the most stable.

We do not consider the contribution of higher-order graphs to the deuteron current, such as graphs where the photon couples to a meson or a nucleon while a meson is present. The omission of the meson-exchange currents does not affect the rotational properties of the current, although it does affect the overall values of the deuteron form factors. This is acceptable since we are only concerned with the rotational properties in this work, not in the detailed results.

The neglect of the graphs where the photon couples to a nucleon while a meson is present may affect the rotational properties of the current. This is because the deuteron current shown in Fig. 4.2(a) is not formally conserved [93], but current conservation is necessary (although not sufficient) for the current to have the correct

properties under rotation. To construct the conserved current operator associated with a given wave function, the current must include diagrams that are related to the potential used to calculate the wave function. We expect that these diagrams are small since they contain meson propagators, and that neglecting them should not significantly affect the conservation of the deuteron current or the rotational properties of the current.

### *Symmetries of the Electromagnetic Current*

Now, we use symmetries to relate the components of  $\langle k', m' | J^+(q) | k, m \rangle$ . Although in light-front dynamics some generators of Lorentz transformations are dynamic, such as the generators of rotations from the  $x$ - $y$  plane into the  $x$  direction are dynamic, we are free to boost in the plane perpendicular to the  $z$ -axis, boost in the plus direction, and rotate about the  $z$ -axis, since the generators of those transformations are kinematic. In addition, we will find how the states and the current operator transforms under parity and time-reversal.

The kinematic generators allow us to choose which frame to evaluate the current in. We choose the Breit frame [80], where  $q^+ = q^- = q_\perp^y = 0$  and  $q_\perp^x = Q$ . We also choose the plus momentum of the deuteron to be  $M_d$ , since  $M_d$  is value of the plus momentum in deuteron's rest frame. To simplify notation, we define the matrix elements of  $J^+$  as

$$I_{m',m}^+(Q) = \left\langle \frac{\mathbf{q}_\perp}{2}, m' \left| J^+(Q) \right| -\frac{\mathbf{q}_\perp}{2}, m \right\rangle. \quad (4.24)$$

This quantity is represented with  $I_{m'm}$  instead of  $J_{m'm}$  because  $J_{m'm}$  is used to represent the matrix elements of  $J$  using the instant-form spin basis. This distinction is discussed later in this section.

Next, we consider rotation about the  $z$ -axis by  $\pi$  ( $R_z(\pi)$ ), parity ( $\Pi$ ), and time-

reversal ( $\Theta$ ). First note that the current operator transforms as

$$R_z(\pi)J^\pm R_z(\pi) = J^\pm, \quad (4.25)$$

$$\Pi J^\pm \Pi = J^\mp, \quad (4.26)$$

$$\Theta J^\pm \Theta = J^\mp. \quad (4.27)$$

Obviously, we must use both parity and time reversal to retain the plus component of the current. Now look at how the deuteron states transform:

$$R_z(\pi)|-\mathbf{k}_\perp, m\rangle = |+\mathbf{k}_\perp, m\rangle(-1)^m, \quad (4.28)$$

$$\Theta\Pi|-\mathbf{k}_\perp, m\rangle = |-\mathbf{k}_\perp, -m\rangle(-1)^m. \quad (4.29)$$

Although the symmetry operators can introduce extra, constant phase factors, they are omitted here since they cancel when calculating matrix elements. These results make it easy to find what each of these symmetry operators does to the matrix element. Under rotations a rotation of  $\pi$  about the  $z$ -axis, the current matrix element transforms to

$$I_{m',m}^+(Q) \rightarrow (-1)^{m-m'} \left\langle -\frac{\mathbf{q}_\perp}{2}, m' \left| J^+(Q) \right| +\frac{\mathbf{q}_\perp}{2}, m \right\rangle. \quad (4.30)$$

Under parity followed by time reversal, the matrix element becomes

$$I_{m',m}^+(Q) \rightarrow (-1)^{m-m'} \left\langle -\frac{\mathbf{q}_\perp}{2}, -m \left| J^+(Q) \right| +\frac{\mathbf{q}_\perp}{2}, -m' \right\rangle. \quad (4.31)$$

$$(4.32)$$

Since  $J^\mu$  is Hermitian, we can also take the complex conjugate of the matrix element to get

$$I_{m',m}^+(Q) \rightarrow \left\langle -\frac{\mathbf{q}_\perp}{2}, m \left| J^+(Q) \right| +\frac{\mathbf{q}_\perp}{2}, m' \right\rangle. \quad (4.33)$$

The appropriate combinations of Eqs. (4.30-4.33) give [79]

$$I_{m',m}^+(Q) = (-1)^{m-m'} I_{-m',-m}^+(Q), \quad (4.34)$$

$$= (-1)^{m-m'} I_{m,m'}^+(Q). \quad (4.35)$$

The same relations also apply for  $J_{m'm}^+$  matrix elements. Eqs. (4.34) and (4.35) imply that of the nine possible matrix elements of  $J^+$ , there are only four independent components. We choose those components to be  $I_{11}^+$ ,  $I_{10}^+$ ,  $I_{1-1}^+$ , and  $I_{00}^+$ . It is helpful to express the matrix elements in a matrix to see the symmetry properties explicitly.

$$I_{m',m}^+ = \begin{pmatrix} I_{11}^+ & I_{10}^+ & I_{1-1}^+ \\ -I_{10}^+ & I_{00}^+ & I_{10}^+ \\ I_{1-1}^+ & -I_{10}^+ & I_{11}^+ \end{pmatrix}. \quad (4.36)$$

### *Rotational Invariance and the Angular Condition*

This is as far as we can go with light-front dynamics, but there should be an additional redundancy in our matrix elements. We have derived four independent components, whereas in a fully covariant framework there are only three form factors. The resolution of this conflict is that full rotational invariance imposes an *angular condition* on the light-front matrix elements.

The angular condition can be found by using the deuteron polarization vectors for the Breit frame to calculate the current given in Eq. (4.3) in terms of  $F_1$ ,  $F_2$ , and  $G_1$ . By comparing that result with Eq. (4.36), we obtain linear relations between the current matrix elements ( $I_{11}^+$ ,  $I_{10}^+$ ,  $I_{1-1}^+$ , and  $I_{00}^+$ ) and the form factors ( $F_1$ ,  $F_2$ , and  $G_1$ ) and also find that in general there is a deviation from the angular condition, which we denote with  $\Delta$ , given by [83]

$$\Delta = -I_{00}^+ + (1 + 2\eta)I_{11}^+ + I_{1-1}^+ - 2\sqrt{2\eta}I_{10}^+, \quad (4.37)$$

where  $\eta$  is defined by Eq. (4.11). Since  $\Delta$  vanishes when the deuteron current transforms correctly under rotations, we interpret  $\Delta$  as a measure of the extent to which the current matrix elements transform incorrectly.

The form factors are overdetermined by the current matrix elements, which means there are many different ways to express the form factors in terms of the current matrix elements. In order to make a definite prescription, one the current matrix

elements (or a linear combination of matrix elements) is identified as “bad”, and the angular condition is used to eliminate it from the expressions for the form factors. This classification of matrix elements as “good” or “bad” is similar to the one made for choosing which component of the current to use.

When  $\Delta$  is zero, all the prescriptions must be equivalent, while a non-zero  $\Delta$  means that the form factors depend on which prescription is chosen. Since  $\Delta$  is non-zero in general, it is important to choose the best prescription to obtain the form factor.

We consider four different prescriptions [83] in this work. This allows us to study how sensitively the form factors depend on the prescription used. First, Grach and Kondratyuk (GK) derive a relation in which  $I_{00}^+$  is considered bad. Using the angular condition to eliminate the  $I_{00}^+$  for the equations, they obtain [96]

$$G_{0,GK} = \frac{1}{3} \left[ (3 - 2\eta)I_{11}^+ + 2\sqrt{2\eta}I_{10}^+ + I_{1-1}^+ \right], \quad (4.38)$$

$$G_{1,GK} = 2 \left( I_{11}^+ - \frac{1}{\sqrt{2\eta}}I_{10}^+ \right), \quad (4.39)$$

$$G_{2,GK} = \frac{2\sqrt{2}}{3} \left( -\eta I_{11}^+ + \frac{2\eta^+}{I_{10}} - I_{1-1}^+ \right). \quad (4.40)$$

Brodsky and Hiller (BH) use a prescription where  $I_{11}^+$  is bad, which results in [97]

$$G_{0,BH} = \frac{1}{3(1 + 2\eta)} \left[ (3 - 2\eta)I_{00}^+ + 8\sqrt{2\eta}I_{10}^+ + 2(2\eta - 1)I_{1-1}^+ \right], \quad (4.41)$$

$$G_{1,BH} = \frac{2}{1 + 2\eta} \left[ I_{00}^+ - I_{1-1}^+ + (2\eta - 1)\frac{I_{10}^+}{\sqrt{2\eta}} \right], \quad (4.42)$$

$$G_{2,BH} = \frac{2\sqrt{2}}{3(1 + 2\eta)} \left[ \sqrt{2\eta}I_{10}^+ - \eta I_{00}^+ - (1 + \eta)I_{1-1}^+ \right]. \quad (4.43)$$

Frankfurt, Frederico, and Strikman (FFS) start by analyzing the deuteron current using an equal-time spin basis, where the current matrix elements are  $J_{m'm}^+$  [80]. Their prescription uses the Cartesian basis to find that  $J_{zz}^+$  is the bad current. Upon transformation to the spherical basis and use of the Melosh transformation [82, 98] to

relate  $J_{m'm}^+$  to  $I_{m'm}^+$ , they find

$$G_{0,FFS} = \frac{1}{3(1+\eta)} \left[ (2\eta+3)I_{11}^+ + 2\sqrt{2\eta}I_{10}^+ - \eta I_{00}^+ + (2\eta+1)I_{1-1}^+ \right], \quad (4.44)$$

$$G_{1,FFS} = \frac{1}{1+\eta} \left[ I_{11}^+ + I_{00}^+ - I_{1-1}^+ - \frac{2(1-\eta)}{\sqrt{2\eta}} I_{10}^+ \right], \quad (4.45)$$

$$G_{2,FFS} = \frac{\sqrt{2}}{3(1+\eta)} \left[ -\eta I_{11}^+ + 2\sqrt{2\eta}I_{10}^+ - \eta I_{00}^+ - (\eta+2)I_{1-1}^+ \right]. \quad (4.46)$$

Chung, Polyzou, Coester, and Keister (CCKP) choose the canonical expressions for the form factors  $G_0$ ,  $G_1$ , and  $G_2$  in terms of the equal-time current as the starting point [79,90]. They use rotations and the Melosh transformation to express the equal-time current matrix elements in terms of the light-front current matrix elements, and find that

$$G_{0,CCKP} = \frac{1}{6(1+\eta)} \left[ (3-2\eta)(I_{11}^+ + I_{00}^+) + 10\sqrt{2\eta}I_{10}^+ + (4\eta-1)I_{1-1}^+ \right], \quad (4.47)$$

$$G_{1,CCKP} = G_{1,FFS}, \quad (4.48)$$

$$G_{2,CCKP} = G_{2,FFS}. \quad (4.49)$$

Note that all the prescriptions reviewed here are related by the angular condition. When  $\Delta$  is zero, each prescription gives the same results.

#### 4.1.3 Impulse Approximation on the Light Front

We now are ready to relate the deuteron wave function to the current expressed in Eq. (4.24). The deuteron wave functions solved in Chapter 3 are used. We use the representation of the wave function in the spin  $|\mathbf{p}_\perp, p^+, m_1, m_2\rangle$  basis, as discussed in Sec. 3.5.4. Note that these spins are expressed in the usual Bjorken and Drell representation [99]. By inserting a two complete sets of states into Eq. (4.24) and

making the momentum of particle 1 explicit, we get

$$\begin{aligned}
J_{m',m}^+(q) = & \int d^2p_\perp dp^+ \sum_{m'_1, m_1, m_2} \left\langle \frac{\mathbf{q}_\perp}{2}, m' \left| p^+, \mathbf{p}_\perp + \frac{\mathbf{q}_\perp}{2}, m'_1, m_2 \right\rangle \right. \\
& 2 \left\langle p^+, \mathbf{p}_\perp + \frac{\mathbf{q}_\perp}{2}, m'_1 \left| J_{(S)}^+(\mathbf{q}_\perp) \left| p^+, \mathbf{p}_\perp - \frac{\mathbf{q}_\perp}{2}, m_1 \right\rangle \right. \right. \\
& \left. \left. \left\langle p^+, \mathbf{p}_\perp - \frac{\mathbf{q}_\perp}{2}, m_1, m_2 \left| -\frac{\mathbf{q}_\perp}{2}, m \right\rangle \right. \right. \quad (4.50)
\end{aligned}$$

where the spin directions of particles 1 and 2 are labeled  $m_1$  and  $m_2$ , respectively. Also, since the deuteron is an isoscalar combination of nucleons, the isovector component of the nucleon current does not contribute and the isoscalar nucleon current is the same for both nucleons. This allows us to simply double the isoscalar current of particle 1 instead of using the isoscalar currents of both particle 1 and 2.

We want to boost the deuteron wave functions to the rest frame, since that is where the wave functions are calculated. Note that the boosts in the  $x$ - $y$  plane transforms a general vector  $(\mathbf{k}_\perp, k^+)$  by  $\mathbf{k}_\perp \rightarrow \mathbf{k}_\perp - \mathbf{q}_\perp \frac{k^+}{q^+}$ , leaving  $k^+$  unchanged. This means that the boost that puts the deuteron in its rest frame transforms the individual nucleon momentum by

$$\mathbf{p}_\perp - \frac{\mathbf{q}_\perp}{2} \rightarrow \mathbf{p}_\perp - (1-x) \frac{\mathbf{q}_\perp}{2}, \quad (4.51)$$

where we use the Bjorken  $x$ -variable  $x = \frac{p^+}{M_d}$ . Note that the spin labels do not change. This is because the boost is in the perpendicular direction, so the spin labels (defined to point in the  $z$  direction) are not affected.

This allows Eq. (4.50) to be written as [84]

$$\begin{aligned}
J_{m',m}^+(q) = & \int d^2p_\perp dp^+ \sum_{m'_1, m_1, m_2} \left\langle m' \left| p^+, \mathbf{p}_\perp + (1-x) \frac{\mathbf{q}_\perp}{2}, m'_1, m_2 \right\rangle \right. \\
& 2 \left\langle p^+, \mathbf{p}_\perp + \frac{\mathbf{q}_\perp}{2}, m'_1 \left| J_{(S)}^+(\mathbf{q}_\perp) \left| p^+, \mathbf{p}_\perp - \frac{\mathbf{q}_\perp}{2}, m_1 \right\rangle \right. \right. \\
& \left. \left. \left\langle p^+, \mathbf{p}_\perp - (1-x) \frac{\mathbf{q}_\perp}{2}, m_1, m_2 \left| m \right\rangle \right. \right. \quad (4.52)
\end{aligned}$$

We have dropped explicit mention of the deuteron's momentum.

Before we continue, we note that we can write the nucleon current matrix elements using the  $u$  spinors,

$$\begin{aligned} & \left\langle p^+, \mathbf{p}_\perp + \frac{\mathbf{q}_\perp}{2}, m'_1 \left| J_{(S)}^+(\mathbf{q}_\perp) \right| p^+, \mathbf{p}_\perp - \frac{\mathbf{q}_\perp}{2}, m_1 \right\rangle \\ &= \bar{u}_{\text{BD}} \left( p^+, \mathbf{p}_\perp + \frac{\mathbf{q}_\perp}{2}, m'_1 \right) J_{(S)}^+(\mathbf{q}_\perp) u_{\text{BD}} \left( p^+, \mathbf{p}_\perp - \frac{\mathbf{q}_\perp}{2}, m_1 \right), \end{aligned} \quad (4.53)$$

where we have used the ‘‘BD’’ subscript to denote these as Bjorken and Drell spinors. Since the nucleons are on-shell, as they must be in a Hamiltonian theory, we interpret  $u_{\text{BD}}(p^+, \mathbf{p}_\perp, m)$  as  $u_{\text{BD}}(p_x = p_{\perp,x}, p_y = p_{\perp,y}, p_z = \frac{p^+ - p^-}{2})$ , where  $p^- = \frac{M^2 + p_\perp^2}{p^+}$ .

However, the matrix elements can be calculated easily if we convert the Bjorken and Drell spinors to light-front spinors. This transformation is formally accomplished with the Melosh transformation  $R_M$ , given by [79, 80],

$$R_M = \frac{p^+ + M - i\boldsymbol{\sigma} \cdot (\mathbf{n} \times \mathbf{p}_\perp)}{\sqrt{(p^+ + M)^2 + p_\perp^2}}, \quad (4.54)$$

where  $\mathbf{n}$  points in the direction of the light front. Note that the Melosh transformation is unitary.

This transformation converts a Bjorken and Drell spinor to a light-front spinor in the following manner,

$$u_{\text{LF}}(p^+, \mathbf{p}_\perp, m) = \sum_{m'} (R_M^\dagger)_{m,m'} u_{\text{BD}}(p^+, \mathbf{p}_\perp, m'). \quad (4.55)$$

Using this transformation, we rewrite Eq. (4.52) as

$$\begin{aligned} J_{m',m}^+(q) &= \int d^2 p_\perp dp^+ \sum_{m'_1, m_1, m_2} \left[ \sum_{m''_1} \left\langle m' \left| p^+, \mathbf{p}_\perp + (1-x) \frac{\mathbf{q}_\perp}{2}, m''_1, m_2 \right\rangle (R_M)_{m''_1, m'_1} \right] \\ & \quad 2\bar{u}_{\text{LF}} \left( p^+, \mathbf{p}_\perp + \frac{\mathbf{q}_\perp}{2}, m'_1 \right) J_{(S)}^+(\mathbf{q}_\perp) u_{\text{LF}} \left( p^+, \mathbf{p}_\perp - \frac{\mathbf{q}_\perp}{2}, m_1 \right) \\ & \quad \left[ \sum_{m'''_1} (R_M^\dagger)_{m'''_1, m_1} \left\langle p^+, \mathbf{p}_\perp - (1-x) \frac{\mathbf{q}_\perp}{2}, m'''_1, m_2 \left| m \right\rangle \right]. \end{aligned} \quad (4.56)$$

#### 4.1.4 The Nucleon Form Factors

From Lorentz covariance, current conservation, parity invariance, and time reversal invariance [86, 87], the isoscalar part of the nucleon current can be expressed as

$$J_{(S)}^\mu(q) = \gamma^\mu F_1^{(S)}(q) + i \frac{\sigma^{\mu\nu} q_\nu}{2M} F_2^{(S)}(q). \quad (4.57)$$

Taking the matrix elements of  $J^+$  with the light-front spinors gives

$$\begin{aligned} \bar{u}(k', \lambda') J_{(S)}^+(\mathbf{q}_\perp) u(k, \lambda) &= F_1^{(S)}(q) \bar{u}_{\text{LF}}(k', \lambda') \gamma^+ u_{\text{LF}}(k, \lambda) \\ &+ F_2^{(S)}(q) \frac{q_\perp^i}{2M} \bar{u}_{\text{LF}}(k', \lambda') \gamma^+ \gamma_\perp^i u_{\text{LF}}(k, \lambda), \end{aligned} \quad (4.58)$$

where we have parameterized

$$k'^+ = k^+, \quad (4.59)$$

$$\mathbf{k}_\perp = \mathbf{p}_\perp + \frac{\mathbf{q}_\perp}{2}, \quad (4.60)$$

$$\mathbf{k}'_\perp = \mathbf{p}_\perp - \frac{\mathbf{q}_\perp}{2}. \quad (4.61)$$

We use the representation of the spinors given in Appendix F to simplify the spinor matrix elements appearing in Eq. 4.58. First consider

$$\begin{aligned} \bar{u}_{\text{LF}}(k', \lambda') \gamma^+ u_{\text{LF}}(k, \lambda) &= \frac{1}{Mk^+} \chi_{\text{LF}, \lambda'}^\dagger \left[ (M - \boldsymbol{\alpha}^\perp \cdot \mathbf{k}'^\perp) \Lambda_+ + k^+ \Lambda_- \right] \gamma^+ \\ &\times \left[ \Lambda_- (M + \boldsymbol{\alpha}^\perp \cdot \mathbf{k}^\perp) + \Lambda_+ k^+ \right] \chi_{\text{LF}, \lambda}, \end{aligned} \quad (4.62)$$

$$= \frac{k^+}{M} \delta_{\lambda' \lambda}. \quad (4.63)$$

Next,

$$\begin{aligned} \bar{u}_{\text{LF}}(k', \lambda') \gamma^+ \gamma_\perp^i u_{\text{LF}}(k, \lambda) &= \frac{1}{Mk^+} \chi_{\text{LF}, \lambda'}^\dagger \left[ (M - \boldsymbol{\alpha}^\perp \cdot \mathbf{k}'^\perp) \Lambda_+ + k^+ \Lambda_- \right] \gamma^+ \gamma^i \\ &\times \left[ \Lambda_- (M + \boldsymbol{\alpha}^\perp \cdot \mathbf{k}^\perp) + \Lambda_+ k^+ \right] \chi_{\text{LF}, \lambda}, \end{aligned} \quad (4.64)$$

$$= \frac{k^+}{M} \chi_{\text{LF}, \lambda'}^\dagger \gamma^+ \gamma_\perp^i \chi_{\text{LF}, \lambda}, \quad (4.65)$$

$$= -i \epsilon^{ij3} \frac{k^+}{M} \chi_{\lambda'}^\dagger \sigma^j \chi_\lambda. \quad (4.66)$$

Combining these, we find [80, 82]

$$\langle k', \lambda' | J_{(S)}^+(\mathbf{q}_\perp) | k, \lambda \rangle = \frac{k^+}{M} \chi_{\lambda'}^\dagger \left[ F_1^{(S)}(q) - \frac{1}{2M} F_2^{(S)}(q) (i q_\perp^i \epsilon^{ij3} \sigma_\perp^j) \right] \chi_\lambda \quad (4.67)$$

We can rewrite Eq. (4.67) as

$$\begin{aligned} \langle k', \lambda' | J_{(S)}^+(\mathbf{q}_\perp) | k, \lambda \rangle &= F_1^{(S)}(q) \langle k', \lambda' | J_{(1S)}^+(\mathbf{q}_\perp) | k, \lambda \rangle + \\ &F_2^{(S)}(q) \langle k', \lambda' | J_{(2S)}^+(\mathbf{q}_\perp) | k, \lambda \rangle, \end{aligned} \quad (4.68)$$

which, when inserted into Eq. (4.56), gives

$$I_{m',m}^+(q) = F_1^{(S)}(q) I_{(1)m',m}^+(q) + F_2^{(S)}(q) I_{(2)m',m}^+(q), \quad (4.69)$$

where we define

$$\begin{aligned} I_{(i)m',m}^+(q) &= \int d^2 p_\perp dp^+ \sum_{m'_1, m_1, m_2} \langle m' | p^+, \mathbf{p}_\perp + (1-x) \frac{\mathbf{q}_\perp}{2}, m'_1, m_2 \rangle \\ &2 \langle p^+, \mathbf{p}_\perp + \frac{\mathbf{q}_\perp}{2}, m'_1 | J_{(iS)}^+(\mathbf{q}_\perp) | p^+, \mathbf{p}_\perp - \frac{\mathbf{q}_\perp}{2}, m_1 \rangle \\ &\langle p^+, \mathbf{p}_\perp - (1-x) \frac{\mathbf{q}_\perp}{2}, m_1, m_2 | m \rangle, \end{aligned} \quad (4.70)$$

for  $i = 1, 2$ . Note that both  $J_{(1)m',m}^+(q)$  and  $J_{(2)m',m}^+(q)$  must satisfy the same equations as  $J_{m',m}^+(q)$  does. In particular, this means that the angular condition should apply to  $J_{(1)m',m}^+(q)$  and  $J_{(2)m',m}^+(q)$  independently, so we consider the deviation from the angular condition for each.

There are many parameterizations of the isoscalar nucleon form factors  $F_1^{(S)}(q)$  and  $F_2^{(S)}(q)$ . Since the measurement of the electron-nucleon cross section is difficult, the data have large errors and are consistent with several different models of the nucleon form factors. Some of the models representative of those proposed in the literature are: the dipole model, fit 8.2 of Hohler [100], Gari:1985 [101], model 3 of Gari:1992 [102, 103], best fit for the multiplicative parameterization of Mergell [104], and model DR-GK(1) of Lomon [105]. The  $F_1^{(S)}(q)$  and  $F_2^{(S)}(q)$  form factors for each of these models are shown in Fig. 4.3.

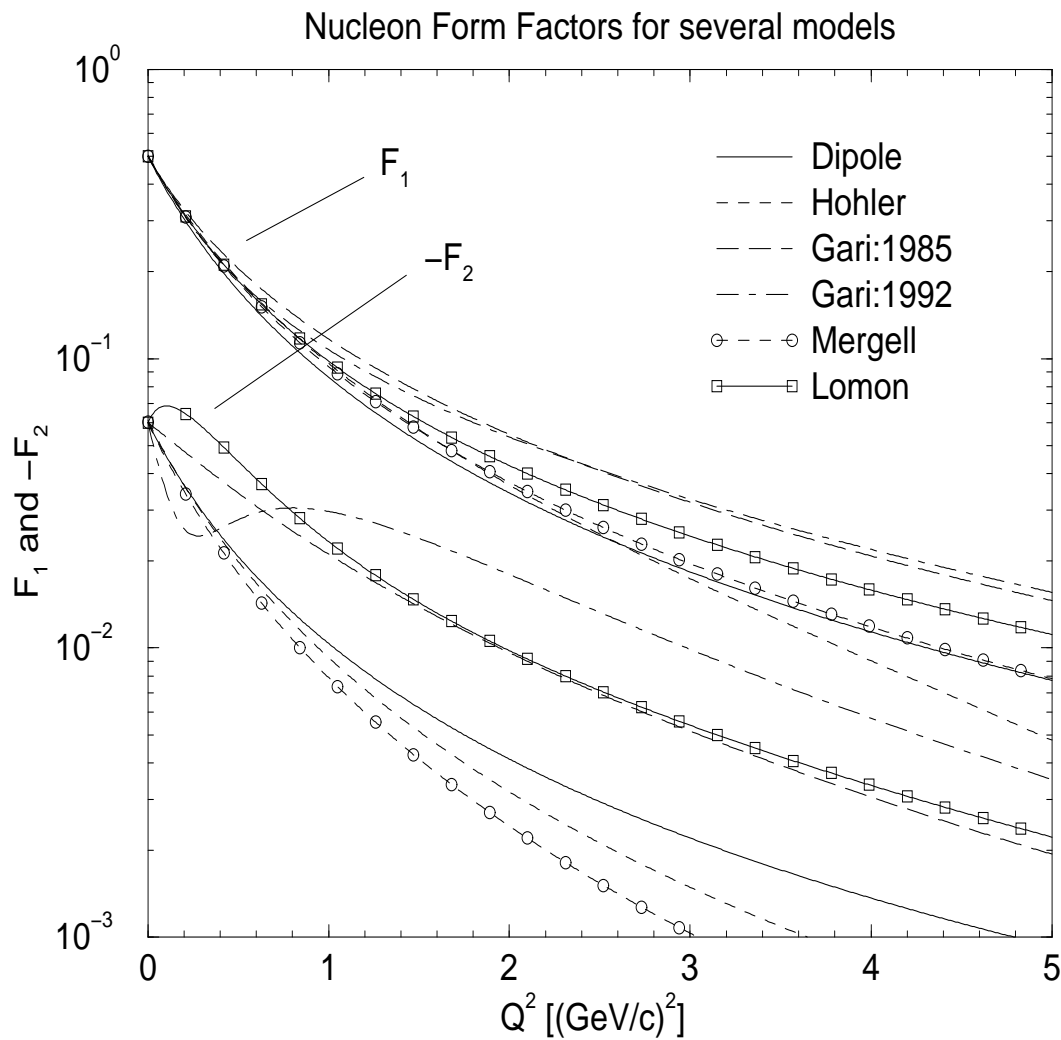


Figure 4.3: The  $F_1$  and  $-F_2$  isoscalar nucleon form factors for six different models: the dipole model, Hohler [100], Gari:1985 [101], Gari:1992 [102, 103], Mergell [104], and Lomon [105].

We can relate the isovector form factors to  $G_{Ep}$ ,  $G_{Mp}$ ,  $G_{En}$ , and  $G_{Mn}$ , the proton electric, proton magnetic, neutron electric, and neutron magnetic form factors, respectively, with [106]

$$F_1^{(S)} = \frac{G_{Ep} + G_{En} + \tau (G_{Mp} + G_{Mn})}{2(1 + \tau)}, \quad (4.71)$$

$$F_2^{(S)} = \frac{-G_{Ep} - G_{En} + G_{Mp} + G_{Mn}}{2(1 + \tau)}, \quad (4.72)$$

where  $\tau \equiv \frac{Q^2}{4M}$ . The value of  $\tau$  is approximately 1 at a momentum transfer of about 5 GeV<sup>2</sup>, the upper range of momentum transfers that we consider. Since the overall magnitudes of the form factors are similar at this momentum transfer, it is important to measure each of the form factors with the same accuracy and cover the same range of momentum transfers. Currently, the most poorly known form factor is  $G_{En}$ , both in terms of the magnitude of the error and in the number of data points [105].

In Section 4.3, we will find that for momentum transfers greater than about 2 GeV<sup>2</sup>, the spread in the values of the deuteron form factors due to the breaking of rotational invariance on the light front is smaller than the spread in values due to using the various nucleon form factors. It is uncertainty of the nucleon form factors, not the use of the light front, that limits the accuracy of the deuteron form factors at large momentum transfers. Only more accurate measurements of the nucleon form factors, especially  $G_{En}$ , will allow for more accurate deuteron form factor calculations.

## 4.2 Axial Form Factors

The formalism used for the axial current and form factor is very similar to that used for the electromagnetic current and form factor. Thus, most of the discussion from the previous section carries over here with only slight modifications. We highlight only the differences.

The derivation of the symmetries of the axial current matrix elements is almost

the same as in Section 4.1.2, with the exception that under parity, the axial current picks up a negative sign

$$\Pi J_5^\pm \Pi = - J_5^\mp. \quad (4.73)$$

When this is propagated through the algebra, we find that

$$I_{(5)m',m}^+(Q) = - (-1)^{m-m'} I_{(5)-m',-m}^+(Q), \quad (4.74)$$

$$= (-1)^{m-m'} I_{(5)m,m'}^+(Q). \quad (4.75)$$

Eqs. (4.74) and (4.75) imply that of the nine possible matrix elements of  $J_5^+$ , there are only two independent components. We choose those components to be  $I_{(5)11}^+$ , and  $I_{(5)10}^+$ . It is helpful to express the matrix elements in a matrix to see the symmetry properties explicitly.

$$I_{(5)m',m}^+ = \begin{pmatrix} I_{(5)11}^+ & I_{(5)10}^+ & 0 \\ -I_{(5)10}^+ & 0 & -I_{(5)10}^+ \\ 0 & I_{(5)10}^+ & -I_{(5)11}^+ \end{pmatrix}. \quad (4.76)$$

We have derived two independent components, but an analysis of the covariant theory shows that only one deuteron form factor ( $F_A$ ) contributes for the plus component of the axial current [81]. This implies that the requirement of full rotational invariance imposes an angular condition on the light-front axial current matrix elements. The deviation from the angular condition, denoted by  $\Delta$ , given by [81],

$$\Delta = \frac{\sqrt{2\eta}}{2} I_{(5)11}^+ - I_{(5)10}^+. \quad (4.77)$$

Since the deuteron axial form factor is overdetermined by the current matrix elements, we need to classify the current matrix elements as either “good” or “bad” to eliminate ambiguity. We consider two such choices.

Frankfurt, Frederico, and Strikman (FFS) find that the  $J_{(5)zz}^+$  is the bad matrix element [80]. After transforming to the spherical basis and using the Melosh transformation, they find that

$$F_A = \frac{1}{2(1+\eta)} \left( I_{(5)11}^+ + \sqrt{2\eta} I_{(5)10}^+ \right). \quad (4.78)$$

Frederico, Henley, and Miller (FHM) use the behavior of the matrix elements in the non-relativistic limit to determine that the bad element is  $I_{(5)10}^+$  [81]. This means that

$$F_A = \frac{1}{2} I_{(5)11}^+. \quad (4.79)$$

The current matrix elements are calculated using the nucleon axial current. The general form of nucleon axial current is given by [81],

$$J_{(5)n}^\mu = \gamma^\mu \gamma^5 F_A^n + q^\mu \gamma^5 F_P^n. \quad (4.80)$$

Since we choose to  $\mu = +$  and work in the Breit frame, where  $q^+ = 0$ , Eq. (4.80) reduces to

$$J_{(5)n}^+ = \gamma^+ \gamma^5 F_A^n. \quad (4.81)$$

The light-front spinor matrix elements of Eq. (4.81) can be computed using expressions given in Appendix F. The result is

$$\langle k', \lambda' | J_{(5)n}^+(\mathbf{q}_\perp) | k, \lambda \rangle = \frac{k^+}{M} F_A^n(q) \chi_{\lambda'} \sigma^3 \chi_\lambda. \quad (4.82)$$

We consider only one model for the nucleon axial form factor since the deuteron axial current has such a simple dependence on it. We choose to use the dipole model

$$F_A(Q^2) = \frac{F_A(0)}{\left(1 + \frac{Q^2}{M_A^2}\right)^2}, \quad (4.83)$$

where  $M_A$  is the axial mass. For our calculations, we use the value for the axial mass determined by Liesenfeld *et al.* [107].

### 4.3 Results for the Form Factors

We use the deuteron wave functions obtained for the light-front nucleon-nucleon potential in Chapter 3 to calculate the deuteron currents and form factors. This gives a

solution where light-front dynamics is used consistently throughout. For the potential, we choose the light-front nucleon-nucleon potential with  $f_\sigma = 1.2815$ . We have verified that the results do not change significantly when  $f_\sigma = 1.22$  is used.

Figure 4.4 show the currents and the associated angular condition for  $I_{(1)}^+$ , given by Eq. (4.70), for several different deuteron wave functions. Results are shown for the wave function from the OME, OME+TME, and OME+TPE potentials (calculated in Chapter 3), and the parameterization of the deuteron wave function for the energy independent Bonn potential [58]. The current matrix elements (but not  $\Delta$ ) are approximately the same regardless of which wave function is used. This consistency is important, since it verifies that the gross features of all the models are the same.

We find that  $\Delta$  for  $I_{(1)}^+$  is much smaller than the largest matrix elements when using the OME wave function. This means that the matrix elements of the  $I_{(1)}^+$  current operator transform very well under rotations. This is somewhat surprising, since we found earlier that the binding energies for the OME wave functions have a large splitting, indicating that OME wave functions transforms poorly under rotations.

To understand this apparent discrepancy, note that some diagrams are not included in the calculation of the current although they are required for manifest current conservation. This problem is addressed in Section 4.1.2. The missing graphs should have a small effect on the rotational properties of the current, but they may have a large effect on  $\Delta$ . In particular, since the OME+TME current is missing more graphs than the OME current, it is reasonable that the OME+TME current transforms more poorly under rotations than the OME current.

Comparing the current calculated with the OME wave function to those calculated with other potentials, we find that for momentum transfers of more than  $1 \text{ GeV}^2$  the OME  $I_{(1)}^+$  current has the best transformation properties under rotation of all the  $I_{(1)}^+$  currents shown.

For smaller momentum transfers, the transformation properties of the Bonn and OME+TME wave functions are the best. This is expected, since in the limit of

no momentum transfer, the current  $I_{(1)m'm}^+$  is simply the overlap of deuteron wave functions,  $\langle m'|m\rangle$ . If the initial and final states have the same mass, the matrix element is simply  $\delta_{m'm}$ , which satisfies the angular condition. However, if the states do not have the same mass (which implies that  $m' \neq m$ ), there will be a non-zero overlap between the two states, which violates the angular condition. Since the masses of the deuteron states are exactly the same for the Bonn wave function, and approximately the same for the OME+TPE wave function, they have a small  $\Delta$  at low momentum transfer. However, the OME wave functions, having the largest mass splitting, have the largest  $\Delta$  at low momentum transfers.

Figures 4.5 and 4.6 show the current matrix elements and the angular condition for  $I_{(2)}^+$  and  $I_{(5)}^+$ , respectively. The general features of these figures are the same as in Figure 4.4, with one important exception. In both figures, the  $\Delta$  for the OME wave function has about the same magnitude as the  $\Delta$ 's for the other wave functions. This means that the rotational properties of  $I_{(2)}^+$  and  $I_{(5)}^+$  currents are approximately the same regardless of which wave function is used. This is a surprising result since it indicates that the rotational properties of the current depend more on how the current is constructed than on which wave function is used.

In Fig. 4.5, we find that the magnitude of  $\Delta$  is almost the same as the magnitude of the largest matrix element of  $I_{(1)}^+$ . This means there is a large deviation from the angular condition, and that form factors calculated with this current may depend strongly on which matrix element is chosen as “bad”. We show below that this is not the case for the electromagnetic form factors.

We find that  $\Delta$  is much smaller than the largest matrix element of the axial currents shown in Fig. 4.6 for most values of momentum transfer. This means that the deuteron axial form factor will be essentially independent of which matrix element is chosen as “bad”, except for within the range of 1.5 to 2 GeV<sup>2</sup>.

Now we combine the two parts of the electromagnetic current,  $I_{(1)}^+$  and  $I_{(2)}^+$ , with the nucleon form factors  $F_1$  and  $F_2$  to get the total current. Figure 4.7 shows the

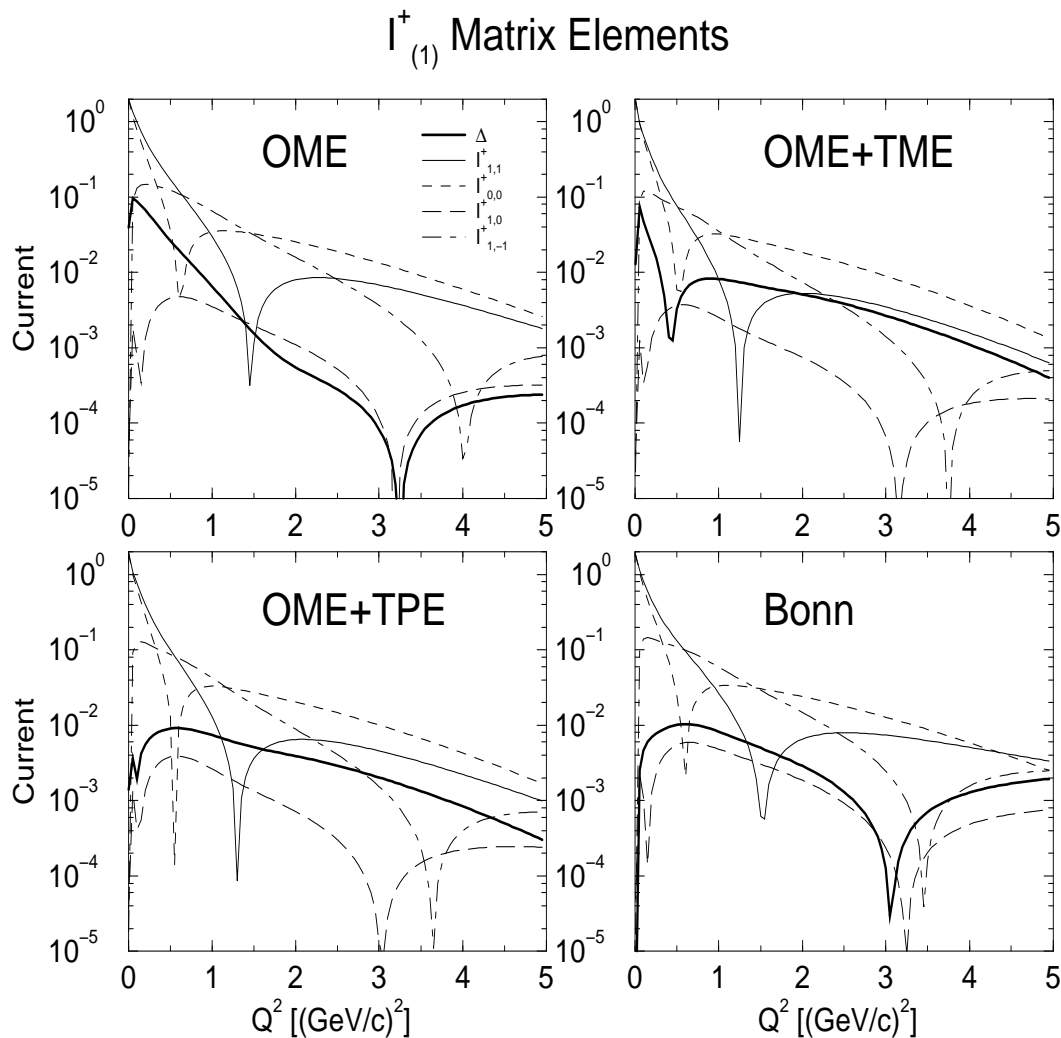


Figure 4.4: The matrix elements of  $I_{(1)m'm}^+$ , the component of the electromagnetic current which multiplies the nucleon  $F_1$  form factor, calculated with the wave function from the OME, OME+TME, OME+TPE, and Bonn potentials.

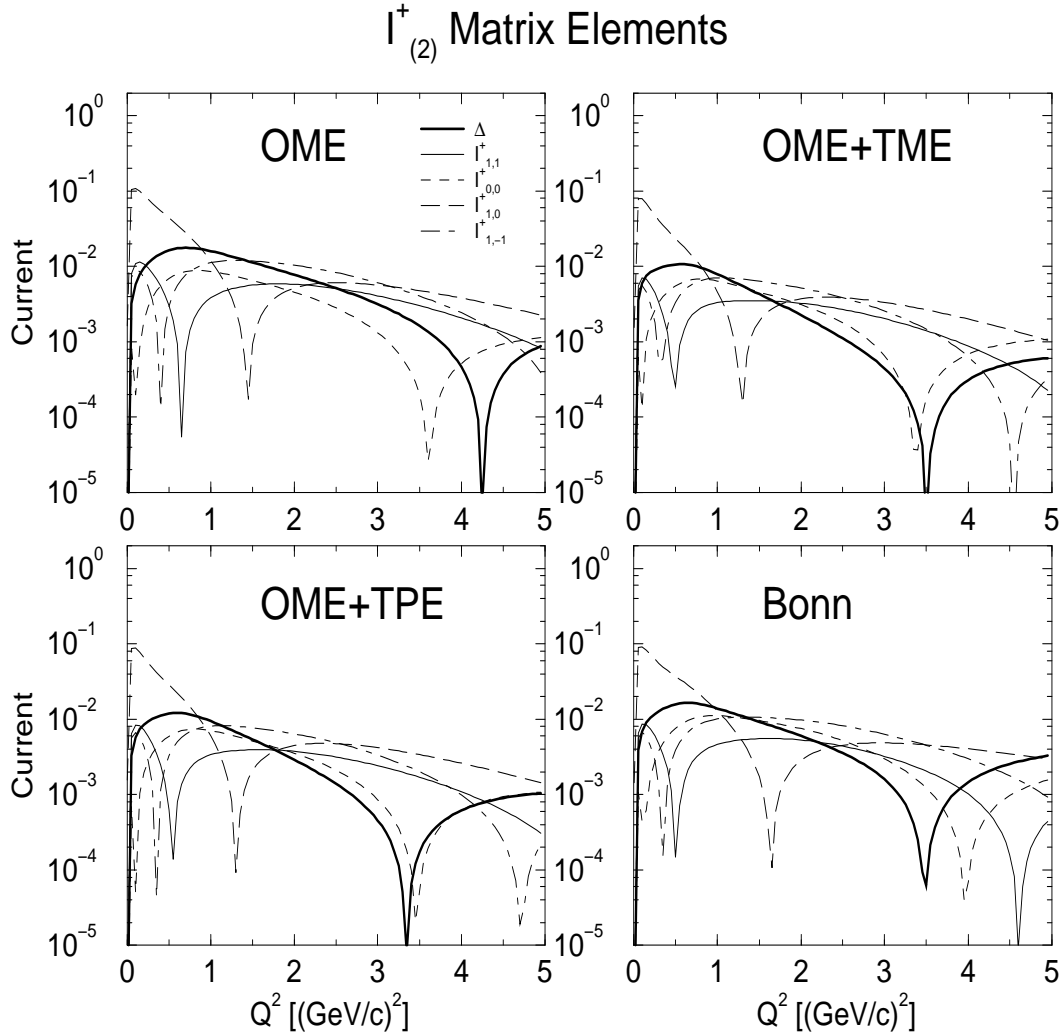


Figure 4.5: The matrix elements of  $I_{(2)m'm}^+$ , the component of the electromagnetic current which multiplies the nucleon  $F_2$  form factor, calculated with the wave function from the OME, OME+TME, OME+TPE, and Bonn potentials.

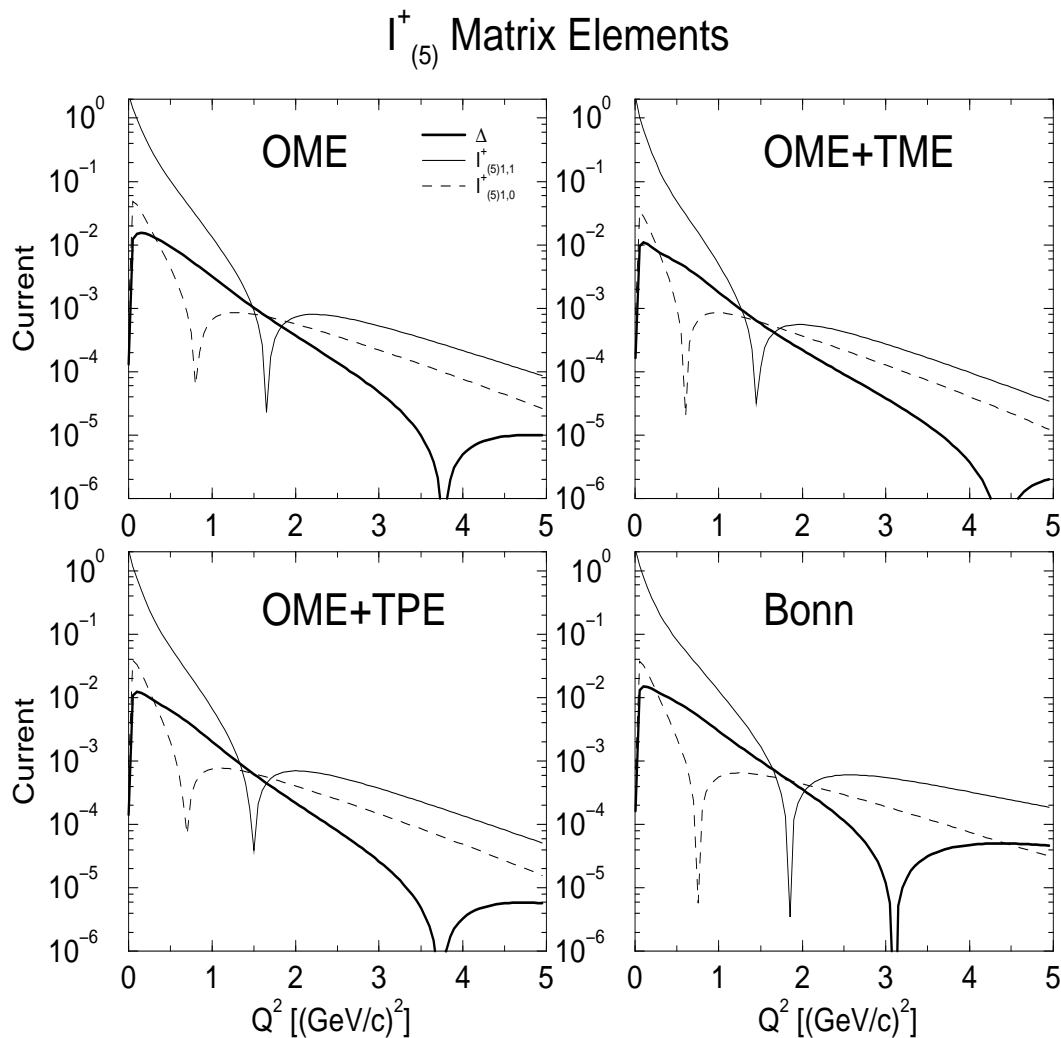


Figure 4.6: The matrix elements of  $I_{(5)m'm}^+$ , the deuteron axial current including the nucleon axial form factor, calculated with the wave function from the OME, OME+TME, OME+TPE, and Bonn potentials.

currents for  $F_1 I_{(1)}^+$  and  $F_2 I_{(2)}^+$ , as well as the sum,  $I^+$ . The Gari:1985 nucleon form factors are used [101]. We find that  $F_1 I_{(1)}^+$  gives the largest contribution to the total current, and because  $\Delta$  is small for  $I_{(1)}^+$ ,  $\Delta$  is also small for the total current, meaning that the total current transforms well under rotations. Thus, in spite of the fact that  $\Delta$  is approximately the same size as the current matrix elements for  $I_{(2)}^+$ , the deuteron electromagnetic form factors should not depend too strongly on the choice of the “bad” matrix element. This is especially true for the form factors calculated with the OME wave function.

We calculate the form factors  $A$ ,  $B$ ,  $T_{20}$ , and  $F_A$  using the OME wave function, and show the results in Fig. 4.8. In general, the form factors do not depend strongly on which matrix element is chosen as “bad”, in agreement with what we predicted in the previous paragraph. The only exception is for the  $B$  form factor, and to a lesser extent the  $F_A$  form factor, near where they cross zero. This is not too surprising, since a small constant shift in any function near a zero-crossing has a large effect in a logarithmic plot. Also, we note that the FFS and CCKP choices of the “bad” matrix element give the same value for  $B$ . This is a consequence of Eqs. (4.48) and (4.49).

We also use the OME+TME wave function to calculate the form factors  $A$ ,  $B$ ,  $T_{20}$ , and  $F_A$ , which we show in Fig. 4.9. We argued earlier that these electromagnetic form factors depend more strongly on which matrix element is chosen as “bad” than those calculated with the OME wave function, and that dependence is clear in this figure. At low momentum transfers, the dependence on the choice is fairly small, but as the momentum transfer increases, so does the dependence. The axial form factor is not affected as strongly, primarily because each wave function generates an axial current which violates the angular condition by approximately the same amount.

Since there are many different models of the nucleon electromagnetic form factors, we calculate the deuteron electromagnetic form factors using each of them to see what effect the differences have. The results are shown in Fig. 4.10. At low momentum transfers, all the nucleon form factors give close to the same results. However,

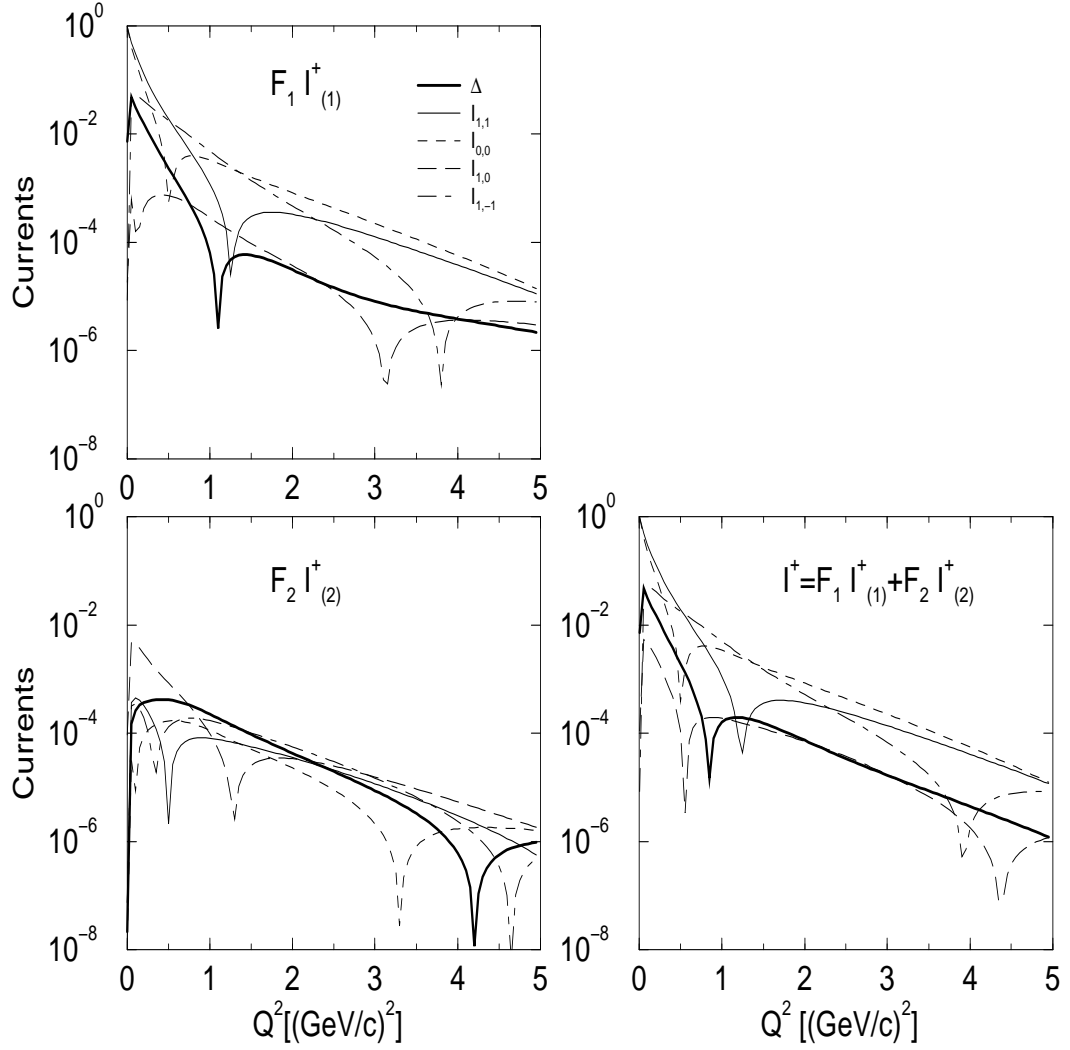


Figure 4.7: The matrix elements for  $F_1 I_{(1)m'm}^+$ ,  $F_2 I_{(2)m'm}^+$ , and  $I_{m'm}^+$  calculated with the OME wave functions. The Gari:1985 nucleon isoscalar form factors are used for  $F_1$  and  $F_2$  [101].

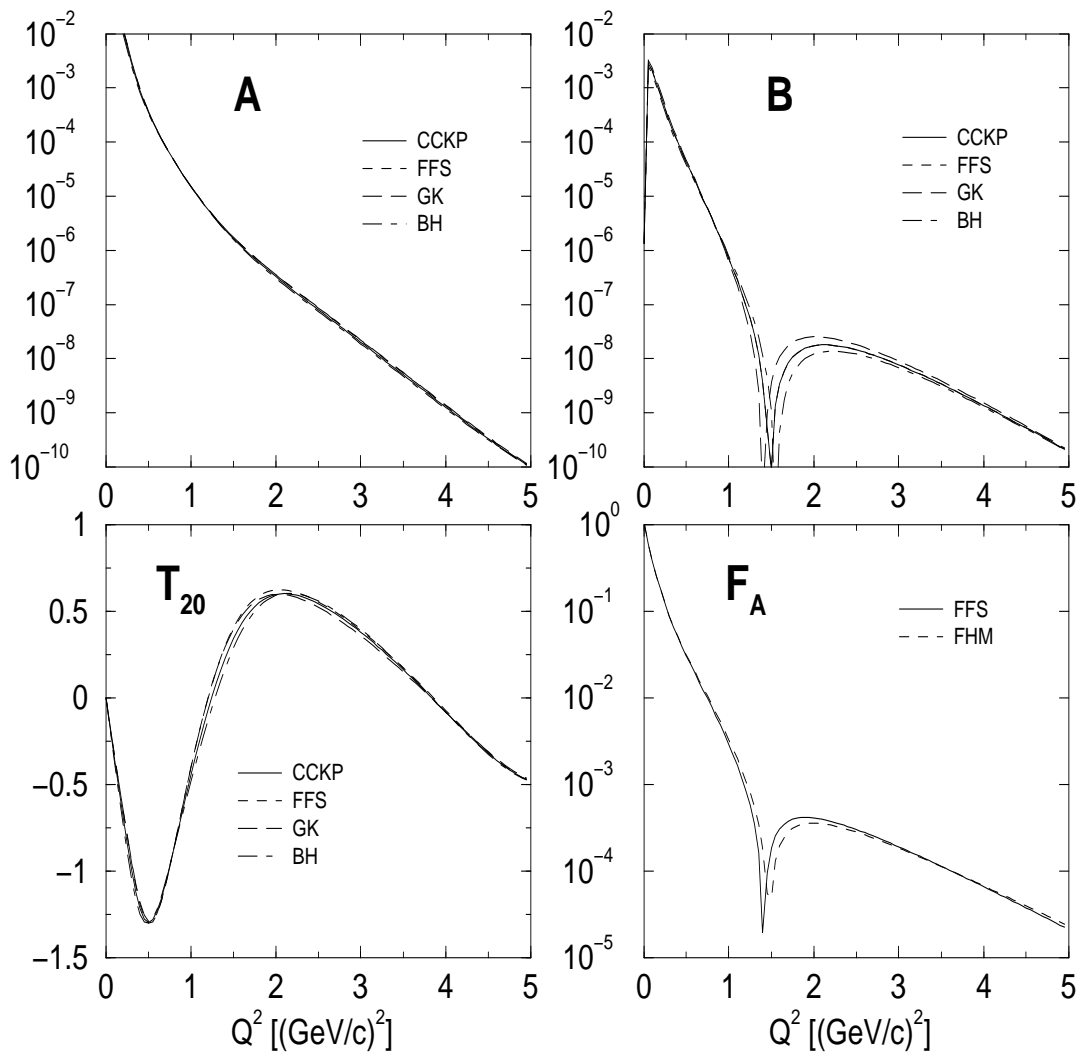


Figure 4.8: The form factors  $A$ ,  $B$ ,  $T_{20}$ , and  $F_A$  calculated using the various choices of the “bad” matrix element. The definitions of the “bad” matrix elements are given in Sections 4.1.2 and 4.2. The OME wave function is used, along with the Lomon nucleon form factors [105] for the electromagnetic form factors, and the Liesenfeld nucleon form factor [107] for the axial form factor.

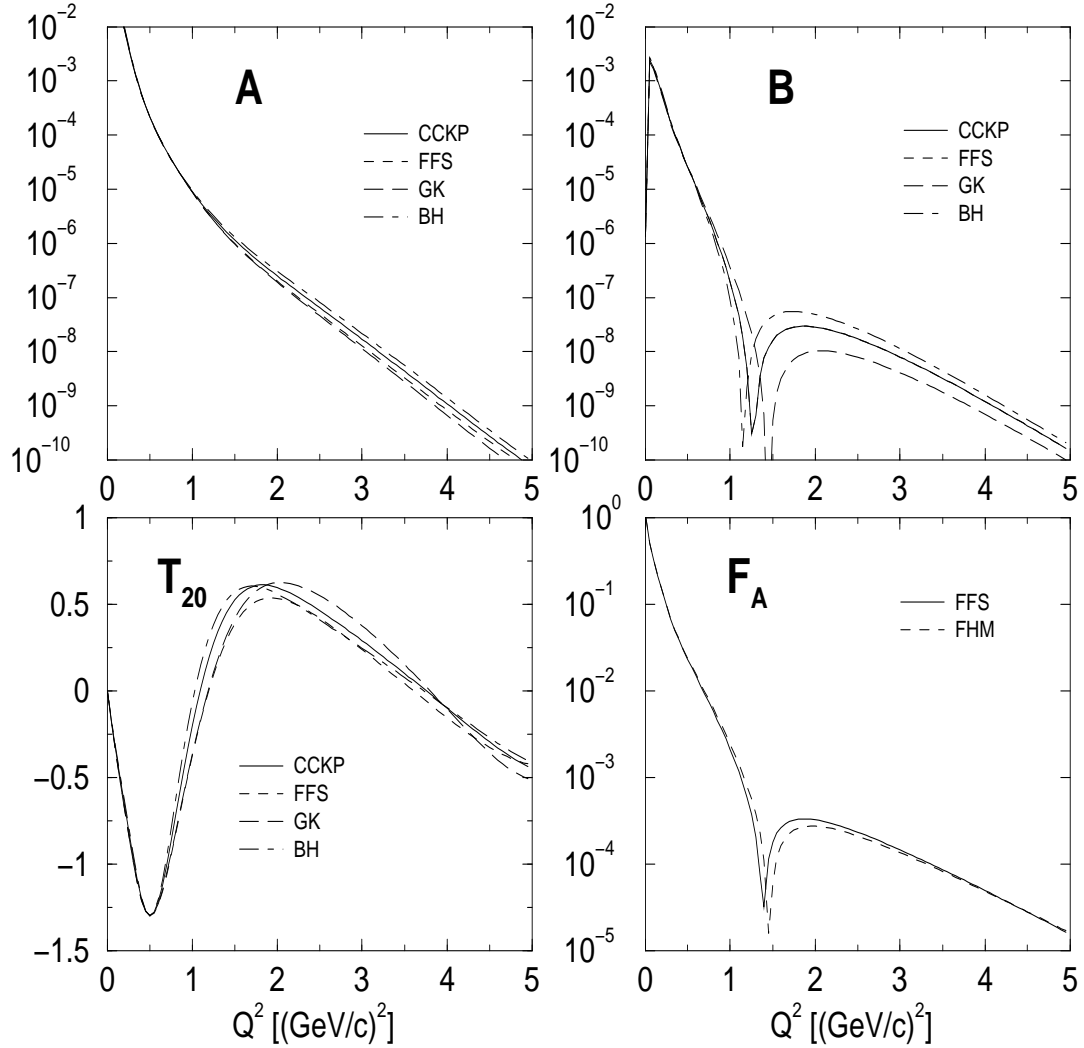


Figure 4.9: The form factors  $A$ ,  $B$ ,  $T_{20}$ , and  $F_A$  calculated using the various choices of the “bad” matrix element. The definitions of the “bad” matrix elements are given in Sections 4.1.2 and 4.2. The OME+TME wave function is used, along with the Lomon nucleon form factors [105] for the electromagnetic form factors, and the Liesenfeld nucleon form factor [107] for the axial form factor.

when the momentum transfers is large, we find a large spread in the values due to nucleon form factors. In fact, this spread in  $A$  and  $B$  is larger than the spread of values obtained from using different “bad” matrix elements with the OME+TME wave functions. In other words, in order to obtain accurate results for  $A$  and  $B$  at momentum transfers over  $2 \text{ GeV}^2$ , it is more important to determine which nucleon form factor to use than when “bad” matrix to use. The spread in  $T_{20}$  is about the same size regardless of whether the different “bad” matrix elements or the different nucleon form factors are used.

Finally, in Fig. 4.11, we compare the  $A$ ,  $B$ ,  $T_{20}$ , and  $F_A$  form factors for the OME and OME+TME wave functions to experimental data. The “bad” component was chosen according to FFS, and the nucleon form factors of Lomon were used for  $A$ ,  $B$ , and  $T_{20}$ , while the Liesenfeld axial nucleon form factor was used for  $F_A$ . The data for  $A$  is from: Buchanan *et al.* [108], Elias *et al.* [109], Galster *et al.* [110], Platchkov *et al.* [111], Abbott *et al.* [112], and Alexa *et al.* [1]; the data for  $B$  is from: Buchanan *et al.* [108], Auffret *et al.* [113], and Bosted *et al.* [114]; and the data for  $T_{20}$  is from: Schulze *et al.* [115], Gilman *et al.* [116], Boden *et al.* [117], Garcon *et al.* [118], Ferro-Luzzi *et al.* [119], Bouwhuis *et al.* [120], and Abbott *et al.* [121].

There is a rather large difference between the form factors calculated with the OME and OME+TME wave functions. This difference is due primarily to the fact that the OME wave functions are more deeply bound than the OME+TME wave functions, and it can be reduced by choosing a different sigma coupling constant  $f_\sigma$  for the OME and OME+TME potentials. However, for our analysis of rotational invariance, it is important to keep  $f_\sigma$  fixed.

The difference between the calculated form factors and the data is also quite large. This is not unexpected, since in our model of the current, meson exchange currents are not included. It is known that these have a large effect on the form factors at large momentum transfers [93,122,123]. Including these effects would bring the form factors into better agreement with the data. However, we emphasize again that agreement

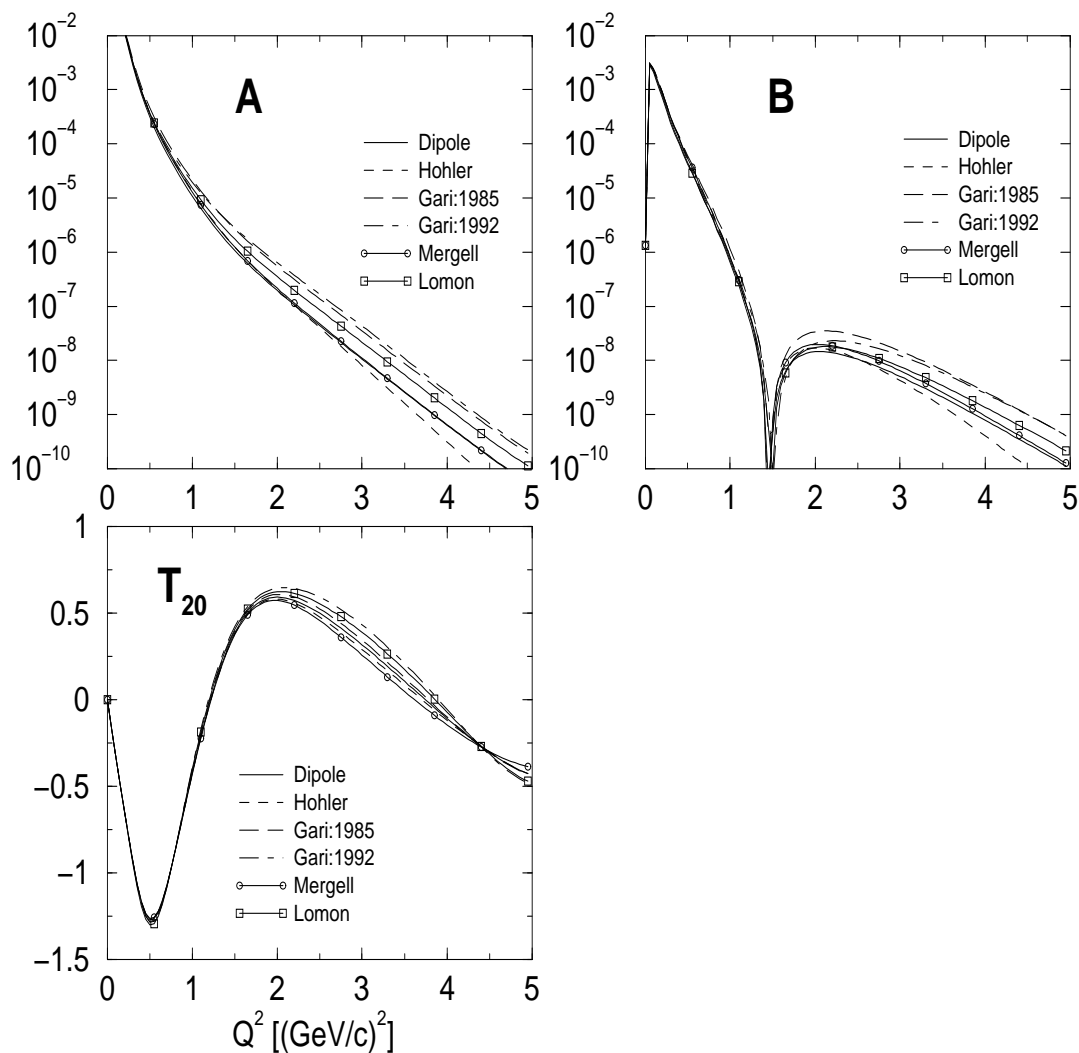


Figure 4.10: The electromagnetic form factors  $A$ ,  $B$ , and  $T_{20}$  calculated using the various choices of the nucleon isoscalar form factors. The OME wave function is used, along with the FFS choice of the “bad” deuteron current matrix. The axial form factor is not shown since its dependence on different form factors is trivial.

with the data is not a priority of this work. Our goal is to gain a better understanding of the breaking of rotational invariance by the light front, and how to restore that invariance. Only after we have that understanding can we pursue accurate calculation of the form factors with light-front dynamics.

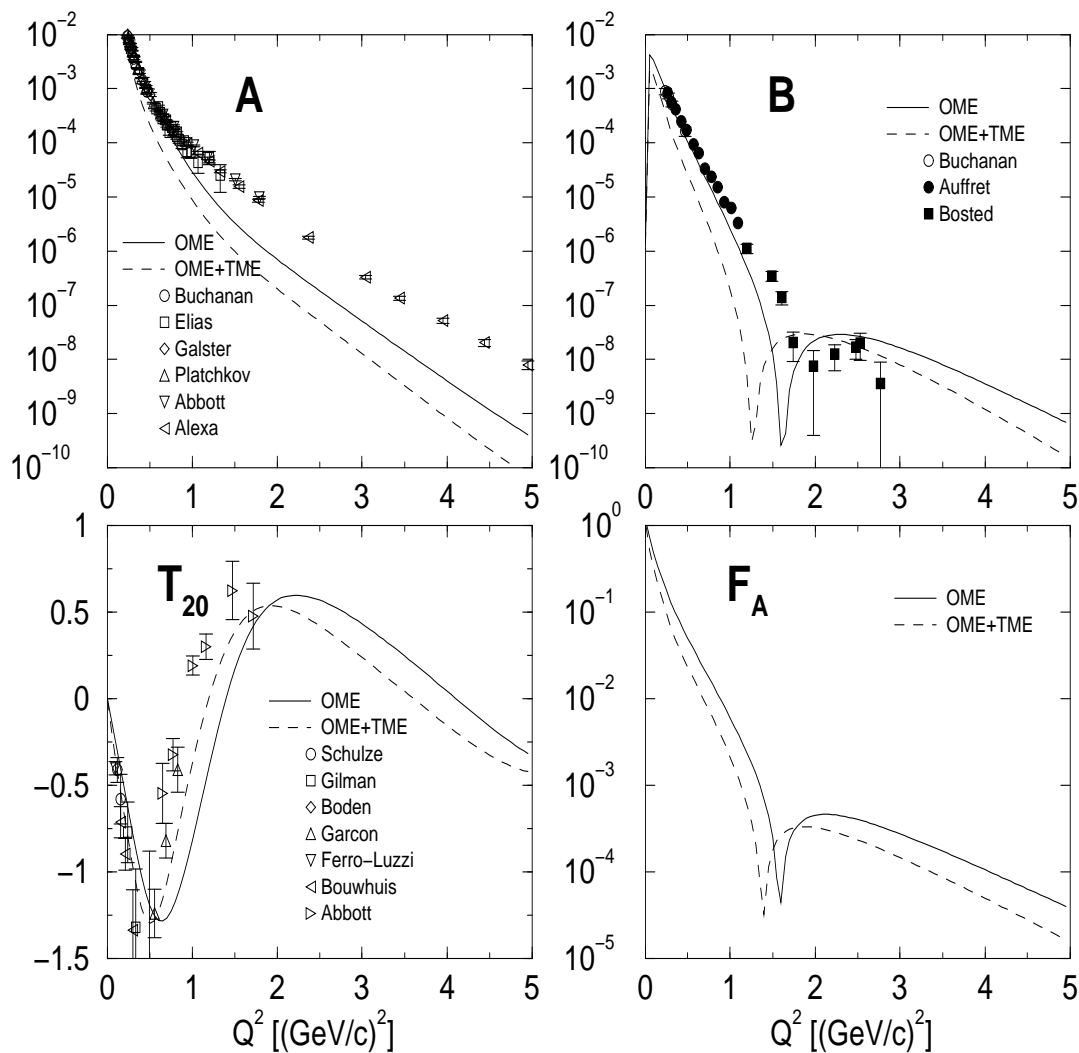


Figure 4.11: The  $A$ ,  $B$ ,  $T_{20}$ , and  $F_A$  form factors for the OME and OME+TME potentials, along with data. See the accompanying text for an explanation of the data.

## Chapter 5

## CONCLUSIONS

“If a thing can not go on forever, it will come to an end.”

—*Herbert Stein*

The issue of rotational invariance in light-front dynamics must be addressed before one attempt to use light-front dynamics for high-precision calculations. In this work, we have sought to find ways to quantify the level to which rotational invariance is broken. In addition, we have investigated potentials of different orders, since we know that if all orders of the potential were included, rotational invariance would be restored. We have used light-front dynamics to obtain one-meson-exchange (OME) and two-meson-exchange (TME) potentials for several different nuclear theory Lagrangians.

In Chapter 2, the massive Wick-Cutkosky model is used to investigate the breaking of rotational invariance in deeply bound states. We studied the pseudo angular momentum decomposition of each wave function into different eigenstates of pseudo angular momentum. In general, we found that most states are approximately angular momentum eigenstates. That is, a partial-wave decomposition of the wave functions shows that most states have one dominant (highest percentage) angular momentum component. Including the TBE potentials increases the fraction of the dominant component in most states. We also showed that the spectra generated by the Bethe-Salpeter equation using the ladder and crossed ladder are well approximated with the spectra generated by the matching OME+TME potentials. In addition, we found that the spectra for the full ground state calculation cannot be reproduced accurately

for deeply bound states using either the light-front Hamiltonian or the Bethe-Salpeter equation.

In Chapter 3, a model Lagrangian for nuclear physics which includes chiral symmetry was used to derive two models, a light-front pion-only model, and a new light-front nucleon-nucleon potential. Those potentials are then used to calculate the binding energy and wave function for the  $m = 0$  and  $m = 1$  states of the deuteron. We find that for both models, the splitting between the  $m = 0$  and  $m = 1$  states was smaller for the OME+TME potential as compared to the OME potential gives. We also find that the effects of chiral symmetry must be included to obtain sensible results for the OPE+TPE pion-only model.

In Chapter 4, the wave functions obtained in Chapter 3 are used to calculate the form factors of the deuteron using only light-front dynamics throughout. In light-front dynamics, there are four independent components of the deuteron current. However, the requirement of rotational invariance introduces an angular condition that the four components must satisfy, reducing the number of physically independent components to three. The deviation of the calculated current components from the angular condition is denoted by  $\Delta$ . We find that  $\Delta$  is very small for the deuteron wave functions calculated with the OME potential. This is an important result, since it means that although *in principle* the light-front calculation of the deuteron current does not transform correctly under rotations, *in practice* it does quite well. The smallness of  $\Delta$  means that any reasonable prescription for eliminating the dependent component of the current gives essentially the same results; the uncertainty introduced by the various nucleon form factors is greater for  $A$  and  $B$ , and about the same size for  $T_{20}$ .

We also found that  $\Delta$  is significantly larger when the TME potentials are used. Since the previous results in Chapters 2 and 3 indicate that the rotational properties of the TME wave function are better than for the OME wave function, we interpret the increase in  $\Delta$  as an indication that extra diagrams need to be included in the current

calculation to restore rotational invariance. That is, having a wave function with good rotational properties is not sufficient to obtain matrix elements of the current operator with good rotational properties.

### ***Future Extensions***

“I never see what has been done; I only see what remains to be done.”

—*Marie Curie*

This work can be extended in many ways. Perhaps the most important addition is to add the higher-order graphs to the deuteron current that are required for current conservation. This may improve the quality of the deuteron form factors when the wave function is calculated using the two-meson-exchange potentials.

Another obvious extension is to include the crossed TME diagrams. This would have two effects. Recall that we included the chiral contact diagrams using a prescription to maintain approximate chiral symmetry. When the crossed diagrams are included, we simply include the full contact potentials which included chiral symmetry without approximation. The second effect is that the crossed diagrams are needed in principle to obtain an accurate solution for the deuteron. However, these effects are not needed to study the breaking of rotational invariance.

The contribution to the deuteron form factors from the meson form factors is another effect that could be investigated. This is possible since our potential is derived from a Lagrangian, and we can calculate the mesonic components of the deuteron wave function. Obviously, the contribution to the form factor due to the mesons must be taken into account when attempting a high precision calculation. However, including these components, like including the crossed diagrams, does not affect the overall rotational invariance properties of the deuteron form factors.

## BIBLIOGRAPHY

“One could not be a successful scientist without realizing that, in contrast to the popular conception supported by newspapers and mothers of scientists, a goodly number of scientists are not only narrow-minded and dull, but also just stupid.”

—*James Watson*

- [1] Jefferson Lab Hall A, L. C. Alexa *et al.*, Phys. Rev. Lett. **82**, 1374 (1999), nucl-ex/9812002.
- [2] Y. A. Simonov and J. A. Tjon, Annals Phys. **228**, 1 (1993).
- [3] Y. Nambu, Prog. Theor. Phys. **5**, 614 (1950).
- [4] J. Schwinger, Proc. Nat. Acad. Sci. **37**, 452 (1951).
- [5] J. Schwinger, Proc. Nat. Acad. Sci. **37**, 455 (1951).
- [6] M. Gell-Mann and F. Low, Phys. Rev. **84**, 350 (1951).
- [7] E. E. Salpeter and H. A. Bethe, Phys. Rev. **84**, 1232 (1951).
- [8] F. Gross, Phys. Rev. **C26**, 2203 (1982).
- [9] G. E. Brown and A. D. Jackson, *The Nucleon-Nucleon Interaction* (North-Holland, Amsterdam, 1976), chap. VII.
- [10] R. Blankenbecler and R. Sugar, Phys. Rev. **142**, 1051 (1966).

- [11] F. Gross, Phys. Rev. **186**, 1448 (1969).
- [12] P. A. M. Dirac, Rev. Mod. Phys. **21**, 392 (1949).
- [13] J. Carbonell, B. Desplanques, V. A. Karmanov, and J. F. Mathiot, Phys. Rept. **300**, 215 (1998), nucl-th/9804029.
- [14] N. C. J. Schoonderwoerd, B. L. G. Bakker, and V. A. Karmanov, Phys. Rev. **C58**, 3093 (1998), hep-ph/9806365.
- [15] S. J. Brodsky, H.-C. Pauli, and S. S. Pinsky, Phys. Rept. **301**, 299 (1998), hep-ph/9705477.
- [16] A. Harindranath, (1996), hep-ph/9612244.
- [17] T. Heinzl, (1998), hep-th/9812190.
- [18] G. A. Miller, Phys. Rev. **C56**, 2789 (1997), nucl-th/9706028.
- [19] U. Trittman and H.-C. Pauli, (1997), hep-th/9705021.
- [20] D. R. Phillips and I. R. Afnan, Phys. Rev. **C54**, 1542 (1996), nucl-th/9605004.
- [21] D. R. Phillips, (private communication).
- [22] T. Nieuwenhuis and J. A. Tjon, Phys. Rev. Lett. **77**, 814 (1996), hep-ph/9606403.
- [23] G. Baym, Phys. Rev. **117**, 886 (1960).
- [24] J. J. Wivoda and J. R. Hiller, Phys. Rev. **D47**, 4647 (1993).

- [25] C. Savkli, J. Tjon, and F. Gross, Phys. Rev. **C60**, 055210 (1999), hep-ph/9906211.
- [26] R. Rosenfelder and A. W. Schreiber, Phys. Rev. **D53**, 3337 (1996), nucl-th/9504002.
- [27] R. Rosenfelder and A. W. Schreiber, Phys. Rev. **D53**, 3354 (1996), nucl-th/9504005.
- [28] G. C. Wick, Phys. Rev. **96**, 1124 (1954).
- [29] R. E. Cutkosky, Phys. Rev. **96**, 1135 (1954).
- [30] V. A. Karmanov, M. Mangin-Brinet, and J. Carbonell, Nucl. Phys. **A684**, 366 (2001), hep-th/0008244.
- [31] M. Mangin-Brinet, J. Carbonell, and V. A. Karmanov, (2001), hep-th/0107235.
- [32] J. H. O. Sales, T. Frederico, B. V. Carlson, and P. U. Sauer, Phys. Rev. **C63**, 064003 (2001).
- [33] M. J. Levine, J. A. Tjon, and J. Wright, Phys. Rev. Lett. **16**, 962 (1966).
- [34] M. J. Levine, J. Wright, and J. A. Tjon, Phys. Rev. **154**, 1433 (1967).
- [35] M. J. Levine and J. Wright, Phys. Rev. **D2**, 2509 (1970).
- [36] J. R. Cooke, G. A. Miller, and D. R. Phillips, Phys. Rev. **C61**, 064005 (2000), nucl-th/9910013.
- [37] J. R. Cooke and G. A. Miller, Phys. Rev. **C62**, 054008 (2000), nucl-th/0002016.

- [38] J. H. O. Sales, T. Frederico, B. V. Carlson, and P. U. Sauer, Phys. Rev. **C61**, 044003 (2000), nucl-th/9909029.
- [39] M. V. Terentev, Sov. J. Nucl. Phys. **24**, 106 (1976).
- [40] B. C. Tiburzi and G. A. Miller, Phys. Rev. **C63**, 044014 (2001), nucl-th/0011074.
- [41] S. Weinberg, Phys. Rev. **150**, 1313 (1966).
- [42] A. Klein, Phys. Rev. **90**, 1101 (1953).
- [43] D. R. Phillips and S. J. Wallace, Phys. Rev. **C54**, 507 (1996), nucl-th/9603008.
- [44] A. D. Lahiff and I. R. Afnan, Phys. Rev. **C56**, 2387 (1997), nucl-th/9708037.
- [45] N. E. Ligterink and B. L. G. Bakker, Phys. Rev. **D52**, 5954 (1995), hep-ph/9412315.
- [46] N. C. J. Schoonderwoerd and B. L. G. Bakker, (1996), hep-ph/9610361.
- [47] M. Krautgartner, H. C. Pauli, and F. Wolz, Phys. Rev. **D45**, 3755 (1992).
- [48] J. A. Eden and M. F. Gari, Phys. Rev. **C53**, 1510 (1996), nucl-th/9601025.
- [49] S. Okubo, Prog. Theor. Phys. **12**, 603 (1954).
- [50] S. J. Wallace, Two-body dirac equation and applications to atomic hyperfine splittings, in *Nuclear and Particle Physics on the Light Cone (LAMPF Workshop), 1988*, p. 477, World Scientific, Singapore, 1989.
- [51] S. J. Wallace and V. B. Mandelzweig, Nucl. Phys. **A503**, 673 (1989).

- [52] R. M. Woloshyn and A. D. Jackson, Nucl. Phys. **B64**, 269 (1973).
- [53] C. Schwartz, Phys. Rev. **137**, B717 (1965).
- [54] L. Theussl and B. Desplanques, Prog. Part. Nucl. Phys. **44**, 123 (2000), nucl-th/9908007.
- [55] G. A. Miller and R. Machleidt, Phys. Rev. **C60**, 035202 (1999), nucl-th/9903080.
- [56] J. L. Friar, B. F. Gibson, and G. L. Payne, Phys. Rev. **C30**, 1084 (1984).
- [57] F. Gursey, Nuovo Cim. **16**, 230 (1960).
- [58] R. Machleidt, K. Holinde, and C. Elster, Phys. Rept. **149**, 1 (1987).
- [59] R. Machleidt, One-boson-exchange potentials and nucleon-nucleon scattering, in *Computational Nuclear Physics 2—Nuclear Reactions*, edited by K. Langanke, J. A. Maruhn, and S. E. Koonin, chap. 1, p. 1, Springer, New York, 1993.
- [60] D. Black, A. H. Fariborz, F. Sannino, and J. Schechter, Phys. Rev. **D59**, 074026 (1999), hep-ph/9808415.
- [61] D. Black, A. H. Fariborz, and J. Schechter, Phys. Rev. **D61**, 074030 (2000), hep-ph/9910351.
- [62] D. Black, A. H. Fariborz, S. Moussa, S. Nasri, and J. Schechter, Phys. Rev. **D64**, 014031 (2001), hep-ph/0012278.
- [63] G. A. Miller, Phys. Rev. **C56**, 8 (1997), nucl-th/9702036.

- [64] S.-J. Chang, R. G. Root, and T.-M. Yan, Phys. Rev. **D7**, 1133 (1973).
- [65] S.-J. Chang and T.-M. Yan, Phys. Rev. **D7**, 1147 (1973).
- [66] T.-M. Yan, Phys. Rev. **D7**, 1760 (1973).
- [67] T.-M. Yan, Phys. Rev. **D7**, 1780 (1973).
- [68] D. E. Soper, SLAC-R-0137.
- [69] J. B. Kogut and D. E. Soper, Phys. Rev. **D1**, 2901 (1970).
- [70] J. D. Bjorken, J. B. Kogut, and D. E. Soper, Phys. Rev. **D3**, 1382 (1971).
- [71] D. E. Soper, Phys. Rev. **D4**, 1620 (1971).
- [72] N. C. J. Schoonderwoerd and B. L. G. Bakker, Phys. Rev. **D57**, 4965 (1998).
- [73] N. C. J. Schoonderwoerd and B. L. G. Bakker, Phys. Rev. **D58**, 025013 (1998),  
hep-ph/9801433.
- [74] N. Schoonderwoerd, (1998), hep-ph/9811317.
- [75] B. H. Brandson and R. G. Moorhouse, *The Pion-Nucleon System* (Princeton University Press, Princeton, 1973), .
- [76] S. L. Adler and R. F. Dashen, *Current Algebras* (W. A. Benjamin, New York, 1968), .
- [77] J. Carbonell and V. A. Karmanov, In \*Williamsburg 1994, Few-body problems in physics\* 891- 894.
- [78] J. Carbonell and V. A. Karmanov, Nucl. Phys. **A581**, 625 (1995).

- [79] P. L. Chung, W. N. Polyzou, F. Coester, and B. D. Keister, Phys. Rev. **C37**, 2000 (1988).
- [80] L. L. Frankfurt, T. Frederico, and M. Strikman, Phys. Rev. **C48**, 2182 (1993).
- [81] T. Frederico, E. M. Henley, and G. A. Miller, Nucl. Phys. **A533**, 617 (1991).
- [82] L. A. Kondratyuk and M. I. Strikman, Nucl. Phys. **A426**, 575 (1984).
- [83] F. Cardarelli, I. L. Grach, I. M. Narodetsky, G. Salme, and S. Simula, Phys. Lett. **B349**, 393 (1995), hep-ph/9502360.
- [84] D. Arndt and C.-R. Ji, Phys. Rev. **D60**, 094020 (1999), hep-ph/9905360.
- [85] E. Hummel and J. A. Tjon, Phys. Rev. **C42**, 423 (1990).
- [86] M. J. Zuilhof and J. A. Tjon, Phys. Rev. **C22**, 2369 (1980).
- [87] G. Rupp and J. A. Tjon, Phys. Rev. **C41**, 472 (1990).
- [88] M. Garcon and J. W. Van Orden, (2001), arXiv:nucl-th/0102049.
- [89] R. G. Arnold, C. E. Carlson, and F. Gross, Phys. Rev. **C23**, 363 (1981).
- [90] F. Coester and A. Ostebee, Phys. Rev. **C11**, 1836 (1975).
- [91] T. E. O. Ericson and M. Rosa-Clot, Nucl. Phys. **A405**, 497 (1983).
- [92] P. J. Mohr and B. N. Taylor, Rev. Mod. Phys. **72**, 351 (2000).
- [93] D. R. Phillips, S. J. Wallace, and N. K. Devine, Phys. Rev. **C58**, 2261 (1998), nucl-th/9802067.

- [94] JLAB t20, D. Abbott *et al.*, Eur. Phys. J. **A7**, 421 (2000), nucl-ex/0002003.
- [95] R. Dashen and M. Gell-Mann, Phys. Rev. Lett. **17**, 340 (1966).
- [96] I. L. Grach and L. A. Kondratyuk, Sov. J. Nucl. Phys. **39**, 198 (1984).
- [97] S. J. Brodsky and J. R. Hiller, Phys. Rev. **D46**, 2141 (1992).
- [98] H. J. Melosh, Phys. Rev. **D9**, 1095 (1974).
- [99] J. D. Bjorken and S. D. Drell, *Relativistic Quantum Mechanics* (McGraw-Hill, Inc., New York, 1964), chap. 3.
- [100] G. Hohler *et al.*, Nucl. Phys. **B114**, 505 (1976).
- [101] M. F. Gari and W. Krümpelmann, Z. Phys. **A322**, 689 (1985).
- [102] M. F. Gari and W. Krümpelmann, Phys. Lett. **B274**, 159 (1992).
- [103] M. F. Gari and W. Krümpelmann, Phys. Lett. **B282**, 483 (1992).
- [104] P. Mergell, U. G. Meissner, and D. Drechsel, Nucl. Phys. **A596**, 367 (1996), hep-ph/9506375.
- [105] E. L. Lomon, Phys. Rev. **C64**, 035204 (2001), nucl-th/0104039.
- [106] K. de Jager, (1999), hep-ex/0003034.
- [107] A1, A. Liesenfeld *et al.*, Phys. Lett. **B468**, 20 (1999), nucl-ex/9911003.
- [108] Buchanan *et al.*, Phys. Rev. Lett. **15**, 303 (1965).
- [109] Elias *et al.*, Phys. Rev. **177**, 2075 (1969).

- [110] S. Galster *et al.*, Nucl. Phys. **B32**, 221 (1971).
- [111] S. Platchkov *et al.*, Nucl. Phys. **A510**, 740 (1990).
- [112] Jefferson Lab t(20), D. Abbott *et al.*, Phys. Rev. Lett. **82**, 1379 (1999), nucl-ex/9810017.
- [113] Auffret *et al.*, Phys. Rev. Lett. **54**, 649 (1985).
- [114] P. Bosted *et al.*, Phys. Rev. **C42**, 38 (1990).
- [115] M. E. Schulze *et al.*, Phys. Rev. Lett. **52**, 597 (1984).
- [116] R. Gilman *et al.*, Phys. Rev. Lett. **65**, 1733 (1990).
- [117] B. Boden *et al.*, Z. Phys. **C49**, 175 (1991).
- [118] M. Garcon *et al.*, Phys. Rev. **C49**, 2516 (1994).
- [119] M. Ferro-Luzzi *et al.*, Phys. Rev. Lett. **77**, 2630 (1996).
- [120] M. Bouwuis *et al.*, Phys. Rev. Lett. **82**, 3755 (1999), nucl-ex/9810004.
- [121] JLAB t(20), D. Abbott *et al.*, Phys. Rev. Lett. **84**, 5053 (2000), nucl-ex/0001006.
- [122] R. B. Wiringa, V. G. J. Stoks, and R. Schiavilla, Phys. Rev. **C51**, 38 (1995), nucl-th/9408016.
- [123] R. Schiavilla and D. O. Riska, Phys. Rev. **C43**, 437 (1991).
- [124] W. H. Press, S. A. Teukolsky, W. T. Vetterling, and B. P. Flannery, *Numerical Recipes in C*, Second ed. (Cambridge University Press, New York, 1992), p. 147.

- [125] B. T. Smith *et al.*, Matrix Eigensystem Routines – EISPACK Guide, in *Lecture Notes in Computer Science*, volume 6, New York-Heidelberg-Berlin, 1976, Springer-Verlag.
- [126] B. S. Garbow, J. M. Boyle, J. J. Dongarra, and C. B. Moler, Matrix Eigensystem Routines – EISPACK Guide Extension, in *Lecture Notes in Computer Science*, volume 51, New York-Heidelberg-Berlin, 1977, Springer-Verlag.
- [127] J. J. Sakurai, *Modern Quantum Mechanics*, Revised ed. (Addison-Wesley, Massachusetts, 1994), pp. 194–202.
- [128] R. A. Rice and Y. E. Kim, *Few Body Syst.* **14**, 127 (1993).
- [129] M. Chaichian and R. Hagedorn, *Symmetries in Quantum Mechanics* (Institute of Physics, Bristol, 1998), chap. 5, p. 144.

## Appendix A

**NOTATION, CONVENTIONS, AND USEFUL  
RELATIONS**

“The best way to be boring is to leave nothing out.”

—*Voltaire*

For a general four-vector  $a$  with components  $(a^0, a^1, a^2, a^3)$  in the equal-time basis, we define the light-front variables

$$a^\pm = a^0 \pm a^3, \tag{A.1}$$

$$\mathbf{a}_\perp = (a^1, a^2), \tag{A.2}$$

so the 4-vector  $a^\mu$  can be denoted in the light-front basis as

$$a = (a^+, a^-, \mathbf{a}_\perp). \tag{A.3}$$

Using this, we find that the scalar product is

$$a \cdot b = a^\mu b_\mu = \frac{1}{2} (a^+ b^- + a^- b^+) - \mathbf{a}_\perp \cdot \mathbf{b}_\perp. \tag{A.4}$$

This defines  $g_{\mu\nu}$ , with  $g_{+-} = g_{-+} = 1/2$ ,  $g_{11} = g_{22} = -1$ , and all other elements of  $g$  vanish. The elements of  $g^{\mu\nu}$  are obtained from the condition that  $g^{\mu\nu}$  is the inverse of  $g_{\mu\nu}$ , so  $g^{\alpha\beta} g_{\beta\lambda} = \delta^\alpha_\lambda$ . Its elements are the same as those of  $g_{\mu\nu}$ , except that  $g^{-+} = g^{+-} = 2$ . Thus,

$$a^\pm = 2a_\mp. \tag{A.5}$$

and the partial derivatives are similarly given by

$$\partial^\pm = 2\partial_\mp = 2\frac{\partial}{\partial x^\mp}. \tag{A.6}$$

To find the physical consequences of this coordinate system, consider the commutation relations  $[p^\mu, x^\nu] = ig^{\mu\nu}$ , which yield

$$[p^\pm, x^\mp] = 2i, \quad (\text{A.7})$$

$$[\mathbf{p}_\perp^i, \mathbf{x}_\perp^j] = -i\delta_{i,j}, \quad (\text{A.8})$$

with the other commutators equal to zero. This means that  $\mathbf{x}_\perp^i$  is canonically conjugate to  $\mathbf{p}_\perp^i$ , and  $x^\pm$  is conjugate to  $p^\mp$ . Since  $x^+$  plays the role of time (the light-front time) in light-front dynamics, and  $p^-$  is canonically conjugate to  $x^+$ , this means that  $p^-$  is the light-front energy and that the light-front Hamiltonian is given by  $P^-$ .

In any Hamiltonian theory, particles have the an energy defined by the on-shell constraint  $k^2 = m^2$ . This implies that the light-front energy of a particle is

$$k^- = \frac{m^2 + \mathbf{k}_\perp^2}{k^+}. \quad (\text{A.9})$$

The independent components of the momentum can be written as a light-front three-vector  $\mathbf{k}_{\text{LF}}$ , denoted by

$$\mathbf{k}_{\text{LF}} = (k^+, \mathbf{k}_\perp). \quad (\text{A.10})$$

For dealing with spin, we require the Pauli sigma matrices, which are

$$(\sigma^1, \sigma^2, \sigma^3) = \left( \left( \begin{array}{cc} 0 & 1 \\ 1 & 0 \end{array} \right), \left( \begin{array}{cc} 0 & -i \\ i & 0 \end{array} \right), \left( \begin{array}{cc} 1 & 0 \\ 0 & -1 \end{array} \right) \right). \quad (\text{A.11})$$

The Bjorken and Drell convention [99] for the gamma matrices is used in this work. They specify that

$$\gamma^0 = \beta = \begin{pmatrix} 1 & 0 \\ 0 & -1 \end{pmatrix}, \quad (\text{A.12})$$

$$\boldsymbol{\gamma} = \beta \boldsymbol{\alpha} = \begin{pmatrix} 0 & \boldsymbol{\sigma} \\ -\boldsymbol{\sigma} & 0 \end{pmatrix}, \quad (\text{A.13})$$

$$\gamma^5 = i\gamma^0\gamma^1\gamma^2\gamma^3 = \begin{pmatrix} 0 & 1 \\ 1 & 0 \end{pmatrix}. \quad (\text{A.14})$$

The spin matrices  $S^i$  then are

$$S^i = \frac{1}{2}\Sigma^i = -\frac{1}{2}\gamma^5\gamma^i, \quad (\text{A.15})$$

$$\Sigma^i = \begin{pmatrix} \sigma^i & 0 \\ 0 & -\sigma^i \end{pmatrix}. \quad (\text{A.16})$$

Using  $\Sigma$ , we can express the helicity operator as  $H = \hat{p} \cdot \Sigma$ , which has eigenvalues  $\pm 1$ . This is useful since the helicity is invariant under rotations, a property that is used in Appendix G.

It is useful to define the spinor projection operators  $\Lambda_{\pm}$  by

$$\Lambda_{\pm} = \frac{1}{4}\gamma^{\mp}\gamma^{\pm} = \frac{1}{2}\gamma^0\gamma^{\pm} = \frac{1}{2}(I \pm \alpha^3). \quad (\text{A.17})$$

These satisfy the requirements for projection operators,

$$\Lambda_+ + \Lambda_- = 1, \quad (\text{A.18})$$

$$(\Lambda_{\pm})^2 = \Lambda_{\pm}, \quad (\text{A.19})$$

$$\Lambda_{\pm}\Lambda_{\mp} = 0. \quad (\text{A.20})$$

We summarize the effect these projection operators have on the gamma matrices:

$$\Lambda_{\pm}\gamma^0 = \gamma^0\Lambda_{\mp}, \quad (\text{A.21})$$

$$\Lambda_{\pm}\gamma^{\pm} = 0 = \gamma^{\pm}\Lambda_{\mp}, \quad (\text{A.22})$$

$$\Lambda_{\pm}\gamma^{\mp} = \gamma^{\mp} = \gamma^{\mp}\Lambda_{\mp}, \quad (\text{A.23})$$

$$\Lambda_{\pm}\gamma^{\perp} = \gamma^{\perp}\Lambda_{\pm}, \quad (\text{A.24})$$

and under conjugation,

$$\gamma^0\Lambda_{\pm}^{\dagger}\gamma^0 = \Lambda_{\mp}. \quad (\text{A.25})$$

## Appendix B

### CONVERSION TO MATRIX FORM

“Let us work without theorizing. It’s the only way to make life enduring.”

—*Voltaire*

To solve for the bound-state wave function for the Wick-Cutkosky model numerically, the light-front Schrödinger equation given in Eq. (2.49) must be discretized and cast in matrix form. The solution of the light-front nucleon-nucleon model proceeds along similar lines. The equation is first symmetrized to get

$$-\int_0^\infty dp_{\text{ET}} \int_0^{\pi/2} d\theta_p V_{p,m}^S(k_{\text{ET}}, \theta_k; p_{\text{ET}}, \theta_p) \psi_{p,m}^S(p_{\text{ET}}, \theta_p) = \psi_{p,m}^S(k_{\text{ET}}, \theta_k), \quad (\text{B.1})$$

where

$$V_{p,m}^S(k_{\text{ET}}, \theta_k; p_{\text{ET}}, \theta_p) = B(k_{\text{ET}}) A(k_{\text{ET}}, \theta_k) V_{p,m}(k_{\text{ET}}, \theta_k; p_{\text{ET}}, \theta_p) A(p_{\text{ET}}, \theta_p) B(p_{\text{ET}}), \quad (\text{B.2})$$

$$\psi_{p,m}^S(k_{\text{ET}}, \theta_k) = B(k_{\text{ET}})^{-1} A(k_{\text{ET}}, \theta_k) \psi_{p,m}(k_{\text{ET}}, \theta_k), \quad (\text{B.3})$$

$$A(k_{\text{ET}}, \theta_k) = \sqrt{\frac{2k_1^+ k_2^+ k_{\text{ET}}^2 \sin \theta_k}{(k^0)}}, \quad (\text{B.4})$$

$$B(k_{\text{ET}}) = \sqrt{\frac{-1}{E^2 - 4(k^0)^2}}. \quad (\text{B.5})$$

Before discretizing the integrals, note that we may write [37]

$$\int_0^\infty dp f(p) = a \int_0^1 du \left( f(au) + \frac{f(a/u)}{u^2} \right). \quad (\text{B.6})$$

Using this trick, the integral in Eq. B.1 over  $p_{\text{ET}}$  can be written as an integral over a finite range. Since we are concerned with a bound state, the wave function is damped

for large momenta, and the second term of Eq. (B.6) converges as  $u$  approaches zero. Another choice that can be used is [58, 59]

$$\int_0^\infty dp f(p) = \frac{a\pi}{4} \int_{-1}^1 \frac{dx}{\cos^2\left(\frac{\pi(x+1)}{4}\right)} f\left(a \tan\left(\frac{\pi(x+1)}{4}\right)\right). \quad (\text{B.7})$$

After using Eq. (B.6) or Eq. (B.7), the integrals in Eq. B.1 are over a finite range and can be discretized using Gauss-Legendre quadrature. The specific routines for the quadrature are given by *Numerical Recipes in C* [124]. This conversion gives a matrix equation that approximates the original Eq. B.1,

$$-V_{p,m}^S(g(E), E)\psi_{p,m}^S = \psi_{p,m}^S, \quad (\text{B.8})$$

where the explicit dependence of  $V_{p,m}^S$  on the binding energy  $E$  and the coupling constant  $g$  is shown. This equation must be solved self-consistently for the spectrum  $g(E)$ .

The approach we use is to first solve for the spectrum for the OBE potential. The eigenvalue equation

$$V_{p,m,\text{OBE}}^S(E)\psi_{p,m}^S = \alpha\psi_{p,m}^S, \quad (\text{B.9})$$

where

$$\alpha = \frac{-1}{g_{\text{OBE}}(E)^2}. \quad (\text{B.10})$$

The ground-state wave function is the eigenvector that corresponds to the smallest eigenvalue  $\alpha$ . We calculate the wave function and the smallest coupling constant using EISPACK [125, 126] routines for a range of energies to map out the spectrum.

Using the coupling constant for the OBE potential as a starting point, we can use Eq. B.8 for higher-order potentials that include  $N$  meson exchanges. For a given energy, the coupling constant  $g(E)$  is initially chosen as  $g_{\text{OBE}}(E)$ , then we take the equation

$$\left[ \sum_{n=1}^N g(E)^{2n} V_{p,m,n\text{BE}}^S(E) \right] \psi_{p,m}^S = \beta\psi_{p,m}^S, \quad (\text{B.11})$$

where  $V_{n\text{BE}}$  is the  $n$ -boson-exchange potential, and solve it as an eigenvalue equation for  $\beta$ . The coupling constant  $g(E)$  is varied until the the lowest eigenvalue is  $\beta = -1$ , at which point  $g(E)$  is the correct value of the spectrum corresponding to the ground-state wave function  $\psi_{p,m}^S$ .

## Appendix C

### AZIMUTHAL-ANGLE AND LOOP INTEGRALS

We outline the methods used to perform the azimuthal-angle integrations for OBE, TME, and MGF potentials, and the loop integrals for the TME potentials. Although these methods are specifically for the Wick-Cutkosky potentials (presented in Chapter 2), they can easily be generalized for the light-front nucleon-nucleon potentials (presented in Chapter 3) by using the integrals discussed in Appendix D.

#### ***C.1 Azimuthal-angle Integration of the OBE and MGF Potentials***

“Never express yourself more clearly than you are able to think.”

—*Niels Bohr*

In this section, we evaluate the azimuthal-angle integration of the OBE potential in Eq. (2.61) and the first term in MGF potential in Eq. (2.123), using the prescription for azimuthal-angle integration given in Eq. (2.52). One of the integrals is easily done since since the potential is independent of the azimuthal angle between the two perpendicular momenta, so

$$V(k^+, k_\perp; p^+, p_\perp) \propto \left[ \theta(x - y) \int_0^{2\pi} \frac{d\phi}{A_1 + B \cos \phi} + \theta(y - x) \int_0^{2\pi} \frac{d\phi}{A_2 + B \cos \phi} \right], \quad (\text{C.1})$$

where

$$A_1 = (k_1^+ - p_1^+)(E - p_1^- - k_2^-) - \mu^2 - p_\perp^2 - k_\perp^2, \quad (\text{C.2})$$

$$A_2 = (p_1^+ - k_1^+)(E - k_1^- - p_2^-) - \mu^2 - p_\perp^2 - k_\perp^2, \quad (\text{C.3})$$

$$B = 2k_\perp p_\perp. \quad (\text{C.4})$$

The integrals in Eq. C.1 are easily done to give

$$\int_0^{2\pi} \frac{d\phi}{A + B \cos \phi} = \frac{-2\pi}{\sqrt{A^2 - B^2}}, \quad (\text{C.5})$$

which is negative since  $A < 0$ . Using this, the azimuthal-angle-averaged OBE potential is given by

$$V_{\text{OBE}}(k^+, k_\perp; p^+, p_\perp) = -2\pi \left(\frac{M}{E}\right)^2 E \left[ \frac{\theta(x-y)}{\sqrt{A_1^2 - B^2}} + \frac{\theta(y-x)}{\sqrt{A_2^2 - B^2}} \right]. \quad (\text{C.6})$$

It is straightforward to rewrite this equation for the potential in terms of the equal-time coordinates.

When the other terms in the MGF potential are azimuthal-angle averaged, integrations similar to the one given in Eq. C.5 are encountered, with the denominator squared or cubed. We note that

$$\int_0^{2\pi} \frac{d\phi}{(A + B \cos \phi)^2} = \frac{-2\pi}{\sqrt{A^2 - B^2}} \frac{A}{A^2 - B^2}, \quad (\text{C.7})$$

$$\int_0^{2\pi} \frac{d\phi}{(A + B \cos \phi)^3} = \frac{-2\pi}{\sqrt{A^2 - B^2}} \frac{2A^2 + B^2}{(A^2 - B^2)^2}, \quad (\text{C.8})$$

so the azimuthal-angle-averaged MGF potential is given by

$$\begin{aligned} V_{\text{MGF}}(\mathbf{k}_1, \mathbf{p}_1; P) &= -2\pi \left(\frac{M}{E}\right)^2 \left[ \frac{\theta(x-y)}{\sqrt{A_1^2 - B^2}} \left( 1 + \frac{N_{p,21} + N_{k,12}}{2D_{1,2}} + \frac{N_{p,21}N_{k,12}}{2D_{1,3}} \right) \right. \\ &\quad \left. + \frac{\theta(y-x)}{\sqrt{A_2^2 - B^2}} \left( 1 + \frac{N_{k,21} + N_{p,12}}{2D_{2,2}} + \frac{N_{p,12}N_{k,21}}{2D_{2,3}} \right) \right], \end{aligned} \quad (\text{C.9})$$

where

$$D_{i,2} \equiv \frac{A^2 - B^2}{A}, \quad (\text{C.10})$$

$$D_{i,3} \equiv \frac{(A^2 - B^2)^2}{2A^2 + B^2}, \quad (\text{C.11})$$

and  $i = 1, 2$ .

## C.2 Azimuthal-angle and Loop Integration of the TBE Potentials

“A child of five would understand this. Send someone to fetch a child of five.”

—*Groucho Marx*

As in Section C.1, we want the azimuthal-angle integrals of the TBE potentials given in Eqs. (2.67-2.73). For these potentials, there is also a loop integral that has to be done. We start by analyzing the equations schematically. Each of the terms in the TBE potentials can be written in the following form,

$$\begin{aligned}
 & V_{\text{TBE}}(k^+, k_\perp; p^+, p_\perp) \\
 &= \int_0^\infty \frac{q_\perp dq_\perp}{2(2\pi)^3} \int_0^1 dz J(k^+, q^+, p^+) I(k^+, k_\perp, q^+, q_\perp, p^+, p_\perp), \quad (\text{C.12}) \\
 & I(k^+, k_\perp, q^+, q_\perp, p^+, p_\perp) \\
 &= \int_0^{2\pi} d\phi_q d\phi_p \frac{1}{A_1 + B_1 \cos \phi_q} \\
 & \quad \times \frac{1}{A_2 + B_2 \cos \phi_q + C_2 \cos \phi_p + D_2 \cos(\phi_p - \phi_q)} \\
 & \quad \times \frac{1}{A_3 + B_3 \cos \phi_q + C_3 \cos \phi_p + D_3 \cos(\phi_p - \phi_q)}, \quad (\text{C.13})
 \end{aligned}$$

where the  $A$ 's,  $B$ 's,  $C$ 's, and  $D$ 's may have dependence on  $k^+$ ,  $k_\perp$ ,  $p^+$ ,  $p_\perp$ ,  $q^+ = zE$ , and  $q_\perp$ ; they are independent of the azimuthal angles. These functions can be easily determined for each potential by examining the forms of the original equations. The rotational invariance of the potential about the  $z$ -axis allows the  $\phi_k$  integration to be done trivially.

In the integrand of  $I$ , only the last two terms depend on  $\phi_p$ . To emphasize this, we write

$$I(k^+, k_\perp, q^+, q_\perp, p^+, p_\perp) = \int_0^{2\pi} d\phi_q \frac{I_2(k^+, k_\perp, \mathbf{q}, p^+, p_\perp)}{(A_1 + B_1 \cos \phi_q)(A_2 + B_2 \cos \phi_q)(A_3 + B_3 \cos \phi_q)}, \quad (\text{C.14})$$

$$I_2(k^+, k_\perp, \mathbf{q}, p^+, p_\perp) = \int_0^{2\pi} \frac{d\phi_p}{(1 + a_2 \cos \phi_p + b_2 \sin \phi_p)(1 + a_3 \cos \phi_p + b_3 \sin \phi_p)}, \quad (\text{C.15})$$

where, for  $i = 2, 3$ ,

$$a_i = \frac{C_i + D_i \cos \phi_q}{A_i + B_i \cos \phi_q}, \quad (\text{C.16})$$

$$b_i = \frac{D_i \sin \phi_q}{A_i + B_i \cos \phi_q}. \quad (\text{C.17})$$

The integral in  $I_2$  is evaluated to obtain

$$I_2(k^+, k_\perp, \mathbf{q}, p^+, p_\perp) = \frac{2\pi}{(a_2 - a_3)^2 + (b_2 - b_3)^2 - (a_2 b_3 - a_3 b_2)^2} \times \left( \frac{a_2(a_2 - a_3) + b_2(b_2 - b_3)}{\sqrt{1 - a_2^2 - b_2^2}} + \frac{a_3(a_3 - a_2) + b_3(b_3 - b_2)}{\sqrt{1 - a_3^2 - b_3^2}} \right). \quad (\text{C.18})$$

The remaining three-dimensional loop integral in  $V_{\text{TBE}}$  on  $\mathbf{q}$  is done using numeric techniques. The trick introduced in Appendix B is used to convert the semi-infinite  $q_\perp$  integration into an integration on a compact range. Before doing the  $z$  integral, the range of integration is limited by using the step functions. Gauss-Legendre quadrature, given by *Numerical Recipes in C* [124], is used to evaluate all the integrals.

Since each of the parts of the full TBE potential (TBE:SB, TBE: SX, ...) given in Chapter 2 should be Hermitian and invariant under interchange of particle 1 and 2, these invariances can be used as a self-consistency check. Each matrix element is calculated twice, first by using the straightforward approach, then particle labels 1 and 2 are interchanged and it is calculated again. The results are compared, and if they

differ by an unacceptable amount, the number of quadrature points is increased and the element is recalculated. In order to get the numerical accuracy of the potentials correct to within 1%, we start with ten points for the  $q_{\perp}$  integral, six points for the  $\phi_q$  integral, and three points for the  $z$  integral, resulting in a three-dimensional integral using 180 points.

## Appendix D

## COSINE INTEGRALS

“According to my point of view, logic and aesthetics cannot be in conflict with one another. Perhaps there is something lacking in my logical reasoning.”

—*M.C. Escher*

We wish to solve

$$I = \int_0^{2\pi} \frac{d\phi}{2\pi} e^{i\phi m} \prod_{j=1}^N \frac{1}{(a_j + b_j \cos \phi)^{n_j}}, \quad (\text{D.1})$$

where  $m$  is an integer,  $n_j$  are a positive integers, and  $a_j$  and  $b_j$  real numbers. Note that if one of the  $b_j$ 's is zero, then we can reduce the integral to one with  $N - 1$  sets of parameters. We therefore assume that  $b_j \neq 0$ .

Some things to note about this integral:

1. Since the range of integration is  $2\pi$ , and all the functions in the integrand are periodic in that range, the range of integration can be shifted by an arbitrary amount.
2. When the variable of integration is changed from  $\phi$  to  $-\phi$ , the limits of integration can be rewritten as

$$\int_0^{2\pi} d\phi \rightarrow \int_0^{-2\pi} d(-\phi) = \int_{-2\pi}^0 d\phi = \int_0^{2\pi} d\phi. \quad (\text{D.2})$$

Here we have used item number 1. Since  $\cos(-z) = \cos(z)$ , the only thing that changes in the integrand is the sign in the exponential. Hence,  $I(m) = I(-m)$ , or the integral is only a function of the magnitude of  $m$ .

3. The integral is real, since  $I(m)^* = I(-m) = I(m)$ .

In addition,

$$\frac{d^m}{da^m} \frac{1}{a + b \cos \phi} = (-1)^m m! \frac{1}{(a + b \cos \phi)^{m+1}}, \quad (\text{D.3})$$

so that

$$\begin{aligned} & \int_0^{2\pi} \frac{d\phi}{2\pi} e^{i\phi m} \prod_{j=1}^N \frac{1}{(a_j + b_j \cos \phi)^{n_j}} \\ &= \prod_{l=1}^N \frac{(-1)^{(n_l-1)}}{(n_l-1)!} \frac{d^{n_l-1}}{da_l^{n_l-1}} \int_0^{2\pi} \frac{d\phi}{2\pi} e^{i\phi m} \prod_{j=1}^N \frac{1}{a_j + b_j \cos \phi}. \end{aligned} \quad (\text{D.4})$$

Since  $b_j \neq 0$ , we can factor out a  $\prod_{j=1}^N \frac{1}{b_j^{n_j}}$ , and we relabel  $\frac{a_j}{b_j} \rightarrow a_j$ . Then, the non-trivial integral is

$$\begin{aligned} I(\{a_i\}, m, N) &= \int_0^{2\pi} \frac{d\phi}{2\pi} e^{i\phi|m|} \prod_{j=1}^N \frac{1}{a_j + \cos \phi} \\ &= \int_0^{2\pi} \frac{d\phi}{2\pi} e^{i\phi|m|} \prod_{j=1}^N \frac{2e^{i\phi}}{e^{2i\phi} + 2a_j e^{i\phi} + 1}. \end{aligned} \quad (\text{D.5})$$

Now we let  $z = e^{i\phi}$ , so  $d\phi e^{i\phi} = dz/i$ , which allows the integral to be converted to a contour integral over the contour  $C$ , a unit circle in the complex plane. Then,

$$\begin{aligned} I(\{a_i\}, m, N) &= \int_C \frac{dz}{2\pi i} z^{|m|-1} \prod_{j=1}^N \frac{2z}{z^2 + 2a_j z + 1} \\ &= \int_C \frac{dz}{2\pi i} z^{|m|-1} \prod_{j=1}^N \frac{2z}{(z - z_{j+})(z - z_{j-})}, \end{aligned} \quad (\text{D.6})$$

where

$$z_{j\pm} = \left\{ \begin{array}{ll} -a_j \pm \text{sign}(a_j) \sqrt{a_j^2 - 1} & \text{if } |a_j| > 1 \\ -a_j \mp i \sqrt{1 - a_j^2} = -e^{\pm i\phi_j} & \text{if } |a_j| \leq 1 \end{array} \right\}. \quad (\text{D.7})$$

Here  $\phi_i = \arccos \sqrt{1 - a_i^2}$ .

We will only consider the case where  $|a_j| > 1$ . In this case, only the only poles that contribute are the ones at  $z = z_{j+}$ . The contour integral is done by inspection to obtain

$$I(\{a_i\}, m, N) = \sum_{k=1}^N \int_{z_{k+}} \frac{dz}{2\pi i} \frac{2z^{|m|}}{(z - z_{k+})(z - z_{k-})} \prod_{j=1, j \neq k}^N \frac{2z}{z^2 + 2a_j z + 1} \quad (\text{D.8})$$

$$= \sum_{k=1}^N \frac{2z_{k+}^{|m|}}{z_{k+} - z_{k-}} \prod_{j=1, j \neq k}^N \frac{2z_{k+}}{z_{k+}^2 + 2a_j z_{k+} + 1}. \quad (\text{D.9})$$

Note that

$$z_{k\pm}^2 + 2a_j z_{k\pm} + 1 = z_{k\pm}^2 + 2a_k z_{k\pm} + 1 + 2(a_j - a_k)z_{k\pm} = 2(a_j - a_k)z_{k\pm}, \quad (\text{D.10})$$

$$z_{k+} - z_{k-} = 2 \text{sign}(a_k) \sqrt{a_k^2 - 1}. \quad (\text{D.11})$$

We define  $c_k$  and  $d_k$  by

$$c_k \equiv \frac{z_{k+} - z_{k-}}{2}, \quad (\text{D.12})$$

$$k_k \equiv z_{k+}^{|m|}. \quad (\text{D.13})$$

With the appropriate replacements, we obtain

$$I(\{a_i\}, m, N) = \sum_{k=1}^N \frac{d_k}{c_k} \prod_{j=1, j \neq k}^N \frac{1}{a_j - a_k}. \quad (\text{D.14})$$

Putting the  $b_j$ 's back in using the  $a_i \rightarrow \frac{a_i}{b_i}$ , we get

$$c_k = \text{sign}(a_k) \sqrt{a_k^2 - b_k^2}, \quad (\text{D.15})$$

$$d_k = \left( \frac{c_k - a_k}{b_k} \right)^{|m|}, \quad (\text{D.16})$$

$$\int_0^{2\pi} \frac{d\phi}{2\pi} e^{i\phi m} \prod_{j=1}^N \frac{1}{a_j + b_j \cos \phi} = \sum_{k=1}^N \frac{d_k}{c_k} \prod_{j=1, j \neq k}^N \frac{1}{a_j - a_k \frac{b_j}{b_k}}. \quad (\text{D.17})$$

This expression is used in Eq. (D.4) get

$$\begin{aligned} & \int_0^{2\pi} \frac{d\phi}{2\pi} e^{i\phi m} \prod_{j=1}^N \frac{1}{(a_j + b_j \cos \phi)^{n_j}} \\ &= \prod_{l=1}^N \frac{(-1)^{(n_l-1)}}{(n_l-1)!} \frac{d^{n_l-1}}{da_l^{n_l-1}} \sum_{k=1}^N \frac{d_k}{c_k} \prod_{j=1, j \neq k}^N \frac{1}{a_j - a_k \frac{b_j}{b_k}}. \end{aligned} \quad (\text{D.18})$$

Specificly, for  $N = 1$ , we can drop the subscripts. For  $n = 1$ ,

$$\int_0^{2\pi} \frac{d\phi}{2\pi} e^{i\phi m} \frac{1}{a + b \cos \phi} = \frac{d}{c}, \quad (\text{D.19})$$

and for  $n = 2$ ,

$$\int_0^{2\pi} \frac{d\phi}{2\pi} e^{i\phi m} \frac{1}{(a + b \cos \phi)^2} = -\frac{d}{da} \frac{d}{c} = f_2 \frac{d}{c} \quad (\text{D.20})$$

$$f_2 = \frac{a + |m|c}{c^2}. \quad (\text{D.21})$$

Since  $I(a, b, m)$  is like an eigenfunction of  $\frac{d}{da}$ , (but not exactly, since the “eigenvalue” is a function of  $a$ ), we can use recursion to find that for general  $n > 2$ ,

$$\int_0^{2\pi} \frac{d\phi}{2\pi} e^{i\phi m} \frac{1}{(a + b \cos \phi)^n} = f_n I(a, b, m), \quad (\text{D.22})$$

$$f_n = \frac{1}{n-1} \left( f_2 f_{n-1} - \frac{d}{da} f_{n-1} \right), \quad (\text{D.23})$$

Using this we get

$$f_1 = 1, \quad (\text{D.24})$$

$$f_2 = \frac{a + |m|c}{c^2}, \quad (\text{D.25})$$

$$f_3 = \frac{3a^2 + c^2(m^2 - 1) + 3a|m|c}{2c^4}. \quad (\text{D.26})$$

The higher-order  $f_i$ 's can easily be found from analytic iteration using a program like *Mathematica*, but apparently they do not have a nice analytic form. We note that in general,  $f_i$  is multiplied by a factor of  $c^{-2(i-1)}$ .

We now check the equation for situations that may be numerically unstable. First note that as  $c \rightarrow 0$ , the  $f$ 's are singular, which is due to the form of the original integral. Since the singular part is multiplicative, it can easily be treated.

Instabilities appear when  $b$  is very small. in which case we have to take care of  $d$  carefully as it appears to be singular. Let  $b = 2a\delta$ , so we can write

$$d_k = \left( \frac{\sqrt{1 - 4\delta^2} - 1}{2\delta} \right)^{|m|} \approx [-\delta(1 + \delta^2(1 + \delta^2(2 + \delta^2(5 + \delta^2(14 + \delta^2 \dots)))))]^{|m|}.$$

This expression demonstrates that  $d_k$  is not go as  $b^{-|m|}$ , but as  $b^{+|m|}$  as  $b \rightarrow 0$ .

Now we analyze what happens where there is more than one term in the denominator. We note first that

$$\left[ \left( \frac{d}{dx} \right)^n f(x)g(x) \right] = \sum_{m=0}^n \frac{n!}{m!(n-m)!} \left[ \left( \frac{d}{dx} \right)^m f(x) \right] \left[ \left( \frac{d}{dx} \right)^{n-m} g(x) \right]. \quad (\text{D.27})$$

This means that Eq. (D.18) can be written as

$$\begin{aligned} & \int_0^{2\pi} \frac{d\phi}{2\pi} e^{i\phi m} \prod_{j=1}^N \frac{1}{(a_j + b_j \cos \phi)^{n_j}} \\ &= \sum_{k=1}^N \left[ \prod_{l=1}^N \sum_{i_l=0}^{n_l-1} \right] \left[ \frac{(-1)^{(n_l-1-i_l)}}{(n_l-1-i_l)!} \frac{d^{n_l-1-i_l}}{da_l^{n_l-1-i_l}} \left\{ \frac{d_k}{c_k} \right\}_{\text{on}} \right] \\ & \quad \times \left[ \frac{(-1)^{(i_l)}}{(i_l)!} \frac{d^{i_l}}{da_l^{i_l}} \left\{ \prod_{j=1, j \neq k}^N \frac{1}{a_j - a_k \frac{b_j}{b_k}} \right\}_{\text{on}} \right]. \end{aligned} \quad (\text{D.28})$$

The product can be broken into two parts, one where  $l = k$  and another where  $l \neq k$ .

$$\begin{aligned} & \int_0^{2\pi} \frac{d\phi}{2\pi} e^{i\phi m} \prod_{j=1}^N \frac{1}{(a_j + b_j \cos \phi)^{n_j}} \\ &= \sum_{k=1}^N \left[ \prod_{l=1, l \neq k}^N \sum_{i_l=0}^{n_l-1} \right] \left[ \frac{(-1)^{(n_l-1-i_l)}}{(n_l-1-i_l)!} \frac{d^{n_l-1-i_l}}{da_l^{n_l-1-i_l}} \left\{ \frac{d_k}{c_k} \right\}_{\text{on}} \right] \\ & \quad \times \left[ \frac{(-1)^{(i_l)}}{(i_l)!} \frac{d^{i_l}}{da_l^{i_l}} \left\{ \prod_{j=1, j \neq k}^N \frac{1}{a_j - a_k \frac{b_j}{b_k}} \right\}_{\text{on}} \right] \\ & \quad \times \left[ \sum_{i_k=0}^{n_k-1} \right] \left[ \frac{(-1)^{(n_k-1-i_k)}}{(n_k-1-i_k)!} \frac{d^{n_k-1-i_k}}{da_k^{n_k-1-i_k}} \left\{ \frac{d_k}{c_k} \right\}_{\text{on}} \right] \\ & \quad \times \left[ \frac{(-1)^{(i_k)}}{(i_k)!} \frac{d^{i_k}}{da_k^{i_k}} \left\{ \prod_{j=1, j \neq k}^N \frac{1}{a_j - a_k \frac{b_j}{b_k}} \right\}_{\text{on}} \right]. \end{aligned} \quad (\text{D.29})$$

Now we note that  $\frac{d}{da_l} \frac{d_k}{c_k} = 0$ , and so on, to get

$$\begin{aligned}
& \int_0^{2\pi} \frac{d\phi}{2\pi} e^{i\phi m} \prod_{j=1}^N \frac{1}{(a_j + b_j \cos \phi)^{n_j}} \\
&= \sum_{k=1}^N \prod_{l=1, l \neq k}^N \left[ \frac{(-1)^{(n_l-1)}}{(n_l-1)!} \frac{d^{n_l-1}}{da_l^{n_l-1}} \left\{ \prod_{j=1, j \neq k}^N \frac{1}{a_j - a_k \frac{b_j}{b_k}} \right\}_{\text{on}} \right] \\
& \quad \times \frac{d_k}{c_k} \sum_{i_k=0}^{n_k-1} f_{n_k-i_k} \left[ \frac{(-1)^{i_k}}{i_k!} \frac{d^{i_k}}{da_k^{i_k}} \left\{ \prod_{j=1, j \neq k}^N \frac{1}{a_j - a_k \frac{b_j}{b_k}} \right\}_{\text{on}} \right]. \tag{D.30}
\end{aligned}$$

The first derivative term in Eq. (D.30) can be written as

$$\begin{aligned}
& \int_0^{2\pi} \frac{d\phi}{2\pi} e^{i\phi m} \prod_{j=1}^N \frac{1}{(a_j + b_j \cos \phi)^{n_j}} \\
&= \sum_{k=1}^N \frac{d_k}{c_k} \sum_{i_k=0}^{n_k-1} f_{n_k-i_k} \frac{(-1)^{i_k}}{i_k!} \frac{d^{i_k}}{da_k^{i_k}} \prod_{j=1, j \neq k}^N \frac{1}{\left(a_j - a_k \frac{b_j}{b_k}\right)^{n_j}}. \tag{D.31}
\end{aligned}$$

Now, we consider the situation where all the  $b_i$  have the same value,  $b$ . In the case where  $k = N$ , the complicated part of Eq. (D.31) is

$$h_N(i_N, N) \equiv \frac{1}{i_N!} \frac{d^{i_N}}{da_N^{i_N}} \prod_{j=1}^{N-1} \frac{1}{(a_j - a_N)^{n_j}} \tag{D.32}$$

$$\begin{aligned}
&= \sum_{i_{N-1}=0}^{i_N} h_{N-1}(i_{N-1}, N-1) \frac{1}{(i_N - i_{N-1})!} \\
& \quad \times \frac{d^{(i_N - i_{N-1})}}{da_N^{(i_N - i_{N-1})}} \frac{1}{(a_{N-1} - a_N)^{n_{N-1}}} \tag{D.33}
\end{aligned}$$

$$\begin{aligned}
&= \sum_{i_{N-1}=0}^{i_N} h_{N-1}(i_{N-1}, N-1) \frac{(i_N - i_{N-1} + n_{N-1} - 1)!}{(i_N - i_{N-1})! (n_{N-1} - 1)!} \\
& \quad \times \frac{1}{(a_{N-1} - a_N)^{n_{N-1} + i_N - i_{N-1}}} \tag{D.34}
\end{aligned}$$

$$= \prod_{l=3}^N \left[ \sum_{i_{l-1}=0}^{i_l} \frac{(i_l - i_{l-1} + n_{l-1} - 1)!}{(i_l - i_{l-1})! (n_{l-1} - 1)!} \frac{1}{(a_{l-1} - a_N)^{n_{l-1} + i_l - i_{l-1}}} \right] \tag{D.35}$$

$$\times \frac{(i_2 + n_1 - 1)!}{i_2! (n_1 - 1)!} \frac{1}{(a_1 - a_N)^{n_1 + i_2}}. \tag{D.36}$$

From this, we can cyclically permute (or shuffle in any order) the labels to get a similar expression for  $k \neq N$ .

For definiteness, we consider a few special cases. If  $n_j = 1$  for all  $j$  except  $N$ , we find that

$$h_2(i, 1) = \frac{\delta_{i,0}}{(a_2 - a_1)^{n_2}}, \quad (\text{D.37})$$

$$h_2(i, 2) = \frac{1}{(a_1 - a_2)^{i+1}}, \quad (\text{D.38})$$

and

$$h_3(i, 1) = \frac{\delta_{i,0}}{(a_2 - a_1)(a_3 - a_1)^{n_3}}, \quad (\text{D.39})$$

$$h_3(i, 2) = \frac{\delta_{i,0}}{(a_1 - a_2)(a_3 - a_2)^{n_3}}, \quad (\text{D.40})$$

$$h_3(i, 3) = \sum_{j=0}^i \frac{1}{(a_1 - a_3)^{j+1}(a_2 - a_3)^{i-j+1}}. \quad (\text{D.41})$$

Using these we can write

$$g_k = \sum_{i_k=0}^{n_k-1} (-1)^{i_k} f_{n_k-i_k} h_N(i_k, k), \quad (\text{D.42})$$

$$\int_0^{2\pi} \frac{d\phi}{2\pi} e^{i\phi m} \prod_{j=1}^N \frac{1}{(a_j + b_j \cos \phi)^{n_j}} = \sum_{k=1}^N \frac{d_k}{c_k} g_k. \quad (\text{D.43})$$

### Approximations

For  $N = 2$ , consider what happens when  $a_1 \approx a_2$ . We can write  $a_2 = a$ ,  $a_1 = a - \delta$ , so that

$$\begin{aligned} & I(a_1, a_2, b, n_1, n_2, m) \\ &= \int_0^{2\pi} \frac{d\phi}{2\pi} e^{i\phi m} \frac{1}{(a_2 + b \cos \phi - \delta)^{n_1}} \frac{1}{(a_2 + b \cos \phi)^{n_2}} \end{aligned} \quad (\text{D.44})$$

$$= \int_0^{2\pi} \frac{d\phi}{2\pi} e^{i\phi m} \frac{1}{(a_2 + b \cos \phi)^{n_1+n_2}} \sum_{j=0}^{\infty} \frac{(n_1 - 1 + j)!}{(n_1 - 1)! j!} \frac{\delta^j}{(a + b \cos \phi)^j} \quad (\text{D.45})$$

$$= \left[ \sum_{j=0}^{\infty} (a_2 - a_1)^j \frac{(n_1 - 1 + j)!}{(n_1 - 1)! j!} f_{n_1+n_2+j} \right] \frac{d_2}{c_2}. \quad (\text{D.46})$$

For  $N = 3$ , we could have  $a_2 \approx a_3$  (or equivalently  $a_1 \approx a_3$ ). In this case,

$$I(a_1, a_2, a_3, b, 1, 1, n, m) = \sum_{j=0}^{\infty} (a_3 - a_2)^j \int_0^{2\pi} \frac{d\phi}{2\pi} e^{i\phi m} \frac{1}{a_1 + b \cos \phi} \frac{1}{(a_3 + b \cos \phi)^{n+j+1}} \quad (\text{D.47})$$

$$= \sum_{j=0}^{\infty} (a_3 - a_2)^j I(a_1, a_3, b, 1, n + j + 1, m). \quad (\text{D.48})$$

When  $a_1 \approx a_2$  but  $a_1 \not\approx a_3$ , we get

$$I(a_1, a_2, a_3, b, 1, 1, n, m) = \sum_{j=0}^{\infty} (a_2 - a_1)^j I(a_1, a_3, b, 2 + j, n, m). \quad (\text{D.49})$$

## Summary

We define

$$I(\{a_i\}, b, \{n_i\}, m) = \int_0^{2\pi} \frac{d\phi}{2\pi} e^{i\phi m} \prod_i \frac{1}{(a_i + b \cos \phi)^{n_i}}, \quad (\text{D.50})$$

$$c_k = a_k \sqrt{1 - \left(\frac{b_k}{a_k}\right)^2}, \quad (\text{D.51})$$

$$d_k = \left(\frac{c_k - a_k}{b_k}\right)^{|m|}. \quad (\text{D.52})$$

We assume that  $n_i > 0$  and  $b_i \neq 0$ .

For  $N = 1$ , the integral is

$$I(a, b, n, m) = f_n \frac{d}{c}, \quad (\text{D.53})$$

and for  $N = 2$ , the integral is

$$I(a_1, a_2, b, n_1, n_2, m) = (-1)^{n_2} \left( \sum_{j=0}^{n_1-1} f_{n_1-j} \frac{(j+n_2-1)!}{j!(n_2-1)!} \frac{1}{(a_1 - a_2)^{j+n_2}} \right) \frac{d_1}{c_1} + (-1)^{n_1} \left( \sum_{j=0}^{n_2-1} f_{n_2-j} \frac{(j+n_1-1)!}{j!(n_1-1)!} \frac{1}{(a_2 - a_1)^{j+n_1}} \right) \frac{d_2}{c_2}. \quad (\text{D.54})$$

For  $N = 2$ , and with  $n_1 = 1$  the integral simplifies to

$$I(a_1, a_2, b, 1, n, m) = \frac{1}{(a_2 - a_1)^n} \frac{d_1}{c_1} - \left( \sum_{j=0}^{n-1} f_{n-j} \frac{1}{(a_2 - a_1)^{j+1}} \right) \frac{d_2}{c_2}. \quad (\text{D.55})$$

When  $N = 3$  and  $n_1 = n_2 = 1$  the integral is

$$\begin{aligned} & I(a_1, a_2, a_3, b, 1, 1, n, m) \\ &= \frac{1}{(a_2 - a_1)(a_3 - a_1)^n} \frac{d_1}{c_1} + \frac{1}{(a_1 - a_2)(a_3 - a_2)^n} \frac{d_2}{c_2} \\ &+ \left[ \sum_{i=0}^{n-1} (-1)^i f_{n-i} \sum_{j=0}^i \frac{1}{(a_1 - a_3)^{j+1} (a_2 - a_3)^{i-j+1}} \right] \frac{d_3}{c_3}. \end{aligned} \quad (\text{D.56})$$

## Appendix E

### CHECK OF THE UNCROSSED APPROXIMATION

“For every problem, there is one solution which is simple, neat and wrong.”

—*H. L. Mencken*

In this section, we want to check that how well the approximation

$$K_{\text{cross}} \approx K_{\text{ladder}} G_C K_{\text{ladder}}, \quad (\text{E.1})$$

works. Since we are using a Hamiltonian theory and are interested in the potentials, we compare the potentials defined by

$$V_{\text{TBE:X}} = \frac{1}{E} g_0^{-1} \langle G_0 K_{\text{cross}} G_0 \rangle g_0^{-1}, \quad (\text{E.2})$$

$$V_{\text{TBE:UX}} = \frac{1}{E} g_0^{-1} \langle G_0 K_{\text{ladder}} G_C K_{\text{ladder}} G_0 \rangle g_0^{-1}. \quad (\text{E.3})$$

The notation used here is defined in sections 2.3.3 and 2.3.4.

The TBE crossed potential (TBE:X) can be written as

$$V_{\text{TBE:X}} = V_{\text{TBE:SX}} + V_{\text{TBE:TX}} + V_{\text{TBE:WX}} + V_{\text{TBE:ZX}}, \quad (\text{E.4})$$

where the potentials on the right-hand side are defined in section 2.2.2. Calculation of the TBE approximate uncrossed potential (TBE:UX) is straightforward, but tedious. We find that

$$V_{\text{TBE:UX}}(E; \mathbf{k}_1, \mathbf{p}_1) = \frac{1}{2} \left[ V_{\text{TBE:UX1}}(E; \mathbf{k}_1, \mathbf{p}_1) + V_{\text{TBE:UX1}}(E; \mathbf{p}_1, \mathbf{k}_1) \right. \\ \left. + V_{\text{TBE:UX2}}(E; \mathbf{k}_1, \mathbf{p}_1) + V_{\text{TBE:UX2}}(E; \mathbf{p}_1, \mathbf{k}_1) \right], \quad (\text{E.5})$$

where

$$\begin{aligned}
V_{\text{TBE:UX1}}(E; \mathbf{k}_1, \mathbf{p}_1) &= \left(\frac{M}{E}\right)^4 \int \frac{d^2 q_\perp}{2(2\pi)^3} \left[ \int_0^1 dz \frac{\theta(x-z)\theta(z-y)}{(x-z)z^2(z-y)} \right. \\
&\quad \times \frac{1}{E - p_1^- - k_2^- - \omega^-(\mathbf{q}_1 - \mathbf{p}_1) - \omega^-(\mathbf{k}_1 - \mathbf{q}_1)} \\
&\quad \left. \times \left( \frac{1}{E - q_1^- - k_2^- - \omega^-(\mathbf{k}_1 - \mathbf{q}_1)} \right)^2 \right] \\
&\quad + \{1 \leftrightarrow 2\}, \tag{E.6}
\end{aligned}$$

$$\begin{aligned}
V_{\text{TBE:UX2}}(E; \mathbf{k}_1, \mathbf{p}_1) &= \left(\frac{M}{E}\right)^4 \int \frac{d^2 q_\perp}{2(2\pi)^3} \left[ \int_0^1 dz \frac{\theta(x-z)\theta(y-z)}{(x-z)z^2(y-z)} \right. \\
&\quad \times \frac{1}{E - q_1^- - p_2^- - \omega^-(\mathbf{p}_1 - \mathbf{q}_1)} \\
&\quad \left. \times \left( \frac{1}{E - q_1^- - k_2^- - \omega^-(\mathbf{k}_1 - \mathbf{q}_1)} \right)^2 \right] \\
&\quad + \{1 \leftrightarrow 2\}. \tag{E.7}
\end{aligned}$$

Now consider the azimuthal-angle and loop integrals for these potentials. The approach used is similar to that of Section C.2. Analyzing the potentials reveals that each of the terms can be written in the following schematic form,

$$\begin{aligned}
V_{\text{TBE:UX},i}(k^+, k_\perp; p^+, p_\perp) &= \int_0^\infty \frac{q_\perp dq_\perp}{2(2\pi)^3} \int_0^1 dz J(k^+, q^+, p^+) I_i(k^+, k_\perp, q^+, q_\perp, p^+, p_\perp) \tag{E.8}
\end{aligned}$$

$$\begin{aligned}
I_i(k^+, k_\perp, q^+, q_\perp, p^+, p_\perp) &= \int_0^{2\pi} \frac{d\phi_q d\phi}{A_{1,i} + B_{1,i} \cos \phi_q + C_{1,i} \cos \phi} \left( \frac{1}{A_2 + B_2 \cos \phi_q} \right)^2, \tag{E.9}
\end{aligned}$$

where  $\phi = -\phi_q + \phi_p$ , and the  $A$ 's,  $B$ 's, and  $C$ 's may have dependence on  $k^+$ ,  $k_\perp$ ,  $p^+$ ,  $p_\perp$ ,  $q^+ = zE$ , and  $q_\perp$ ; they are independent of the azimuthal angles. These factors can be easily determined for each potential by examining the forms of the original equations. The rotational invariance of the potential about the three-axis allows the

$\phi_k$  integration to be done trivially. The  $\phi$  integral is easily done to obtain

$$I(k^+, k_\perp, q^+, q_\perp, p^+, p_\perp) = -2\pi \int_0^{2\pi} d\phi_q \frac{1}{\sqrt{a_i^2 - C_{1,i}^2}} \left( \frac{1}{A_2 + B_2 \cos \phi_q} \right)^2, \quad (\text{E.10})$$

where

$$a_i = A_{1,i} + B_{1,i} \cos \phi_q. \quad (\text{E.11})$$

Further simplification is possible for  $V_{\text{TBE:UX2}}$ , since for that potential  $B_{1,2} = 0$ ,

$$I(k^+, k_\perp, q^+, q_\perp, p^+, p_\perp) = \frac{(2\pi)^2 A_2}{\sqrt{A_{1,2}^2 - C_{1,2}^2} \sqrt{A_2^2 - B_2^2} (A_2^2 - B_2^2)}. \quad (\text{E.12})$$

The techniques discussed in the Section C.2 are used to do the remaining loop integrals.

The spectra for the OBE+TBE:SB+TBE:UX potential can be calculated and compared to the OBE+TBE:SB+TBE:X potential (recall that this is the same as the OBE+TBE potential), the modified-Green's-function potential, and the ladder plus crossed Bethe-Salpeter equation. The spectra are plotted in Fig. E.1. The spectra for the TBE:UX, TBE:X and BSE all lie close to each other, which shows that that the uncrossed approximation is valid.

This shows that the important approximation in the modified-Green's-function approach is not the uncrossed approximation, but the addition of the extra interaction terms in Eq. (2.102) which serve to mimic the higher order interactions.

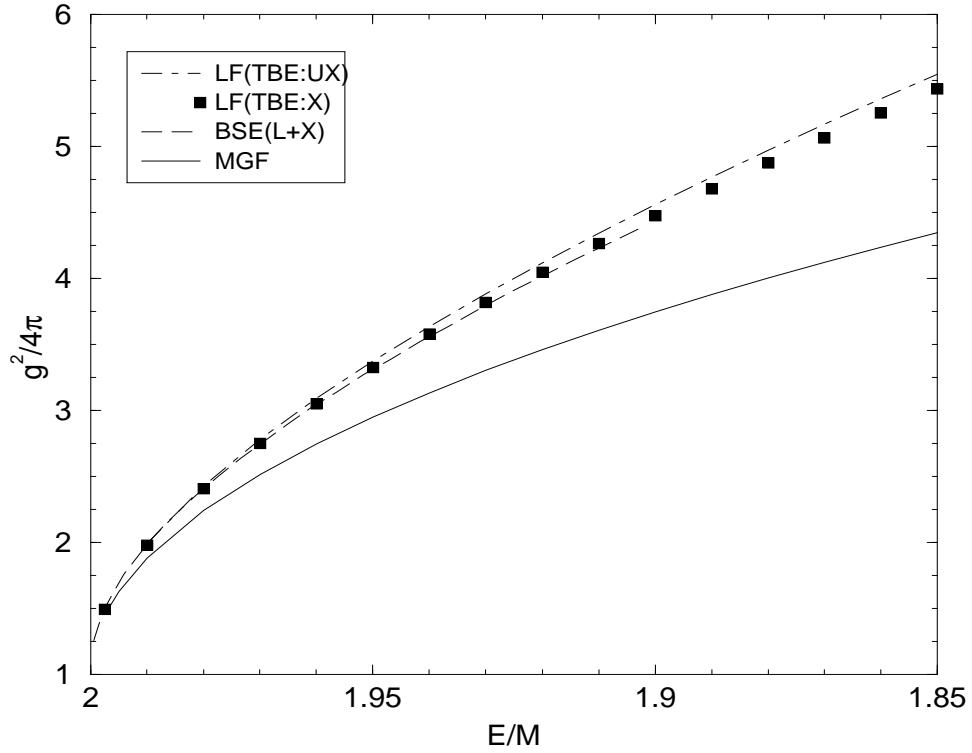


Figure E.1: The spectra for the potential derived from the TBE truncation of the uncrossed approximation (OBE+TBE:SB+TBE:UX, denoted in the figure by TBE:UX), the TBE potential (OBE+TBE, denoted by TBE:X), the ladder plus crossed Bethe-Salpeter equation (BSE(L+X)), and the modified-Green's-function potential (MGF). Except for the MGF spectrum, all the curves lie close to each other.

## Appendix F

### SPINORS

“Everything should be made as simple as possible, but not simpler.”

—*Albert Einstein*

#### **F.1 Definition of the Spinors**

The Dirac equation is

$$(i\rlap{/}\partial - M)\psi(x) = 0. \quad (\text{F.1})$$

We can multiply the Dirac equation by  $(i\rlap{/}\partial + M)$  to get

$$0 = (i\rlap{/}\partial + M)(i\rlap{/}\partial - M)\psi(x) = (-\rlap{/}\partial^2 + M^2)\psi(x) = (-\partial^2 + M^2)\psi(x). \quad (\text{F.2})$$

This means that for an eigenstate of momentum,  $\psi_p(x) \propto e^{\pm ip_\mu x^\mu}$ , with  $p^2 = M^2$ . The energy component of  $p_\mu$  is chosen to be positive.

Looking at the positive energy part of  $\psi(x)$ , (the part where the sign in the exponent is negative), we let

$$\psi_{p,+}(x) = u(\mathbf{p})e^{-ip_\mu x^\mu}, \quad (\text{F.3})$$

and for the negative energy part,

$$\psi_{p,-}(x) = v(\mathbf{p})e^{+ip_\mu x^\mu}. \quad (\text{F.4})$$

The  $u(\mathbf{p})$  and  $v(\mathbf{p})$  are column vectors. They depend on only the spatial part of  $p$ , since the momentum is required to be on shell. The column vectors satisfy

$$(\rlap{/}p - M)u(\mathbf{p}) = (\rlap{/}p + M)v(\mathbf{p}) = 0, \quad (\text{F.5})$$

$$\bar{u}(\mathbf{p})(\rlap{/}p - M) = \bar{v}(\mathbf{p})(\rlap{/}p + M) = 0. \quad (\text{F.6})$$

From this point on, we will only be concerned with these momentum space representations.

To get a Hamiltonian version of the Dirac equation, we multiply by  $\gamma^0$  to get

$$(E - \boldsymbol{\alpha} \cdot \mathbf{p} - \beta M)u(\mathbf{p}) = 0, \quad (\text{F.7})$$

$$(E - \boldsymbol{\alpha} \cdot \mathbf{p} + \beta M)v(\mathbf{p}) = 0. \quad (\text{F.8})$$

Using the Bjorken and Drell representation, we can write the Hamiltonian version of the Dirac equation as

$$\begin{pmatrix} E - M & -\boldsymbol{\sigma} \cdot \mathbf{p} \\ -\boldsymbol{\sigma} \cdot \mathbf{p} & E + M \end{pmatrix} \begin{pmatrix} \chi(\mathbf{p}) \\ u_B(\mathbf{p}) \end{pmatrix} = \begin{pmatrix} 0 \\ 0 \end{pmatrix}. \quad (\text{F.9})$$

We find that  $u_B(\mathbf{p}) = \frac{\boldsymbol{\sigma} \cdot \mathbf{p}}{E+M}\chi(\mathbf{p})$ , so

$$u(\mathbf{p}) = c \begin{pmatrix} 1 \\ \frac{\boldsymbol{\sigma} \cdot \mathbf{p}}{E+M} \end{pmatrix} \chi(\mathbf{p}), \quad (\text{F.10})$$

$$v(\mathbf{p}) = c \begin{pmatrix} \frac{\boldsymbol{\sigma} \cdot \mathbf{p}}{E+M} \\ 1 \end{pmatrix} v_A(\mathbf{p}), \quad (\text{F.11})$$

where  $c$  is the normalization constant.

The normalization we choose is  $\bar{u}(\mathbf{p}, \lambda')u(\mathbf{p}, \lambda) = \delta_{\lambda'\lambda}$ , so

$$\delta_{\lambda'\lambda} = \bar{u}(\mathbf{p}, \lambda')u(\mathbf{p}, \lambda) \quad (\text{F.12})$$

$$= |c|^2 \begin{pmatrix} 1 & \frac{\boldsymbol{\sigma} \cdot \mathbf{p}}{E+M} \end{pmatrix} \begin{pmatrix} 1 & 0 \\ 0 & -1 \end{pmatrix} \begin{pmatrix} 1 \\ \frac{\boldsymbol{\sigma} \cdot \mathbf{p}}{E+M} \end{pmatrix} \chi^\dagger(\mathbf{p}, \lambda')\chi(\mathbf{p}, \lambda) \quad (\text{F.13})$$

$$= |c|^2 \left( 1 - \frac{\mathbf{p}^2}{(E+M)^2} \right) \chi^\dagger(\mathbf{p}, \lambda')\chi(\mathbf{p}, \lambda) \quad (\text{F.14})$$

$$= |c|^2 \frac{M^2 + \mathbf{p}^2 + E^2 + 2EM + M^2 - \mathbf{p}^2}{(E+M)^2} \chi^\dagger(\mathbf{p}, \lambda')\chi(\mathbf{p}, \lambda) \quad (\text{F.15})$$

$$= |c|^2 \frac{2M}{E+M} \chi^\dagger(\mathbf{p}, \lambda')\chi(\mathbf{p}, \lambda). \quad (\text{F.16})$$

If we choose also  $\chi^\dagger(\mathbf{p}, \lambda')\chi(\mathbf{p}, \lambda) = 1$ , then we get that  $c = \sqrt{\frac{W}{2M}}$ , where  $W = E + M$ , so

$$u(\mathbf{p}) = \sqrt{\frac{W}{2M}} \begin{pmatrix} 1 \\ \frac{\boldsymbol{\sigma} \cdot \mathbf{p}}{W} \end{pmatrix} \chi(\mathbf{p}), \quad (\text{F.17})$$

$$v(\mathbf{p}) = \sqrt{\frac{W}{2M}} \begin{pmatrix} \frac{\boldsymbol{\sigma} \cdot \mathbf{p}}{W} \\ 1 \end{pmatrix} v_A(\mathbf{p}). \quad (\text{F.18})$$

We can choose any two linearly independent vectors for  $\chi(\mathbf{p})$  which correspond to the two spins. These different choices lead to the different definitions of the spinors.

### *Assorted Spinor Definitions*

“One day Alice came to a fork in the road and saw a Cheshire cat in a tree. ‘Which road do I take?’ she asked. His response was a question: ‘Where do you want to go?’ ‘I don’t know,’ Alice answered. ‘Then,’ said the cat, ‘it doesn’t matter.’ ”

—*Lewis Carroll*

The spinors used by Bjorken and Drell [99] are polarized in the  $\hat{z}$  direction, and so the  $\chi$ 's are chosen to be

$$\chi_{+1/2} = \begin{pmatrix} 1 \\ 0 \end{pmatrix}, \quad (\text{F.19})$$

$$\chi_{-1/2} = \begin{pmatrix} 0 \\ 1 \end{pmatrix}. \quad (\text{F.20})$$

The light-front spinors are defined to be [18]

$$u_{\text{LF}}(k, \lambda) \equiv \frac{1}{\sqrt{Mk^+}} [M\Lambda_- + (k^+ + \boldsymbol{\alpha}^\perp \cdot \mathbf{k}^\perp)\Lambda_+] \chi_{\text{LF},\lambda} \quad (\text{F.21})$$

$$= \frac{1}{\sqrt{Mk^+}} [\Lambda_-(M + \boldsymbol{\alpha}^\perp \cdot \mathbf{k}^\perp) + \Lambda_+k^+] \chi_{\text{LF},\lambda}, \quad (\text{F.22})$$

$$\chi_{\text{LF},\lambda} \equiv \begin{pmatrix} \chi_\lambda \\ 0 \end{pmatrix}, \quad (\text{F.23})$$

where  $\chi_\lambda$  is the usual Pauli spinor, and the  $\Lambda_\pm$  are the spinor projection operators defined in Appendix A. We find that

$$\bar{u}_{\text{LF}}(k, \lambda) = \frac{1}{\sqrt{Mk^+}} \chi_{\text{LF},\lambda}^\dagger [\Lambda_+ M + \Lambda_- (k^+ + \boldsymbol{\alpha}^\perp \cdot \mathbf{k}^\perp)] \quad (\text{F.24})$$

$$= \frac{1}{\sqrt{Mk^+}} \chi_{\text{LF},\lambda}^\dagger [(M - \boldsymbol{\alpha}^\perp \cdot \mathbf{k}^\perp) \Lambda_+ + k^+ \Lambda_-]. \quad (\text{F.25})$$

Note that these spinors are normalized to satisfy  $\bar{u}_{\text{LF}}(k, \lambda') u_{\text{LF}}(k, \lambda) = \delta_{\lambda'\lambda}$ .

For helicity spinors, we choose the eigenvectors of the helicity operator  $(\boldsymbol{\sigma} \cdot \hat{\mathbf{p}})$  as the  $\chi$ 's. In particular,  $(\hat{\mathbf{p}} \cdot \boldsymbol{\Sigma}) u(\mathbf{p}, \lambda) = h u(\mathbf{p}, \lambda)$ , where  $h = 2\lambda$ . This choice allows us to write

$$u(\mathbf{p}, \lambda) = \sqrt{\frac{W}{2M}} \begin{pmatrix} 1 \\ \frac{h\mathbf{p}}{W} \end{pmatrix} \chi_\lambda(\mathbf{p}) \quad (\text{F.26})$$

where  $(\boldsymbol{\sigma} \cdot \hat{\mathbf{p}}) \chi_\lambda(\mathbf{p}) = h \chi_\lambda(\mathbf{p})$ .

One useful feature of the helicity spinors is the simplification of the  $\boldsymbol{\sigma} \cdot p$  factor living in the prefactor of  $\chi$  in the definition of  $u$ . This is an important feature: all of the directional dependence lives in the  $\chi$  alone. (For the normal spinors, the  $\chi$  are independent of the momentum, but the prefactor has the dependence.)

Now, we proceed to calculate  $\chi_\lambda(\mathbf{p})$ . This will be done by taking two steps: first calculate  $\chi_\lambda(\hat{\mathbf{z}})$ , then rotate that to an arbitrary angle.

The first step is easy. When  $\mathbf{p} = \hat{\mathbf{z}}$ , the helicity eigenvalue equation is

$$(\boldsymbol{\sigma} \cdot \hat{\mathbf{z}}) \chi_\lambda(\mathbf{z}) = \sigma_z \chi_\lambda(\mathbf{z}) \quad (\text{F.27})$$

$$= h \chi_\lambda(\mathbf{z}). \quad (\text{F.28})$$

This means that  $\chi_\lambda(\mathbf{z})$  are just the usual vectors for the spin-1/2 basis,

$$\chi_{+1/2}(\mathbf{z}) = \begin{pmatrix} 1 \\ 0 \end{pmatrix}, \quad (\text{F.29})$$

$$\chi_{-1/2}(\mathbf{z}) = \begin{pmatrix} 0 \\ 1 \end{pmatrix}. \quad (\text{F.30})$$

Now for the second step. To rotate, use the Euler angle representation of the rotation operator [127]:

$$R_{\alpha,\beta,\gamma} = e^{-i\alpha J_z} e^{-i\beta J_y} e^{-i\gamma J_z}. \quad (\text{F.31})$$

This operator allows us to write

$$u(\mathbf{p}, \lambda) = R_{\phi,\theta,\gamma} u(p \times \hat{\mathbf{z}}, \lambda) \quad (\text{F.32})$$

$$= R_{\phi,\theta,\gamma} \sqrt{\frac{W}{2M}} \begin{pmatrix} 1 \\ \frac{hp}{W} \end{pmatrix} \chi_\lambda(\hat{\mathbf{z}}). \quad (\text{F.33})$$

Note that we are free to choose  $\gamma$ , since all it does is give a phase to  $\chi$ . The traditional approach is to set it equal to  $-\phi$ . This is what Brown and Jackson do [9], and in general it is the best thing to do, since it gives the correct rotations starting from a state pointing in an arbitrary direction. However, since our state just points in the  $z$ -direction, this angle just gives a phase. It will turn out to be useful to just set  $\gamma = 0$ . This choice simplifies the equations we will use later, but be warned that these kets transform differently from those that Machleidt [58] and Brown and Jackson use [9], but they are closer to what Rice and Kim [128] use. Note that for totally symmetric potentials, both  $\phi$  and  $\phi'$  can be set to zero, so this distinction is a moot point. However, here (and in Rice and Kim's work), we cannot set them both to zero, and we find that our convention is much easier to work with.

So we have

$$u(\mathbf{p}, \lambda) = R_{\phi,\theta,0} \sqrt{\frac{W}{2M}} \begin{pmatrix} 1 \\ \frac{hp}{W} \end{pmatrix} \chi_\lambda(\hat{\mathbf{z}}). \quad (\text{F.34})$$

The operator will not affect the prefactor. Since the spin and the momentum rotate together, the factor of  $\boldsymbol{\sigma} \cdot \mathbf{p}$  remains unchanged. The rotation operator only hits  $\chi$ , so that

$$\chi_\lambda(\mathbf{p}) = R_{\phi,\theta,0} \chi_\lambda(\hat{\mathbf{z}}). \quad (\text{F.35})$$

The  $\chi$  is an  $SU(2)$  spinor, and the  $SU(2)$  representation of the angular momentum operator  $J$  is  $\sigma/2$ . Note that  $\sigma_i^2 = 1$ , and that in general if  $A^2 = 1$ ,

$$e^{i\theta A} = \sum_{n=0}^{\infty} \frac{(-1)^n}{(2n)!} \theta^{2n} + \sum_{n=0}^{\infty} \frac{(-1)^n}{(2n+1)!} \theta^{2n+1} iA \quad (\text{F.36})$$

$$= \cos \theta + iA \sin \theta. \quad (\text{F.37})$$

Thus,

$$e^{-i\alpha J_z} = \begin{pmatrix} e^{-i\alpha/2} & 0 \\ 0 & e^{+i\alpha/2} \end{pmatrix}, \quad (\text{F.38})$$

$$e^{-i\beta J_y} = \cos \frac{\beta}{2} - i\sigma_y \sin \frac{\beta}{2} = \begin{pmatrix} \cos \frac{\beta}{2} & -\sin \frac{\beta}{2} \\ \sin \frac{\beta}{2} & \cos \frac{\beta}{2} \end{pmatrix}, \quad (\text{F.39})$$

$$e^{-i\theta J_x} = \cos \frac{\theta}{2} - i\sigma_x \sin \frac{\theta}{2} = \begin{pmatrix} \cos \frac{\theta}{2} & -i \sin \frac{\theta}{2} \\ -i \sin \frac{\theta}{2} & \cos \frac{\theta}{2} \end{pmatrix}. \quad (\text{F.40})$$

This means that  $R$  is

$$R_{\phi,\theta,0} = \begin{pmatrix} e^{-i\phi/2} c_2 & -e^{-i\phi/2} s_2 \\ e^{+i\phi/2} s_2 & e^{+i\phi/2} c_2 \end{pmatrix}, \quad (\text{F.41})$$

where  $c_2 = \cos \frac{\theta}{2}$  and  $s_2 = \sin \frac{\theta}{2}$ . This gives

$$\chi_\lambda(\mathbf{k}) = R_{\phi,\theta,0} \chi_\lambda(\hat{\mathbf{z}}) = \chi_\lambda(\hat{\mathbf{p}}) = \begin{cases} \begin{pmatrix} c_2 e^{-i\phi/2} \\ s_2 e^{+i\phi/2} \end{pmatrix} & \text{if } h = +1 \\ \begin{pmatrix} -s_2 e^{-i\phi/2} \\ c_2 e^{+i\phi/2} \end{pmatrix} & \text{if } h = -1 \end{cases} \quad (\text{F.42})$$

## F.2 Two Helicity Spinors in the Center of Momentum Frame

We now address the problem of two particles with spin. We work in the center-of-momentum frame, and consider the relative momentum between the particles.

To start with, consider having the relative momentum pointing in the  $\hat{\mathbf{z}}$  direction. The first particle has momentum  $p\hat{\mathbf{z}}$  and helicity  $\lambda_1$ . The helicity spinor for this particle is just what was discussed in the previous section.

The second particle will have momentum  $-p\hat{\mathbf{z}}$  and helicity  $\lambda_2$ . We can relate this to a spinor with the momentum pointing in the  $\hat{\mathbf{z}}$  direction via a rotation,

$$u(-p\hat{\mathbf{z}}, \lambda_2) = R_{\phi, \pi, 0} u(p\hat{\mathbf{z}}, \lambda_2), \quad (\text{F.43})$$

where  $\phi$  is a free parameter because it has no meaning when pointing along the  $z$ -axis. As argued in the previous section, this can be recast as

$$\chi_{\lambda_2}(-\hat{\mathbf{z}}) = R_{\phi, \pi, 0} \chi_{\lambda_2}(\hat{\mathbf{z}}). \quad (\text{F.44})$$

Using Eq. (F.41), we can write

$$R_{\phi, \pi, 0} = \begin{pmatrix} 0 & -e^{-i\phi/2} \\ e^{+i\phi/2} & 0 \end{pmatrix}. \quad (\text{F.45})$$

If we choose  $\phi = \pi$ , this becomes

$$R_{\pi, \pi, 0} = \begin{pmatrix} 0 & i \\ i & 0 \end{pmatrix}, \quad (\text{F.46})$$

so that

$$\chi_{\lambda_2}(-\hat{\mathbf{z}}) = i\chi_{-\lambda_2}(\hat{\mathbf{z}}). \quad (\text{F.47})$$

When the relative momentum points in an arbitrary direction, we find that for particle 2,

$$\chi_{\lambda_2}(-\mathbf{p}) = R_{\phi, \theta, 0} \chi_{\lambda_2}(-\hat{\mathbf{z}}) \quad (\text{F.48})$$

$$= iR_{\phi, \theta, 0} \chi_{-\lambda_2}(\hat{\mathbf{z}}) \quad (\text{F.49})$$

$$= i\chi_{-\lambda_2}(\mathbf{p}). \quad (\text{F.50})$$

This is rather simple.

### F.3 Helicity Spinor Summary

We have

$$u(\mathbf{p}, \lambda) = \sqrt{\frac{W}{2M}} \begin{pmatrix} 1 \\ f \end{pmatrix} \chi_\lambda(\hat{\mathbf{p}}), \quad (\text{F.51})$$

and

$$\chi_\lambda(\hat{\mathbf{p}}) = \begin{cases} \begin{pmatrix} c_2 e^{-i\phi/2} \\ s_2 e^{+i\phi/2} \end{pmatrix} & \text{if } h = +1 \\ \begin{pmatrix} -s_2 e^{-i\phi/2} \\ c_2 e^{+i\phi/2} \end{pmatrix} & \text{if } h = -1 \end{cases} \quad (\text{F.52})$$

where  $c_2 = \cos \frac{\theta}{2}$ ,  $s_2 = \sin \frac{\theta}{2}$ ,  $f = \frac{hp}{W}$ , and  $h = 2\lambda$ .

When there are two fermions in the center-of-momentum frame, we can define  $\phi \equiv \phi_1$  and  $\theta \equiv \theta_1$  and for particle two  $\phi_2 = \pi + \phi$  and  $\theta_2 = \pi - \theta$ . This means that

$$u(\mathbf{p}_i, \lambda_i) = \sqrt{\frac{W}{2M}} \begin{pmatrix} 1 \\ f_i \end{pmatrix} \chi_{i,\lambda_i}(\hat{\mathbf{p}}), \quad (\text{F.53})$$

where  $i = 1, 2$  and

$$\chi_{1,\lambda_1}(\hat{\mathbf{p}}) = \chi_{\lambda_1}(\hat{\mathbf{p}}), \quad (\text{F.54})$$

$$\chi_{2,\lambda_2}(\hat{\mathbf{p}}) = i\chi_{-\lambda_2}(\hat{\mathbf{p}}). \quad (\text{F.55})$$

### F.4 Breakup of Dirac Spinor Matrix Elements

We are interested in matrix elements with the form

$$\begin{aligned} \bar{u}(\mathbf{p}', \lambda') \Gamma u(\mathbf{p}, \lambda) &= \frac{\sqrt{W'W}}{2M} \chi_{\lambda'}^\dagger(\mathbf{p}') \left[ \begin{pmatrix} 1 & -f' \end{pmatrix} \begin{pmatrix} \Gamma_{AA} & \Gamma_{AB} \\ \Gamma_{BA} & \Gamma_{BB} \end{pmatrix} \begin{pmatrix} 1 \\ f \end{pmatrix} \right] \chi_\lambda(\mathbf{p}) \\ &= \frac{\sqrt{W'W}}{2M} \left( \chi_{\lambda'}^\dagger \Gamma_{AA} \chi_\lambda + \chi_{\lambda'}^\dagger \Gamma_{AB} \chi_\lambda f \right. \\ &\quad \left. - \chi_{\lambda'}^\dagger \Gamma_{BA} \chi_\lambda f' - \chi_{\lambda'}^\dagger \Gamma_{BB} \chi_\lambda f' f \right). \end{aligned} \quad (\text{F.56})$$

The elements of the  $\Gamma_{ab}$  matrices will be either the identity matrix or Pauli sigma matrices.

For example, we have

$$\bar{u}(p', \lambda') u(p, \lambda) = \chi_{\lambda'}^\dagger \chi_\lambda \frac{\sqrt{W'W}}{2M} (1 - f'f), \quad (\text{F.57})$$

$$\bar{u}(p', \lambda') \gamma^0 u(p, \lambda) = \chi_{\lambda'}^\dagger \chi_\lambda \frac{\sqrt{W'W}}{2M} (1 + f'f), \quad (\text{F.58})$$

$$\bar{u}(p', \lambda') \gamma^5 u(p, \lambda) = \chi_{\lambda'}^\dagger \chi_\lambda \frac{\sqrt{W'W}}{2M} (f - f'), \quad (\text{F.59})$$

and some more complicated ones,

$$\bar{u}(p', \lambda') \gamma^i u(p, \lambda) = \chi_{\lambda'}^\dagger \sigma^i \chi_\lambda \frac{\sqrt{W'W}}{2M} (f + f'), \quad (\text{F.60})$$

$$\begin{aligned} \bar{u}(p', \lambda') \sigma^{\mu\nu} i(p' - p)_\nu u(p, \lambda) &= 2M \bar{u}(p', \lambda') \gamma^\mu u(p, \lambda) \\ &\quad - (p' + p)^\mu \bar{u}(p', \lambda') u(p, \lambda). \end{aligned} \quad (\text{F.61})$$

We used the Gordon decomposition (Section F.5) to simplify the last equation. This simplification of the tensor allows us to only worry about two tricky matrix elements for vector mesons.

With the Gordon decomposition, we can further simplify the vector meson coupling by using the Dirac equation. Note that the expression for  $\Gamma$  is only valid in this context.

$$\Gamma_i^\mu = \left(1 + \frac{f}{g}\right) \gamma^\mu - \frac{f}{g} \frac{1}{2M} (p'_i + p_i)^\mu, \quad (\text{F.62})$$

$$U_v = \bar{u}(\mathbf{p}'_1, \lambda'_1) \Gamma_1^\mu u(\mathbf{p}_1, \lambda_1) (-g_{\mu\nu}) \bar{u}(\mathbf{p}'_2, \lambda'_2) \Gamma_2^\nu u(\mathbf{p}_2, \lambda_2) \quad (\text{F.63})$$

$$\begin{aligned} &= \left(1 + \frac{f}{g}\right)^2 \bar{u}(\mathbf{p}'_1, \lambda'_1) \gamma^\mu u(\mathbf{p}_1, \lambda_1) (-g_{\mu\nu}) \bar{u}(\mathbf{p}'_2, \lambda'_2) \gamma^\nu u(\mathbf{p}_2, \lambda_2) \\ &\quad + \left(1 + \frac{f}{g}\right) \frac{f}{g} \frac{1}{2M} \bar{u}(\mathbf{p}'_1, \lambda'_1) (\mathbf{p}'_2 + \mathbf{p}_2) u(\mathbf{p}_1, \lambda_1) \bar{u}(\mathbf{p}'_2, \lambda'_2) u(\mathbf{p}_2, \lambda_2) \\ &\quad + \left(1 + \frac{f}{g}\right) \frac{f}{g} \frac{1}{2M} \bar{u}(\mathbf{p}'_1, \lambda'_1) u(\mathbf{p}_1, \lambda_1) \bar{u}(\mathbf{p}'_2, \lambda'_2) (\mathbf{p}'_1 + \mathbf{p}_1) u(\mathbf{p}_2, \lambda_2) \\ &\quad - \left(\frac{f}{g}\right)^2 (p'_1 + p_1)^\mu (p'_2 + p_2)_\mu \frac{1}{4M^2} \bar{u}(\mathbf{p}'_1, \lambda'_1) u(\mathbf{p}_1, \lambda_1) \bar{u}(\mathbf{p}'_2, \lambda'_2) u(\mathbf{p}_2, \lambda_2). \end{aligned} \quad (\text{F.64})$$

The Dirac equation can be used to write  $\not{p}_2 u(p_1, \lambda) = (2E\gamma^0 - M)u(p_1, \lambda)$ , and also note that

$$(\mathbf{p}'_1 + p_1)^\mu (\mathbf{p}'_2 + p_2)_\mu = 2(E' + E)^2 - (\mathbf{p}'_1 + p_1)^\mu (\mathbf{p}'_1 + p_1)_\mu \quad (\text{F.65})$$

$$= 2(E' + E)^2 - 2M^2 - 2E'E + 2\mathbf{p}' \cdot \mathbf{p}. \quad (\text{F.66})$$

This means we can write

$$\begin{aligned} U_v &= \left(1 + \frac{f}{g}\right)^2 \bar{u}(\mathbf{p}'_1, \lambda'_1) \gamma^\mu u(\mathbf{p}_1, \lambda_1) (-g_{\mu\nu}) \bar{u}(\mathbf{p}'_2, \lambda'_2) \gamma^\nu u(\mathbf{p}_2, \lambda_2) \\ &\quad - 2 \left(1 + \frac{f}{g}\right) \frac{f}{g} \bar{u}(\mathbf{p}'_1, \lambda'_1) u(\mathbf{p}_1, \lambda_1) \bar{u}(\mathbf{p}'_2, \lambda'_2) u(\mathbf{p}_2, \lambda_2) \\ &\quad + \left(1 + \frac{f}{g}\right) \frac{f}{g} \frac{E' + E}{M} \bar{u}(\mathbf{p}'_1, \lambda'_1) \gamma^0 u(\mathbf{p}_1, \lambda_1) \bar{u}(\mathbf{p}'_2, \lambda'_2) u(\mathbf{p}_2, \lambda_2) \\ &\quad + \left(1 + \frac{f}{g}\right) \frac{f}{g} \frac{E' + E}{M} \bar{u}(\mathbf{p}'_1, \lambda'_1) u(\mathbf{p}_1, \lambda_1) \bar{u}(\mathbf{p}'_2, \lambda'_2) \gamma^0 u(\mathbf{p}_2, \lambda_2) \\ &\quad - \left(\frac{f}{g}\right)^2 \frac{(E' + E)^2 - M^2 - E'E + \mathbf{p}' \cdot \mathbf{p}}{2M^2} \\ &\quad \times \bar{u}(\mathbf{p}'_1, \lambda'_1) u(\mathbf{p}_1, \lambda_1) \bar{u}(\mathbf{p}'_2, \lambda'_2) u(\mathbf{p}_2, \lambda_2). \end{aligned} \quad (\text{F.67})$$

We are interested in the matrix elements for OME and TBE exchange potentials. Thus, we want to look at combinations of two  $\bar{u}u$  matrix elements. To save space, we will write

$$\langle \lambda'_1, \lambda'_2 | \lambda_1, \lambda_2 \rangle = \left( \chi_{\lambda'_1}^\dagger \chi_{\lambda_1} \right) \left( \chi_{-\lambda'_2}^\dagger \chi_{-\lambda_2} \right), \quad (\text{F.68})$$

$$\langle \lambda'_1, \lambda'_2 | \boldsymbol{\sigma}_1 \cdot \boldsymbol{\sigma}_2 | \lambda_1, \lambda_2 \rangle = \left( \chi_{\lambda'_1}^\dagger \sigma^i \chi_{\lambda_1} \right) \left( \chi_{-\lambda'_2}^\dagger \sigma^i \chi_{-\lambda_2} \right). \quad (\text{F.69})$$

We can write the matrix element for the scalar exchange as

$$\begin{aligned} U_s &= \bar{u}(\mathbf{p}'_1, \lambda'_1) u(\mathbf{p}_1, \lambda_1) \times \bar{u}(\mathbf{p}'_2, \lambda'_2) u(\mathbf{p}_2, \lambda_2) \\ &= \frac{W'W}{4M^2} \left(1 - \frac{h'_2 h_1 p' p}{W'W}\right) \left(1 - \frac{h_2 h_2 p' p}{W'W}\right) \langle \lambda'_1, \lambda'_2 | \lambda_1, \lambda_2 \rangle, \end{aligned} \quad (\text{F.70})$$

and the matrix element for the pseudoscalar exchange as

$$\begin{aligned} U_{ps} &= \bar{u}(\mathbf{p}'_1, \lambda'_1) i\gamma^5 u(\mathbf{p}_1, \lambda_1) \times \bar{u}(\mathbf{p}'_2, \lambda'_2) i\gamma^5 u(\mathbf{p}_2, \lambda_2) \\ &= -\frac{W'W}{4M^2} \left(\frac{h_1 p}{W} - \frac{h'_1 p'}{W'}\right) \left(\frac{h_2 p}{W} - \frac{h'_2 p'}{W'}\right) \langle \lambda'_1, \lambda'_2 | \lambda_1, \lambda_2 \rangle. \end{aligned} \quad (\text{F.71})$$

Now for the vector meson. Note that one part is the same as for the scalar meson. The other part is more complicated, the vector-vector part:

$$\begin{aligned}
U_{\text{vv}} &= \bar{u}(\mathbf{p}'_1, \lambda'_1) \gamma^\mu u(\mathbf{p}_1, \lambda_1) (-g_{\mu\nu}) \bar{u}(\mathbf{p}'_2, \lambda'_2) \gamma^\nu u(\mathbf{p}_2, \lambda_2) \\
&= -\frac{W'W}{4M^2} \left[ \left(1 + \frac{h'_1 h_1 p' p}{W'W}\right) \left(1 + \frac{h'_2 h_2 p' p}{W'W}\right) \langle \lambda'_1, \lambda'_2 | \lambda_1, \lambda_2 \rangle - \right. \\
&\quad \left. \left(\frac{h_1 p}{W} + \frac{h'_1 p'}{W'}\right) \left(\frac{h_2 p}{W} + \frac{h'_2 p'}{W'}\right) \langle \lambda'_1, \lambda'_2 | \boldsymbol{\sigma}_1 \cdot \boldsymbol{\sigma}_2 | \lambda_1, \lambda_2 \rangle \right]. \quad (\text{F.72})
\end{aligned}$$

This means that the full  $\bar{u}u$  matrix element for a vector meson with a non-vanishing tensor coupling is

$$U_{\text{v}} = \left(1 + \frac{f}{g}\right)^2 U_{\text{vv}} + \frac{f}{g} \left[2 + \frac{f}{g} \left(\frac{3}{2} + \frac{-E'E + \mathbf{p}' \cdot \mathbf{p}}{2M^2}\right)\right] U_{\text{s}} \quad (\text{F.73})$$

$$\begin{aligned}
&= \left(1 + \frac{f}{g}\right)^2 U_{\text{vv}} + \frac{f}{g} \left[2 + \frac{f}{g} \left(\frac{3}{2} + \frac{-E'E + p'^3 p^3}{2M^2}\right)\right] U_{\text{s}} \\
&\quad + \left(\frac{f}{g}\right)^2 \frac{p'_\perp p_\perp}{4M^2} U_{\text{s}} \left(e^{i(\phi' - \phi)} + e^{-i(\phi' - \phi)}\right). \quad (\text{F.74})
\end{aligned}$$

We can write this out as vector-tensor, and tensor-tensor parts. The vector-vector is just  $U_{\text{vv}}$ .

$$U_{\text{vt}} = \frac{2f}{g} [U_{\text{vv}} + U_{\text{s}}] \quad (\text{F.75})$$

$$\begin{aligned}
&= -\frac{2f}{g} \frac{W'W}{4M^2} \left[2 \left(\frac{h'_1 h_1 p' p}{W'W} + \frac{h'_2 h_2 p' p}{W'W}\right) \langle \lambda'_1, \lambda'_2 | \lambda_1, \lambda_2 \rangle - \right. \\
&\quad \left. \left(\frac{h_1 p}{W} + \frac{h'_1 p'}{W'}\right) \left(\frac{h_2 p}{W} + \frac{h'_2 p'}{W'}\right) \langle \lambda'_1, \lambda'_2 | \boldsymbol{\sigma}_1 \cdot \boldsymbol{\sigma}_2 | \lambda_1, \lambda_2 \rangle \right], \quad (\text{F.76})
\end{aligned}$$

$$U_{\text{tt}} = \left(\frac{f}{g}\right)^2 \left[U_{\text{vv}} + \frac{1}{2} \left(3 - \frac{E'E}{M^2} + \frac{\mathbf{p}' \cdot \mathbf{p}}{M^2}\right) U_{\text{s}}\right] \quad (\text{F.77})$$

$$\begin{aligned}
&= -\left(\frac{f}{g}\right)^2 \frac{W'W}{4M^2} \left[ \langle \lambda'_1, \lambda'_2 | \lambda_1, \lambda_2 \rangle \left\{ \left(1 + \frac{h'_1 h_1 p' p}{W'W}\right) \left(1 + \frac{h'_2 h_2 p' p}{W'W}\right) + \right. \right. \\
&\quad \left. \left. \frac{3M^2 - E'E + \mathbf{p}' \cdot \mathbf{p}}{2M^2} \left(1 - \frac{h'_1 h_1 p' p}{W'W}\right) \left(1 - \frac{h'_2 h_2 p' p}{W'W}\right) \right\} - \right. \\
&\quad \left. \left(\frac{h_1 p}{W} + \frac{h'_1 p'}{W'}\right) \left(\frac{h_2 p}{W} + \frac{h'_2 p'}{W'}\right) \langle \lambda'_1, \lambda'_2 | \boldsymbol{\sigma}_1 \cdot \boldsymbol{\sigma}_2 | \lambda_1, \lambda_2 \rangle \right]. \quad (\text{F.78})
\end{aligned}$$

### F.5 The Gordon Decomposition

“Nothing shocks me. I’m a scientist.”

—*Indiana Jones*

Now, let’s look at the Gordon decomposition. We start by looking at

$$i\sigma^{\mu\nu} = \frac{-1}{2} (\gamma^\mu\gamma^\nu - \gamma^\nu\gamma^\mu) = g^{\mu\nu} - \gamma^\mu\gamma^\nu. \quad (\text{F.79})$$

Then,

$$\begin{aligned} \bar{u}(p', \lambda')\sigma^{\mu\nu}i(p' - p)_\nu u(p, \lambda) &= -\bar{u}(p', \lambda')\sigma^{\mu\nu}ip_\nu u(p, \lambda) - \bar{u}(p', \lambda')ip'_\nu\sigma^{\nu\mu}u(p, \lambda) \\ &= \bar{u}(p', \lambda')\gamma^\mu\not{p}u(p, \lambda) + \bar{u}(p', \lambda')\not{p}'\gamma^\mu u(p, \lambda) \\ &\quad - (p' + p)^\mu\bar{u}(p', \lambda')u(p, \lambda). \end{aligned} \quad (\text{F.80})$$

Using the Dirac equation, we see that

$$\bar{u}(p', \lambda')\sigma^{\mu\nu}i(p' - p)_\nu u(p, \lambda) = 2M\bar{u}(p', \lambda')\gamma^\mu u(p, \lambda) - (p' + p)^\mu\bar{u}(p', \lambda')u(p, \lambda), \quad (\text{F.81})$$

which is the Gordon identity.

## Appendix G

### ROTATION MATRICES

“There comes a time when for every addition of knowledge you forget something that you knew before. It is of the highest importance, therefore, not to have useless facts elbowing out the useful ones.”

—*Arthur Conan Doyle*

#### **G.1 Relations Between Rotation Matrices**

Brown and Jackson give a good introduction to this topic [9]. We start out with the rotation operator, parameterized in terms of the Euler angles,

$$R_{\alpha\beta\gamma} = e^{-i\alpha J_z} e^{-i\beta J_y} e^{-i\gamma J_z}, \quad (\text{G.1})$$

We can take matrix elements of this, to get

$$\langle J' M' | R_{\alpha\beta\gamma} | J M \rangle = \delta_{J' J} \mathcal{D}_{M' M}^J(\alpha\beta\gamma) \quad (\text{G.2})$$

$$= \delta_{J' J} e^{-i(\alpha M' + \gamma M)} d_{M' M}^J(\beta). \quad (\text{G.3})$$

Note that the lower indices in  $d$  are in the same order as in  $\mathcal{D}$ . This is different that the convention in [9, 58], but agrees with [127–129]. However, we also define the matrix elements slightly differently, and the combination of those two effects makes the calculated Jacobi polynomials the same!

An alternative interpretation of the  $\mathcal{D}$ 's is that they are the overlap of  $JM\lambda$  kets with  $\theta\phi\lambda$  kets. To see this, generalize Sakurai's approach for kets without spin [127]. We start out with  $|\hat{z}\lambda\rangle$ . This is a ket for a particle pointed upwards, with  $\lambda$  units of

spin in the  $z$ -direction. This ket can be rotated with  $R$  to get

$$R_{\phi\theta\gamma}|\widehat{z}\lambda\rangle = |\theta\phi\lambda\rangle. \quad (\text{G.4})$$

Brown and Jackson choose  $\gamma = -\phi$ , however our convention is to choose  $\gamma = 0$  and get

$$R_{\phi\theta 0}|\widehat{z}\lambda\rangle = |\theta\phi\lambda\rangle \quad (\text{G.5})$$

Applying a  $\langle J'M'\lambda'|$  bra to the previous equation, we obtain

$$\langle J'M'\lambda'|\theta\phi\lambda\rangle = \langle J'M'\lambda'|R_{\phi\theta 0}|\widehat{z}\lambda\rangle = \sum_{J,M,\lambda''} \langle J'M'\lambda'|R_{\phi\theta 0}|JM\lambda''\rangle \langle JM\lambda''|\widehat{z}\lambda\rangle. \quad (\text{G.6})$$

In the last bra-ket, we must have  $\lambda = \lambda''$ , since the helicity cannot be changed. Furthermore, since  $\lambda$  is the  $J_z$  quantum number for the final state, we also have  $\lambda = M$ . These facts allow us to write

$$\langle JM\lambda''|\widehat{z}\lambda\rangle = \delta_{\lambda''\lambda}\delta_{M\lambda}\langle JM|\widehat{z}\rangle = \delta_{\lambda''\lambda}\delta_{M\lambda}Y_{JM}(0, \phi) = \delta_{\lambda''\lambda}\delta_{M\lambda}\sqrt{\frac{2J+1}{4\pi}}, \quad (\text{G.7})$$

which means that

$$\langle JM\lambda|\theta\phi\lambda\rangle = \langle JM|R_{\phi\theta 0}|J\lambda\rangle\sqrt{\frac{2J+1}{4\pi}} = \sqrt{\frac{2J+1}{4\pi}}\mathcal{D}_{M\lambda}^J(\phi\theta 0). \quad (\text{G.8})$$

Since the  $\phi$  dependence of the  $\mathcal{D}$ 's is essentially trivial, we can replace the 0 with a  $\gamma$  to get

$$\mathcal{D}_{M\lambda}^J(\phi\theta\gamma) = \sqrt{\frac{4\pi}{2J+1}}\langle JM\lambda|\theta\phi\lambda\rangle e^{-i\gamma\lambda}, \quad (\text{G.9})$$

and

$$\langle JM\lambda|\theta\phi\lambda\rangle = \sqrt{\frac{2J+1}{4\pi}}\mathcal{D}_{M\lambda}^J(\phi\theta 0). \quad (\text{G.10})$$

Using these relations, we find that

$$\mathcal{D}_{M'M}^J(\alpha\beta\gamma) = \mathcal{D}_{MM'}^J(-\gamma - \beta - \alpha), \quad (\text{G.11})$$

$$d_{M'M}^J(\beta) = d_{MM'}^J(-\beta), \quad (\text{G.12})$$

$$\mathcal{D}_{M0}^J(\phi, \theta, X) = \sqrt{\frac{4\pi}{2J+1}} Y_{JM}(\Omega) = \sqrt{\frac{(J-M)!}{(J+M)!}} P_J^M(\cos\theta) e^{iM\phi}, \quad (\text{G.13})$$

$$d_{M0}^J(\beta) = \sqrt{\frac{(J-M)!}{(J+M)!}} P_J^M(\cos\beta), \quad (\text{G.14})$$

$$d_{00}^J(\beta) = P_J(\cos\beta), \quad (\text{G.15})$$

$$\mathcal{D}_{M'M}^J(0, 0, 0) = \delta_{M'M} = d_{M'M}^J(0). \quad (\text{G.16})$$

Now, let's use this. Our first thing to do is look at is the addition theorem

$$\begin{aligned} \sum_{M''} \mathcal{D}_{MM''}^J(\alpha_2, \beta_2, \gamma_2) \mathcal{D}_{M''M'}^J(\alpha_1, \beta_1, \gamma_1) \\ = \sum_{M''} \langle JM | R_{\alpha_2, \beta_2, \gamma_2} | JM'' \rangle \langle JM'' | R_{\alpha_1, \beta_1, \gamma_1} | JM' \rangle \end{aligned} \quad (\text{G.17})$$

$$= \langle JM | R_{\alpha_2, \beta_2, \gamma_2} R_{\alpha_1, \beta_1, \gamma_1} | JM' \rangle \quad (\text{G.18})$$

$$= \langle JM | R_{\alpha, \beta, \gamma} | JM' \rangle \quad (\text{G.19})$$

$$= \mathcal{D}_{MM'}^J(\alpha, \beta, \gamma). \quad (\text{G.20})$$

We used the group property of the rotations that the product of two elements gives another element. The expressions for  $(\alpha, \beta, \gamma)$  in terms of the other angles is rather complex in general.

We can also look at the orthogonality relation, considering the  $\mathcal{D}$ 's as overlaps,

$$\begin{aligned}
& \frac{2J+1}{8\pi^2} \int_0^{2\pi} d\alpha \int_0^\pi \sin\beta d\beta \int_0^{2\pi} d\gamma \mathcal{D}_{M'_1 M_1}^{J_1}{}^*(\alpha\beta\gamma) \mathcal{D}_{M'_2 M_2}^{J_2}(\alpha\beta\gamma) \\
&= \frac{2J+1}{8\pi^2} \sqrt{\frac{4\pi}{2J_1+1} \frac{4\pi}{2J_2+1}} \int_0^{2\pi} d\alpha \int_0^\pi \sin\beta d\beta \int_0^{2\pi} d\gamma \\
&\quad \left( \langle J_1 M'_1 M_1 | \alpha\beta M_1 \rangle e^{-i\gamma M_1} \right)^* \langle J_2 M'_2 M_2 | \alpha\beta M_2 \rangle e^{-i\gamma M_2} \\
&= (2J+1) \sqrt{\frac{1}{2J_1+1} \frac{1}{2J_2+1}} \left[ \int_0^{2\pi} \frac{d\gamma}{2\pi} e^{+i\gamma(M_1-M_2)} \right] \\
&\quad \int d\Omega \langle J_2 M'_2 M_2 | \Omega M_2 \rangle \langle \Omega M_1 | J_1 M'_1 M_1 \rangle \\
&= (2J+1) \sqrt{\frac{1}{2J_1+1} \frac{1}{2J_2+1}} \delta_{M_1 M_2} \\
&\quad \int d\Omega \langle J_2 M'_2 M_1 | \Omega M_1 \rangle \langle \Omega M_1 | J_1 M'_1 M_1 \rangle \\
&= (2J+1) \sqrt{\frac{1}{2J_1+1} \frac{1}{2J_2+1}} \delta_{M_1 M_2} \langle J_2 M'_2 M_1 | J_1 M'_1 M_1 \rangle \\
&= \delta_{M_1 M_2} \delta_{J_1 J_2} \delta_{M'_1 M'_2}. \tag{G.21}
\end{aligned}$$

So the conclusion is

$$\begin{aligned}
& \frac{2J+1}{8\pi^2} \int_0^{2\pi} d\alpha \int_0^\pi \sin\beta d\beta \int_0^{2\pi} d\gamma \mathcal{D}_{M'_1 M_1}^{J_1}{}^*(\alpha\beta\gamma) \mathcal{D}_{M'_2 M_2}^{J_2}(\alpha\beta\gamma) \\
&= \delta_{M_1 M_2} \delta_{M'_1 M'_2} \delta_{J_1 J_2}. \tag{G.22}
\end{aligned}$$

Using this, we find

$$\int d\Omega \frac{2J+1}{4\pi} \mathcal{D}_{M_1 M'}^{J_1}{}^*(\phi, \theta, -\phi) \mathcal{D}_{M_2 M'}^{J_2}(\phi, \theta, -\phi) = \delta_{M_1 M_2} \delta_{J_1 J_2}, \tag{G.23}$$

$$\sum_{J, M} \frac{2J+1}{4\pi} \mathcal{D}_{MM'}^J{}^*(\phi', \theta', -\phi') \mathcal{D}_{MM'}^J(\phi, \theta, -\phi) = \delta(\Omega - \Omega'), \tag{G.24}$$

$$\int_{-1}^1 d\cos\theta \frac{2J+1}{2} d_{M'M}^{J_1}(\theta) d_{M'M}^{J_2}(\theta) = \delta_{J_1 J_2}, \tag{G.25}$$

$$\sum_J \frac{2J+1}{2} d_{MM'}^J(\theta') d_{MM'}^J(\theta) = \delta(\cos\theta - \cos\theta'). \tag{G.26}$$

Now, for two particle state in the center-of-momentum frame, we can write the ket as  $|p\theta\phi\lambda_1\lambda_2\rangle$ . The total helicity of this state is  $\lambda = \lambda_1 - \lambda_2$ , which is easily seen

if we choose the momentum to be in the  $z$ -direction. Since this ket has total helicity  $\lambda$ , we can transform it using

$$|pJM\lambda_1\lambda_2\rangle = \int d\Omega |p\theta\phi\lambda_1\lambda_2\rangle \langle p\theta\phi\lambda_1\lambda_2 | pJM\lambda_1\lambda_2\rangle \quad (\text{G.27})$$

$$= \int d\Omega |p\theta\phi\lambda_1\lambda_2\rangle \langle \theta\phi\lambda | JM\lambda\rangle \quad (\text{G.28})$$

$$= \sqrt{\frac{2J+1}{4\pi}} \int d\Omega \mathcal{D}_{M\lambda}^J(\theta\phi 0) |p\theta\phi\lambda_1\lambda_2\rangle, \quad (\text{G.29})$$

where  $\lambda = \lambda_1 - \lambda_2$ .

We can break apart Eq. (G.29) as we did for the orthogonality relations,

$$|pJM\lambda_1\lambda_2\rangle = \sqrt{\frac{2J+1}{4\pi}} \int d\Omega \mathcal{D}_{M\lambda}^J(\phi, \theta, 0) |p\theta\phi\lambda_1\lambda_2\rangle \quad (\text{G.30})$$

$$= \sqrt{\frac{2J+1}{2}} \int_{-1}^1 d\cos\theta d_{M\lambda}^J(\theta) |p\theta M\lambda_1\lambda_2\rangle, \quad (\text{G.31})$$

$$|p\theta M\lambda_1\lambda_2\rangle = \frac{1}{\sqrt{2\pi}} \int_0^{2\pi} d\phi e^{i\phi M} |p\theta\phi\lambda_1\lambda_2\rangle, \quad (\text{G.32})$$

and the inverse relations (obtained using the orthogonality relations)

$$|p\theta\phi\lambda_1\lambda_2\rangle = \frac{1}{\sqrt{2\pi}} \sum_M e^{-i\phi M} |p\theta M\lambda_1\lambda_2\rangle \quad (\text{G.33})$$

$$= \sum_{J,M} \sqrt{\frac{2J+1}{4\pi}} \mathcal{D}_{M\lambda}^J(\phi, \theta, 0) |pJM\lambda_1\lambda_2\rangle, \quad (\text{G.34})$$

$$|p\theta M\lambda_1\lambda_2\rangle = \sum_J \sqrt{\frac{2J+1}{2}} d_{M\lambda}^J(\theta) |pJM\lambda_1\lambda_2\rangle. \quad (\text{G.35})$$

## G.2 Jacobi Polynomials

“Logic, like whiskey, loses its beneficial effect when taken in too large quantities.”

—*Lord Dunsany*

The Jacobi polynomials are neat guys. They are defined by

$$\langle J, M' | R_{0\theta 0} | J, M \rangle = d_{M'M}^J(\theta). \quad (\text{G.36})$$

Note that since the Jacobi polynomials are real,

$$d_{M'M}^J(\theta) = (\langle J, M' | R_{0\theta 0} | J, M \rangle)^* = \langle J, M | R_{0-\theta 0} | J, M' \rangle = d_{MM'}^J(-\theta). \quad (\text{G.37})$$

There are other symmetries that the Jacobi polynomials obey. To see them, we turn to Schwinger's model of angular momentum. In this model, we have

$$|J, M\rangle = \frac{(a_+^\dagger)^{J+M}}{\sqrt{J+M}} \frac{(a_-^\dagger)^{J-M}}{\sqrt{J-M}} |0, 0\rangle, \quad (\text{G.38})$$

where  $a_\pm^\dagger$  essentially adds in one half unit of spin, and changes  $M$  by  $\pm\frac{1}{2}$ .

What does this state do under rotation about the  $y$ -axis? Well,

$$R_{0\theta 0} |J, M\rangle = \frac{(R_{0\theta 0} a_+^\dagger R_{0\theta 0}^\dagger)^{J+M}}{\sqrt{J+M}} \frac{(R_{0\theta 0} a_-^\dagger R_{0\theta 0}^\dagger)^{J-M}}{\sqrt{J-M}} R_{0\theta 0} |0, 0\rangle. \quad (\text{G.39})$$

The vacuum is unaffected by rotations. Now, Sakurai shows that [127]

$$R_{0\theta 0} a_\pm^\dagger R_{0\theta 0}^\dagger = a_\pm^\dagger \cos \frac{\theta}{2} \pm a_\mp^\dagger \sin \frac{\theta}{2}. \quad (\text{G.40})$$

This can be used to get an explicit expression for  $d$ .

Consider now what happens to the state under a rotation by  $\pi$ . We get  $a_\pm^\dagger \rightarrow \pm a_\mp^\dagger$ .

Thus,

$$R_{0\pi 0} |J, M\rangle = \frac{(a_-^\dagger)^{J+M}}{\sqrt{J+M}} \frac{(-a_+^\dagger)^{J-M}}{\sqrt{J-M}} |0, 0\rangle \quad (\text{G.41})$$

$$= (-1)^{J-M} \frac{(a_+^\dagger)^{J-M}}{\sqrt{J-M}} \frac{(a_-^\dagger)^{J+M}}{\sqrt{J+M}} |0, 0\rangle \quad (\text{G.42})$$

$$= (-1)^{J-M} |J, -M\rangle, \quad (\text{G.43})$$

which gives a nice relation for Clebsch-Gordon coefficients

$$\langle J_1 M_1 J_2 M_2 | J M \rangle = (-1)^{J_1+J_2+J-M_1-M_2-M} \langle J_1 - M_1 J_2 - M_2 | J - M \rangle \quad (\text{G.44})$$

$$= (-1)^{J_1+J_2-J} \langle J_1 - M_1 J_2 - M_2 | J - M \rangle. \quad (\text{G.45})$$

Using this result for the Jacobi polynomials,

$$d_{M'M}^J(\pi - \theta) = \langle J, M' | R_{0\pi-\theta 0} | J, M \rangle \quad (\text{G.46})$$

$$= \langle J, M' | R_{0-\theta 0} R_{0\pi 0} | J, M \rangle \quad (\text{G.47})$$

$$= (-1)^{J-M} \langle J, M' | R_{0-\theta 0} | J, -M \rangle = (-1)^{J-M} d_{M'-M}^J(-\theta) \quad (\text{G.48})$$

$$= (-1)^{J-M'} \langle J, -M' | R_{0-\theta 0} | J, M \rangle = (-1)^{J-M'} d_{-M'-M}^J(-\theta). \quad (\text{G.49})$$

We can rotate by a full  $2\pi$ , and get

$$d_{M'M}^J(2\pi + \theta) = d_{M'M}^J(\theta) \quad (\text{G.50})$$

$$= \langle J, M' | R_{0\pi 0} R_{0\theta 0} R_{0\pi 0} | J, M \rangle \quad (\text{G.51})$$

$$= (-1)^{M'-M} \langle J, -M' | R_{0\theta 0} | J, -M \rangle = (-1)^{M'-M} d_{-M'-M}^J(\theta). \quad (\text{G.52})$$

We can also use a trick from Ref. [129]. Note that

$$e^{-i\beta J_y} = e^{+i\pi J_x} e^{+i\beta J_y} e^{-i\pi J_x}. \quad (\text{G.53})$$

The  $J_x$  exponential is calculated in Eq. (F.40), and for an angle of  $\pi$  it is

$$e^{-i\pi J_x} = i \begin{pmatrix} 0 & 1 \\ 1 & 0 \end{pmatrix}, \quad (\text{G.54})$$

so under this rotation  $a_{\pm}^{\dagger} \rightarrow ia_{\mp}^{\dagger}$ , so

$$e^{-i\pi J_x} |J, M\rangle = (i)^{J+M+J-M} |J, -M\rangle = (-1)^J |J, -M\rangle. \quad (\text{G.55})$$

Thus,

$$d_{M'M}^J(\theta) = \langle J, M' | e^{+i\beta J_y} R_{0-\theta 0} e^{-i\beta J_y} | J, M \rangle \quad (\text{G.56})$$

$$= \langle J, -M' | R_{0-\theta 0} | J, -M \rangle \quad (\text{G.57})$$

$$= d_{-M'-M}^J(-\theta). \quad (\text{G.58})$$

Also, we can use the  $x$ -rotation to look at

$$d_{M'M}^J(\pi - \theta) = \langle J, M' | R_{0\pi-\theta_0} | J, M \rangle \quad (\text{G.59})$$

$$= \langle J, M' | R_{0-\theta_0} R_{0\pi_0} | J, M \rangle \quad (\text{G.60})$$

$$= (-1)^{J-M} \langle J, M' | R_{0-\theta_0} | J, -M \rangle = (-1)^{J-M} d_{M'-M}^J(-\theta) \quad (\text{G.61})$$

$$= (-1)^{J-M'} \langle J, -M' | R_{0-\theta_0} | J, M \rangle = (-1)^{J-M'} d_{-M'M}^J(-\theta). \quad (\text{G.62})$$

Summarizing what we have so far,

$$d_{M'M}^J(\theta) = d_{MM'}^J(-\theta) \quad (\text{G.63})$$

$$= d_{-M'-M}^J(-\theta) \quad (\text{G.64})$$

$$= (-1)^{M'-M} d_{-M'-M}^J(\theta), \quad (\text{G.65})$$

$$d_{MM'}^J(\pi - \theta) = (-1)^{J-M} d_{M'-M}^J(-\theta) \quad (\text{G.66})$$

$$= (-1)^{J-M'} d_{-M'M}^J(-\theta). \quad (\text{G.67})$$

What sort of fundamental symmetries do we expect the Jacobi polynomials to obey?

1. Under  $\theta \rightarrow -\theta$ . Combining Eqs. (G.65) and (G.64) gives

$$d_{M'M}^J(\theta) = (-1)^{M'-M} d_{M'M}^J(-\theta). \quad (\text{G.68})$$

2. Under  $m \leftrightarrow m'$ . Combining Eqs. (G.63), (G.64), and (G.65), we get

$$d_{M'M}^J(\theta) = (-1)^{M'-M} d_{MM'}^J(\theta). \quad (\text{G.69})$$

3. Under  $m \rightarrow -m$  and  $m' \rightarrow -m'$ . Looking at Eq. (G.65),

$$d_{M'M}^J(\theta) = (-1)^{M'-M} d_{-M'-M}^J(\theta). \quad (\text{G.70})$$

4. Under  $\theta \rightarrow \pi \pm \theta$ . Apparently this is *not* a symmetry that the Jacobi polynomials have. This must be accompanied with a  $m$  or  $m'$  being negated as well.

5. Under  $\theta \rightarrow \pi - \theta$  and  $m \rightarrow -m$ . Combining Eqs. (G.66) and (G.68) gives

$$d_{M'M}^J(\pi - \theta) = (-1)^{J-M'} d_{M'-M}^J(\theta). \quad (\text{G.71})$$

6. Under  $\theta \rightarrow \pi - \theta$  and  $m' \rightarrow -m'$ . Combining Eqs. (G.67) and (G.68) gives

$$d_{M'M}^J(\pi - \theta) = (-1)^{J-M} d_{-M'M}^J(\theta). \quad (\text{G.72})$$

As a closing note for this section, Sakurai gives an expression for  $d_{M'M}^J$  calculated using Schwinger's angular momentum model [127],

$$\begin{aligned} d_{M'M}^J(\beta) &= \sqrt{(J+M)!(J-M)!(J+M')!(J-M')!} \\ &\times \sum_{k=k_{\min}}^{k_{\max}} (-1)^{k-M+M'} \frac{s_2^k}{k!} \frac{s_2^{k-M+M'}}{(k-M+M')!} \\ &\times \frac{c_2^{J+M-k}}{(J+M-k)!} \frac{c_2^{J-M'-k}}{(J-M'-k)!}, \end{aligned} \quad (\text{G.73})$$

$$k_{\min} = \text{Max}(0, M - M'), \quad (\text{G.74})$$

$$k_{\max} = \text{Min}(J + M, J - M'), \quad (\text{G.75})$$

where  $s_2 = \sin(\beta/2)$  and  $c_2 = \cos(\beta/2)$ .

### G.3 Helicity Applied to Potentials with Full Rotational Invariance

Now, we want to look at matrix elements of the potential

$$\begin{aligned} \langle \mathbf{p}' \lambda'_1 \lambda'_2 | V | \mathbf{p} \lambda_1 \lambda_2 \rangle &= \sum_{J', M'} \sqrt{\frac{2J'+1}{4\pi}} \mathcal{D}_{M'\lambda'}^{J'}(\phi', \theta', 0) \sum_{J, M} \sqrt{\frac{2J+1}{4\pi}} \mathcal{D}_{M\lambda}^J(\phi, \theta, 0) \\ &\langle \mathbf{p}' J' M' \lambda'_1 \lambda'_2 | V | \mathbf{p} J M \lambda_1 \lambda_2 \rangle. \end{aligned} \quad (\text{G.76})$$

But if the potential has full rotational invariance, that means that it is a scalar. We need to use the Wigner-Eckart theorem, which states that

$$\langle \alpha' J' M' | T_m^j | \alpha J M \rangle = \langle J j; M m | J j; J' M' \rangle \frac{\langle \alpha' J' || T^j || \alpha J \rangle}{\sqrt{2j+1}}. \quad (\text{G.77})$$

For a scalar potential,  $V = T_0^0$ , so

$$\langle \alpha' J' M' | V | \alpha J M \rangle = \delta_{MM'} \delta_{JJ'} \frac{\langle \alpha' J || V || \alpha J \rangle}{\sqrt{2J+1}}. \quad (\text{G.78})$$

Thus, the potential matrix element is independent of the  $M$  value, and is diagonal in  $J$ .

This allows us to write

$$\langle \mathbf{p}' \lambda'_1 \lambda'_2 | V | \mathbf{p} \lambda_1 \lambda_2 \rangle = \sum_J \frac{2J+1}{4\pi} \left[ \sum_M \mathcal{D}_{M\lambda'}^J(\phi', \theta', 0) \mathcal{D}_{M\lambda}^J(\phi, \theta, 0) \right] \langle p' J \lambda'_1 \lambda'_2 | V | p J \lambda_1 \lambda_2 \rangle. \quad (\text{G.79})$$

The  $M$  dependence of the matrix element has simply been omitted, since there is no dependence.

Recall the addition theorem for the rotation matrices,

$$\mathcal{D}_{MM'}^J(\alpha\beta\gamma) = \sum_{M''} \mathcal{D}_{MM''}^J(\alpha_1\beta_1\gamma_1) \mathcal{D}_{M''M'}^J(\alpha_2\beta_2\gamma_2), \quad (\text{G.80})$$

where

$$R_{\alpha\beta\gamma} = R_{\alpha_1\beta_1\gamma_1} R_{\alpha_2\beta_2\gamma_2} \quad (\text{G.81})$$

$$e^{-i\alpha J_z} e^{-i\beta J_y} e^{-i\gamma M} = e^{-i\alpha_1 J_z} e^{-i\beta_1 J_y} e^{-i(\gamma_1+\alpha_2) J_z} e^{-i\beta_2 J_y} e^{-i\gamma_2 J_z}. \quad (\text{G.82})$$

Using the addition theorem, we get

$$\sum_M \mathcal{D}_{M\lambda'}^J(\phi', \theta', 0) \mathcal{D}_{M\lambda}^J(\phi, \theta, 0) = \sum_M \mathcal{D}_{\lambda'M}^J(0, -\theta', -\phi') \mathcal{D}_{M\lambda}^J(\phi, \theta, 0) \quad (\text{G.83})$$

$$= \mathcal{D}_{\lambda'\lambda}^J(\phi''_1, \theta'', -\phi''_2). \quad (\text{G.84})$$

In general,  $\phi''_1 \neq \phi''_2$ , and  $\theta'' \neq \theta' - \theta$ . However, we will be able to make some simplifications.

The sum rule allows us to write

$$\langle \mathbf{p}' \lambda'_1 \lambda'_2 | V | \mathbf{p} \lambda_1 \lambda_2 \rangle = e^{-i\phi''_1 \lambda'} e^{i\phi''_2 \lambda} \sum_J \frac{2J+1}{4\pi} d_{\lambda'\lambda}^J(\theta'') \langle p' J \lambda'_1 \lambda'_2 | V | p J \lambda_1 \lambda_2 \rangle. \quad (\text{G.85})$$

All we are interested is the matrix element buried inside the sum, so we invert the equation to get

$$\langle p' J \lambda'_1 \lambda'_2 | V | p J \lambda_1 \lambda_2 \rangle = 2\pi \int_{-1}^1 d \cos \theta'' d_{\lambda' \lambda}^J(\theta'') e^{i\phi'_1 \lambda'} e^{-i\phi'_2 \lambda} \langle p' \lambda'_1 \lambda'_2 | V | p \lambda_1 \lambda_2 \rangle. \quad (\text{G.86})$$

Note that there are three free parameters in the integrand. We can choose  $\phi = \phi' = \theta = 0$ . This means that  $\phi''_1 = \phi''_2 = 0$ , and  $\theta'' = \theta'$ . Thus,

$$\begin{aligned} & \langle p' J \lambda'_1 \lambda'_2 | V | p J \lambda_1 \lambda_2 \rangle \\ &= 2\pi \int_{-1}^1 d \cos \theta' d_{\lambda' \lambda}^J(\theta') \langle (p' \sin \theta', 0, p' \cos \theta') \lambda'_1 \lambda'_2 | V | p \hat{\mathbf{z}} \lambda_1 \lambda_2 \rangle, \end{aligned} \quad (\text{G.87})$$

which is what is advertised in Machleidt's Eq. (E.41) in Ref. [58].

#### G.4 Helicity Applied to Potentials with Cylindrical Invariance

Now, we want to look at matrix elements of the potential

$$\begin{aligned} \langle p' \lambda'_1 \lambda'_2 | V | p \lambda_1 \lambda_2 \rangle &= \sum_{J', M'} \sqrt{\frac{2J'+1}{4\pi}} \mathcal{D}_{M' \lambda'}^{J'}(\phi', \theta', 0) \sum_{J, M} \sqrt{\frac{2J+1}{4\pi}} \mathcal{D}_{M \lambda}^J(\phi, \theta, 0) \\ & \langle p' J' M' \lambda'_1 \lambda'_2 | V | p J M \lambda_1 \lambda_2 \rangle. \end{aligned} \quad (\text{G.88})$$

Now we consider that the potential operator is not a scalar, but it still conserves  $M$ . In terms of spherical tensor operators, we can write

$$V = \sum_J V_{M=0}^{(J)}. \quad (\text{G.89})$$

This does not bode well for an approach like the one that was used in the previous section.

However, we can write

$$\begin{aligned} \langle p' \lambda'_1 \lambda'_2 | V | p \lambda_1 \lambda_2 \rangle &= \sum_{J'} \sqrt{\frac{2J'+1}{4\pi}} \sum_{J, M} \sqrt{\frac{2J+1}{4\pi}} e^{iM(\phi' - \phi)} d_{\lambda' M}^{J'}(\theta') d_{\lambda M}^J(\theta) \\ & \langle p' J' M \lambda'_1 \lambda'_2 | V | p J M \lambda_1 \lambda_2 \rangle. \end{aligned} \quad (\text{G.90})$$

Since the  $M$  is all that is conserved, it makes sense to ignore  $J$  for now. So we change basis to

$$\langle \mathbf{p}'\lambda'_1\lambda'_2|V|\mathbf{p}\lambda_1\lambda_2\rangle = \sum_M \frac{1}{2\pi} e^{i\Delta\phi M} \langle p'\theta' M\lambda'_1\lambda'_2|V|p\theta M\lambda_1\lambda_2\rangle, \quad (\text{G.91})$$

where  $\Delta\phi = \phi' - \phi$ . As in the previous section, all we are interested in is the matrix element buried in the sum. We invert the equation to obtain

$$\langle p'\theta' M\lambda'_1\lambda'_2|V|p\theta M\lambda_1\lambda_2\rangle = \int_0^{2\pi} d(\Delta\phi) e^{-i\Delta\phi M} \langle \mathbf{p}'\lambda'_1\lambda'_2|V|\mathbf{p}\lambda_1\lambda_2\rangle. \quad (\text{G.92})$$

There is one free angle in the integrand. Setting  $\phi = 0$  for simplicity, to get

$$\langle p'\theta' M\lambda'_1\lambda'_2|V|p\theta M\lambda_1\lambda_2\rangle = \int_0^{2\pi} d\phi' e^{-i\phi' M} \langle \mathbf{p}'\lambda'_1\lambda'_2|V|p_3, p_\perp \hat{\mathbf{x}}\lambda_1\lambda_2\rangle. \quad (\text{G.93})$$

How does this relate to what we got before, with the  $J, M$  matrix elements? We need to change basis once more, to get

$$\begin{aligned} \langle p'J'M\lambda'_1\lambda'_2|V|pJM\lambda_1\lambda_2\rangle &= \sqrt{\frac{2J'+1}{2}} \int_{-1}^1 d\cos\theta' d_{M\lambda'}^{J'}(\theta') \\ &\quad \times \sqrt{\frac{2J+1}{2}} \int_{-1}^1 d\cos\theta d_{M\lambda}^J(\theta) \\ &\quad \times \langle p'\theta' M\lambda'_1\lambda'_2|V|p\theta M\lambda_1\lambda_2\rangle. \end{aligned} \quad (\text{G.94})$$

## G.5 Summary of Transformations

“Oh, I have now a mania for shortness. Whatever I read - my own or other people’s works - it all seems to me not short enough.”

—Anton Chekhov

First of all, we would like to be able to transform to  $|JM\lambda S\rangle$ . In particular, we would like

$$\langle JM\lambda S|JM\lambda S\rangle = \int d\Omega \langle JM\lambda S|\theta\phi S\rangle \langle \theta\phi S|JM\lambda S\rangle. \quad (\text{G.95})$$

Looking at the first term,

$$\langle JMS\lambda|\theta\phi S\lambda\rangle = \sqrt{\frac{2J+1}{4\pi}} \mathcal{D}_{M\lambda}^J(\phi, \theta, 0). \quad (\text{G.96})$$

The second term takes a little more work.

$$\begin{aligned} \langle \theta\phi S\lambda|JM LS\rangle &= \langle 00S\lambda|R_{\phi\theta 0}^\dagger|JM LS\rangle \\ &= \sum_{M'} \langle 00S\lambda|JM' LS\rangle \langle JM' SL|R_{\phi\theta 0}^\dagger|JM LS\rangle \\ &= \sum_{M_L, M_S, M'} \langle 00S\lambda|LM_L SM_S\rangle \langle LM_L SM_S|JM' LS\rangle \\ &\quad \times (\langle JM SL|R_{\phi\theta 0}|JM' LS\rangle)^* \\ &= \sum_{M_L, M_S, M'} Y_{LM_L}(0, 0) \delta_{\lambda, M_S} \langle LM_L SM_S|JM'\rangle \mathcal{D}_{MM'}^{J*}(\phi, \theta, 0) \\ &= \sum_{M_L, M_S, M'} \sqrt{\frac{2L+1}{4\pi}} \delta_{M_L, 0} \delta_{\lambda, M_S} \langle LM_L SM_S|JM'\rangle \mathcal{D}_{MM'}^{J*}(\phi, \theta, 0) \\ &= \sqrt{\frac{2L+1}{4\pi}} \langle L0S\lambda|J\lambda\rangle \mathcal{D}_{M\lambda}^{J*}(\phi, \theta, 0) \end{aligned} \quad (\text{G.97})$$

Combining these, we get, by virtue of the orthonormality of the  $\mathcal{D}$ 's,

$$\begin{aligned} \langle JMS\lambda|JM LS\rangle &= \sqrt{\frac{2L+1}{2J+1}} \langle L0S\lambda|J\lambda\rangle \left[ \frac{2J+1}{4\pi} \int d\Omega \mathcal{D}_{M\lambda}^J(\phi, \theta, 0) \mathcal{D}_{M\lambda}^{J*}(\phi, \theta, 0) \right] \\ &= \sqrt{\frac{2L+1}{2J+1}} \langle L0S\lambda|J\lambda\rangle. \end{aligned} \quad (\text{G.98})$$

Using this, we obtain Machleidt's equation Eq. (C18) in Ref. [58],

$$|JM LS\rangle = \sum_{\lambda} \sqrt{\frac{2L+1}{2J+1}} \langle L0; S\lambda|J\lambda\rangle |JMS\lambda\rangle. \quad (\text{G.99})$$

For a one particle state, we start with  $|\theta\phi S\lambda\rangle$ . From that,

$$|\theta MS\lambda\rangle = \frac{1}{\sqrt{2\pi}} \int_0^{2\pi} d\phi e^{iM\phi} |\theta\phi S\lambda\rangle, \quad (\text{G.100})$$

$$|JMS\lambda\rangle = \sqrt{\frac{2J+1}{2}} \int_{-1}^1 d\cos\theta d_{M\lambda}^J(\theta) |\theta MS\lambda\rangle, \quad (\text{G.101})$$

$$|JM LS\rangle = \sqrt{\frac{2L+1}{2J+1}} \langle L0S\lambda|J\lambda\rangle |JMS\lambda\rangle. \quad (\text{G.102})$$

Furthermore, for two particle states, we have  $|\theta\phi S_1\lambda_1 S_2\lambda_2\rangle$ . However, that is rewritten as

$$|\theta\phi S\lambda S_1 S_2\rangle = \sum_{\lambda_1 \lambda_2} \langle \theta\phi S_1\lambda_1 S_2\lambda_2 | \theta\phi S\lambda S_1 S_2 \rangle |\theta\phi S_1\lambda_1 S_2\lambda_2\rangle \quad (\text{G.103})$$

$$= \sum_{\lambda_1 \lambda_2} \langle 00 S_1\lambda_1 S_2\lambda_2 | R_{\phi\theta 0}^\dagger R_{\phi\theta 0} | 00 S\lambda S_1 S_2 \rangle |\theta\phi S_1\lambda_1 S_2\lambda_2\rangle \quad (\text{G.104})$$

$$= \sum_{\lambda_1 \lambda_2} \langle 00 S_1\lambda_1 S_2\lambda_2 | 00 S\lambda S_1 S_2 \rangle |\theta\phi S_1\lambda_1 S_2\lambda_2\rangle \quad (\text{G.105})$$

$$= \sum_{\lambda_1 \lambda_2} \langle S_1 M_1 = \lambda_1 S_2 M_2 = -\lambda_2 | S M = \lambda S_1 S_2 \rangle |\theta\phi S_1\lambda_1 S_2\lambda_2\rangle \quad (\text{G.106})$$

$$= \sum_{\lambda_1 \lambda_2} \langle S_1\lambda_1 S_2 - \lambda_2 | S\lambda \rangle |\theta\phi S_1\lambda_1 S_2\lambda_2\rangle. \quad (\text{G.107})$$

Now, the  $|\theta\phi S\lambda S_1 S_2\rangle$  can be used to get

$$|\theta M S\lambda S_1 S_2\rangle = \frac{1}{\sqrt{2\pi}} \int_0^{2\pi} d\phi e^{iM\phi} |\theta\phi S\lambda S_1 S_2\rangle, \quad (\text{G.108})$$

$$|J M S\lambda S_1 S_2\rangle = \sqrt{\frac{2J+1}{2}} \int_{-1}^1 d\cos\theta d_{M\lambda}^J(\theta) |\theta M S\lambda S_1 S_2\rangle, \quad (\text{G.109})$$

$$|J M L S S_1 S_2\rangle = \sqrt{\frac{2L+1}{2J+1}} \langle L 0 S\lambda | J\lambda \rangle |J M S\lambda S_1 S_2\rangle. \quad (\text{G.110})$$

How does this relate to normal spins? Well, for those,

$$|\theta\phi S M_S S_1 S_2\rangle = \sum_{M_1 M_2} \langle S_1 M_1 S_2 M_2 | S M_S \rangle |\theta\phi S_1 M_1 S_2 M_2\rangle. \quad (\text{G.111})$$

But the relation of these to helicity is complicated, since in general every  $M_1$  is

connected to every  $\lambda_1$ . In particular,

$$\begin{aligned} & \langle \theta \phi S_1 \lambda_1 S_2 \lambda_2 | \theta \phi S_1 M_1 S_2 M_2 \rangle \\ &= \langle 00 S_1 \lambda_1 S_2 \lambda_2 | R_{\phi \theta 0}^\dagger R_{\phi \theta 0}^{(L)} | 00 S_1 M_1 S_2 M_2 \rangle \end{aligned} \quad (\text{G.112})$$

$$= \langle 00 S_1 \lambda_1 S_2 \lambda_2 | e^{i\theta J_y} e^{i\phi J_z} e^{-i\phi L_z} e^{-i\theta L_y} | 00 S_1 M_1 S_2 M_2 \rangle \quad (\text{G.113})$$

$$= \langle 00 S_1 \lambda_1 S_2 \lambda_2 | e^{i\theta J_y} e^{-i\theta L_y} e^{i\phi S_z} | 00 S_1 M_1 S_2 M_2 \rangle \quad (\text{G.114})$$

$$= \langle 00 S_1 \lambda_1 S_2 \lambda_2 | e^{i\theta S_y} e^{i\phi S_z} | 00 S_1 M_1 S_2 M_2 \rangle \quad (\text{G.115})$$

$$= \langle 00 | 00 \rangle \langle S_1 \lambda_1 | e^{-i\phi S_z} e^{-i\theta S_y} | S_1 M_1 \rangle \langle S_2 - \lambda_2 | e^{i\theta S_y} e^{i\phi S_z} | S_2 M_2 \rangle \quad (\text{G.116})$$

$$= \langle S_1 \lambda_1 | e^{i\theta S_y} | S_1 M_1 \rangle \langle S_2 - \lambda_2 | e^{i\theta S_y} | S_2 M_2 \rangle e^{i\phi(M_1+M_2)} \quad (\text{G.117})$$

$$= e^{i\phi(M_1+M_2)} d_{M_1, \lambda_1}^{S_1}(\theta) d_{M_2, -\lambda_2}^{S_2}(\theta). \quad (\text{G.118})$$

This is easily generalizable, to get

$$\langle \theta \phi \{S_i \lambda_i\} | \theta \phi \{S_i M_i\} \rangle = \prod_i e^{i\phi M_i} d_{M_i, \lambda_i}^{S_i}(\theta). \quad (\text{G.119})$$

Well, at least this makes sense for 1 and 2 particle states.

This has an implication for parity,  $\Pi$ . We get

$$\langle \theta \phi \{S_i \lambda_i\} | \theta \phi \{S_i M_i\} \rangle = \langle \theta \phi \{S_i \lambda_i\} | \Pi \Pi | \theta \phi \{S_i M_i\} \rangle \quad (\text{G.120})$$

$$= \delta \langle \pi - \theta \pi + \phi \{S_i - \lambda_i\} | \pi - \theta \pi + \phi \{S_i M_i\} \rangle \quad (\text{G.121})$$

$$= \delta \prod_i e^{i(\pi+\phi)M_i} d_{M_i, -\lambda_i}^{S_i}(\pi - \theta) \quad (\text{G.122})$$

$$= \delta \prod_i e^{i\phi M_i} (-1)^{M_i} (-1)^{S_i - M_i} d_{M_i, \lambda_i}^{S_i}(\theta) \quad (\text{G.123})$$

$$= \left[ \delta \prod_i (-1)^{S_i} \right] \prod_i e^{i\phi M_i} d_{M_i, \lambda_i}^{S_i}(\theta) \quad (\text{G.124})$$

$$= \prod_i e^{i\phi M_i} d_{M_i, \lambda_i}^{S_i}(\theta). \quad (\text{G.125})$$

So we see that  $\delta = \prod_i (-1)^{S_i}$ , so

$$\Pi | \theta \phi S \lambda \rangle = (-1)^S | \pi - \theta \pi + \phi S - \lambda \rangle \quad (\text{G.126})$$

$$\Pi | \theta \phi S_1 \lambda_1 S_2 \lambda_2 \rangle = (-1)^{S_1+S_2} | \pi - \theta \pi + \phi S_1 - \lambda_1 S_2 - \lambda_2 \rangle. \quad (\text{G.127})$$

Continuing on, we can derive other kets from the normal spin kets,

$$|\theta M_L S M_S S_1 S_2\rangle = \frac{1}{\sqrt{2\pi}} \int_0^{2\pi} d\phi e^{iM\phi} |\theta\phi S M_S S_1 S_2\rangle, \quad (\text{G.128})$$

$$|L M_L S M_S S_1 S_2\rangle = \int_{-1}^1 d\cos\theta Y_{LM_L}(\theta, 0) |\theta M_L S M_S S_1 S_2\rangle, \quad (\text{G.129})$$

$$|J M L S S_1 S_2\rangle = \sum_{M_L, M_S} \langle L M_L S M_S | J M \rangle |L M_L S M_S S_1 S_2\rangle. \quad (\text{G.130})$$

## VITA

“The life of every individual, if we survey it as a whole and in general, and only lay stress upon its most significant features, is really always a tragedy, but gone through in detail, it has the character of a comedy. For the deeds and vexations of the day, the restless irritation of the moment, the desires and fears of the week, the mishaps of every hour, are all through chance, which is ever bent upon some jest, scenes of a comedy.

“But the never-satisfied wishes, the frustrated efforts, the hopes unmercifully crushed by fate, the unfortunate errors of the whole life, with increasing suffering and death at the end, are always a tragedy. Thus, as if fate would add derision to the misery of our existence, our life must contain all the woes of tragedy, and yet we cannot even assert the dignity of tragic characters, but in the broad detail of life must inevitably be the foolish characters of a comedy.”

—*Arthur Schopenhauer*

Jason Randolph Cooke was born in Binghamton, New York state in January 26, 1974. After graduating from Owego Free Academy in Owego, New York in 1992, he enrolled at the State University of New York at Stony Brook. He earned a Bachelor of Science degree with honors in both Physics and Mathematics in May, 1996, and subsequently entered graduate school at the University of Washington in Seattle that fall. He earned a Master of Science in Physics and was admitted into candidacy in the doctoral program in December, 1997. In December, 2001, he earned a Doctor of Philosophy in Physics at the University of Washington.